

# Stability of stones on mild slopes

Master of Science Thesis





# Stability of stones on mild slopes

Master of Science Thesis

by

E.A.F. Wendt

Delft, December 2017

Delft University of Technology  
Faculty of Civil Engineering and Geosciences  
Department of Hydraulic Engineering



In collaboration with:

de Vries & van de Wiel  
Dredging & Environmental Solutions



# I Graduation Committee

## Chair member Graduation Committee

Prof.dr.ir. W.S.J. Uijtewaal

*Professor of Experimental Hydraulics  
Delft University of Technology*



## Board members Graduation Committee

Dr.ir. B. Hofland

*Assistant Professor of Coastal Engineering  
Delft University of Technology*



Ing. C. Kuiper

*Guest lecturer of Coastal Engineering  
Delft University of Technology*



Ir. H.D. Jumelet

*Project Engineer  
de Vries & van Wiel  
Dredging & Environmental Solutions*



## II Preface

This report presents the research of the MSc Thesis “*Stability of stones on mild slopes*”. The MSc Thesis is the final part of the Master curriculum of the Hydraulic Engineering track from the Faculty of Civil Engineering at the Delft University of Technology. The research and writing of the thesis is carried out with the assistance and facilities of both the Delft University of Technology and the company de Vries & van de Wiel.

The thesis is a follow-up to the research performed by Marieke Wit, Mark Postma and Roy Kramer. Wit (2015) studied the potential use of the numerical model XBeach-G to design a rock protection on mild slopes. Postma (2016) studied the underlying physics in XBeach-G. Kramer (2016) performed physical scale model tests to validate the conclusions drawn by Postma (2016). Their research will play a fundamental role in my thesis.

I would like to express my sincere gratitude to the members of my graduation committee for their guidance and advice during the project. In particular, I would like to thank my daily supervisor Daan Jumelet for his support and enthusiasm throughout the project. Additionally, I want to thank Mark Postma and Arjan Mol for their assistance with the numerical model XBeach-G.

Finally, I would like to thank my parents and my girlfriend Bonny for their moral support throughout my study.

Emiel Wendt

Delft, December 2017

### III Abstract

The static stability of stones on mild slopes under wave attack is investigated in this research. The first part of the research is focused on reproducing the physical scale model tests regarding profile change of Kramer (2016) numerically with the model XBeach-G. The erosion profiles modelled with the bed-load transport formulas of Nielsen (2006) and Van Rijn (2007) in XBeach-G do not match the erosion profiles of the profile change experiments of Kramer (2016). The bed-load transport formulas of Nielsen (2006) and Van Rijn (2007) are not able to model the sediment transport in XBeach-G accurately. Furthermore, XBeach-G cannot determine the velocity and acceleration near the bed, because the model solves the flow due to currents and waves for a single layer. Therefore, it can be concluded that XBeach-G should not be used to describe static stability of stones on mild slopes under wave attack. For the application of dynamically stable structures (which is not investigated in this research), XBeach-G functions satisfactorily (Postma, 2016). For further research, a model that solves the hydrodynamics for multiple layers should be applied. In this way, the hydrodynamics near the bed can be used to describe the static stability of stones.

The aim of the second part of the research is to develop a design method that describes the static stability of stones on mild slopes under wave attack. The basis of this design method is the initiation of motion of a stone and the hydrodynamic forces that initiate this movement. The hydrodynamic forces and corresponding mobility parameters are determined with the velocity and the acceleration near the bottom. Using Bubble Image Velocimetry (BIV), the velocity and the acceleration are derived from the videos of the BIV experiments of Kramer (2016) with regular waves breaking on a slope. It is found from the results of the BIV analysis that the effective, adapted Shields parameter  $\theta'_{\text{McCall}}$  can be used to describe movements of stones on mild slopes under wave attack. This mobility parameter has been determined with the bed shear stress of McCall (2015), which added an inertia term to include the influence of accelerations. For initiation of motion of stones, it appears that the stability parameter  $\theta_{\text{cr}}$  could be a value of 0.024 (in case no slope correction factor has been applied). To substantiate a design method that describes the static stability of stones on mild slopes under wave attack, the value of 0.024 could be used to define a threshold for initiation of motion of stones. More experiments need to be executed to optimize this value of the stability parameter. Moreover, a statistical value for the stability parameter could be used (like  $\theta_{\text{cr},1\%}$ ) to describe the static stability of stones by means of a certain number of stones that are allowed to move for a certain number of waves.

#### Keywords:

Stability of stones	Design method	BIV analysis	Van der Meer (1988)
Initiation of motion	Mild slopes	XBeach-G	Nielsen (2006)
Shields parameter	Erosion profiles	McCall (2015)	Van Rijn (2007)

## IV Table of Contents

<b>I</b>	<b>Graduation Committee .....</b>	<b>iv</b>
<b>II</b>	<b>Preface .....</b>	<b>v</b>
<b>III</b>	<b>Abstract.....</b>	<b>vi</b>
<b>IV</b>	<b>Table of Contents .....</b>	<b>vii</b>
<b>1</b>	<b>Introduction .....</b>	<b>1</b>
1.1	Background information .....	1
1.2	Problem analysis .....	2
1.3	Research question.....	3
1.4	Scope.....	3
1.5	Structure of report.....	3
<b>2</b>	<b>Literature review .....</b>	<b>4</b>
2.1	Hydrodynamics .....	4
2.1.1	Nearshore processes .....	4
2.1.2	Wave breaking on mild slopes.....	4
2.2	Initiation of motion .....	5
2.2.1	Hydrodynamic forces on a single stone.....	5
2.2.2	Forces caused by accelerations .....	6
2.2.3	Combining forces in oscillating flow .....	6
2.2.4	Force balance .....	6
2.3	Stability of stones on horizontal bed .....	7
2.3.1	Approach of Izbash (1930).....	7
2.3.2	Approach of Shields (1936) .....	7
2.3.3	Research of Sleath (1978).....	9
2.4	Stability of stones in breaking waves.....	9
2.4.1	Formula of Iribarren (1938) and formula of Hudson (1953) .....	9
2.4.2	Formula of Van der Meer (1988).....	10
2.4.3	Research of Schiereck & Fontijn (1996).....	11
2.5	Sediment transport .....	11
2.5.1	Threshold for initiation of motion .....	11
2.5.2	Sediment transport caused by accelerations .....	12
2.5.3	Sediment transport caused by bed shear stress .....	12
2.5.4	Formula of Nielsen (2006) .....	13
2.5.5	Formula of Van Rijn (1984) for currents.....	13
2.5.6	Formula of Van Rijn (2007) for currents and waves .....	14
2.6	Damage characteristics .....	14
2.6.1	Quantitative damage descriptions .....	14
2.6.2	Profile development .....	15
<b>3</b>	<b>Verification of previous physical scale model tests .....</b>	<b>17</b>
3.1	XBeach-G   Reproduce profile change experiments of Kramer (2016) .....	17
3.1.1	XBeach-G   Input parameters .....	17
3.1.2	XBeach-G   Initial and post profile of profile change experiments of Kramer (2016).....	18
3.1.3	XBeach-G   Numerical model XBeach-G .....	18

3.1.4	XBeach-G   Bed-load transport formulas in XBeach-G.....	19
3.1.5	XBeach-G   Output parameters and analyzation of process.....	20
3.2	BIV   Initiation of motion of stones based on BIV analysis.....	20
3.2.1	BIV   BIV experiments of Kramer (2016) .....	20
3.2.2	BIV   Input parameters.....	22
3.2.3	BIV   Analysis of videos of BIV experiments of Kramer (2016) .....	23
3.2.4	BIV   Velocity in Field of View with PIVlab .....	23
3.2.5	BIV   Horizontal velocity and acceleration in Region of Interest .....	24
3.2.6	BIV   Effective, adapted Shields parameter as mobility parameter .....	26
3.2.7	BIV   Stability parameter as threshold for initiation of motion .....	28
3.3	XBeach-G & BIV   Link mobility parameter with XBeach-G .....	29
<b>4</b>	<b>Results of XBeach-G simulations .....</b>	<b>30</b>
4.1	Results of XBeach-G simulations for 1:10 slope and $S_{wit}$ input.....	30
4.2	Overview of results of XBeach-G simulations .....	31
4.3	Analysis of results of XBeach-G simulations .....	32
4.3.1	Comparison of modelled erosion profiles with measured post profiles .....	32
4.3.2	Analysis of bed-load transport formulas applied in XBeach-G .....	32
4.3.3	Sensitivity of formula of Nielsen (2006) to sediment friction factor and phase lag angle .....	33
4.3.4	Validation/falsification of conclusions drawn by Postma (2016) about the bed-load transport formulas of Nielsen (2006) and Van Rijn (2007) .....	33
4.3.5	Comparison of damage for different wave characteristics with same slope angle .....	34
4.3.6	Analysis of damage level $S$ versus damage depth $E_3$ .....	34
4.3.7	Profile development of modelled erosion profiles.....	35
4.4	Discussion.....	35
4.4.1	Sediment friction factor and phase lag angle of formula of Nielsen (2006) .....	35
4.4.2	Minor damage derived from profile change experiments .....	36
4.5	Analysis of dimensionless stability parameter vs. Iribarren number .....	36
<b>5</b>	<b>Results of BIV analysis .....</b>	<b>38</b>
5.1	Results of BIV analysis of video with 1:5 slope .....	38
5.2	Results of BIV analysis of videos with 1:10 and 1:15 slope .....	42
5.3	Overview of velocity, acceleration and mobility parameters per slope .....	42
5.4	Analysis of results of BIV analysis .....	43
5.4.1	Movements of stones according to visual observations and mobility parameters .....	43
5.4.2	Sensitivity of formula of Nielsen (2006) to sediment friction factor and phase lag angle .....	43
5.4.3	Trend: decreasing mobility parameter for milder slopes .....	44
5.4.4	Results of BIV analysis of this research compared to results of Kramer (2016) .....	44
5.5	Discussion.....	45
5.5.1	Glued stones in DOF give no or limited movements of stones .....	45
5.6	Analysis of coefficients $c_f$ and $c_i$ in bed shear stress of $\theta'_{McCall}$ .....	45
5.7	Analysis of stability parameter $\theta_{cr}$ .....	47
5.7.1	Analysis of stability parameters $\theta'_{cr,displacement}$ and $\theta'_{cr,rocking}$ .....	47
5.7.2	New value for stability parameter $\theta_{cr}$ determined with $\theta'_{McCall}$ with new $c_f$ and $c_i$ .....	48
5.7.3	Stability parameter $\theta_{cr}$ in bed-load transport formulas of Nielsen (2006) and Van Rijn (2007). .....	50
5.8	Link mobility parameter $\theta'_{McCall}$ with numerical model XBeach-G .....	50
5.8.1	Mobility parameter $\theta'_{McCall}$ over time along length of slope .....	50

<b>6</b>	<b>Conclusions and recommendations.....</b>	<b>53</b>
6.1	Conclusions .....	53
6.1.1	Main research question.....	53
6.1.2	Research objectives.....	53
6.2	Recommendations .....	54
	<b>References .....</b>	<b>57</b>
	<b>List of Symbols .....</b>	<b>59</b>
	<b>Glossary .....</b>	<b>60</b>
	<b>List of Figures .....</b>	<b>61</b>
	<b>List of Tables .....</b>	<b>63</b>
	<b>Appendices - Table of Contents.....</b>	<b>64</b>
<b>Appendix A</b>	<b>Additional literature .....</b>	<b>66</b>
<b>Appendix B</b>	<b>Verification previous physical scale model tests.....</b>	<b>80</b>
<b>Appendix C</b>	<b>Results of XBeach-G simulations .....</b>	<b>86</b>
<b>Appendix D</b>	<b>Results of BIV analysis .....</b>	<b>92</b>
<b>Appendix E</b>	<b>Results of mobility parameter from XBeach-G.....</b>	<b>105</b>



# 1 Introduction

This chapter introduces the problem description of this research. In Section 1.1 the background information is described briefly. A concise analysis of the problem is given in Section 1.2. The research question and objectives of this study are presented in Section 1.3. Finally, the scope and the structure of the report are elaborated in Section 1.4 and Section 1.5.

## 1.1 Background information

The stability of stones on slopes under wave attack has been investigated by many researchers. These researchers have mainly focused on developing a design formula for rock slopes from 1:6 to steeper slopes, e.g. Van der Meer (1988) and Hudson (1959). However, applications exist with milder slopes, e.g. pipeline landings and foreshore protections at sea defences. An accurate design method to describe the stability of stones on these mild sloped applications under wave attack has not yet been determined.

For recent projects in the Netherlands regarding rock protections on mild slopes, the empirical design formula of Van der Meer (1988) is the prescribed method to determine the static stability for stones under wave attack. The formula, applicable for slopes steeper than 1:6, is extrapolated towards more gentle slopes. The validity of this extrapolation has not been thoroughly investigated. It seems that the method of Van der Meer (1988) overestimates the required stone size for stones on mild slopes due to the change in wave breaking (plunging to spilling breakers). The results of Schiereck & Fontijn (1996) strengthen this assumption and suggest that the formula of Van der Meer (1988) is too conservative for mild slopes, which can be expected as the type of wave breaking changes from plunging onto spilling breakers.

In 2015 de Vries & van de Wiel, a Dutch contractor, has been assigned to install a rock protection on the mild sloped, sandy foreshores of the Eastern Scheldt. The contract had strict design requirements, including the prescription to use the formula of Van der Meer (1988) to design a statically stable protection (allowing no or only minor damage). The result was that a protection with rather large stones was installed at the mild sloping foreshores. It appeared that a more cost efficient design method is preferred for this mild sloped application. Because of this reason, de Vries & van de Wiel has initiated further research with the aim to develop a design method for the static stability of stones on mild slopes under wave attack.

The subject has been investigated by three students from the Delft University of Technology. Wit (2015) studied the potential use of the numerical model XBeach-G<sup>1</sup> to describe the stability of stones on mild slopes under wave attack on homogeneous structures. Postma (2016) continued her work by studying the physics in XBeach-G. Furthermore, he examined the applicability of the model for inhomogeneous structures.

Kramer (2016) carried out physical scale model tests with rock protection on mild slopes. He did profile change experiments in order to examine the validity of the empirical design method of Van der Meer (1988) for mild slopes. Moreover, Kramer (2016) performed experiments with Bubble Image Velocimetry (BIV) to investigate the conclusions drawn by Postma (2016) about the physics in XBeach-G. Not all physical scale model tests performed by Kramer (2016) have been fully analyzed. This research elaborates on the test results of Kramer (2016) and provides feedback to the research of Postma (2016).

---

<sup>1</sup> XBeach-G is a branch of the main XBeach model, developed by McCall (2015), to simulate storm impacts on gravel beaches. XBeach-G uses the one-layer, depth-averaged, non-hydrostatic extension to XBeach.

## 1.2 Problem analysis

The static stability of stones on steep slopes (i.e. slopes with slope ratio  $< 1:6$ ) under wave attack has been described by the empirical design formula of Van der Meer (1988) for plunging breakers. The formula is extrapolated towards more gentle slopes, outside its validity region (only validated on 1:2 slopes for homogeneous structures and up to 1:6 slopes for inhomogeneous structures). According to the experimental results of Schiereck & Fontijn (1996) for 1:10 and 1:25 slopes, the extrapolated formula of Van der Meer (1988) seems to be too conservative due to the fact that the type of wave breaking changes from plunging onto spilling breakers.

A process-based model is preferred over an empirical design formula, provided that the underlying physics are implemented correctly, because such a model can be applied for many conditions governed by those underlying physics. Therefore, both Wit (2015) and Postma (2016) studied the potential use of the process-based model XBeach-G to describe the stability of stones on mild slopes under wave attack. Originally, XBeach-G is an application to determine the profile response of gravel beaches. The design formulas for statically stable breakwaters determine the stability of the rock based on the erosion area  $A_e$  or damage level  $S$  ( $S = A_e/D_{n50}$ ). Both the erosion area and the damage level can be derived from the eroded profile (obtained with XBeach-G). In this way, the XBeach-G results of Wit (2015) and Postma (2016) could (in theory) be compared with the (extrapolated) test results of Van der Meer (1988).

For homogeneous, statically stable structures (fully consisting of gravel), XBeach-G shows that smaller stone diameters provide sufficient stability for slopes ranging from 1:5 up to 1:50 (Wit, 2015). Moreover, physical scale model tests with impermeable structures (with a gravel layer on a sandy core) regarding profile change for 1:5 and 1:10 slopes demonstrate that the static stability is higher than the static stability determined with the extrapolated design formula of Van der Meer (1988) (Kramer, 2016). Both the results of the XBeach-G simulations of Wit (2015) and the results of the physical model tests of Kramer (2016) confirm the suggestion of Schiereck & Fontijn (1996) that the design method of Van der Meer (1988) is a conservative approach to describe the static stability of stones on mild slopes under wave attack.

Postma (2016) studied the underlying physics implemented in XBeach-G. The physical processes are modified to model storm impacts on gravel beaches correctly. The sediment transport is modelled in XBeach-G with the modified bed-load transport formulas of Nielsen (2006) or Van Rijn (2007). Postma (2016) performed XBeach-G simulations with these transport formulas for slopes ranging from 1:4 to 1:12. From the results could be concluded that the model could be used for the design of dynamically stable structures, because the (modified) physical processes in the model are able to predict the erosion profile developments reasonably well (Postma, 2016; Wit, 2015). However, neither the formula of Nielsen (2006) nor Van Rijn (2007) was able to accurately model the erosion area or damage level as used by Van der Meer (1988). A design method, focused on initiation of motion, should be developed to describe the static stability of stones on mild slopes under wave attack.

BIV experiments were executed by Kramer (2016) to investigate the conclusions drawn by Postma (2016) about the physical approaches used in XBeach-G. Several contradictions were found in the results of Postma (2016) and the results of the experiments of Kramer (2016). Whereas Postma (2016) recommends applying the formula of Nielsen (2006) for slopes milder than 1:6, the physical analysis of the BIV results of Kramer (2016) suggests using the method of Van Rijn (2007) to describe the static stability of stones on mild slopes.

### 1.3 Research question

The main research question of this (and previous) research is:

#### **How to describe the static stability of stones on mild slopes under wave attack?**

With the above research question in mind, the following objectives are addressed:

- Objective 1:** To reproduce and analyse the results of the physical scale model tests regarding profile change of Kramer (2016) by means of the numerical model XBeach-G.
- Objective 2:** To validate/falsify the conclusions drawn by Postma (2016) about modelling sediment transport of stones on mild slopes under wave attack using the bed-load transport formulas of Nielsen (2006) and Van Rijn (2007).
- Objective 3:** To describe initiation of motion of a stone by looking at the hydrodynamic forces that act on a stone on a mild sloping bed under wave attack.
- Objective 4:** To develop a design method that describes the static stability of stones on mild slopes under wave attack based on the initiation of motion of stones.

### 1.4 Scope

One part of the research is focused on reproducing the profile change experiments for 1:5, 1:10 and 1:15 slopes of Kramer (2016) numerically with the model XBeach-G. The bed-load transport formulas of Nielsen (2006) and Van Rijn (2007) are used to model the sediment transport in XBeach-G. The results of the modelled erosion profiles and corresponding damage characteristics obtained with the formulas of Nielsen (2006) and Van Rijn (2007) are compared with the results of the profile change experiments of Kramer (2016). The ability of both formulas to describe the static stability of stones on mild slopes under wave attack will be assessed. In this way, the conclusions drawn by Postma (2016) regarding the formulas of Nielsen (2006) and Van Rijn (2007) are validated.

Secondly, an attempt has been made to substantiate a design method that describes the static stability of stones on mild slopes under wave attack. The basis of this design method is the initiation of motion of a stone on a mild sloping bed under wave attack and the hydrodynamic forces that initiate this movement. The hydrodynamic forces and corresponding mobility parameters can be determined with the velocity and the acceleration close to the bottom. The velocity and the acceleration are derived from the videos of waves breaking on a slope using Bubble Image Velocimetry (BIV). The videos are obtained from the BIV experiments of Kramer (2016). The BIV analysis of the videos regarding initiation of motion of stones will be carried out in this report.

Finally, an endeavor is made to link both parts by connecting a mobility parameter, derived from the BIV analysis, with the numerical model XBeach-G.

### 1.5 Structure of report

Chapter 2 presents an introduction to the stability of stones. It includes a literature review that provides insight in the hydrodynamics that apply to mild slopes under wave attack, the initiation of motion of stones, several design formulas regarding the stability of stones in uniform flow or in breaking waves, and sediment transport formulas. Chapter 3 covers the methodology for the XBeach-G simulations to reproduce the profile change experiments of Kramer (2016) with the bed-load transport formulas of Nielsen (2006) and Van Rijn (2007). Besides, Chapter 3 treats the verification of the BIV analysis of the videos from the BIV experiments of Kramer (2016) regarding initiation of motion of stones. The results of XBeach-G simulations are presented and analyzed in Chapter 4. The results of the BIV analysis are elaborated in Chapter 5. The conclusions and recommendations for further research are given in Chapter 6.

## 2 Literature review

This chapter contains a collection of relevant literature that functions as a theoretical background regarding the stability of stones. First, the hydrodynamics are treated briefly in Section 2.1 with the focus on the nearshore processes that apply to mild slopes and the relevant wave breaking types. To gain insight in the stability of stones, the moment when a stone starts to move from its initial position is considered in Section 2.2. This threshold of motion can be described by a certain critical velocity or critical shear stress and is dependent on the hydrodynamic forces acting on a stone. A force balance is worked out and the influence of accelerations in a fluid motion is included. The static stability of stones on mild slopes falls in the transition area between the static stability of rocks on breakwaters (with relatively steep slopes) and the stability of grains on beaches (with relatively gentle slopes). For these different slope applications, much research has been done to describe the stability of stones. Section 2.3 deals with the stability of stones in a uniform flow and on a horizontal bed. Several design methods for breakwaters are derived from the research on the static stability of stones in breaking waves. These design methods are described in Section 2.4. Sediment transport formulas, originally derived for horizontal sandy beds, are treated in Section 2.5. Finally, damage characteristics to indicate the damage of rock protections are described in Section 2.6.

### 2.1 Hydrodynamics

#### 2.1.1 Nearshore processes

The main nearshore processes that apply to mild slopes under wave attack can be divided into the surface water, the groundwater and the surface water-groundwater exchange. The depth-averaged flow of the surface water due to currents and waves can be described with the non-linear shallow water equations (NLSWE), elaborated in Appendix A.1. The groundwater is based on conservation of mass, equations of motion and a parameterization for the non-hydrostatic groundwater pressure. This is worked out in Appendix A.2. The surface water-groundwater exchange is treated in Appendix A.3. Submarine exchange occurs when surface water is connected with groundwater. When surface water and groundwater are not connected, infiltration takes place when the surface water table is above the groundwater table or exfiltration occurs due to a high groundwater table (McCall, 2015).

#### 2.1.2 Wave breaking on mild slopes

The type of wave breaking can be described with the dimensionless Iribarren number  $\xi$ , elaborated in Appendix A.10. The parameter is related to the slope angle and the wave steepness. For this research on relative mild slopes ( $\xi \approx 0.5 - 1.5$ ), the plunging breaker is the relevant breaker type. For even more gentle slopes ( $\xi < 0.3$ ), the spilling breaker needs to be taken into account (Schierack & Verhagen, 2012).

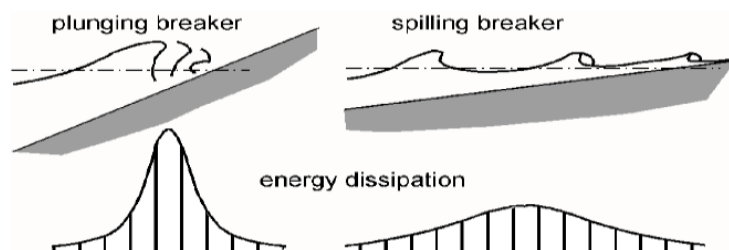


Figure 1 - Energy dissipation of plunging breaker and spilling breaker (Schierack & Verhagen, 2012)

The difference in wave breaking and corresponding energy dissipation of a plunging breaker and a spilling breaker is shown in Figure 1. In case of a plunging breaker, the wave crest becomes very asymmetric and breaks over the lower part of the wave on the slope. In this way, the wave energy is released in one big splash. With a spilling breaker, the wave crest is less asymmetric. Therefore, the wave impact on the slope is less pronounced and the energy dissipation is more spread. Both breaker types have a different effect on the stability of stones. Furthermore, the interaction between surface water and groundwater is high/low for plunging/spilling breakers.

## 2.2 Initiation of motion

### 2.2.1 Hydrodynamic forces on a single stone

To describe the initiation of motion of a stone, the hydrodynamic forces that act on a stone need to be investigated. The hydrodynamic forces can be divided in active forces that try to move the stone and passive forces that keep the stone in place. A stone is brought into motion when the active forces are larger than the passive forces. The forces are shown in Figure 2. The active forces are: drag force  $F_D$ , shear force  $F_S$ , lift force  $F_L$ , and turbulence forces. The drag force is caused by protrusion of the stone in the flow, causing pressure and viscous skin friction. The drag force acts in the direction of the current. The curvature of the flow lines gives a decrease in pressure at the top of the stone, causing a lift force. The lift force acts perpendicular to the drag force. The gravitational force  $F_G$  and the friction force  $F_F$  are the passive forces. The gravitational force acts downward and is caused by the submerged weight of the stone. A dimensionless relation between load and strength can be deduced from the equilibrium of horizontal forces, vertical forces and momentum (Van der Velden, 1989). This is elaborated in Appendix A.4.

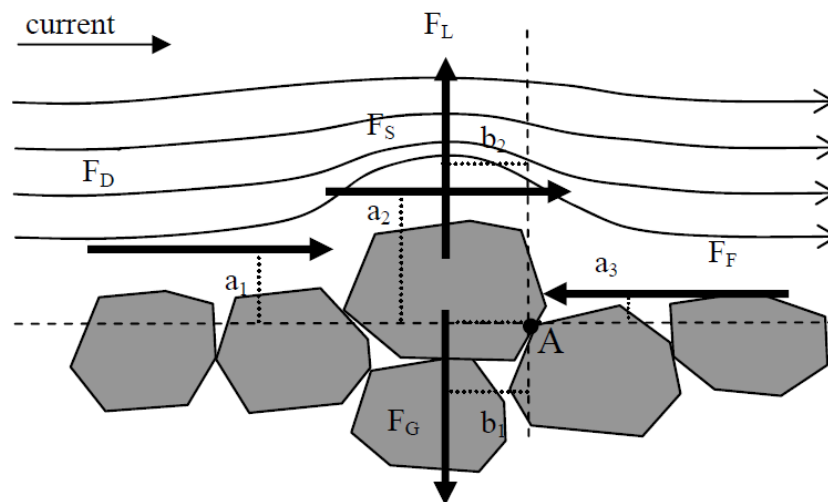


Figure 2 - Hydrodynamic forces acting on a stone (Huijsmans, 2006)

The formulas of the active forces, related to the horizontal velocity of the fluid motion, are given by equation (2.1). The shear force is assumed to be implicitly included in the drag force, because it is also proportional to  $u_b^2$  and works in the same direction (of the current) (Van den Heuvel, 2013).

$$F_D = \frac{1}{2} C_D \rho_w A_D u_b |u_b|, \quad F_S = \frac{1}{2} C_S \rho_w A_S u_b |u_b|, \quad F_L = \frac{1}{2} C_L \rho_w A_L u_b |u_b| \quad (2.1)$$

In which:  $F_x$  is the force (N),  $C_x$  is the coefficient (-),  $\rho_w$  is the density of water ( $\text{kg/m}^3$ ),  $u_b$  is the velocity of the flow near the bottom (m/s) and  $A_x$  is the exposed surface area ( $\text{m}^2$ ). With subscript X for D (drag), S (shear) and L (lift) respectively.

The formulas of the passive forces are given by equation (2.2).

$$F_G = ma = (\rho_s - \rho_w)gV, \quad F_F = C_F(\rho_s - \rho_w)gV \quad (2.2)$$

In which:  $F_G$  is the gravity force (N),  $F_F$  is the friction force (N),  $C_F$  is the friction coefficient (-),  $\rho_s$  is the density of stone ( $\text{kg/m}^3$ ),  $g$  is the gravitational acceleration ( $\text{m/s}^2$ ),  $V$  is the volume of the stone ( $\text{m}^3$ ) (with  $V \propto D_{50}^3$ ) and  $D_{50}$  is the mean diameter of the stone (m).

### 2.2.2 Forces caused by accelerations

In case of a non-stationary flow, accelerations of a fluid motion around a stone create horizontal pressure differences. Dessens (2004) and Tromp (2004) already investigated the influence of accelerations on the initiation of motion. The derivation of the forces due to the horizontal pressure differences is worked out in Appendix A.5. The pressure differences are determined with the theory of Bernoulli. The stones are assumed to be equally sized and small compared to the variations in flow. In case of small stones, the change of velocities along the length of a stone is small as well. The force  $F_{acc}$  due to pressure differences, caused by accelerations of the flow, is then given by equation (2.3). In which:  $a$  ( $= \partial u / \partial t$ ) is the horizontal acceleration ( $m/s^2$ ). The force  $F_{acc}$  becomes larger for increasing stone sizes, because the volume of the stone is related to the diameter of the stone by  $V \propto D_{50}^3$ .

$$F_{acc} = \rho \frac{\partial u}{\partial t} V = \rho a V \quad (2.3)$$

### 2.2.3 Combining forces in oscillating flow

This research looks at an oscillating flow (with waves breaking on a mild slope) where both forces related to the horizontal velocity of the fluid motion and forces due to horizontal pressure differences (created by accelerations of the fluid motion) are present. These forces fluctuate in time, but have an average value of zero over time. The formula for the wave force, as proposed by Morison et al. (1950), is adapted into equation (2.4) by replacing the drag force  $F_D$  with a bulk force  $F_B$  to include also the other forces related to the horizontal velocity of the fluid motion. The formula is now a combination of the bulk force  $F_B$  and the pressure force  $F_{acc}$ , which becomes more dominant for larger stone sizes.

$$F_{combined} = F_B + F_{acc} = \frac{1}{2} C_B \rho A u |u| + C_M \rho V \frac{\partial u}{\partial t} \quad (2.4)$$

In which:  $C_B$  is a bulk coefficient that includes the coefficients  $C_D$  and  $C_L$ , and  $C_M$  is an acceleration coefficient, which also contains a contribution for the added mass. An elaboration of the coefficients  $C_B$ ,  $C_D$ ,  $C_L$  and  $C_M$  is given in Appendix A.6.

### 2.2.4 Force balance

The forces balance of Section 2.2.1 is extended by adding the force due to accelerations (Dessens, 2004; Tromp, 2004). The movement of a stone is initiated when momentum of forces about pivot A in Figure 3 (contact point with adjacent stone) is positive (Van der Velden, 1989). All forces are assumed to have their origin in the center of mass of the stone.

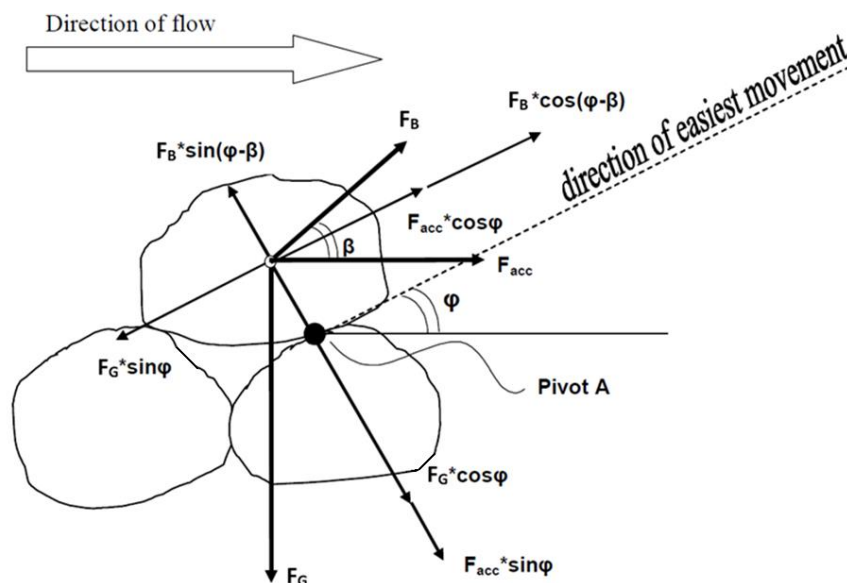


Figure 3 - Schematization of forces acting on a stone in accelerating flow (Tromp, 2004)

According to Kirchner (1990), the angle  $\varphi$  ranges between  $30^\circ$  and  $45^\circ$  for the direction of easiest movement for stones. The forces  $F_B$ ,  $F_{acc}$  and  $F_G$  can be decomposed into normal and tangential components in the direction of easiest movement. The tangential components intersect with pivot A in Figure 3. Therefore, the tangential components do not contribute to the momentum balance and only the normal components of the forces need to be taken into account. The momentum balance is presented in equation (2.5). The combined force of the adapted Morison equation (2.4) can be found in equation (2.5) as  $F_B$  and  $F_{acc}$ . In Figure 3  $F_{acc}$  acts in horizontal direction and  $F_B$  acts at an angle  $\beta$  compared to  $F_{acc}$ . The angle  $\beta$  is determined by means of the contribution of lift, drag and turbulence forces.

$$F_B \cos(\varphi - \beta) + F_{acc} \cos(\varphi) < F_G \sin(\varphi) \quad (2.5)$$

When the left hand side is larger than the right hand side, the stone will start to move. When the right hand side is larger, the stone is stable and will not move.  $F_G \sin(\varphi)$  can be seen as the critical force that has to be exceeded to initiate movement of the stone. The critical mobility parameter  $\theta_{Force}$  can be derived to define a threshold of motion (Van den Heuvel, 2013). The derivation is treated in Appendix A.7 and resulted in a Shields-like stability parameter.

## 2.3 Stability of stones on horizontal bed

For horizontal beds, the two most common used formulas dealing with the stability of stones are: Izbash (1930) and Shields (1936).

### 2.3.1 Approach of Izbash (1930)

Izbash (1930) researched the stability of stones on a horizontal bed using the critical velocity. The approach is based on the critical value for which the forces acting on an individual stone are not in equilibrium anymore. When the critical velocity is exceeded, the particle starts to move. Izbash (1930) has not considered the depth in his formula, because a velocity distribution profile has not been defined. Besides, the location of the velocity acting on the stone is not known and it is unclear how the diameter of the stone is defined. The formula can be used in cases of non-uniform flow and in conditions where velocity does not depend on an equilibrium flow force and bed friction force, e.g. water jets. In other cases, the approach of Shields (1936) should be used.

### 2.3.2 Approach of Shields (1936)

The Shields (1936) approach is probably the best-known formula for the stability of granular material in uniform flow (Chézy-equation has to be valid). The approach considers the friction force caused by the water on the bed, so not on a single particle. When this force exceeds a certain critical value, the bed starts to erode and particles are brought into motion. The initiation of motion is described by a relation between dimensionless shear stress and the particle Reynolds-number. The particle Reynolds number indicates whether the grain protrudes into the turbulent boundary layer or stays within the viscous sublayer (Schierack & Verhagen, 2012). The relation is given in equation (2.6). The Shields parameter is defined as the critical value for which the stability of stones is guaranteed (CIRIA et al., 2007).

$$\Psi_{cr} = \frac{\tau_{cr}}{(\rho_s - \rho_w)gD_{50}} = \frac{u_{*,cr}^2}{\Delta g D_{50}} = f(Re_*) = f\left(\frac{u_* D_{50}}{\nu}\right) \quad (2.6)$$

In which:  $\Psi_{cr}$  is the Shields parameter (-),  $\tau_{cr}$  is the critical bed shear stress ( $N/m^2$ ),  $u_{*,cr}$  is the critical bed shear velocity, defined generally as  $u_* = \sqrt{\tau_b/\rho_w}$  (m/s),  $Re_*$  is the particle Reynolds-number (-),  $\Delta$  is the relative density (-), which is defined as  $\Delta = (\rho_s - \rho_w)/\rho_w$ , and  $\nu$  is the kinematic viscosity of water ( $m^2/s$ ) ( $=10^{-6} m^2/s$ ).

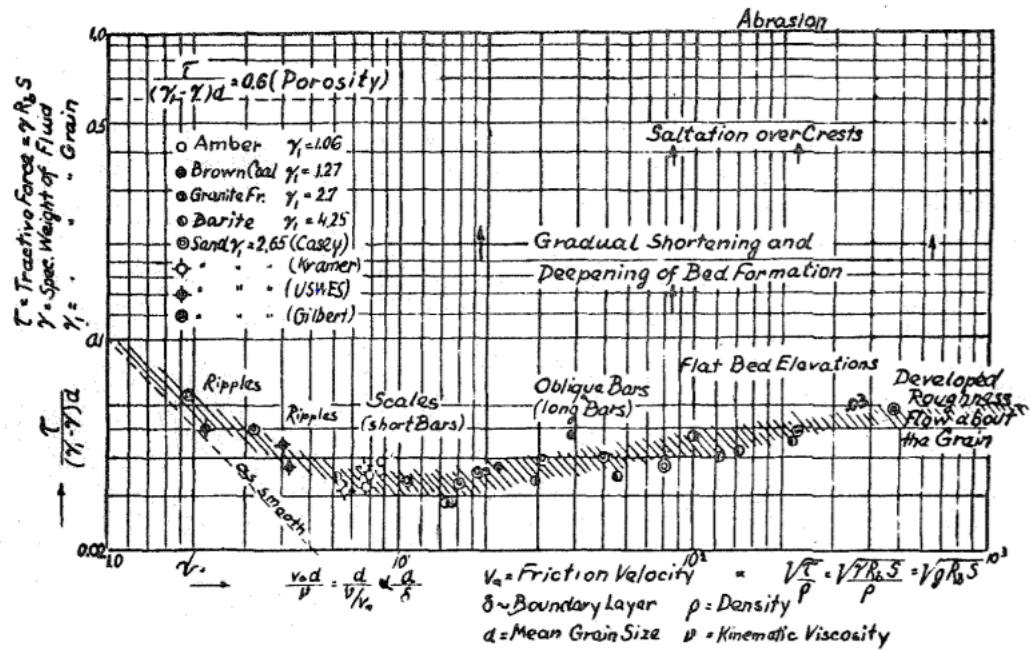


Figure 4 - Original Shields diagram (Shields, 1936)

The relation of Shields (1936) is presented as a curve in Figure 4. The curve shows the critical shear stress as function of the particle Reynolds number. The graph shows that the Shields parameter  $\Psi_{cr}$  becomes constant for a value of 0.055 for high particle Reynolds numbers ( $Re_* > 500$ ). If the Shields parameter has a value that is above the Shields curve, stones will move. For lower values, no movement of stones will occur. This threshold of motion is prone to subjectivity. Breusers & Schukking (1971) investigated initiation of motion and came with seven transport stages, shown in Figure 5 and described in Table 1.

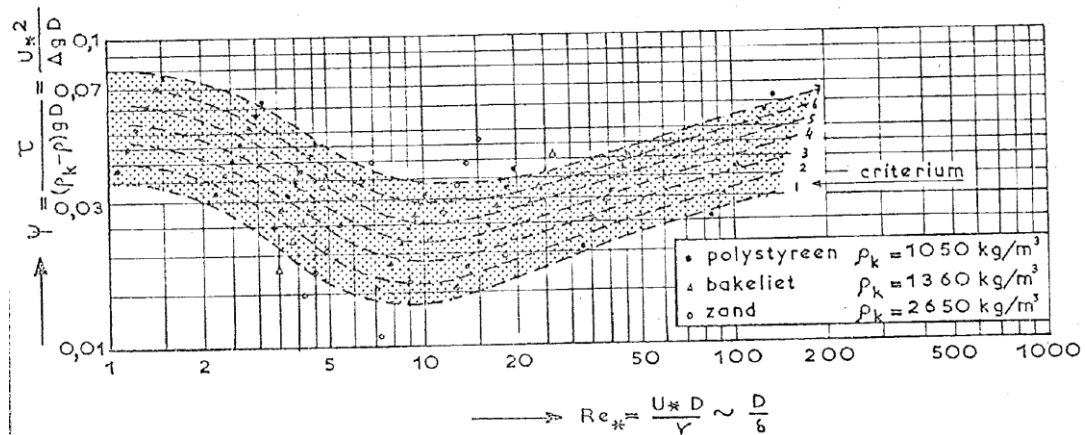


Figure 5 - Seven transport stages (Breusers & Schukking, 1971)

Table 1 - Description of the seven transport stages (Breusers & Schukking, 1971)

Stage	Description
0	No movement at all
1	Occasional movement at some locations
2	Frequent movement at some locations
3	Frequent movement at several locations
4	Frequent movement at many locations
5	Frequent movement at all locations
6	Continuous movement at all locations (matches Shields criterion)
7	General transport of the grains

In this research, the Shields parameter is used as a threshold for the initiation of motion of stones, taking into account the different transport stages.

### 2.3.3 Research of Sleath (1978)

Sleath (1978) elaborated on the research of Shields by investigating the stability of stones in an oscillating flow (with non-breaking waves). He used the bed shear stress related to waves  $\hat{\tau}_{b,w}$  based on Jonsson (1966). The results could be compared directly, see Figure 6 (with  $d_*$  as the dimensionless particle parameter). Sleath (1978) based the graph on several stability measurements of various authors, e.g. Rance & Warren (1968). This resulted in a critical value for  $\Psi_{cr}$  of 0.056 (Sleath, 1978).

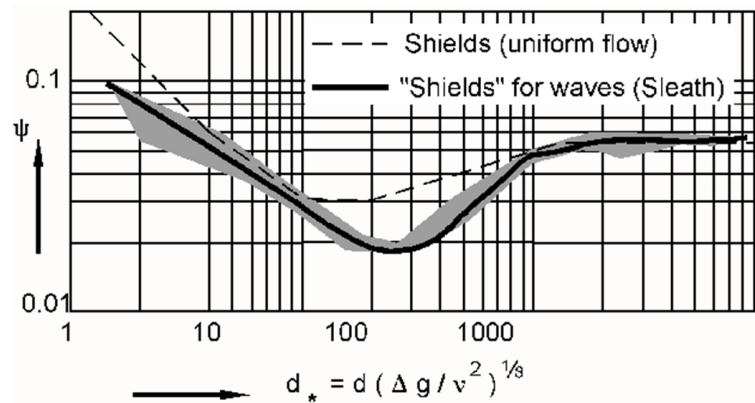


Figure 6 - Modified Shields-diagram for waves by Sleath (1978) (Schierack & Verhagen, 2012)

When making a comparison of the results of the oscillating flow of Sleath (1978) with the Shields-curve (steady flow), it seems to agree reasonably well. However, it is doubtful that for both cases the same amount of stones is in motion, because unstable stones should move less in oscillating flow due to a changing flow regime for the same stress. Therefore, the threshold in oscillating flow is probably assumed rather high compared to the threshold in steady flow. Another reason could be the influence of accelerations in oscillatory flows (in accelerating steady flow  $\Psi$  increases as  $\tau$  increases).

## 2.4 Stability of stones in breaking waves

Many researches have been executed to describe the stability of stones in breaking waves on a sloping bed. In this section an elaboration is given of their research.

### 2.4.1 Formula of Iribarren (1938) and formula of Hudson (1953)

Iribarren (1938) researched the stability of stones on breakwaters on slopes. He tried to add a slope correction factor to the formulas for stability in flow on a horizontal bed. Furthermore, he implemented the influence of breaking waves. The velocity in a breaking or broken wave on a slope is assumed to be proportional to the wave celerity in shallow water with the wave height as a representative measure for the water depth ( $u \propto \sqrt{gH}$ ). This gives relation (2.7).

$$\underbrace{\rho_w g H D_{50}^2}_{\text{load}} \propto \underbrace{(\rho_s - \rho_w) g D_{50}^3}_{\text{strength}} \cdot \underbrace{(\tan \phi \cos \alpha \pm \sin \alpha)}_{\text{slope factor}} \quad (2.7)$$

Iribarren (1938) proposed to raise all terms to the third power, so equation (2.7) can be written into equation (2.8) due to the relation of the mass of stone:  $M \propto \rho_s D_{50}^3$ .

$$M \propto \frac{\rho_s H^3}{\Delta^3 (\tan \phi \cos \alpha \pm \sin \alpha)^3} \quad (2.8)$$

Hudson (1953) presented a more general equation, derived from experimental data, for the weight of armor units necessary to ensure a stable rubble-mound breakwater. He proposed equation (2.9). In which  $K_D$  is an experimentally determined coefficient, dependent on the shape of the armor units.

$$M = \frac{\rho_s H^3}{K_D \Delta^3 \cos \alpha} \quad \text{or} \quad \frac{H}{\Delta D_{n50}} = \sqrt[3]{K_D \cos \alpha} \quad (2.9)$$

For relatively steep slopes, the formula of Hudson and Iribarren are very similar. However, for more gentle slopes the formula of Hudson (1953) does not hold, because the stability becomes infinitely large. Equation (2.9) is therefore only valid from slopes between 1:1.5 and 1:4. The most important limitations of the formula of Iribarren (1938) and Hudson (1953) are listed in Appendix A.8.

#### 2.4.2 Formula of Van der Meer (1988)

Van der Meer (1988) performed scaled model tests and used curve-fitting to come up with two design formulas to describe the static stability of stones on slopes (one formula for plunging breakers and one for surging breakers). Because these design formulas include more parameters than the formula of Hudson (1953), this was a step forward. The most governing parameters were tested with a certain range, presented in an overview in Appendix A.9. The design formula of Van der Meer (1988) for plunging breakers is given in equation (2.10).

$$\frac{H_s}{\Delta D_{n50}} = 6.2 \cdot P^{0.18} \cdot \left( \frac{S}{\sqrt{N}} \right)^{0.2} \cdot \xi_m^{-0.5} \quad (2.10)$$

In which:  $H_s/\Delta D_{n50}$  is a dimensionless stability parameter that describes both the load (significant wave height) on and strength (own weight) of the stone,  $H_s$  is the significant wave height (m),  $D_{n50}$  is the median nominal stone diameter (m) with  $D_{n50} = 0.85 D_{50}$ , according to Laan (1981),  $P$  is the notional permeability (-),  $N$  is the number of waves (-),  $S$  is damage level (-) ( $S = A_e/D_{n50}^2$  with  $A_e$  as the eroded area (m<sup>2</sup>)), and  $\xi_m$  is the Iribarren number related to the mean wave period (-).

The design formula of Van der Meer (1988) for surging breakers, the formula to determine the transition between plunging and surging breakers, and an elaboration on the above implemented parameters are given in Appendix A.10.

For recent projects in the Netherlands regarding rock protections on mild slopes, the design formula of Van der Meer (1988) for plunging breakers is the prescribed method to determine the static stability for stones on mild slopes under wave attack. The formula, applicable for slopes steeper than 1:6, is extrapolated towards more gentle slopes. The validity of this extrapolation has not been thoroughly investigated. It seems that the method of Van der Meer (1988) overestimates the required stone size for stones on mild slopes due to the change in wave breaking (plunging to spilling breakers). The XBeach-G results of Wit (2015) already confirmed this for homogeneous, statically stable structures (fully consisting of gravel) (see Figure 7 (left)).

Kramer (2016) performed physical scale model tests to research the applicability of the formula of Van der Meer (1988) to describe the static stability of stones for inhomogeneous structures. This research continues with the work of Kramer (2016) by trying to develop a design method for the static stability of stones on mild slopes under wave attack (which is more accurate than the formula of Van der Meer (1988)).

### 2.4.3 Research of Schiereck & Fontijn (1996)

Schiereck & Fontijn (1996) compared the experimental results (with slope ratios of 1:10 and 1:25) of Sijm (1993) and Ye (1996) with computational results and with the formula of Van der Meer (1988) to investigate the stability of stones on mild slopes. The computational results are obtained with the wave model ENDEC according to Rance & Warren (1968) and according to Jonsson (1966) & Sleath (1978). The formulas to compute the diameter of stones on slopes are given in Appendix A.11.

The experimental results and the formula of Van der Meer (1988) for plunging breakers are shown in Figure 7 (right). The trend of the experimental results is that the stability parameter  $H_s/\Delta d_{n50}$  increases for decreasing Iribarren number  $\xi$ . Furthermore, the stability of stones on mild slopes is larger than the stability determined with the extrapolated curve of Van der Meer (1988) (only validated for  $\xi > 1$ ), suggesting that the extrapolated formula of Van der Meer (1988) is conservative. As can be seen in Figure 7 (left), Wit (2015) confirms this suggestion.

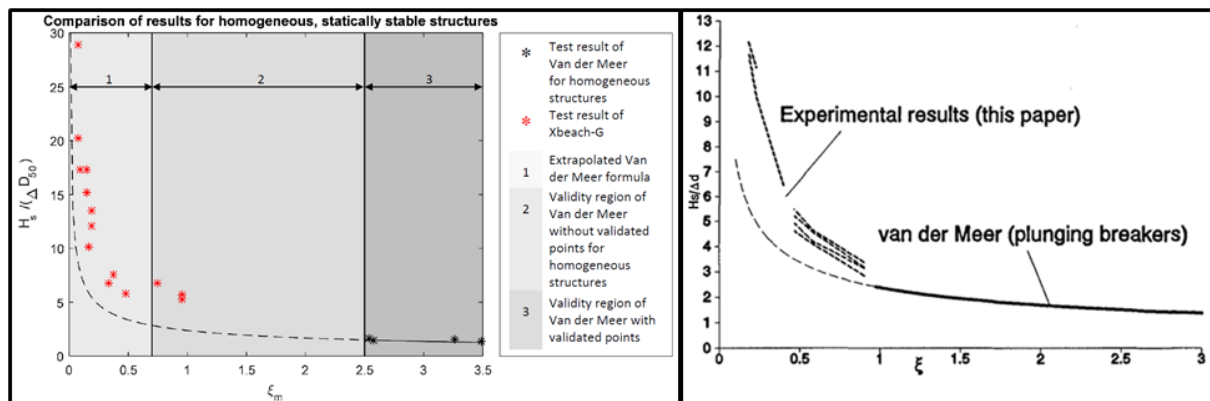


Figure 7 - Comparison of formula of Van der Meer (1988) for plunging breakers with XBeach-G results of Wit (2015) (left) and comparison with experimental results of Schiereck & Fontijn (1996) (right)

## 2.5 Sediment transport

Sediment transport can be divided in bed-load transport and suspended load transport. Bed-load transport can be described as sediment transport that is in close contact with the bed. The transport consists of gliding, jumping, rolling and saltating stones. Bed-load transport is dominated by drag forces (related to the horizontal velocity) and gravity forces acting on the stones. Suspended load transport is defined as the transport of (smaller) particles through the water column due to the irregular motion of the flow (related to turbulence) (Van Rijn, 1993).

In this research, the cross-shore sediment transport of stones is assumed to occur via bed-load transport. Suspended transport will not take place, because the settling velocity of gravel is assumed to be too high. The determination of the bed level change due to sediment transport is treated in Appendix A.12.

### 2.5.1 Threshold for initiation of motion

The Shields parameter, presented in equation (2.11), is included in the bed-load formulas of Nielsen (2006) and Van Rijn (2007) to define a threshold for the initiation of motion. The approach of Shields (1936) is elaborated in Section 2.3.2. Because the acceleration is included,  $\theta$  is called the adapted Shields parameter.

$$\theta = \frac{\tau_b}{(\rho_s - \rho_w)gD_{50}} = \frac{u_*^2}{\Delta gD_{50}} \quad (2.11)$$

**Note:** the (adapted) Shields parameter is a **stability parameter** when a certain critical value of the bed shear stress or the bed shear velocity is used to define a threshold for initiation of motion of stones. When the actual bed shear stress or the actual bed shear velocity is used, the (adapted)

Shields parameter is a **mobility parameter**. The stability parameter can also be called the critical mobility parameter, because movements of stones occur when the mobility parameter exceeds the stability parameter (i.e. threshold with a certain critical value of the mobility parameter).

To account for bed slope effects on the sediment transport, equation (2.11) is modified into the effective, adapted Shields parameter  $\theta'$  in equation (2.12), according to Fredsøe & Deigaard (1992).

$$\theta' = \theta \cos \beta \left( 1 \pm \frac{\tan \beta}{\tan \phi} \right) \quad (2.12)$$

In which:  $\beta$  is the angle of the bed (°) and  $\phi$  is the internal angle of repose (°). When these angles are equal to each other, the stone is brought into motion by any load (Schierack & Verhagen, 2012). A steeper profile has a larger slope effect than a profile with a milder slope.

### 2.5.2 Sediment transport caused by accelerations

Both approaches of Nielsen (2006) and Van Rijn (2007) have a term to account for sediment transport caused by acceleration due to wave asymmetry. Waves become asymmetric when they approach the shore. Due to this change in wave shape, wave energy gets compressed and the wave crest increases until it breaks on the slope. The cross-shore sediment transport due to the mean current/undertow, (horizontal wave) skewness and bound long waves is treated in Appendix A.13.

In case of vertical wave asymmetry, no sediment transport seems to occur as the free stream velocity is not skewed. However, a net sediment transport does occur and is generated by significant acceleration skewness (Nielsen, 2002). This acceleration skewness is explained in Appendix A.13.

### 2.5.3 Sediment transport caused by bed shear stress

The bed shear stress  $\tau_b$ , presented in equation (2.13), is used by McCall (2015) to determine the effective, adapted Shields parameter (equation (2.12)). The bed shear stress is created by currents and waves and functions as the driving force in equation (2.18). In equation (2.13), the drag term is the bed shear stress due to currents (with the velocity is included) and the inertia term is the bed shear stress due to waves. The inertia term has been added by McCall (2015) as an additional term to the bed shear stress due to drag to include the influence of accelerations (cf. (Morison et al., 1950; Puleo et al., 2003)).

$$\tau_b = \underbrace{c_f \rho u |u|}_{\text{drag}} + \underbrace{\rho c_m c_v c_n D_{50} \frac{\partial u}{\partial t}}_{\text{inertia}} \quad (2.13)$$

In which:  $c_f$  is the dimensionless friction factor (-),  $c_m$  is an inertia coefficient ( $c_m = 1 + c_a$ ) with the added mass coefficient  $c_a$  ( $= 0.5$  for spheres with zero autonomous acceleration),  $c_v$  is the volume shape factor ( $c_v = \pi/6$  for spheres), and  $c_n$  is a coefficient for the number of particles on the surface influenced by accelerations per unit of area. These coefficients can be replaced by one calibration coefficient for inertia  $c_i = c_m c_v c_n \approx O(1)$  (McCall, 2015).

The dimensionless friction factor in the drag term and the coefficients in the inertia term of the bed shear stress are worked out in more detail in Appendix A.14.

In this research, the bed shear stress, described in equation (2.13), is applied in XBeach-G to model the sediment transport with the bed-load transport formula of Van Rijn (2007) (McCall, 2015). Originally, the formula of Van Rijn (2007) uses the bed shear stress  $\tau'_{b,cw}$ , which is only determined with the velocity and not with an inertia term (see elaboration in Appendix A.17).

Furthermore, the bed shear stress is used in the second part of this research to determine the effective, adapted Shields parameter regarding initiation of motion of stones.

#### 2.5.4 Formula of Nielsen (2006)

Sediment transport due to acceleration skewness, described in Section 2.5.2, is included in the sediment transport by Nielsen (2002), using a sediment friction factor  $f_s$  and a phase lag angle  $\varphi_\tau$  to determine the bed shear stress (equation (A.40)) for a certain free stream velocity  $u_\infty(t)$ .

The effective, adapted Shields parameter (equation (2.12)) can be determined with the sediment mobilizing velocity  $u_\theta(t)$  (i.e. the bed shear velocity), given by equation (2.14) (Nielsen, 2002).

$$u_\theta(t) = \sqrt{\frac{f_s}{2}} \left( \underbrace{\cos \varphi_\tau u_\infty}_{\text{velocity}} + \underbrace{\frac{T_{m-1.0}}{2\pi} \sin \varphi_\tau \frac{\partial u_\infty}{\partial t}}_{\text{acceleration}} \right) \quad (2.14)$$

In which:  $u_\theta(t)$  is a sediment mobilizing velocity,  $\varphi_\tau$  is the phase lag angle between the wave induced current and the period of the bed shear velocity ( $\varphi_\tau = 35-40^\circ$ ),  $f_s$  is the sediment friction factor (-) (for which a standard value of 0.025 is taken in XBeach-G) and  $T_{m-1.0}$  is the spectral mean period (s).

The influence of the phase lag angle and the sediment friction factor on the accuracy of the formula of Nielsen (2006) is significant. An elaboration of these two parameters is given in Appendix A.15.

The bed-load transport formula of Nielsen (2006) to compute the sediment transport is given in equation (2.15). The instantaneous sediment transport rate is determined with a modification of the formula of Meyer-Peter & Müller (1948) (Nielsen, 2006). The effective, adapted Shields parameter, given in equation (2.12), is included in equation (2.15) as a mobility parameter, using a value of 0.05 as the stability parameter (i.e. to define a threshold for initiation of motion of stones).

$$q_s(t) = 12[\theta'(t) - 0.05] \sqrt{\theta'(t)} \sqrt{\Delta g D_{50}^3} \frac{u_\theta(t)}{|u_\theta(t)|} \quad (2.15)$$

In this research, the bed-load transport formula of Nielsen (2006) is used to model the sediment transport of the simulations executed in XBeach-G.

#### 2.5.5 Formula of Van Rijn (1984) for currents

The bed-load transport formula of Van Rijn (1984) for currents only is presented in equation (2.16) (for particles in the range of 200 to 2,000  $\mu\text{m}$ ).

$$q_b = 0.053 \sqrt{\Delta g D_{50}^3} \frac{T^{2.1}}{D_*^{0.3}} \quad (2.16)$$

Van Rijn derived this formula by means of the saltation height  $\delta_b/D$ , the particle velocity  $u_b$  and the bed-load concentration  $c_b$  (Van Rijn, 1984). Furthermore, he used a dimensionless particle parameter  $D_*$  and a transport stage parameter  $T$  to describe the bed-load transport rate. The parameters are elaborated in Appendix A.16.

### 2.5.6 Formula of Van Rijn (2007) for currents and waves

The bed-load transport formula of Van Rijn (2007) for currents and waves is given in equation (2.17). The sediment transport is determined by means of the bed shear stress due to currents and waves.

$$q_b = \gamma \rho_s f_{silt} D_{50} D_*^{-0.3} \sqrt{\frac{\tau'_{b,cw}}{\rho}} \left[ \frac{(\tau'_{b,cw} - \tau_{b,cr})}{\tau_{b,cr}} \right]^\eta \quad (2.17)$$

In which:  $q_b$  is the volumetric bed-load transport rate (excluding pore space) (kg/s/m),  $\gamma$  is a calibration coefficient ( $\gamma = 0.5$  according to Van Rijn (2007)),  $D_*$  is the non-dimensional particle diameter, and for gravel beaches, both  $f_{silt}$  and  $\eta$  have a value of 1.  $\tau_{b,cr}$  is the critical bed-shear stress according to Shields (1936) and  $\tau'_{b,cw}$  is the instantaneous grain-related bed-shear stress due to currents and waves and can be determined with the friction related to currents  $f'_c$  (based on the Darcy-Weisbach approach (Van Rijn, 2007)) and the friction caused by waves  $f'_w$  (according to Swart (1974) (Saers, 2005)). The parameters of  $\tau'_{b,cw}$  are worked out in Appendix A.17.  $\tau'_{b,cw}$  is only determined with the velocity and an inertia term is not included.

In XBeach-G, the modified formula of Van Rijn (2007) is given by equation (2.18) (McCall, 2015). As can be seen in equation (2.18), McCall (2016) included the effective, adapted Shields parameter, given in equation (2.12), as a mobility parameter. The bed shear stress  $\tau_b$  in equation (2.18) is worked out in Section 2.5.3 and consists of a drag term and an inertia term.

$$q_b = \gamma D_{50} D_*^{-0.3} \sqrt{\frac{\tau_b}{\rho}} \frac{\theta' - \theta_{cr}}{\theta_{cr}} \frac{\tau_b}{|\tau_b|} \quad (2.18)$$

In which:  $\theta_{cr}$  is used as the stability parameter to define a threshold for initiation of motion of stones.  $\theta_{cr}$  can be determined with equation (2.19) (Soulsby & Whitehouse, 1997).

$$\theta_{cr} = \frac{0.30}{1 + 1.2D_*} + 0.055 (1 - e^{-0.020D_*}) \quad (2.19)$$

McCall (2015) recommends applying the formula of Van Rijn (2007) in XBeach-G, because the predictive skill of XBeach-G is greater than when applying other (examined) bed-load transport equations.

A simplified formula of Van Rijn (2007) to compute bed-load transport for steady flow (with or without waves) is derived using the detailed, numerical intra-wave TR2004 model (Van Rijn, 2007). The simplified bed-load transport formula of Van Rijn (2007) is presented in Appendix A.18.

## 2.6 Damage characteristics

### 2.6.1 Quantitative damage descriptions

The damage of a rock protection on a slope under wave attack is shown in Figure 8. The damage can be described by looking at profile change, which is the difference between the initial profile and the (post) erosion profile. The erosion area  $A_e$  (m<sup>2</sup>), the cover depth  $d_c$  (m), the erosion depth  $d_e$  (m) and the erosion length  $l_e$  (m) are parameters that can be determined and used for a damage description.

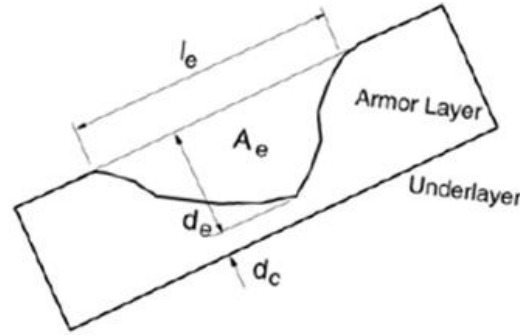


Figure 8 - Damage of a rock protection with erosion parameters  $A_e$ ,  $d_c$ ,  $d_e$  and  $l_e$  (Melby & Kobayashi, 1998)

The damage level  $S$  of Van der Meer (1988) is defined as the erosion area divided by the square of the mean nominal diameter of the stone, see equation (2.20) (see also Figure 24 in Appendix A.10). Static stability is described by a damage level  $S$  of 2, but higher values are acceptable for milder slopes (Van der Meer, 1988). A damage level  $S$  of 10 is often used to describe failure (Schierneck & Verhagen, 2012).

$$S = \frac{A_e}{D_{n50}^2} \quad (2.20)$$

The distribution of the erosion area is not defined in this damage description, so the same value of  $S$  is found for an erosion area with a relatively large  $l_e$  and a small  $d_e$ , and an erosion area with a relatively small  $l_e$  and a large  $d_e$ . In case of a rock protection with smaller stones (with the size of gravel) on a mild slope, a damage description based on the erosion depth  $d_e$  seems to be a better way to indicate the damage (Melby & Kobayashi, 1998). Therefore, the relative erosion depth  $d_e/D_{n50}$  and the damage depth  $E_3$  are also determined when examining the damage of the modelled erosion profiles in this research.

The damage depth  $E_3$  is defined as the erosion depth, averaged in a circle with a diameter of three times  $D_{n50}$ , divided by the mean nominal diameter of the stone (Hofland et al., 2011), see equation (2.21).

$$E_3 = \frac{\langle d_e \rangle_{3D_{n50}}}{D_{n50}} \quad (2.21)$$

For a rock protection with a layer thickness of  $2D_{n50}$ , the damage is classified in three degrees in Table 2, according to Hofland et al. (2011).

Table 2 - Damage classification of  $E_3$  for rock protection with layer thickness of  $2D_{n50}$  (Hofland et al., 2011)

$E_3$ (-)	Degree
0.2 - 0.3	Initial damage
0.5 - 0.6	Intermediate damage
1.5 - 1.6	Failure

## 2.6.2 Profile development

The damage of the modelled erosion profiles can also be analyzed qualitatively. By visual comparison, the type of profile development of the modelled erosion profile can be determined. The profile can develop into a bar profile or a crest profile. Both types are schematized in Figure 9.

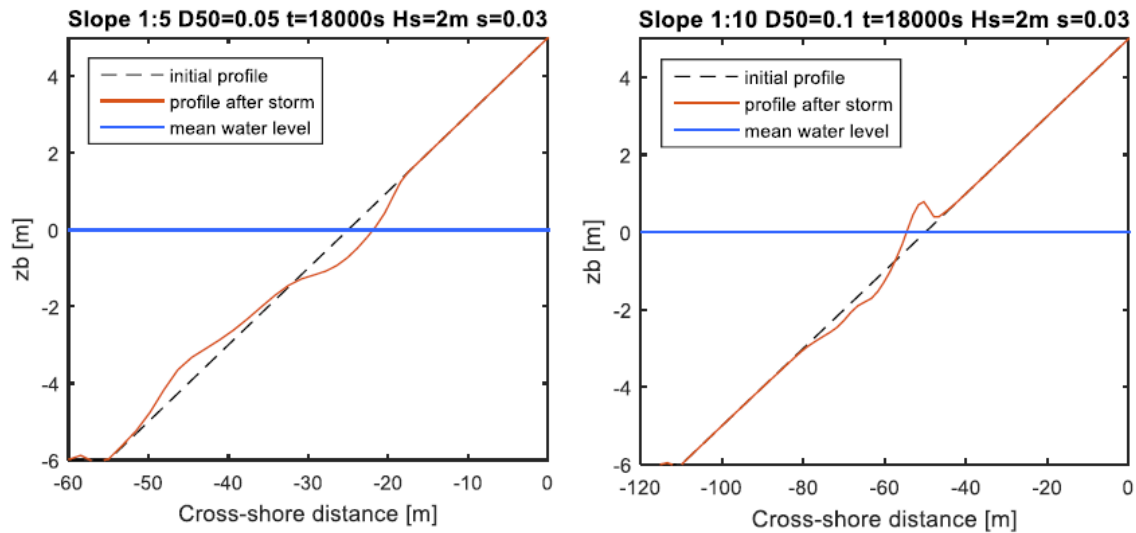


Figure 9 - XBeach-G results with submerged bar profile (left) and crest profile (right) (Wit, 2015)

A submerged bar profile is formed when material is transported downslope. An erosion hole, located around still water level, is created above the bar. A crest profile is formed when material is transported upslope. The crest is located around still water level. An erosion hole is created at the foot of the crest. According to Wit (2015), the stone diameter and the slope angle are the main parameters that influence the type of profile development (for homogeneous structures).

### 3 Verification of previous physical scale model tests

The research is divided into two parts, as explained in the scope of the research (see Section 1.4). The first part is about reproducing the profile change experiments of Kramer (2016) for 1:5, 1:10 and 1:15 slope with the bed-load transport formulas of Nielsen (2006) and Van Rijn (2007) using the numerical model XBeach-G. The analysis of this part is treated in Section 3.1, and elaborates briefly on the numerical model XBeach-G. Section 3.2 covers the verification of the BIV analysis of the videos of the BIV experiments of Kramer (2016) regarding initiation of motion of stones. An endeavor is made to link the two parts investigated in this research. This is elaborated in Section 3.3.

#### 3.1 XBeach-G | Reproduce profile change experiments of Kramer (2016)

For a comprehensive explanation of the execution of the profile change experiments and the analysis of the test results by Kramer (2016) is referred to Appendix A.2.2 and Appendix B.1 of the report of Kramer (2016). A schematization of the test set up for the profile change experiments is shown in Figure 27 in Appendix B.1.

##### 3.1.1 XBeach-G | Input parameters

The erosion profiles of the profile change experiments of Kramer (2016) were obtained for two different wave characteristics per slope. The input of the wave characteristics has also been used to model the erosion profiles with the bed-load transport formulas of Nielsen (2006) and Van Rijn (2007), using XBeach-G. The constant parameters that were used in the experiments of Kramer (2016) and the simulations executed in this research are given in Table 3.

Table 3 - Constant input parameters profile change experiments of Kramer (2016) and XBeach-G simulations

Parameter		Unit	Value	
Gravitational acceleration	g	m/s <sup>2</sup>	9.81	Assumed
Density of stone	$\rho_s$	kg/m <sup>3</sup>	2,685	Measured by Kramer (2016)
Density of water	$\rho_w$	kg/m <sup>3</sup>	1,000	Assumed
Relative density	$\Delta$	-	1.685	Determined
Mean nominal diameter of stone	$D_{n50}$	m	0.0162	Measured by Kramer (2016)
Internal angle of repose	$\phi$	°	40	Assumed
Water depth	h	m	0.65	Measured by Kramer (2016)
Number of waves	N	-	3,000	Chosen
Wave steepness	s	-	0.04	Chosen
Wave spectrum	-	-	JONSWAP	Assumed
Notional permeability	P	-	0.1	Assumed
Darcy-flow permeability coefficient	$k_x$	m/s	0.0995	Measured by Kramer (2016)

The two wave characteristics per slope are based on the (theoretical) damage levels  $S_{norm}$ ,  $S_{Wit}$ , and  $S_{S\&F}$ . The input parameters of the two wave characteristics per slope are given in Table 4. The input for one of the wave characteristics for the 1:5 slope is based on  $S_{norm}$  with an acceptable damage of 2.00. The input for  $S_{Wit}$  is based on higher acceptable damage levels for milder slopes (Van der Meer, 1988; Wit, 2015). The input for  $S_{S\&F}$  is derived from the research of Schiereck & Fontijn (1996), using the stability parameter  $H_s/\Delta D_{n50}$  (Kramer, 2016).

The value of the Iribarren number per slope will not change, because Kramer (2016) kept the wave steepness constant. Thus, the type of wave breaking is the same per slope. In this way, Kramer (2016) could compare the results of the profile change experiments of the two wave characteristics with each other (for example, comparing the results of the 1:5 slope with  $S_{Wit}$  input with the results of the 1:5 slope with  $S_{norm}$  input). A comparison of results with different slope angles is not correct, because the type of wave breaking is not the same (as the Iribarren number is not constant).

**Table 4 - Variable input parameters of two wave characteristics, per slope**

<b>Slope</b>	<b><math>S_{norm}</math> (-)</b>	<b><math>T_m</math> (s)</b>	<b><math>T_{m-1,0}</math> (s)</b>	<b><math>H_{m0}</math> (m)</b>	<b><math>\xi_m</math> (-)</b>	<b><math>t_{model}</math> (s)</b>
1:5	2.00	0.96	1.02	0.054	1.00	3,066

<b>Slope</b>	<b><math>S_{Wit}</math> (-)</b>	<b><math>T_m</math> (s)</b>	<b><math>T_{m-1,0}</math> (s)</b>	<b><math>H_{m0}</math> (m)</b>	<b><math>\xi_m</math> (-)</b>	<b><math>t_{model}</math> (s)</b>
1:5	3.00	0.96	1.05	0.058	1.00	3,159
1:10	5.91	1.27	1.34	0.094	0.50	4,023
1:15	8.84	1.46	1.56	0.125	0.33	4,677

<b>Slope</b>	<b><math>H_s/\Delta D_{n50}</math> (-)</b>	<b><math>T_m</math> (s)</b>	<b><math>T_{m-1,0}</math> (s)</b>	<b><math>H_{m0}</math> (m)</b>	<b><math>\xi_m</math> (-)</b>	<b><math>t_{model}</math> (s)</b>
1:10	5.00	1.47	1.56	0.129	0.50	4,686
1:15	8.00	1.79	1.94	0.173	0.33	5,826

In which:  $T_m$  is the mean wave period from the time signal (s),  $T_{m-1,0}$  is the spectral mean wave period, measured at the wave gauge in front of the toe of the slope (see Figure 27 in Appendix B.1) (s),  $H_{m0}$  is the significant wave height (m),  $\xi_m$  is the Iribarren number related to the mean wave period (-), and  $t_{model}$  is the model time to run a simulation.

### 3.1.2 XBeach-G | Initial and post profile of profile change experiments of Kramer (2016)

Kramer (2016) obtained the data of the profile change experiments by measuring the 3D profile with a laser scanner (Leica C10) before and after execution of the experiment. The profile measured before the execution of the experiment of is called the initial profile. The preparation of the initial profile slope in the wave flume is shown in Figure 28 (left & middle) in Appendix B.1. The obtained slope after the experiment is named the post profile. Both initial profile and post profile have been determined in 2D by averaging the profile change over the width of the flume. The damage characteristics have been derived from the difference between the averaged profiles (in 2D).

In this research, the initial profiles are used as the bathymetry input for the simulations with XBeach-G. Furthermore, the measured post profiles and the damage characteristics of the experiments of Kramer (2016) are compared with the results from the simulations in XBeach-G, consisting of the modelled erosion profiles and corresponding damage characteristics.

For the 1:15 slope of the profile change experiments of Kramer (2016), the sediment transport is restricted by the upslope boundary when running XBeach-G simulations with the original length of the initial profile. The boundary restricted erosion profile for 1:15 slope with  $S_{Wit}$  input, modelled with the bed-load transport formula of Nielsen (2006) with standard values, is shown in Figure 29 in Appendix B.2. The right boundary restricts the sediment transport. Therefore, the original length of the 1:15 slope of the profile change experiments of Kramer (2016) is extended in upslope direction to overcome this problem.

### 3.1.3 XBeach-G | Numerical model XBeach-G

The numerical model XBeach-G is a branch of the main XBeach model, developed by McCall (2015). XBeach-G is a process-based model that simulates storm impacts on gravel beaches (with slopes in the order of 1:5 and 1:10 and gravel with diameters between 0.01 m and 0.08 m). These diameters are in the range of stones used as a rock protection on mild slopes under wave attack. This is the reason why both Wit (2015) and Postma (2016) (each with different objectives) used the numerical model XBeach-G as a tool to model the stability of stones on mild slopes under wave attack.

XBeach-G is used as a tool in this research to reproduce the profile change experiments of Kramer (2016) (executed with stones with a  $D_{n50}$  of 0.0162 m). The conclusions drawn by Postma (2016) regarding the sediment transport modelled with XBeach-G can be validated/falsified.

XBeach-G describes the depth-averaged flow of the surface water due to currents and waves with the non-linear shallow water equations (NLSWE) in which a non-hydrostatic pressure term is included to model short waves (see elaboration in Appendix A.1). XBeach-G applies the non-hydrostatic extension to the XBeach model (i.e.  $nonh = 1$ ) to solve wave-by-wave flow and surface elevation variations due to short waves in intermediate and shallow water depths. The groundwater dynamics and the surface water-groundwater exchange are included in XBeach-G with the XBeach groundwater model (i.e.  $gwflow = 1$ ). In this way, XBeach-G takes into account the interaction between the surface water and the groundwater, of which the sediment transport on gravel beaches is strongly dependent (see elaboration in Appendix A.3). For the cross-shore sediment transport (i.e. longshore uniformity, as XBeach-G is a 1D model), bed-load transport formulas have been included to simulate the sediment transport of gravel during storms. (McCall, 2015)

An extensive elaboration on the model XBeach-G is given in Chapter 4 of the report of Postma (2016), in which he describes the modelling of the hydrodynamics and morphodynamics, and the validation and the limitations of the model. The research of McCall (2015) regarding the model XBeach-G is described in his PhD thesis '*Process-based modelling of storm impacts on gravel coasts*'.

For the simulations, the 2015 release of the numerical model XBeach-G is used (which is the same version Postma (2016) used to run simulations in XBeach-G for his research).

The model input, which needs to be determined for each simulation, is listed below. The constant and variable input parameters, given in Section 3.1.1, are also part of the model input. An overview of all simulations performed with the numerical model XBeach-G is given in Table 14.

- The bathymetry of the model needs to be determined. The bathymetry is based on the initial profile of the profile change experiments of Kramer (2016) averaged over the width (see Section 3.1.2). The grid size  $\Delta x$  remains constant and has a value of 0.05 m. The length and the height of the slope is test dependent.
- The simulations are executed with a layer of stones with a layer thickness of two times  $D_{n50}$  to represent the rock protection on an impermeable sandy core. The impermeable layer is implemented in XBeach-G as an aquifer layer, which can be modelled with the code 'aquiferbotfile = zandlaag.dep' with a text file (called zandlaag.dep) that contains the y-coordinates with the values for the depth of the impermeable layer. Postma (2016) also applied the impermeable layer in this way. Although, no validation of the method is found in literature.
- The bed-load transport formula that models the sediment transport in XBeach-G needs to be determined, see below.

### 3.1.4 XBeach-G | Bed-load transport formulas in XBeach-G

The bed-load transport formulas, which are used to model the erosion profiles for a certain slope and wave characteristics, are listed below. Postma (2016) researched the formula of Nielsen (2006) for standard values and Van Rijn (2007) in XBeach-G (see elaboration of formulas in Section 2.5).

- Bed-load transport formula of Nielsen (2006) with standard values for  $f_s$  and  $\varphi_\tau$ .
- Bed-load transport formula of Nielsen (2006) with test values for  $f_s$  and  $\varphi_\tau$ , derived from the BIV experiments of Kramer (2016).
- Bed-load transport formula of Van Rijn (2007).

Two other sediment transport formulas (i.e. Soulsby (1997) & Van Rijn (1985), and Van Thiel (2009) & Van Rijn (2007)) could also be used in XBeach-G to model the sediment transport (McCall, 2015). In a first stage of this research regarding the stability of stones (with a size of gravel) on mild slopes is decided to focus only on the bed-load transport formulas of Nielsen (2006) and Van Rijn (2007), listed as bullet points above.

When modelling with the bed-load transport formula of Nielsen (2006) in XBeach-G, the user needs to define the sediment friction factor  $f_s$  and the phase lag angle  $\varphi_\tau$ . The magnitude and direction of the predicted sediment transport is strongly dependent on both parameters, and calibration is necessary. The sensitivity of XBeach-G using the formula of Nielsen (2006) to the sediment friction factor  $f_s$  and the phase lag angle  $\varphi_\tau$  is investigated by McCall (2015). The standard values are  $f_s = 0.025$  and  $\varphi_\tau = 25^\circ$  (McCall, 2015). The test values, derived from the BIV experiments, are shown in Table 5 per slope. The difference between the standard values and test derived values of the sediment friction factor  $f_s$  and the phase lag angle  $\varphi_\tau$  is large and will affect the results.

**Table 5 - Sediment friction factor and phase lag angle (test values) derived from BIV experiments, per slope**

Slope	$f_s$ (-)	$\varphi_\tau$ (°)
1:5	0.3611	72.8
1:10	0.2091	65.0
1:15	0.2914	69.6

No user-defined parameters are included in the bed-load transport formula of Van Rijn (2007).

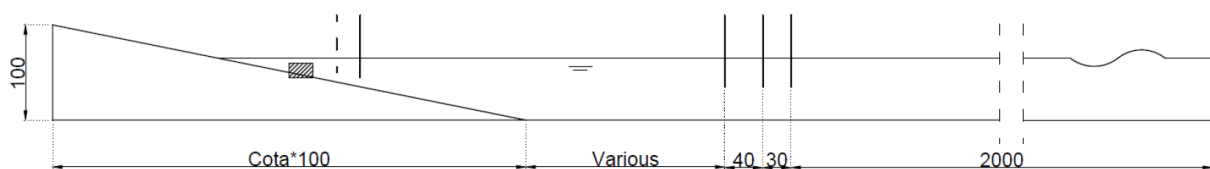
### 3.1.5 XBeach-G | Output parameters and analyzation of process

The result of an XBeach-G simulation is a modelled erosion profile, which is based on the model input parameters specified in the previous sections. This erosion profile can be used to derive the erosion area  $A_e$ , damage level  $S$ , relative erosion depth  $d_e/D_{n50}$  and the damage depth  $E_3$  (see elaboration in Section 2.6.1). The modelled erosion profiles can be compared qualitatively with the post profiles of experiments of Kramer (2016). The comparison includes an analysis of the magnitude of the sediment transport, which is incorporated in the damage characteristics.

## 3.2 BIV | Initiation of motion of stones based on BIV analysis

### 3.2.1 BIV | BIV experiments of Kramer (2016)

The BIV experiments of Kramer (2016) consist of regular waves breaking on a certain slope. The test set up is schematized in Figure 10. A camera (type 'DFK 23GP031') makes videos of the Field of View (FOV), which can be explained as the focus region where the waves are breaking and movement of stones occurs (based on the damage zone of the profile change experiments of Kramer (2016) in combination with visual observations of the location of movement of stones (Kramer, 2016)).



**Figure 10 - Test set up for BIV experiments of Kramer (2016) (length in cm) (Kramer, 2016)**

In which: the Field of View (FOV) is indicated by the black striped box on the slope, the bold lines are wave gauges. The length of the slope on the left is dependent on the slope angle (i.e. the same slope ratio (1:5, 1:10 and 1:15) is used with the profile change experiments). A wave board on the right generates the regular waves.

Kramer (2016) started filming the BIV experiments after the first couple of waves had broken on the slope, so the wave height of the waves had become constant and the BIV experiments were executed with regular waves. Furthermore, this gave the stones some time to settle (Kramer, 2016).

The preparation of the stone layer with a layer thickness of  $2D_{n50}$  is done in the same way as was done with the profile change experiments (see Figure 28 (left & middle) in Appendix B.1). For the BIV experiments, the stones located in the FOV are colored black, so they do not reflect the beam of light created by two 50W LED lights. The beam of light limits a Depth of Field (DOF), which is located in the FOV, so only the bubbles and particles in the DOF are visible.

The slope with black stones in the FOV (left) and the setup of the LED lights (right) are shown in Figure 30 in Appendix B.3. The DOF and FOV are schematized in Figure 11.

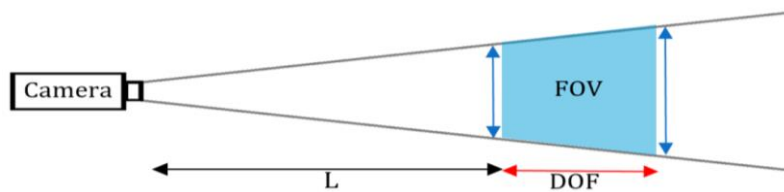


Figure 11 - Schematization of DOF and FOV (Kramer, 2016)

In which:  $L$  is the distance between the camera and the FOV and has a length of 80 cm, the Depth of Field (DOF) is 4.5 cm, and the FOV is approximately 12 cm x 9 cm. Because 2D images are obtained with the camera, the location where the particle moves (in front or in the back of the FOV) is not known. This causes an error of 2.8%, see equation (3.1) (Kramer, 2016).

$$error = \frac{0.5DOF}{L} * 100\% = \frac{0.5 * 4.5}{80} * 100\% = 2.8\% \quad (3.1)$$

The black colored stones in the DOF are glued on a strip (with a width of  $2D_{n50}$ ), so their movements through the FOV are limited and only the black colored stones that are placed around the strip of glued stones are allowed to move. Kramer (2016) thought that the restriction of the movement of stones in the DOF would lead to more accurate measurements of the velocities around the stones with Bubble Image Velocimetry (BIV). Therefore, only the movements of stones, which are located in the FOV around the strip of glued stones, can be examined in this research.

During the profile change experiments of Kramer (2016) significant movements of stones were observed (visually) under the highest (irregular) waves of the spectrum for each slope. The wave characteristics of the regular waves used for the BIV experiments are based on the highest one percent waves of the spectrum used for the profile change experiments (see Section 3.2.2). Therefore, Kramer (2016) assumed that significant movements of stones should also be present during the BIV experiments in case the stones were not glued on a strip (Kramer, 2016). Furthermore, from videos of the preparation of the BIV experiments of Kramer (2016) with regular waves could be observed that frequent movements of stones occur at many locations over the width of the flume.

For an extensive elaboration on the execution of the BIV experiments by Kramer (2016) is referred to Section 3.2.2, Section 3.3.2 and Appendix A.2.3 of the report of Kramer (2016).

In this research, the videos of the BIV experiments of Kramer (2016) are used to derive the velocities and accelerations close to the bottom using Bubble Image Velocimetry (BIV). The hydrodynamic forces (and corresponding mobility parameters) that initiate the movement of stones can be determined with these velocities and accelerations.

For the 1:5, 1:10 and 1:15 slope (and wave characteristics of Table 7), the significant movements of stones in the videos of the profile change experiments and the videos of the preparation of the BIV experiments of Kramer (2016) are observed. Rocking of many stones and displacements of some stones occur at several locations. These movements of stones in the videos of the experiments executed with 1:5 and 1:10 slopes seem to agree with transport stage 3 (described as: frequent movement at several locations) of Breusers & Schukking (1971). Transport stage 3 relates to a Shields number of 0.04. For the videos with 1:15 slopes, rocking of some stones (and sometimes displacements) occurs. This can be described as occasional movements of stones at some locations, and corresponds to transport stage 1 with a Shields number of 0.03. Both values are taken into account per slope when examining the mobility parameters derived from the BIV analyzed videos.

The values of the Shields parameters (determined above) are checked by looking at four videos of flume experiments (executed with uniform flow) regarding the movements of stones. For a constant water depth of 0.20 m and a certain set averaged velocity (of 0.60 m/s, 0.70 m/s, 0.90 m/s and 0.97 m/s respectively), the movements of stones during the experiment are related by means of visual observations to a Shields number (with a value of 0.03, 0.04, 0.055 and 0.07 respectively). The videos are obtained from the course CIE4310 Bed, Bank and Shore Protection, TU Delft (tab: Documents/video/Video3/Shields number).

### 3.2.2 BIV | Input parameters

The constant parameters that are used in the BIV experiments of Kramer (2016) are given in Table 6.

Table 6 - Constant input parameters used in BIV experiments of Kramer (2016)

Parameter		Unit	Value	
Gravitational acceleration	g	m/s <sup>2</sup>	9.81	Assumed
Density of stone	$\rho_s$	kg/m <sup>3</sup>	2,685	Measured by Kramer (2016)
Density of water	$\rho_w$	kg/m <sup>3</sup>	1,000	Assumed
Relative density	$\Delta$	-	1.685	Determined
Mean diameter of stone	$D_{50}$	m	0.0192	Measured by Kramer (2016)
Internal angle of repose	$\phi$	°	40	Assumed
Water depth	h	m	0.65	Measured by Kramer (2016)
Wave steepness	s	-	0.04	Chosen
Notional permeability	P	-	0.1	Assumed

The wave characteristics of the BIV experiments of Kramer (2016), given in Table 7, are based on the highest one percent (irregular) waves ( $H_{1\%}$ ) of the  $S_{wit}$  input of the profile change experiments of Kramer (2016). The choice to use  $H_{1\%}$  is because these waves generate the highest velocities and accelerations, which induce the largest forces on the bed that could cause initiation of motion of stones. The JONSWAP wave spectrum is assumed to be a Rayleigh distributed, so the significant wave height of the BIV experiments can be determined with equation (3.2).

$$H_{m0,BIV} = H_{1\%,profile} = 1.5H_{m0,profile} \quad (3.2)$$

Table 7 - Wave characteristics of BIV experiments of Kramer (2016), per slope

Slope	$T_{m-1,0}$ (s)	$H_{m0}$ (m)	$\xi_m$ (-)
1:5	1.22	0.088	1.00
1:10	1.55	0.146	0.50
1:15	1.79	0.187	0.33

The BIV experiments of Kramer (2016) are executed with regular waves. This gives a high repeatability of the experiments, because each time the same wave is generated. For regular waves, the spectral mean wave period  $T_{m-1,0}$  is assumed to be equal to the mean wave period  $T_m$ .

### 3.2.3 BIV | Analysis of videos of BIV experiments of Kramer (2016)

The videos of the BIV experiments of Kramer (2016), presented in Table 8, are analyzed in this research. The number of regular waves breaking in the video can be determined with the length of the video and the wave period (see Table 7).

**Table 8 - Analyzed videos of BIV experiments of Kramer (2016), per slope**

<b>Slope</b>	<b>Video</b>	<b><math>t_{\text{video}}</math> (s)</b>	<b><math>N_{\text{frames}}</math> (-)</b>	<b><math>N_{\text{waves}}</math> (-)</b>
1:5	05_BIV_0001	7.09	937	6
1:10	10_BIV_0003	4.71	623	3
1:15	15_BIV_0005	8.96	1183	5

For each video is determined by means of visual observation if and when movements of one or more stones occur. Furthermore, the type and the direction of the movement of the stones are determined. Two definitions to describe the movement of stones are used: rocking and displacement. The rocking of a stone can be described as vibrating, tilting or overturning of a stone at the same location. The displacement of a stone is defined as the movement of a stone (by gliding, jumping, rolling or saltating) from its original location to another location. The direction of the movement can be upslope or downslope directed. The methodology of the visual analysis of the movements of stones is treated in Appendix B.4, using the frames of video 05\_BIV\_0001. With the results of the visual analysis, the horizontal velocity and acceleration can be determined at the specific moment in time when the stone starts to move (i.e. initiation of motion of stone).

After the visual observations, the videos are analyzed with Bubble Image Velocimetry (BIV) to derive the velocities and accelerations close to the bottom. BIV can be seen as a complementary velocity measurement tool for Particle Image Velocimetry (PIV), because the flow velocity can accurately be determined in both the highly aerated flow with bubbles caused by waves and the non-aerated return flow (in case of plunging breakers) (Ryu et al., 2005). Kramer (2016) added particles with a size of 0.1 mm (= 25% of pixel size) to the water, because no or little bubbles were present in the FOV during return flow. In this way, he improved the color change per pixel and was able to derive the flow velocity more accurately due to the tracking of both bubbles and particles (Kramer, 2016).

The camera used to make videos of the BIV experiments of Kramer (2016) is of the type 'DFK 23GP031'. For a set resolution of 720 pixels x 480 pixels, the camera is capable of shooting video images with a frame rate of 132 frames per second (fps). A pixel density of 28 pixels per  $\text{mm}^2$  (with a pixel size of approximately 0.2 mm x 0.2 mm) is found by combining the resolution of the camera with the size of the FOV, which is approximately 12 cm x 9 cm. The movement between two frames is 7.6 mm for a frame rate per second of 132. This can be translated to a movement of approximately 35 a 40 pixels per time step. According to Kramer (2016), this seems to be sufficient movement for the BIV analysis of the flow velocity in the FOV.

### 3.2.4 BIV | Velocity in Field of View with PIVlab

The BIV analysis of the videos is done with the software PIVlab (version: 1.41), developed by Thielicke and Stamhuis (2014). Thielicke developed PIVlab for his PhD research '*The Flapping Flight of Birds*' (Thielicke, 2014). PIVlab is an open-source, time-resolved digital Particle Image Velocimetry Tool for MATLAB. The software is used to calculate the velocity distribution between consecutive frames of a video. The part of the BIV analysis with PIVlab is elaborated below.

The analyzed videos of BIV experiments of Kramer (2016) (see Table 8) need to be split into separate images (132 frames per second). The images are imported into PIVlab. The sequencing style for the frames is 1-2, 2-3, 3-4, ..., n-n+1 (i.e. the pixels of frame 1 are compared with frame 2, followed by a comparison of the pixels between frame 2 and frame 3, etcetera). Then, the analyses settings need to be defined. A mask is drawn over the lowest area of the images to exclude this part of the image from the BIV analysis, because no movements of water and stones occur at this location. Moreover, images pre-processing techniques (CLAHE (20 pixels), high-pass (20 pixels), and intensity capping) are enabled to improve the images. The effects of pre-processing techniques are shown in Figure 32 in Appendix B.5, including a brief elaboration. A direct Fourier transform correlation with multiple passes and deforming windows is used as the PIV correlation algorithm to analyze the frames, because it gives the most accurate results (Thielicke & Stamhuis, 2014). This algorithm is called FFT window deformation. The analysis of the frames is done in three consecutive passes with interrogation areas decreasing in size (128 pixels, 64 pixels and 32 pixels respectively). In this way, the displacements of the pixels are determined with a good signal-to-noise ratio and a high vector resolution. Now that the analyses settings are defined, all frames can be analyzed in PIVlab.

After the analysis of the frames in PIVlab, the post processing of the data needs to be done. The post processing consists of the interpolation of missing data. Next, the calibration is done by importing an external calibration image (of a ruler in the FOV) and selecting the reference distance, which can be converted from the number of pixels to a real distance in millimeters. In order to convert the vectors with the unit pixel per frame to meter per second, the calibration also includes the time step ( $\Delta t = 1/132 * 1000 = 7.576 \text{ ms}$ ). A screenshot of the calibration for the BIV analysis of the 1:5 slope is shown in Figure 33 in Appendix B.6.

### 3.2.5 BIV | Horizontal velocity and acceleration in Region of Interest

The BIV analysis of the videos continues using MATLAB (version: R2016b). The PIVlab results per frame are saved as MATLAB data files and loaded into the MATLAB program for further processing. Velocity vector fields can be made of the FOV. Two velocity vector fields are shown in Figure 12 (left: frame 54 during run-down, and right: frame 82 during run-up).

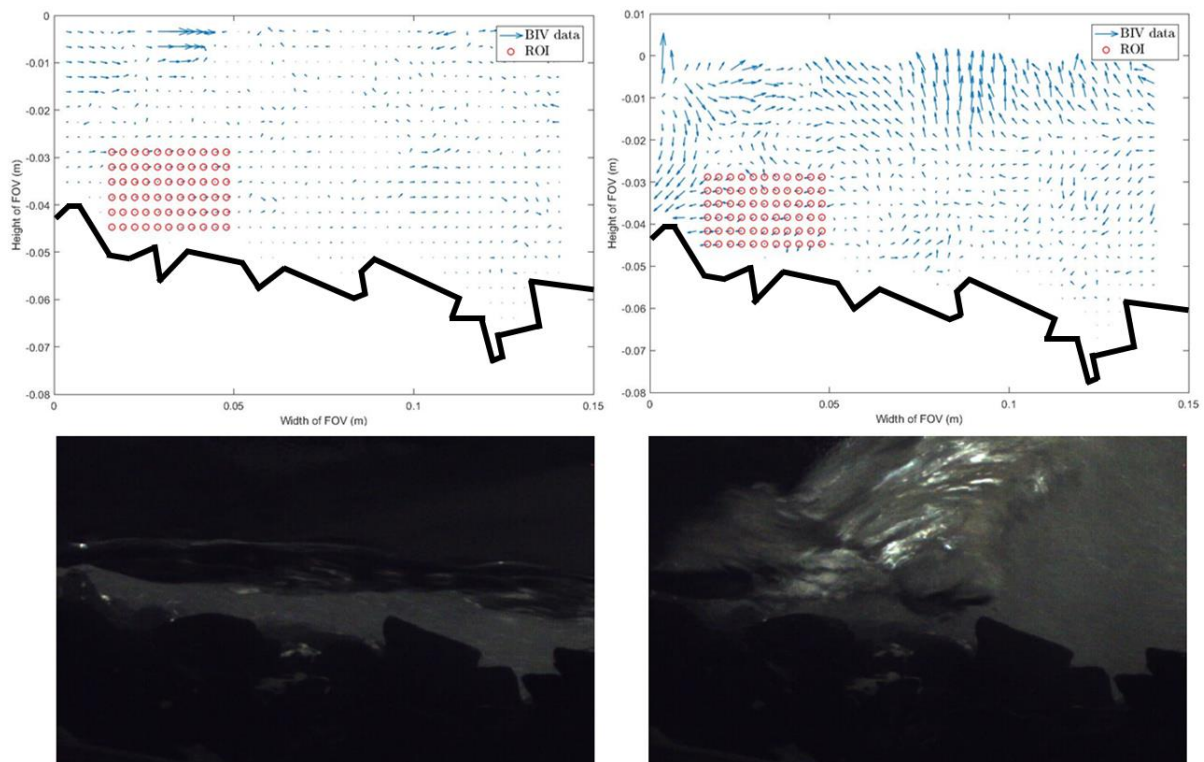


Figure 12 - Velocity vector field with ROI during run-down (left) and during run-up (right) for 1:5 slope

The red circles indicate the vectors in the Region of Interest (ROI), which is the area, located just above the bed, where movements of stone(s) occur (as rocking or displacement). The velocities and accelerations in the ROI have a large influence on the stability of the stones at this location. Therefore, the velocities and accelerations in the ROI are used to derive the hydrodynamic forces at this location, which are analyzed in this research regarding the initiation of motion of stones. The ROI is determined by means of visual observation. The area of the ROI has a width of  $2D_{n50}$  ( $1D_{n50}$  upslope of the center of ROI, and  $1D_{n50}$  downslope) and a height of  $1D_{n50}$  (Kramer, 2016). In MATLAB, the area of the ROI consists of  $11 \times 6$  vectors.

The horizontal velocity  $U$  is averaged over the ROI per velocity vector field (so per frame). In this way, a time signal of the horizontal velocity is obtained for each frame with a time step of  $\Delta t$ . The extreme values of the horizontal velocity, derived from the video of the BIV experiment with 1:5 slope, are in agreement with the values calculated with linear wave theory (see Appendix B.7).

Both the horizontal velocity  $U$  and the acceleration  $dU/dt$  in the ROI are shown over time for the 1:5 slope in Figure 13. The graph is elaborated given below.

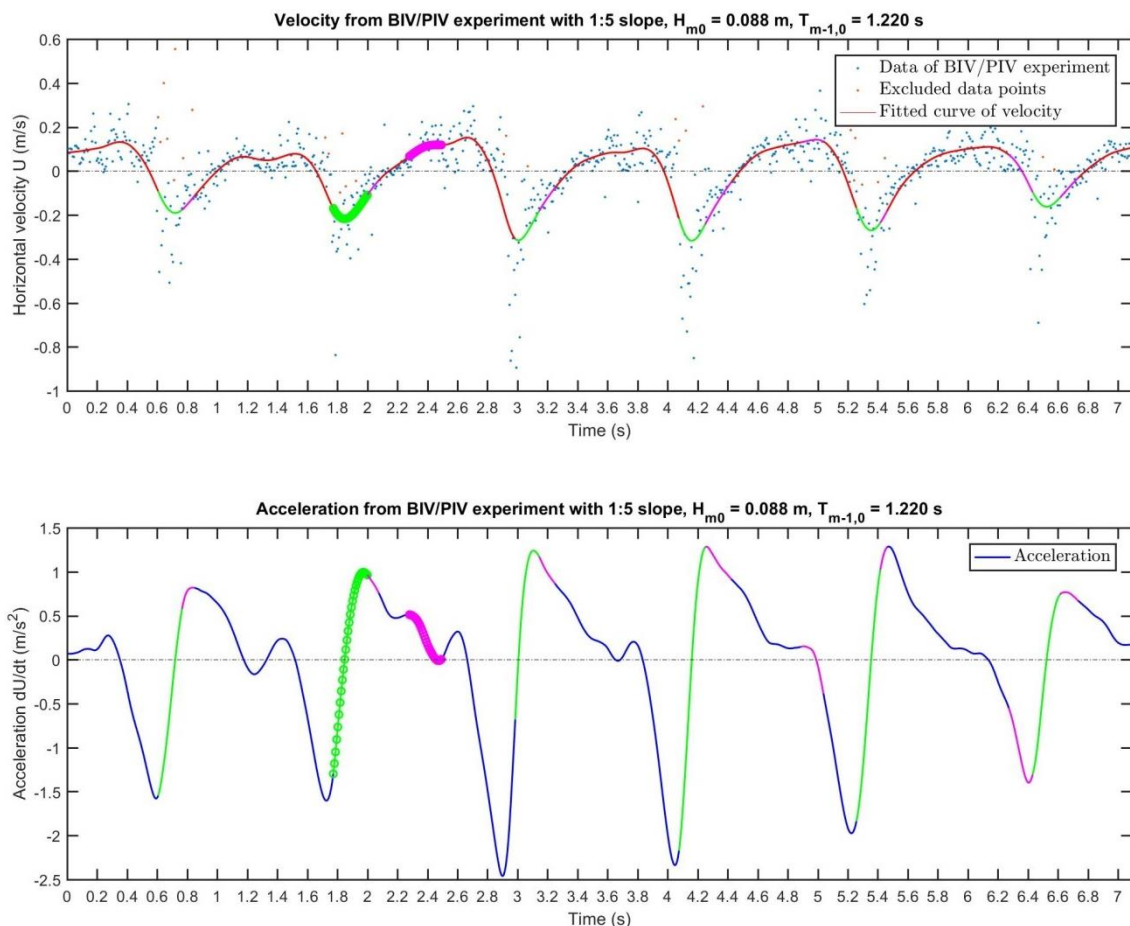


Figure 13 - Velocity (top) and acceleration (bottom) in ROI over time for 1:5 slope

In which: the velocities have a negative value during run-up (in case of incoming waves) and the values of the velocities are positive during run-down (in case of return flow).

Furthermore, the type and the direction of the movements of the stone (from the visual analysis, see Section 3.2.3) are indicated in the plots of the horizontal velocity and the acceleration. The green line with circles indicates displacement of a stone in upslope direction. The pink line with circles indicates displacement of a stone in downslope direction. The green line (without circles) shows

rocking of a stone in upslope direction. The pink line (without circles) indicates rocking of a stone in downslope direction. In this way (with the results of the visual analysis), the horizontal velocity and acceleration can be determined at the specific moment in time when the stone starts to move (i.e. initiation of motion of stone).

### Elaboration of Figure 13

For the 1:5 slope, the time signal of the horizontal velocity is shown as blue data points in Figure 13. A smoothing spline curve is fitted through the scattered data points with the fit-function in MATLAB using 'smoothingspline' as the model type to fit. The option 'SmoothingParam' with a value of 0.997 is included as the smoothing parameter. The option has also been used by Kramer (2016) with a value of 0.990. By applying this value, Kramer (2016) smoothed the data too much. A value of 0.997, which has been determined iteratively in this research, seems to give a better fit of the scattered data. Moreover, data points are excluded from the fit with the option 'Exclude' with a vector of integers indexing the data points that are excluded (e.g. [80 82 ... 858 868]). Both additional options are specified to fit the smoothing spline curve of the horizontal velocity more through the peaks of negative data points, assuming that these peaks influence the initiation of motion of the stone.

The acceleration  $dU/dt$  is determined by taking the derivative over time of the fitted curve of the horizontal velocity  $U$ .

After the derivation, the horizontal velocity  $U$  and the acceleration  $dU/dt$  are substituted into the formulas of the bed shear stress of McCall (2015), as used in XBeach-G with the modified bed-load transport formula of Van Rijn (2007), and the bed shear velocity, as used in the bed-load transport formula of Nielsen (2006).

### Check horizontal velocity with ensemble averaging

Because the BIV experiments are executed with regular waves, the methodology of curve fitting of the horizontal velocity is further investigated with ensemble averaging in Appendix B.8.

### 3.2.6 BIV | Effective, adapted Shields parameter as mobility parameter

The effective, adapted Shields parameter  $\theta'$ , derived in Section 2.5.1, is included in the bed-load formulas of Nielsen (2006) and Van Rijn (2007). In this research, three effective, adapted Shields parameter are defined. They are used as a mobility parameter to describe the stability of stones on mild slopes under wave attack. An overview of the three mobility parameters that are investigated is given in Table 9.

Table 9 - Overview of mobility parameters

Derived from		Mobility parameter
1	Bed-load transport formula of Nielsen (2006) with effective, adapted Shields (1936), using $u_\theta$ as $u_*$ with test values for $f_s$ and $\varphi_\tau$	$\theta'_{Nielsen,Test} = \frac{u_*^2}{\Delta g D_{50}} \cos \beta \left( 1 \pm \frac{\tan \beta}{\tan \phi} \right)$
2	Bed-load transport formula of Nielsen (2006) with effective, adapted Shields (1936), using $u_\theta$ as $u_*$ with standard values for $f_s$ and $\varphi_\tau$	$\theta'_{Nielsen,Standard} = \frac{u_*^2}{\Delta g D_{50}} \cos \beta \left( 1 \pm \frac{\tan \beta}{\tan \phi} \right)$
3	Formula of McCall (2015) for bed shear stress with effective, adapted Shields (1936), using $\tau_b$ with $c_f$ and $c_i$ (as in XBeach-G)	$\theta'_{McCall} = \frac{\tau_b}{(\rho_s - \rho_w) g D_{50}} \cos \beta \left( 1 \pm \frac{\tan \beta}{\tan \phi} \right)$

The mobility parameters  $\theta'_{Nielsen,Test}$  and  $\theta'_{Nielsen,Standard}$  are determined with the bed shear velocity, given in equation (3.3) (and worked out in Section 2.5.4). The mobility parameter  $\theta'_{McCall}$  is obtained with the bed shear stress, given in equation (3.4) (and treated in Section 2.5.3). Both equation (3.3)

and equation (3.4) have a velocity/drag term and an acceleration/inertia term, in which the horizontal velocity  $U$  and the acceleration  $dU/dt$  (derived from the BIV analysis, see Section 3.2.5) are substituted.

$$u_* = \sqrt{\frac{f_s}{2}} \left( \underbrace{\cos \varphi_\tau U}_{\text{velocity}} + \underbrace{\frac{T_{m-1.0}}{2\pi} \sin \varphi_\tau \frac{dU}{dt}}_{\text{acceleration}} \right) \quad (3.3)$$

$$\tau_b = \underbrace{c_f \rho U |U|}_{\text{drag}} + \underbrace{\rho c_m c_v c_n D_{50} \frac{dU}{dt}}_{\text{inertia}} \quad (3.4)$$

The variable input parameters that are used to determine the bed shear velocity and the shear stress per slope are presented in Table 10.

**Table 10 - Variable input parameters used to determine bed shear velocity and shear stress, per slope**

Slope	Shear velocity of Nielsen (2006)					Shear stress of McCall (2015)	
	var(U) (-)	Test values		Standard values		$h_{ROI}$ (m)	$c_f$ (-)
		$f_s$ (-)	$\varphi_\tau$ (°)	$f_s$ (-)	$\varphi_\tau$ (°)		
1:5	0.0284	0.3611	72.8	0.0250	25.0	0.035	0.054
1:10	0.0846	0.2091	65.0	0.0250	25.0	0.059	0.031
1:15	0.0430	0.2914	69.6	0.0250	25.0	0.077	0.025

In which: var(U) is the variance of the velocity,  $f_s$  is the sediment friction factor (-),  $\varphi_\tau$  is the phase lag angle between the wave induced current and the period of the bed shear velocity (°),  $h_{ROI}$  is the water depth at the ROI (m), and  $c_f$  is the dimensionless friction factor. The sediment friction factor  $f_s$  and phase lag angle  $\varphi_\tau$  are treated in Appendix A.15. An elaboration on the dimensionless friction factor  $c_f$  can be found in Appendix A.14.

The constant input parameters that are used to determine the bed shear stress of Van Rijn (2007) are given in Table 11.

**Table 11 - Constant input parameters used to determine mobility parameter  $\theta'_{McCall}$  with bed shear stress**

Parameter		Unit	Value	
Diameter of stone with 90% passing	$D_{90}$	m	0.025	Measured by Kramer (2016)
Characteristic roughness (= $3D_{90}$ )	$k_s$	m	0.075	Assumed (determined with $D_{90}$ )
Inertia coefficient (= $1 + c_a$ )	$c_m$	-	1.50	Determined (with $c_a$ )
Added mass coefficient (for spheres)	$c_a$	-	0.50	Assumed
Volume shape factor (for spheres)	$c_v$	-	0.52	Assumed
Coefficient for number of particles	$c_n$	-	1.00	Assumed

The term of the slope effect  $\cos \beta \left( 1 \pm \frac{\tan \beta}{\tan \phi} \right)$  of the mobility parameters can be determined for each slope ratio when the internal angle of repose ( $\phi = 40^\circ$ ) and the slope angles are known. The slope effect can be defined as a correction factor, which is given per slope in Table 12. The slope effect becomes less when the slope becomes milder (see Table 12).

Table 12 - Slope correction factors, per slope (according to Fredsøe and Deigaard (1992))

Slope ratio	Slope angle (°)	Factor downslope	Factor upslope
1:5	11.3	0.747	1.214
1:10	5.7	0.877	1.114
1:15	3.8	0.919	1.077

### 3.2.7 BIV | Stability parameter as threshold for initiation of motion

An attempt is made to derive a certain critical value of the effective, adapted Shields parameter that can function as a threshold for the initiation of motion of stones on mild slopes under wave attack. When this stability parameter is not exceeded by the mobility parameter(s) of Section 3.2.6, no or limited movements of stone(s) occur and the stability of stones is guaranteed. The stability parameter should be applicable for each slope (taking the slope effect into account).

A critical value based on the seven transport stages of Breusers and Schukking (1971), elaborated in Section 2.3.2, could be used. In *paragraph 5.2.1.3 of The Rock Manual*, certain values for the critical Shields parameter  $\theta_{cr}$  are presented (CIRIA et al., 2007). These critical Shields parameters are given for a certain acceptable movement of stones (using the transport stages 1, 2, 5 and 6 of Breusers and Schukking (1971)), see the two bullet points below.

- $\theta_{cr} = 0.030 - 0.035$  For the point at which stones first start to move (CIRIA et al., 2007).
- $\theta_{cr} \cong 0.050 - 0.055$  For which limited movement of stones occurs (CIRIA et al., 2007).

**Note:** the values are derived for uniform flow on a horizontal bed. This research deals with an oscillating flow with waves breaking on a slope.

The stability parameters (elaborated above) do not take into account the slope effect, because they have been derived for horizontal bottom protections. The slope correction factors of Table 12 are used to derive the effective stability parameters  $\theta'_{cr}$  per slope, given as a range in Table 13.

Table 13 - Effective stability parameters, per slope

Slope	Description of movements of stones		Direction	$\theta'_{cr}$	
1:5	Rocking	First stones start to move	Upslope	-0.036	-0.042
			Downslope	0.022	0.026
	Displacement	Beginning of transport of stones	Upslope	-0.061	-0.067
			Downslope	0.037	0.041
1:10	Rocking	First stones start to move	Upslope	-0.033	-0.039
			Downslope	0.026	0.031
	Displacement	Beginning of transport of stones	Upslope	-0.056	-0.061
			Downslope	0.044	0.048
1:15	Rocking	First stones start to move	Upslope	-0.032	-0.038
			Downslope	0.028	0.032
	Displacement	Beginning of transport of stones	Upslope	-0.054	-0.059
			Downslope	0.046	0.051
<b>No correction factor</b>	Rocking	First stones start to move	-	0.030	0.035
	Displacement	Beginning of transport of stones	-	0.050	0.055

In which: the values of  $\theta'_{cr}$  are positive during run-down and  $\theta'_{cr}$  has a negative value during run-up. The values of  $\theta'_{cr}$  without slope correction factor (shown in the bottom rows) are for a horizontal bottom.

The applicability of the stability parameter as a threshold for the initiation of motion of stones is examined in Section 5.7. The aim is to find a value for the stability parameter that indicates initiation of motion of stones for each slope.

### 3.3 XBeach-G & BIV | Link mobility parameter with XBeach-G

An endeavor is made to link both parts of this research by connecting the mobility parameter  $\theta'_{McCall}$  regarding initiation of motion of stones (part 2) with the numerical model XBeach-G (part 1). The mobility parameter  $\theta'_{McCall}$  has been investigated for a few regular waves (i.e.  $N = 3 - 6$ ) and is now examined for irregular waves with  $N = 3000$ .

**Note:** the wave characteristics of the regular waves in the BIV experiments of Kramer (2016), given in Table 7, are based on the highest one percent (irregular) waves ( $H_{1\%}$ ) of the  $S_{Wit}$  input of the profile change experiments of Kramer (2016).

The mobility parameter  $\theta'_{McCall}$  is used to describe the stability of the stones along the length of the slope. The mobility parameter is determined with the bed shear stress computed with XBeach-G using the velocity and the acceleration.

The values of the velocity and the acceleration are investigated to check if the hydrodynamics are implemented correctly in the numerical model XBeach-G. Assuming this is true, the velocity and the acceleration calculated with XBeach-G can be used to determine the mobility parameter  $\theta'_{McCall}$ . The mobility parameter is plotted along the length of the slope of the modelled erosion profiles with  $S_{Wit}$  input.

## 4 Results of XBeach-G simulations

The results of the XBeach-G simulations to reproduce the profile change experiments of Kramer (2016) are presented and analyzed in this chapter. To give an impression of the results, the erosion profiles of the XBeach-G simulations for the 1:10 slope with  $S_{Wit}$  input are shown in Section 4.1. The erosion profiles, simulated in XBeach-G with other input parameters (i.e. slope angle and wave characteristics), are presented in Appendix C. The input parameters of the executed XBeach-G simulations are treated in Section 3.1.1. An overview of the results of the XBeach-G simulations is given in Section 4.2 and the analysis of the results is done in Section 4.3. The results are discussed in Section 4.4.

### 4.1 Results of XBeach-G simulations for 1:10 slope and $S_{Wit}$ input

The erosion profiles of the XBeach-G simulations for the 1:10 slope with  $S_{Wit}$  input, modelled with the bed-load transport formulas of Nielsen (2006) and Van Rijn (2007), are shown in Figure 14.

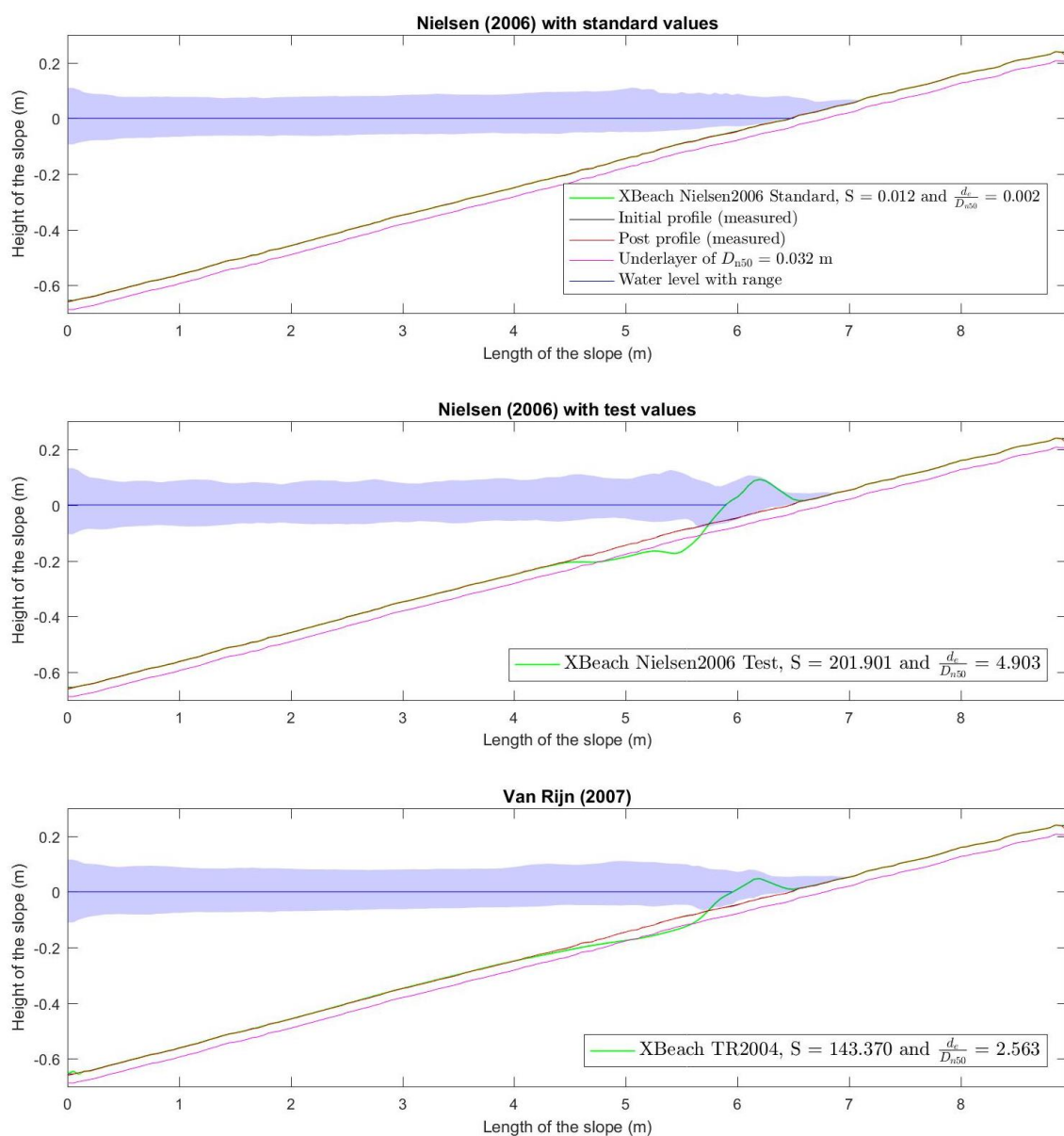


Figure 14 - Erosion profiles for 1:10 slope and  $S_{Wit}$  input

In which: the green line shows the erosion profile modelled in XBeach-G with the relevant bed-load transport formula. The initial profile is the black line and the post profile is the red line. Both profiles

are measured by Kramer (2016) before and after the execution of his profile change experiments, see Section 3.1.2. The under layer with a layer thickness of two times the nominal mean diameter of the stone is shown as a pink line. The layer represents the rock protection on an impermeable sandy core; see Section 3.1.3 for the elaboration on how the layer is implemented in XBeach-G. The blue line indicates the water level, including the range.

## 4.2 Overview of results of XBeach-G simulations

An overview of all simulations performed using the numerical model XBeach-G is given in Table 14. The overview includes the erosion area  $A_e$  and the damage characteristics: the damage level  $S$ , the relative erosion depth  $d_e/D_{n50}$  and the damage depth  $E_3$ . The damage characteristics have been derived from the modelled erosion profiles, which are presented in Appendix C. The profile development is evaluated qualitatively by looking at the direction of transport (by means of visual observation). An elaboration on the damage characteristics is given in Section 2.6.

Table 14 - Overview of all simulations, including damage obtained from the erosion profiles

	1:5 slope & $S_{norm}$ input	$A_e$ (m <sup>2</sup> )	$S$ (-)	$d_e/D_{n50}$ (-)	$E_3$ (%)	Profile development
1	Experiment of Kramer (2016)	-1.44E-04	0.55	-	35.8	-
2	XBeach-G Nielsen (2006) Standard	0.00	0.00	0.000	0.0	No erosion profile
3	XBeach-G Nielsen (2006) Test	-9.10E-03	34.67	2.029	203.1	Reversed transport, crest profile
4	XBeach-G Van Rijn (2007)	-2.20E-03	8.21	0.788	79.0	Reversed transport, crest profile

	1:5 slope & $S_{wit}$ input	$A_e$ (m <sup>2</sup> )	$S$ (-)	$d_e/D_{n50}$ (-)	$E_3$ (%)	Profile development
1	Experiment of Kramer (2016)	-2.77E-04	1.02	-	6.3	-
2	XBeach-G Nielsen (2006) Standard	0.00	0.00	0.000	0.0	No erosion profile
3	XBeach-G Nielsen (2006) Test	-7.30E-03	27.87	2.290	229.0	Reversed transport, crest profile
4	XBeach-G Van Rijn (2007)	-2.80E-03	10.81	0.750	74.7	Reversed transport, crest profile

	1:10 slope & $S_{wit}$ input	$A_e$ (m <sup>2</sup> )	$S$ (-)	$d_e/D_{n50}$ (-)	$E_3$ (%)	Profile development
1	Experiment of Kramer (2016)	-5.29E-04	2.01	-	44.4	-
2	XBeach-G Nielsen (2006) Standard	-3.02E-06	0.01	0.002	0.2	No erosion profile
3	XBeach-G Nielsen (2006) Test	-5.30E-02	201.90	4.903	490.1	Very large crest profile
4	XBeach-G Van Rijn (2007)	-3.76E-02	143.37	2.563	255.6	Very large crest profile




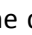
	1:10 slope & $S_{s\&f}$ input	$A_e$ (m <sup>2</sup> )	$S$ (-)	$d_e/D_{n50}$ (-)	$E_3$ (%)	Profile development
1	Experiment of Kramer (2016)	-3.07E-04	1.07	-	50.0	-
2	XBeach-G Nielsen (2006) Standard	-4.40E-03	16.62	0.577	57.4	Wide erosion profile
3	XBeach-G Nielsen (2006) Test	-1.25E-01	475.27	5.044	504.3	Very large crest profile
4	XBeach-G Van Rijn (2007)	-8.10E-02	308.80	3.713	371.6	Very large crest profile

	1:15 slope & $S_{wit}$ input	$A_e$ (m <sup>2</sup> )	$S$ (-)	$d_e/D_{n50}$ (-)	$E_3$ (%)	Profile development
1	Experiment of Kramer (2016)	-2.76E-04	1.05	-	33.3	-
2	XBeach-G Nielsen (2006) Standard	-1.00E-03	3.96	0.078	8.0	Wide erosion profile
3	XBeach-G Nielsen (2006) Test	-1.90E-01	723.03	5.844	584.6	Very large crest profile
4	XBeach-G Van Rijn (2007)	-8.46E-02	322.49	3.124	312.3	Very large crest profile

	1:15 slope & $S_{s\&f}$ input	$A_e$ (m <sup>2</sup> )	$S$ (-)	$d_e/D_{n50}$ (-)	$E_3$ (%)	Profile development
1	Experiment of Kramer (2016)	-1.85E-04	0.70	-	46.3	-
2	XBeach-G Nielsen (2006) Standard	-2.52E-02	96.11	0.946	94.4	Very wide crest profile
3	XBeach-G Nielsen (2006) Test	-4.51E-01	1717.34	9.012	901.2	Very large crest profile
4	XBeach-G Van Rijn (2007)	-1.92E-01	731.00	4.612	461.1	Very large crest profile

In which: damage levels with a background color of  indicates an underestimation of the damage and damage levels with a background color of  means an overestimation of the damage. The damage depths with a background color of  indicate intermediate damage, while the damage levels have values that indicate failure. The damage depths with a background color of  indicate intermediate damage, while the damage levels have values that indicate failure.

### 4.3 Analysis of results of XBeach-G simulations

#### 4.3.1 Comparison of modelled erosion profiles with measured post profiles

A general comparison of the erosion profiles modelled in XBeach-G with the erosion profiles of the profile change experiments of Kramer (2016) is given below.

- As can be seen in Figure 14 and in Appendix C, the formed erosion profiles modelled with XBeach-G are not in agreement with the post profiles of the profile change experiments of Kramer (2016).
- The values of the damage characteristics derived from the erosion profiles modelled with XBeach-G differ significantly from the damage characteristics obtained from the post profiles of the profile change experiments of Kramer (2016). The difference in damage is shown in Table 14.

From the above two points, it can be concluded that the applied bed-load transport formulas are not able to model the sediment transport correctly in XBeach-G.

#### 4.3.2 Analysis of bed-load transport formulas applied in XBeach-G

The results of the bed-load transport formulas applied in XBeach-G are analyzed below, using the damage characteristics, presented in Table 14, and the profile development of the modelled erosion profiles, shown in Figure 14 and in Appendix C.

- Bed-load transport formula of Nielsen (2006) with standard values for  $f_s$  and  $\varphi_\tau$ 
  - No erosion profiles are modelled for 1:5 slope &  $S_{norm}$  input, 1:5 slope &  $S_{wit}$  input, 1:10 slope &  $S_{wit}$  input. Because the damage characteristics are related to the erosion profile with the eroded area  $A_e$  or eroded depth  $d_e$ , the damage characteristics have a value of zero. This results in an underestimation of the expected damage, derived from the erosion profiles of the profile change experiments of Kramer (2016).
  - Wide or very wide erosion profiles are modelled for the other cases, overestimating the expected damage.
  - The XBeach-G results using this bed-load transport formula are closest to the results of the profile change experiments of Kramer (2016) with respect to the other applied bed-load transport formulas.
- Bed-load transport formula of Nielsen (2006) with test values for  $f_s$  and  $\varphi_\tau$ 
  - In all cases, large or very large erosion profiles are modelled. The expected damage is overestimated significantly.
  - The XBeach-G results using this bed-load transport formula deviate most from the results of the profile change experiments of Kramer (2016) with respect to the other applied bed-load transport formulas.
- Bed-load transport formula of Van Rijn (2007)
  - In all cases, large or very large erosion profiles are modelled. This results in a significant overestimation of the expected damage.

- The XBeach-G results using this bed-load transport formula deviate less from the results of the profile change experiments of Kramer (2016) than using the bed-load transport formula of Nielsen (2006) with test values for the sediment friction factor and the phase lag angle.
- The XBeach-G results using this bed-load transport formula deviate more from the results of the profile change experiments of Kramer (2016) than using the bed-load transport formula of Nielsen (2006) with standard values.

#### 4.3.3 Sensitivity of formula of Nielsen (2006) to sediment friction factor and phase lag angle

The sensitivity of the numerical model XBeach-G to the sediment friction factor and the phase lag angle when modelling the erosion profiles with the bed-load transport formula of Nielsen (2006) is demonstrated in Table 14. The bed-load transport formula of Nielsen (2006) has been applied with standard values ( $f_s = 0.025$  and  $\varphi_\tau = 25^\circ$  (McCall, 2015)) and with test values (derived from the BIV experiments of Kramer (2016)). The following points have been found.

- As can be seen in Table 14, large differences are found qualitatively when looking at the values of the damage characteristics of the modelled erosion profiles (see the damage characteristics of Nielsen (2006) Standard in green and the damage characteristics of Nielsen (2006) Test in red).
- When looking at the profile development of the modelled erosion profiles, shown in Figure 14 and in Appendix C, the quantitative results differ significantly as well.

From the above two points, it can be concluded that the results obtained with the bed-load transport formula of Nielsen (2006) are very sensitive to the sediment friction factor and the phase lag angle. This has already been concluded by McCall (2015), when modelling sediment transport with the formula of Nielsen (2006) in XBeach-G. Examining the results of the simulations obtained with the bed-load transport formula of Nielsen (2006) should be done with care.

#### 4.3.4 Validation/falsification of conclusions drawn by Postma (2016) about the bed-load transport formulas of Nielsen (2006) and Van Rijn (2007)

Postma (2016) examined the bed-load transport formula of Nielsen (2006) with standard values for the sediment friction factor and the phase lag angle and the bed-load transport formula of Van Rijn (2007) in XBeach-G, using the data of the experiments of Van der Meer (1988) as input. He concluded that the erosion profiles modelled in XBeach-G with both bed-load transport formulas differ too much from the measured erosion profiles of the experiments of Van der Meer (1988) (Postma, 2016). The conclusions regarding the bed-load transport formula of Nielsen (2006) with standard values for the sediment friction factor and the phase lag angle and the bed-load transport formula of Van Rijn (2007) drawn by Postma (2016) are given below.

The XBeach-G results obtained in this research are in agreement with the conclusions indicated in green. The conclusions shown in red are falsified in this research (elaborated in black behind the red conclusion of Postma (2016)).

- Bed-load transport formula of Nielsen (2006) with standard values for  $f_s$  and  $\varphi_\tau$ 
  - Gives more accurate and consistent results for slopes milder than 1:6.  
For the cases with 1:5 slope & Snorm input, 1:5 slope & SWit input, 1:10 slope & SWit input (examined in this research), the expected damage of the profile change experiments of Kramer (2016) is underestimated by the damage derived from the erosion profiles modelled with the bed-load transport formula of Nielsen (2006) with standard values for the sediment friction factor and the phase lag angle. The expected damage is overestimated significantly for the case with 1:10 slope & SS&F input and the cases with 1:15 slopes. Therefore, the bed-load transport formula of Nielsen (2006) with standard values for the sediment friction

factor and the phase lag angle does not give more accurate and consistent results for slopes milder than 1:6.

- In a lot of cases the expected damage is underestimated.
- The XBeach-G results are closer to the results of the experiments of Van der Meer (1988).
- Bed-load transport formula of Van Rijn (2007)
  - Is more applicable for steep slopes (i.e. slopes towards 1:4).  
For the cases with 1:5 slope (examined in this research), the values of the damage characteristics derived from the erosion profiles modelled with the bed-load transport formula of Van Rijn (2007) indicate failure. Thus, the expected damage of the profile change experiments of Kramer (2016) is overestimated significantly. Therefore, the bed-load transport formula of Van Rijn (2007) is not more applicable for steep slopes.
  - Gives more conservative damage levels.
  - Overestimates the expected damage in all cases.
  - High values of damage level  $S$  do not give high values for the relative erosion depth  $d_e/D_{n50}$ .

Furthermore, the velocity and the acceleration in the hydrodynamics are modelled well in the numerical model XBeach-G, according to Postma (2016). However, the values of the velocity and the acceleration obtained with XBeach-G are significantly higher than the values derived from the BIV analyzed videos.

#### 4.3.5 Comparison of damage for different wave characteristics with same slope angle

In Section 3.1.1 is already explained that the results of the XBeach-G simulations for the same slope angle with the two different wave characteristics can be compared with each other (for example, comparing the results of the 1:5 slope with  $S_{Wit}$  input with the results of the 1:5 slope with  $S_{norm}$  input). This is possible because the Iribarren number is kept constant per slope, and thus, the type of wave breaking is the same per slope. The following points have been found.

- When comparing the XBeach-G simulations modelled with a certain bed-load transport for the 1:5 slope, more damage is found for the simulations modelled with the wave characteristics based on  $S_{Wit}$  input than the simulations modelled with the wave characteristics based on  $S_{norm}$  input. This result was expected, because the wave height is larger for  $S_{Wit}$  input.
- For a certain bed-load transport with a 1:10 or 1:15 slope, the damage obtained with the simulations modelled with the wave characteristics based on  $S_{S\&F}$  input is larger than the damage derived from the erosion profiles modelled with the wave characteristics based on  $S_{Wit}$  input. These results were also expected, because the wave height is larger for  $S_{S\&F}$  input.

The results with different slope angles cannot be compared with each other, because the type of wave breaking is not the same (as the Iribarren number is not constant, see Table 4).

#### 4.3.6 Analysis of damage level $S$ versus damage depth $E_3$

The analysis of the damage level  $S$  and the damage depth  $E_3$  to describe damage of stones on mild slopes under wave attack is elaborated below.

- For the simulation with 1:5 slope and  $S_{norm}$  input and the simulation with 1:5 slope and  $S_{Wit}$  input, the damage levels derived from the erosion profiles modelled with the bed-load transport formula of Van Rijn (2007) indicate failure ( $S \approx 10$ ). However, the values of the damage depths (shown with a green background color in Table 14) are closer to the range of intermediate damage ( $E_3 = 50 - 60\%$ ) than failure ( $E_3 = 150 - 160\%$ ).
- The same results are found for the simulation with 1:10 slope and  $S_{S\&F}$  input and the simulation with 1:15 slope and  $S_{S\&F}$  input when modelling the erosion profiles with the bed-load transport formula of Nielsen (2006) using standard values for the sediment friction factor and the phase

lag angle. For these results, the relative erosion depth is also below the criteria of  $d_e/D_{n50} < 1$ , which means that the layer of stones on the impermeable structure is still present with a layer thickness of at least one times  $D_{n50}$ .

- Both the values of  $E_3$  and  $d_e/D_{n50}$  show that the erosion holes have a relatively long erosion length and a relatively small erosion depth. These results were also found by Wit (2015) and Postma (2016). Both argued the use of the damage level S for mild slopes and suggested an alternative damage description that is dependent on the erosion depth. In this way, the length/depth ratio is taken into account of the erosion profiles, which become wider and less deep for milder slopes. The damage level S is determined by means of the erosion area  $A_e$ , in which the length/depth ratio is not included (see explanation in Section 2.6.1).
- For all simulations modelled with the bed-load transport formula of Nielsen with test values for the sediment friction factor and the phase lag angle and the remaining simulation modelled with the formula of Van Rijn (2007), the values of the damage levels and the damage depths (shown with a yellow background color in Table 14) are very high and unrealistic. Both the damage characteristics and the very large crest profiles (modelled) deviate significantly from the results obtained from the profile change experiments of Kramer (2016).

#### 4.3.7 Profile development of modelled erosion profiles

According to Wit (2015), the slope angle and the stone diameter are the two main parameters that determine the type of profile. Based on the results of the XBeach-G simulations of Wit (2015), a submerged bar profile is expected to occur in the erosion profiles of the XBeach-G simulations with a 1:5 slope (and a  $D_{n50}$  of 0.0162 m). Because the slope is relatively steep and the stones are relatively small, the stones are expected to move downslope, creating a submerged bar profile (Wit, 2015).

- When examining the profile development of the modelled erosion profiles with 1:5 slopes in this research, the sediment transport is transported upslope, leading to the formation of a crest profile. The crest profiles of the simulations with 1:5 slopes are shown in Figure 35 in Appendix C.1 and in Figure 36 in Appendix C.2. The crest profiles could be formed due to the fact that, besides the slope angle and the stone diameter, the wave characteristics have an influence on the profile development as well. In this research, the significant wave heights used in the simulations with 1:5 slopes are  $H_{m0} = 0.054 \text{ m}$  and  $H_{m0} = 0.058 \text{ m}$ , while Wit (2015) researched the profile development with  $H_s = 1 \text{ m}$  and  $H_s = 2 \text{ m}$ . The difference in wave height is significant and could have an influence on the profile development.
- The profile development of the erosion profiles of the XBeach-G simulations with 1:10 and 1:15 slopes is in agreement with the research of Wit (2015), because the expected crest profiles are formed (although very large).

### 4.4 Discussion

#### 4.4.1 Sediment friction factor and phase lag angle of formula of Nielsen (2006)

A point of interest is the determination of the test values of the sediment friction factor and the phase lag angle. The test values of the sediment friction factor and the phase lag angle, derived from the BIV experiments of Kramer (2016), are obtained for other wave characteristics (i.e. with regular waves) (shown in Table 7) than the wave characteristics (i.e. with irregular waves) (see Table 4) that were used for the profile change experiments of Kramer (2016) and the XBeach-G simulations executed in this research. However, the type of wave breaking is the same per slope, because Kramer (2016) kept the Iribarren number constant per slope for both the profile change experiments and the BIV experiments.

#### 4.4.2 Minor damage derived from profile change experiments

The wave characteristics used the profile change experiments of Kramer (2016) are based on theoretical damage levels  $S$  with values between 2.00 (for a 1:5 slope) and 8.84 (for a 1:15 slope) (see Section 3.1.1). The corresponding wave characteristics are relatively small. Therefore, the profile change is small and only minor damage is derived from the measured erosion profiles (called post profiles in this research) determined from the profile change experiments of Kramer (2016). Van der Meer (1988) would describe the damage of the profile change experiments with a damage level  $S$  of zero, because he based the damage description of the damage level on damage that is actually visible. Although stones are moved during the profile change experiments of Kramer (2016) (i.e. gradients in displacement), the profile change was only limited (i.e. net transport of zero). Therefore, the wave characteristics used to model the profile change experiments in XBeach-G are arguable, because the values of the wave characteristics are not in agreement with the theoretical damage level on which the values of the wave characteristics are based. This is explained with the following example. One of the wave characteristics for the 1:5 slope is based on  $S_{\text{norm}}$  input, which has a (theoretical) damage level  $S$  of 2.00. However, the damage level derived from the profile change experiment of Kramer (2016) has a value of 1.06, which is significantly lower. The difference between the damage levels is shown in Table 15.

Table 15 - Theoretical damage levels and damage levels derived by Kramer (2016), per slope

Slope	$S_{\text{norm}} (-)$	$S_{\text{Kramer(2016)}} (-)$
1:5	2.00	1.06

Slope	$S_{\text{Wit}} (-)$	$S_{\text{Kramer(2016)}} (-)$
1:5	3.00	0.55
1:10	5.91	2.01
1:15	8.84	1.05

Slope	$S_{\text{S&F}} (-)$	$S_{\text{Kramer(2016)}} (-)$
1:10	20.02	3.51
1:15	30.38	0.70

#### 4.5 Analysis of dimensionless stability parameter vs. Iribarren number

For static stability, the dimensionless stability parameter  $H_s/\Delta D_{n50}$  has been determined iteratively. For each slope, the wave characteristics are tuned to obtain an erosion profile that corresponds to a damage level  $S$  with a value close to two. The erosion profiles have been modelled with the bed-load transport formula of Van Rijn (2007) in XBeach-G. The results are shown in Table 16 and Figure 15.

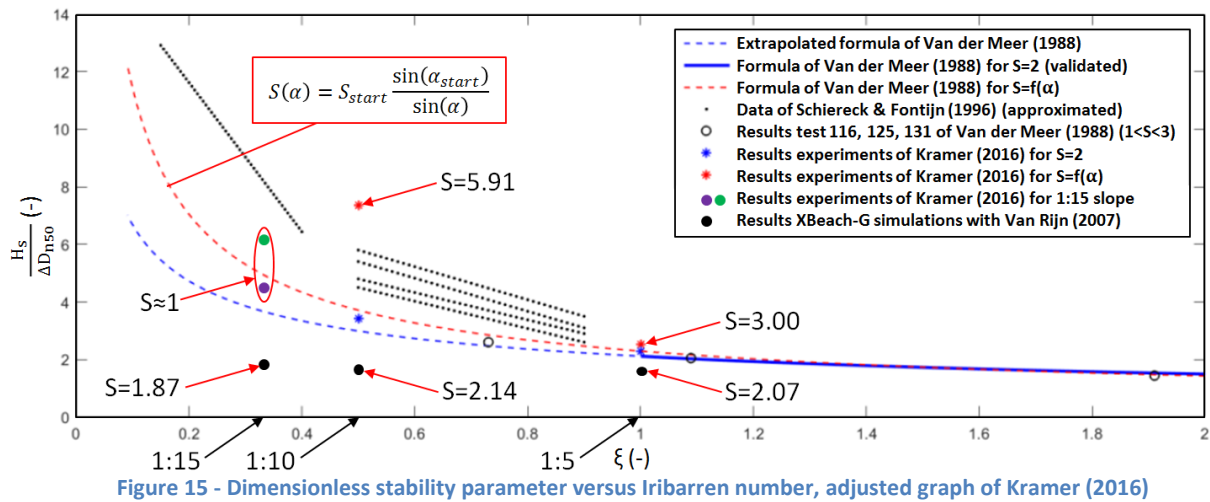
Table 16 - Dimensionless stability parameter  $H_s/\Delta D_{n50}$  determined with bed-load transport formula of Van Rijn (2007) using the numerical model XBeach-G, per slope (and corresponding wave characteristics)

Input					Output	
Slope	$T_m (s)$	$T_p (s)$	$H_{m0} (m)$	$\xi_m (-)$	$S_{\text{norm}} (-)$	$H_s/\Delta D_{n50} (-)$
1:5	0.84	0.97	0.044	1.00	2.07	1.61
1:10	0.86	0.99	0.046	0.50	2.14	1.69
1:15	0.89	1.02	0.049	0.33	1.87	1.80

As can be seen in Figure 15, the values of the dimensionless stability parameter obtained with the XBeach-G simulations remain below the extrapolated formula of Van der Meer (1988). This demonstrates that (when modelling with the bed-load transport formula of Van Rijn (2007)) the

numerical model XBeach-G gives more conservative results than using the extrapolated formula of Van der Meer (1988), which is already a conservative design approach (explained in Section 2.4).

**Note:** in Section 4.3.1 is already concluded that the bed-load transport formula of Van Rijn is not able to model the sediment transport correctly in XBeach-G. The use of XBeach-G simulations with this bed-load transport formula to describe static stability should be examined carefully.



In which:  $\alpha$  is the slope angle ( $^{\circ}$ ).

## 5 Results of BIV analysis

The results of the BIV analysis regarding initiation of motion of stones are presented and analyzed in this chapter. The results of the BIV analysis of the video with the 1:5 slope of the BIV experiments of Kramer (2016) are elaborated in Section 5.1. The results of the BIV analysed videos with 1:10 and 1:15 slope are treated in Appendix D. An overview of the results of the BIV analysis is given in Section 5.3. The analysis of these results is treated in Section 5.4 and the results are discussed in Section 5.5. Further analyses are done in Section 5.6 and Section 5.7. The sediment friction factor and the inertia coefficient used in the bed shear stress formula to determine the mobility parameter  $\theta'_{McCall}$  are analyzed in Section 5.6. Section 5.7 covers the analysis of the stability parameter  $\theta_{cr}$ . Finally, an endeavor is made to link the mobility parameter  $\theta'_{McCall}$  with the numerical model XBeach-G in Section 5.8.

### 5.1 Results of BIV analysis of video with 1:5 slope

#### Visual analysis of video 05\_BIV\_0001

The results of the visual analysis of the movements of the stone of video 05\_BIV\_0001 are shown in Table 17. The methodology of the visual analysis of the movements of the stone is treated Section 3.2.3 and elaborated in Appendix B.4.

Table 17 - Movements of stone for 1:5 slope (video 05\_BIV\_0001)

Type of movement	Direction	Time (s)		Frame (-)	
		from	to	from	to
Rocking	Upslope	0.606	0.765	80	101
Rocking	Downslope	0.765	0.848	101	112
Displacement	Upslope	1.773	2.000	234	264
Rocking	Downslope	2.000	2.076	264	274
Displacement	Downslope	2.280	2.492	301	329
Rocking	Upslope	2.985	3.144	394	415
Rocking	Downslope	3.144	3.250	415	429
Rocking	Upslope	4.076	4.250	538	561
Rocking	Downslope	4.250	4.424	561	584
Rocking	Downslope	4.886	5.038	645	665
Rocking	Upslope	5.258	5.417	694	715
Rocking	Downslope	5.417	5.462	715	721
Rocking	Downslope	6.273	6.432	828	849
Rocking	Upslope	6.432	6.614	849	873
Rocking	Downslope	6.614	6.735	873	889

#### Horizontal velocity and acceleration

After the visual analysis of the movements of stone, the horizontal velocity  $U$  and the acceleration  $dU/dt$  are derived from the BIV analysis of video 05\_BIV\_0001. The horizontal velocity  $U$  and the acceleration  $dU/dt$  over time are presented in Figure 16.

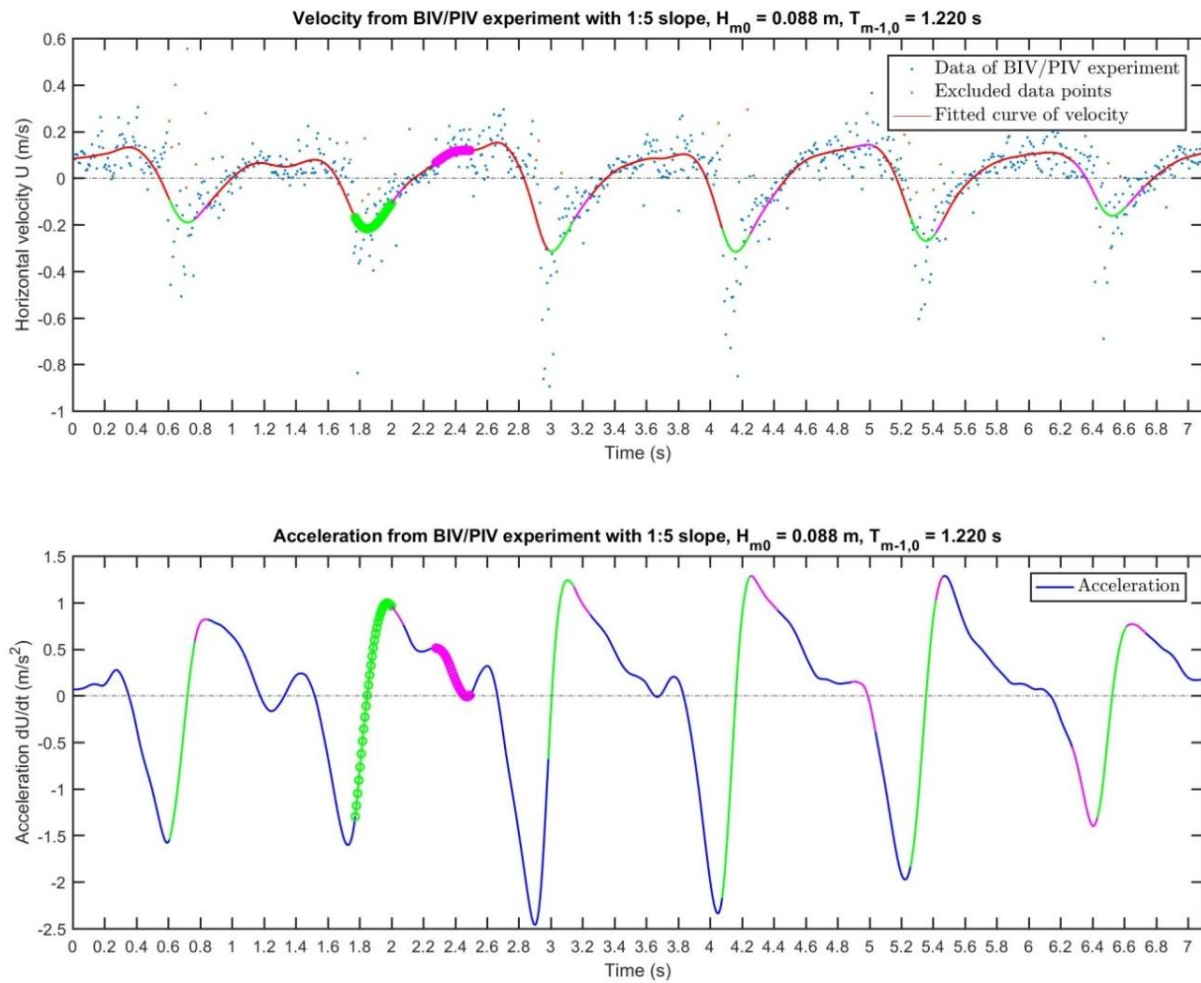


Figure 16 - Velocity (top) and acceleration (bottom) in ROI over time for 1:5 slope

In which: the velocities have a negative value during run-up (in case of incoming waves) and the values of the velocities are positive during run-down (in case of return flow). Furthermore, the type and the direction of the movements of the stone (from the visual analysis, see Table 17) are indicated in the plots of the horizontal velocity and the acceleration. The green line with circles indicates displacement of a stone in upslope direction. The pink line with circles indicates displacement of a stone in downslope direction. The green line (without circles) shows rocking of a stone in upslope direction. The pink line (without circles) indicates rocking of a stone in downslope direction. In this way (with the results of the visual analysis), the horizontal velocity and acceleration can be determined at the specific moment in time when the stone starts to move (i.e. initiation of motion of stone).

As can be seen in Figure 16, the negative peaks (during run-up) are larger in magnitude than the positive peaks (during run-down) for both the velocity and the acceleration. In Figure 16, the incoming waves initiate movement of stones in upslope direction (indicated in green) just before the moments where the velocity reaches the negative peak. At these moments, the gradient in acceleration from negative to positive is large. After the waves had passed, the flow reverses and movements of stones in downslope direction are observed (shown in pink). The corresponding accelerations have maximum values. Moreover, movements of stones in downslope direction are found when the velocity is increasing in positive direction (at  $t = 2.280$  s and at  $t = 4.886$  s), and when the acceleration reaches the negative peak at  $t = 6.273$  s.

### Bed shear stress and bed shear velocity

The horizontal velocity  $U$  and acceleration  $dU/dt$  are substituted into the velocity/drag term and the acceleration/inertia term of the formula of the bed shear stress of McCall (2015), as used in XBeach-G with the modified bed-load transport formula of Van Rijn (2007), and the formula of the bed shear velocity, as used in the bed-load transport formula of Nielsen (2006). The bed shear stress and bed shear velocity are treated in Section 2.5.3 and Section 2.5.4.

For the 1:5 slope, the bed shear velocity over time and the bed shear stress over time are presented in Figure 41 and Figure 42, in Appendix D.1 respectively. The dominance of the velocity/drag term with respect to the acceleration/inertia term for both the bed shear stress and bed shear velocity has been examined by plotting the terms separately in time. The acceleration/inertia term (shown in blue) is very dominant over the velocity/drag term (shown in red) for both the bed shear stress and the bed shear velocity. This dominance relationship has also been found by Kramer (2016). The effect of the acceleration/inertia term is significant on the total term of the bed shear stress or bed shear velocity over time (as the blue line of the acceleration/inertia term is almost the same as the black line of the total term). This means that the acceleration/inertia term plays an important role in the stability of stones under wave attack.

### Mobility parameters

The bed shear stress and the bed shear velocity over time are substituted in the formulas of the mobility parameters  $\theta'_{\text{Nielsen,Test}}$ ,  $\theta'_{\text{Nielsen,Standard}}$  and  $\theta'_{\text{McCall}}$ . An elaboration on how these three mobility parameters (i.e. effective, adapted Shields parameters) are determined is given in Section 3.2.6. The mobility parameters over time are presented in Figure 17.

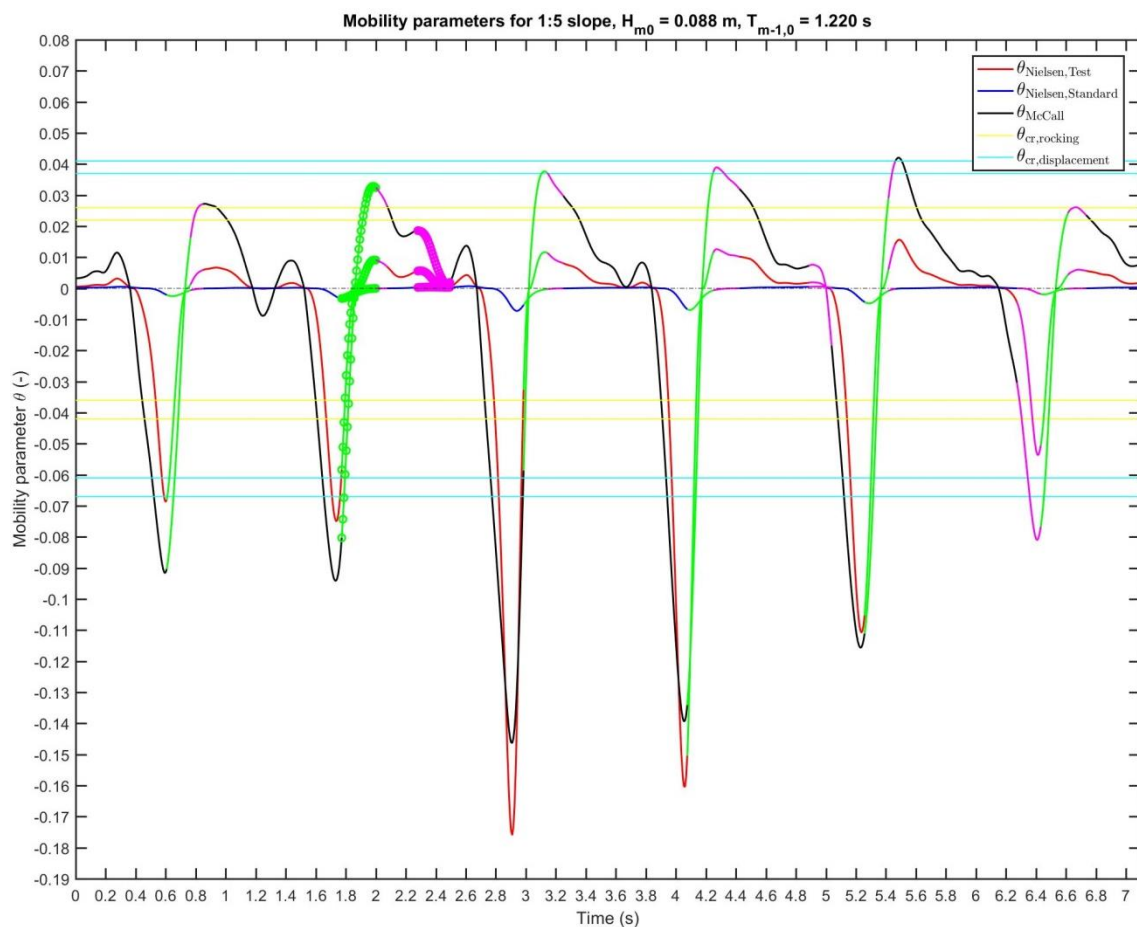


Figure 17 - Mobility parameters over time for 1:5 slope

In which: the mobility parameters have a negative value during run-up and the values of the mobility parameters are positive during run-down.

Furthermore, the type and the direction of the movements of the stone (from the visual analysis, see Table 17) are indicated in Figure 17. The green line with circles indicates displacement of a stone in upslope direction. The pink line with circles indicates displacement of a stone in downslope direction. The green line (without circles) shows rocking of a stone in upslope direction. The pink line (without circles) indicates rocking of a stone in downslope direction. In this way (with the results of the visual analysis), the stability parameters can be determined at the specific moment in time when the stone starts to move (i.e. initiation of motion of stone).

The critical, effective Shields parameters for rocking  $\theta'_{cr,rocking}$  and displacement  $\theta'_{cr,displacement}$  are shown in Figure 17 as horizontal lines. The critical, effective Shields parameters for the 1:5 slope are given in Table 18 (and elaborated in Section 3.2.7).

**Table 18 - Critical, effective Shields parameter for 1:5 slope**

Slope	Description of movements of stones		Direction	$\theta'_{cr}$	
1:5	Rocking	First stones start to move	Upslope	-0.036	-0.042
			Downslope	0.022	0.026
	Displacement	Beginning of transport of stones	Upslope	-0.061	-0.067
			Downslope	0.037	0.041

In which: the values of  $\theta'_{cr}$  are positive during run-down and  $\theta'_{cr}$  has a negative value during run-up.

As can be seen in Figure 17, the positive peaks of the mobility parameter  $\theta'_{McCall}$  (shown with black line) are between the stability parameters  $\theta'_{cr,rocking}$  and  $\theta'_{cr,displacement}$  for downslope movement (indicated with yellow and blue lines respectively). The positive values of  $\theta'_{Nielsen,Test}$  remain below  $\theta'_{cr,rocking}$ . Both the negative peaks of the mobility parameters  $\theta'_{Nielsen,Test}$  and  $\theta'_{McCall}$  exceed the stability parameter  $\theta'_{cr,displacement}$  for upslope movement significantly, and movements of stones in upslope direction occur (type: rocking and displacements). The values of  $\theta'_{Nielsen,Standard}$  are very small and are not in agreement with the values of  $\theta'_{Nielsen,Test}$  and  $\theta'_{McCall}$ .

When the stability parameters are exceeded by the mobility parameters, movements of stones are expected, according to theory (CIRIA et al., 2007; McCall, 2015; Nielsen, 2006; Shields, 1936). Once the values of the mobility parameters come below the stability parameters, no movements should occur. However, this is not observed in Figure 17. Movements of stones in upslope direction (indicated in green) start to occur when the mobility parameter  $\theta'_{McCall}$  is already decreasing in negative value (from the negative peaks towards positive values) and not when the stability parameters  $\theta'_{cr,displacement}$  and  $\theta'_{cr,rocking}$  for upslope movement are exceeded for the first time. The movements of stones are expected to stop if  $\theta'_{McCall}$  decreases to a value below the stability parameters  $\theta'_{cr,displacement}$  and  $\theta'_{cr,rocking}$  for upslope movement. However, the stones keep moving. Even when  $\theta'_{McCall}$  has a value of zero or become positive, movements of stones in upslope direction are observed. For the positive peaks of  $\theta'_{McCall}$ , movements of stones in downslope direction (shown in pink) occur. Moreover, movements of stones in downslope direction (type: rocking) are found when the mobility parameter does not exceed the stability parameters  $\theta'_{cr,displacement}$  and  $\theta'_{cr,rocking}$  for downslope movement (at  $t = 2.280$  s, at  $t = 4.886$  s, and at  $t = 6.273$  s).

## 5.2 Results of BIV analysis of videos with 1:10 and 1:15 slope

The results of the BIV analysis of the videos with 1:10 and 1:15 slope are elaborated extensively in Appendix D. The results are analyzed in the same way as has been done in Section 5.1.

The movements of stones in the videos with 1:10 and 1:15 slopes are limited because the FOV contains stones that are glued to a strip (explained in Section 3.2.1). However, from the videos of the profile change experiments and the videos of the preparation of the BIV experiments of Kramer (2016) with regular waves for the (1:5 and) 1:10 slopes could be observed that rocking of many stones and displacements of some stones occur at several locations. These movements of stones occur at several locations over the width of the flume and corresponds to transport stage 3 of Breusers and Schukking (1971). In the videos from the experiments with 1:15 slopes fewer movements of stones are observed. These movements seem to agree with transport stage 1 (described as: occasional movements of stones at some locations). The difference in movements per slope is taken into account when examining the mobility parameters derived from the BIV analyzed videos.

## 5.3 Overview of velocity, acceleration and mobility parameters per slope

An overview of the results of the BIV analysis of the videos of the BIV experiments of Kramer (2015) for the 1:5, 1:10 and 1:15 slope is given in Table 19. The minimum, the mean and the maximum values of the velocity, the acceleration and the mobility parameters are presented. The methodology of the BIV analysis to determine the horizontal velocity and acceleration is elaborated in Section 3.2.5. The derivation of the mobility parameters is treated in Section 3.2.6.

Table 19 - Values of velocity, acceleration and mobility parameters from BIV analysis of videos, per slope

Slope		1:5	1:10	1:15
Video		05_BIV_0001	10_BIV_0003	15_BIV_0005
<b>U</b> (m/s)	min	-0.317	-0.348	-0.293
	mean	-0.007	0.050	-0.014
	max	0.152	0.295	0.164
<b>dU/dt</b> (m/s <sup>2</sup> )	min	-2.462	-2.599	-1.488
	mean	0.003	0.101	0.001
	max	1.286	1.761	1.467
<b>θ'<sub>Nielsen,Test</sub></b> (-)	min	-0.176	-0.141	-0.096
	mean	-0.010	-0.006	-0.005
	max	0.016	0.038	0.056
<b>θ'<sub>Nielsen,Standard</sub></b> (-)	min	-0.006	-0.007	-0.004
	mean	0.000	0.000	0.000
	max	0.001	0.004	0.001
<b>θ'<sub>McCall</sub></b> (-)	min	-0.146	-0.137	-0.077
	mean	-0.008	0.001	-0.002
	max	0.042	0.071	0.063

In which: the values are negative during run-up and the values are positive during run-down. The largest negative values and the largest positive values have a background color of   and the smallest values have a background color of  . The values in between have a background color of  . The values of the mobility parameter  $\theta'_{Nielsen,Standard}$  are indicated with a background color of  , because they are very small and do not agree with the values of the mobility parameters  $\theta'_{Nielsen,Test}$  and  $\theta'_{McCall}$ .

## 5.4 Analysis of results of BIV analysis

### 5.4.1 Movements of stones according to visual observations and mobility parameters

The analysis of the movements of stones has been done by means of visual observations and by means of the mobility parameters. The following points have been found.

- From the visual observations, of the movements of stones in the videos of the preparation of the BIV experiments of Kramer (2016) with regular waves for the 1:5, 1:10 and 1:15 slopes it is found that more movements of stones occur for the 1:5 and 1:10 slopes (i.e. rocking of many stones and displacements of some stones occur at several locations) than for the 1:15 slopes (i.e. rocking of some stones (and sometimes displacements) at some locations).
- From the visual observations, the movements of stones (type: rocking and displacements) occur mainly during run-up and fewer movements (type: rocking) of stones are observed during run-down.
- As can be seen in Table 19, the extreme minimum values (during run-up) of the mobility parameters  $\theta'_{\text{Nielsen,Test}}$  and  $\theta'_{\text{McCall}}$  for the 1:5 and 1:10 slopes are larger than the extreme minimum values of the mobility parameters for the 1:15 slope.
- The extreme minimum values (during run-up) of the mobility parameters  $\theta'_{\text{Nielsen,Test}}$  and  $\theta'_{\text{McCall}}$  are larger in magnitude than the extreme maximum values (during run-down). Thus, run-up causes more movements of stones than run-down. This is true for all three slopes.

From the above four points, it can be concluded that the results in Table 19 match the visual observations of the videos regarding the movements of stones.

### 5.4.2 Sensitivity of formula of Nielsen (2006) to sediment friction factor and phase lag angle

The sensitivity of the bed-load transport formula of Nielsen (2006) is shown in Table 19. The bed-load transport formula of Nielsen (2006) has been applied with standard values ( $f_s = 0.025$  and  $\varphi_\tau = 25^\circ$  (McCall, 2015)) and with test values (derived from the BIV experiments of Kramer (2016)). The following points have been found.

- Standard values (from McCall (2015)) for the sediment friction factor and the phase lag angle are used. Thus, the parameters are not calibrated for the specified conditions. This results in significantly small values of the mobility parameter  $\theta'_{\text{Nielsen,Standard}}$ , shown in Table 19.
- The extreme minimum and maximum values of the mobility parameter  $\theta'_{\text{Nielsen,Standard}}$  (indicated with a yellow background colour), determined with the bed-load transport formula of Nielsen (2006) with standard values for the sediment friction factor and the phase lag angle are very small compared with the values of the mobility parameter  $\theta'_{\text{Nielsen,Test}}$ .
- The values of  $\theta'_{\text{Nielsen,Standard}}$  are not in agreement with the movements of stones observed in the videos and do not match to the values of the critical, effective Shields parameters (corresponding to the visual observations and derived from the transport stages of Breusers & Schukking (1971) (see Section 3.2.1)).
- For all three slopes, the values of the mobility parameter  $\theta'_{\text{Nielsen,Test}}$  determined with test values for the sediment friction factor and the phase lag angle, are more or less in agreement with the movements of stones observed in the videos.

From the above three points, it can be concluded that the results obtained with the bed-load transport formula of Nielsen (2006) are very sensitive to the sediment friction factor and the phase lag angle. This has already been found in Section 4.3.3. Again, the results obtained with the bed-load transport formula of Nielsen (2006) should be examined carefully.

### 5.4.3 Trend: decreasing mobility parameter for milder slopes

The magnitude of the extreme minimum and maximum values of the mobility parameters  $\theta'_{\text{Nielsen,Test}}$  and  $\theta'_{\text{McCall}}$  for the 1:5 and 1:10 slopes are examined, because the same amount of movements of stones was observed in the videos for these slopes.

According to theory (see Table 12 and Table 13 in Section 3.2.7), the extreme minimum and maximum values of  $\theta'_{\text{Nielsen,Test}}$  and  $\theta'_{\text{McCall}}$  should become smaller when the slope becomes milder. This is true for the minimum values of  $\theta'_{\text{Nielsen,Test}}$  and  $\theta'_{\text{McCall}}$  (shown bold and in red in Table 19). However, this is not the case when looking at the extreme maximum values (shown bold and in black in Table 19). For both  $\theta'_{\text{Nielsen,Test}}$  and  $\theta'_{\text{McCall}}$ , the extreme maximum values increase when the slope becomes milder (from 1:5 to 1:10 slope).

**Note:** The values of the mobility parameters for different slopes are compared with each other, because the hydrodynamic forces that act on a stone are determined with the local velocity and acceleration near the bed (in the ROI) are examined. However, it should be taken into account that the type of wave breaking for the different slopes is not the same (as the Iribarren number is not constant, see Table 7). The type of wave breaking is implicitly included in the velocity and the acceleration with the difference in wave impact on the slope (i.e. plunging or surging breakers, elaborated in Section 2.1.2).

### 5.4.4 Results of BIV analysis of this research compared to results of Kramer (2016)

The results of the BIV analysis executed in this research are compared with the results of the BIV analysis done by Kramer (2016). Different videos are analyzed by Kramer (2016) for the 1:5 and 1:10 slopes. However, because all BIV experiments of Kramer (2016) are performed with regular waves, the values of the velocity and the acceleration derived from the BIV analysis should be in the same order of magnitude. The results of Kramer (2016) are presented in Table 20.

Table 20 - Values of U and dU/dt from BIV analysis derived by Kramer (2016), per slope

Slope		1:5	1:10	1:15
Video		05_BIV_0002	10_BIV_0006	15_BIV_0005
U (m/s) Kramer (2016)	min	-0.187	-0.208	-0.258
	max	0.124	0.238	0.173
dU/dt (m/s <sup>2</sup> ) Kramer (2016)	min	-1.146	-1.574	-1.111
	max	0.872	1.282	0.828

In which: the values are negative during run-up and the values are positive during run-down. The largest negative values and the largest positive values have a background color of   and the smallest values have a background color of  . Values in between have a background color of  .

As can be seen in Table 19 and in Table 20, the extreme minimum and maximum values of the velocity and the acceleration of the BIV analysis in this research are larger than the values (shown in black in Table 20) obtained by Kramer (2016) (except for the maximum velocity of 1:15 slope, shown in red). This can be clarified by the different methodologies applied when fitting the curve through the scattered data points of the horizontal velocity (see Section 3.2.5). In this research, the curve is fitted more through the peaks of negative data points, whereas Kramer (2016) smoothed the data more. The negative and positive peaks of the fitted curve of the horizontal velocity of Kramer (2016) are therefore less extreme. The lower values of the horizontal velocity derived by Kramer (2016) resulted in lower values of the acceleration, which is the derivative of the velocity over time. Both parameters are used to determine the mobility parameters  $\theta'_{\text{Nielsen,Test}}$  and  $\theta'_{\text{VanRijn}}$  (called  $\theta'_{\text{McCall}}$  in this research). Therefore, the values of the mobility parameters are lower as well.

Besides, the same trend with highest values (with green background color in Table 20) for the 1:10 slope is observed (except for the minimum velocity (see 1:15 slope)).

## 5.5 Discussion

### 5.5.1 Glued stones in DOF give no or limited movements of stones

Only limited movements of stones is observed in the video with a 1:5 slope, while hardly any movements of stones are visible in the videos with 1:10 and 1:15 slopes. The movements of stones are limited in the DOF due to the strip of glued stones. However, from visual observations of the profile change experiments by Kramer (2016) and the videos of the preparation of the BIV experiments of Kramer (2016) with regular waves could be observed that movements of stones occur at several locations over the width of the flume. This is taken into account when analyzing the results of the BIV analysis regarding the initiation of motion of stones for the different slopes.

### 5.6 Analysis of coefficients $c_f$ and $c_i$ in bed shear stress of $\theta'_{McCall}$

The mobility parameter  $\theta'_{McCall}$  in equation (5.1) is obtained with the bed shear stress, given in equation (5.2) (and treated in Section 2.5.3). In the formula of the bed shear stress, the drag term consists of the sediment friction factor  $c_f$  (determined with equation (5.3)), the density  $\rho$  and the horizontal velocity  $U$  (derived from the BIV analysis). The inertia term is determined with the density  $\rho$ , the inertia coefficient  $c_i$  ( $= c_m c_v c_n$ ), the mean diameter of the stone  $D_{50}$  and the acceleration  $dU/dt$  (derived from the BIV analysis).

$$\theta'_{McCall} = \frac{\tau_b}{(\rho_s - \rho_w)gD_{50}} \cos \beta \left( 1 \pm \frac{\tan \beta}{\tan \phi} \right) \quad (5.1)$$

$$\tau_b = \underbrace{c_f \rho U |U|}_{drag} + \underbrace{\rho c_m c_v c_n D_{50} \frac{\partial u}{\partial t}}_{inertia} = \underbrace{c_f \rho U |U|}_{drag} + \underbrace{\rho c_i D_{50} \frac{\partial u}{\partial t}}_{inertia} \quad (5.2)$$

$$c_f = \frac{9.81}{\left( 18 \log \left( \frac{12 h_{ROI}}{k_s} \right) \right)^2} \quad (5.3)$$

In which:  $h_{ROI}$  is the water depth at the ROI (m), and  $k_s$  is the characteristic roughness height (assumed to be  $3D_{90}$ , as for flat beds according to Van Rijn (1982)). The values of the all relevant input parameters that are used to determine the sediment friction factor  $c_f$  and the inertia coefficient  $c_i$  are given in Table 10 and Table 11 in Section 3.2.6.

The sediment friction factor  $c_f$  and the inertia coefficient  $c_i$  can be seen as calibration coefficients for the drag and inertia term of the bed shear stress. For each slope, the mobility parameter  $\theta'_{McCall}$  has been obtained with the bed shear stress using the values of  $c_f$  and  $c_i$ , shown in Table 21. The sediment friction factor  $c_f$  varies per slope (due to different values for  $h_{ROI}$  per slope). The inertia coefficient  $c_i$  has a constant value.

Table 21 - Values of coefficients  $c_f$  and  $c_i$  per slope (this research)

Slope	$c_f$ (-)	$c_i$ (-)	Ratio $c_i/c_f$ (-)
1:5	0.054	0.780	14.4
1:10	0.031	0.780	25.2
1:15	0.025	0.780	31.2

The use of equation (5.3) to determine the sediment friction factor  $c_f$  per slope is arguable. Normally, the formula is applied in case of a developed, uniform flow with a logarithmic velocity profile over the entire water depth. In this research, the state of the flow is different (i.e. oscillating flow with breaking waves), and the only a small part of the water depth is used to determine the horizontal velocity (i.e. the ROI with a height of  $1D_{n50}$ ). Therefore, a constant value of the sediment friction factor seems to be better applicable. The values in Table 21 are used in the first instance to compare the results of the BIV analysis with the results of Kramer (2016), who also applied the equation (5.3). A constant value of the sediment friction factor (that is not dependent on the water depth) is investigated below.

The values of the coefficients  $C_B$  and  $C_M$  (representing  $c_f$  and  $c_i$  respectively) from previous research into the influence of flow accelerations on the stability of stones on a horizontal bed (Dean & Dalrymple, 1991; Dessens, 2004; Steenstra et al., 2016) or sloping bed (Tromp, 2004) can be used for reference. The values of  $C_B$  and  $C_M$  and the corresponding ratio are presented in Table 22. The ratio  $c_f/c_i$  of the 1:5, 1:10 and 1:15 slopes (shown in Table 21) are in the range of the ratio  $C_M/C_B$  found by Dessens (2004) and Tromp (2004). The average of the ratios in Table 21 is 23.6, which is almost equal to the ratio  $C_M/C_B$  of Steenstra et al. (2016). According to Steenstra et al. (2016), the ratio  $C_M/C_B$  with a value of 23.0 predicts the influence of accelerations on the mobility parameter correctly.

**Table 22 - Values of coefficients  $C_B$  and  $C_M$  from previous research**

Research of	$C_B$ (-)	$C_M$ (-)	Ratio $C_M/C_B$ (-)
Dean and Dalrymple (1991)	0.4	2.0	5.0
Dessens (2004)	0.10 - 0.14	3.92 - 5.55	39.2 - 39.6
Tromp (2004)	0.40 - 0.55	2.67 - 3.75	4.9 - 9.4
Steenstra et al. (2016)	-	-	23.0

The extreme minimum and maximum values of the mobility parameter  $\theta'_{McCall}$  (after slope correction) for the 1:5 slope should match the extreme minimum and maximum values of  $\theta'_{McCall}$  (after slope correction) for the 1:10 slope, because the same amount of movements of stones is observed in the videos of both slopes. Because the movements of stones occur mainly during run-up and fewer movements of stones are observed during run-down, the negative peaks of  $\theta'_{McCall}$  are used to calibrate the sediment friction factor  $c_f$  and the inertia coefficient  $c_i$ . The negative peaks of  $\theta'_{McCall}$  (after slope correction) for the 1:5 and 1:10 slope are in agreement with each other for the coefficients  $c_f$  and  $c_i$  given in equation (5.4). These values have been derived iteratively. The ratio  $c_f/c_i$  is 20.0, which is in the range of the ratios  $c_f/c_i$  shown in Table 21 and the ratios  $C_M/C_B$  of previous research presented in Table 22.

$$c_f = 0.04, \quad c_i = 0.80 \quad (5.4)$$

The extreme minimum and maximum values of the mobility parameter  $\theta'_{McCall}$  determined with the new values for the coefficients  $c_f$  and  $c_i$  for the 1:5 and 1:10 slopes are shown in Table 23. The values of  $\theta'_{McCall}$  for the 1:15 slope are included as well.

**Table 23 - Values of mobility parameter  $\theta'_{McCall}$  with new  $c_f$  and  $c_i$  from BIV analysis of videos, per slope**

Slope		1:5	1:10	1:15
Video		05_BIV_0001	10_BIV_0003	15_BIV_0005
$\theta'_{McCall}$ (-) (new $c_f$ & $c_i$ )	min	-0.148	-0.141	-0.080
	max	0.044	0.073	0.064

In which: the values are negative during run-up and the values are positive during run-down.

The mobility parameter  $\theta'_{McCall}$  determined with the new values for the coefficients  $c_f$  and  $c_i$  for the 1:5, 1:10 and 1:15 slopes are plotted over time in Figure 18 in Section 5.7, and in Figure 47 and Figure 52 in Appendix D respectively. The extreme maximum values of  $\theta'_{McCall}$  (after slope correction) for the 1:5 and 1:10 slopes do not match. As can be seen in Figure 18 and in Figure 47, the values (with a range of 0.027 - 0.044) of the positive peaks of  $\theta'_{McCall}$  for the 1:5 slope are smaller than the values (with a range of 0.049 - 0.073) of the positive peaks of  $\theta'_{McCall}$  for the 1:10 slope. This can be explained by the difference in the maximum value of the horizontal velocity (shown in Table 19 in Section 4.2), derived from the BIV analyzed videos. The maximum value of the horizontal velocity of the 1:10 slope is larger than the maximum value of the horizontal velocity of the 1:5 slope. This outcome cannot be altered with other constant values for the coefficients  $c_f$  and  $c_i$ .

## 5.7 Analysis of stability parameter $\theta_{cr}$

### 5.7.1 Analysis of stability parameters $\theta'_{cr,displacement}$ and $\theta'_{cr,rocking}$

When the stability parameters  $\theta'_{cr,displacement}$  and  $\theta'_{cr,rocking}$  are exceeded by the mobility parameter  $\theta'_{McCall}$ , movements of stones are expected, according to theory (CIRIA et al., 2007; McCall, 2015; Nielsen, 2006; Shields, 1936). Once the value of the mobility parameter comes below the stability parameters, no movements should occur.

This is not observed in Figure 17 (in Section 5.1) for the 1:5 slope and in Figure 46 (in Appendix D.2) for the 1:10 slope.

- No movements of stones are initiated when the stability parameters  $\theta'_{cr,displacement}$  and  $\theta'_{cr,rocking}$  for upslope movement are exceeded for the first time.
- Movements of stones in upslope direction (indicated in green in the figures) start to occur when the value of the mobility parameter  $\theta'_{McCall}$  is already near the negative peak or has already passed the negative peak and decreases in value.
- The movements of stones are expected to stop if the mobility parameter  $\theta'_{McCall}$  decreases to a value below the stability parameters  $\theta'_{cr,displacement}$  and  $\theta'_{cr,rocking}$  for upslope movement. However, the stones keep moving. Even when the mobility parameter  $\theta'_{McCall}$  has a value of zero or becomes positive, movements of stones occur.

From the above points, it can be concluded that  $\theta'_{cr,displacement}$  and  $\theta'_{cr,rocking}$  (with the applied values, given in Table 13 in Section 3.2.7) are not able to function as an instantaneous threshold for movements of stones on mild slopes under wave attack (i.e. not able to determine the occurrence of movements of stones). However, the stability parameters can be used to determine the initiation of motion of stones.

The values of  $\theta'_{cr,displacement}$  and  $\theta'_{cr,rocking}$  are originally derived for uniform flow, in which the hydrodynamic forces related to the horizontal velocity near the bottom plays an important role (see Section 2.2.1). This research looks at an oscillating flow (with waves breaking on a mild slope) where the hydrodynamic due to horizontal pressure differences (created by accelerations) have a large influence on the stability of stones (according to the mobility parameter  $\theta'_{McCall}$ ). The stability parameters  $\theta'_{cr,displacement}$  and  $\theta'_{cr,rocking}$  are used to get a first estimation of the critical value for which initiation of motion of stones occurs. When downslope movements of stones (type: rocking) are observed, the positive values of the mobility parameter  $\theta'_{McCall}$  (during run-down) are mainly in the range of  $\theta'_{cr,rocking}$ . Upslope movements of stones (type: rocking and displacements) occur mainly for the negative values of the mobility parameter  $\theta'_{McCall}$  (during run-up) that exceed  $\theta'_{cr,displacement}$ .

significantly. This has already been found in Section 5.4.1. The stability parameter  $\theta_{cr}$  for downslope and upslope movements of stones is investigated in Section 5.7.2.

**Note:** no movements of stones are found from the visual analysis of the movements of the stone of video 15\_BIV\_0005 (see results in Appendix D.3), because the FOV contains stones that are glued to a strip (explained in Section 3.2.1). Therefore, the ability of  $\theta'_{cr,displacement}$  and  $\theta'_{cr,rocking}$  to function as a threshold for the initiation of motion of stones on 1:15 slopes under wave attack could not be assessed accurately. When the negative peaks of the mobility parameter  $\theta'_{McCall}$  exceed the values of  $\theta'_{cr,rocking}$  and  $\theta'_{cr,displacement}$ , rocking of stones is expected to occur (based on visual observations of the videos of the profile change experiments and videos of the preparation of the BIV experiments of Kramer (2016)).

### 5.7.2 New value for stability parameter $\theta_{cr}$ determined with $\theta'_{McCall}$ with new $c_f$ and $c_i$

An attempt is made to define a new value for the stability parameter  $\theta_{cr}$  for each slope, because the values of  $\theta'_{cr,displacement}$  and  $\theta'_{cr,rocking}$  (given in Table 13 in Section 3.2.7) are not able to describe the initiation of motion of stones accurately.

Because movements of stones are observed in the BIV analyzed video 05\_BIV\_0001 for the 1:5 slope (and hardly any or no movements of stones occurred in the BIV analyzed videos for the 1:10 and 1:15 slopes), the results of the mobility parameter  $\theta'_{McCall}$  for the 1:5 slope are used to find new value for the stability parameter  $\theta_{cr}$  for downslope and upslope movements of stones. The mobility parameter  $\theta'_{McCall}$ , determined with the new values for the coefficients  $c_f$  and  $c_i$ , is plotted over time for the 1:5 in Figure 18.

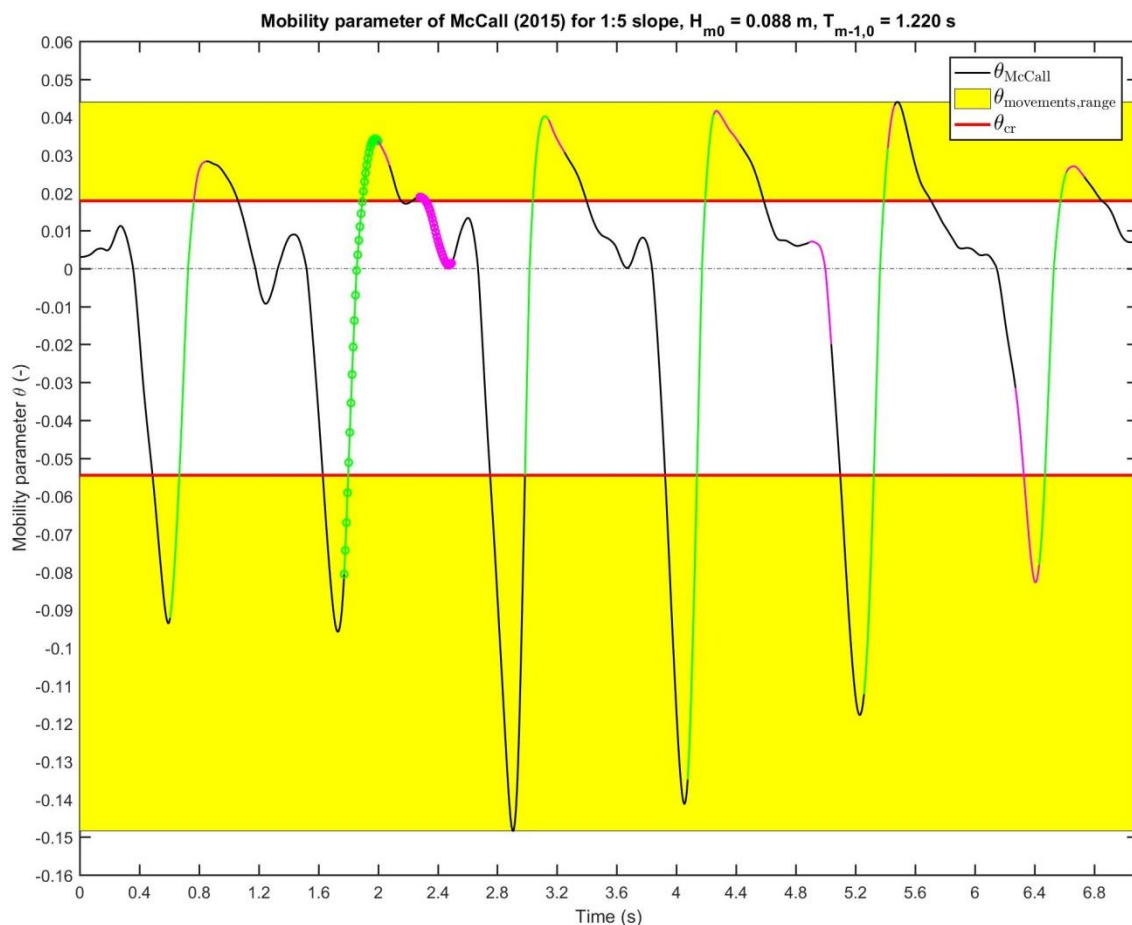


Figure 18 - Mobility parameter  $\theta'_{McCall}$  over time with new  $c_f$  and  $c_i$  for 1:5 slope

In which: the mobility parameters have a negative value during run-up and the values of the mobility parameters are positive during run-down.

Furthermore, the type and the direction of the movements of the stone (from the visual analysis, see Table 17) are indicated in Figure 18. The green line with circles indicates displacement of a stone in upslope direction. The pink line with circles indicates displacement of a stone in downslope direction. The green line (without circles) shows rocking of a stone in upslope direction. The pink line (without circles) indicates rocking of a stone in downslope direction. In this way (with the results of the visual analysis), the stability parameters can be determined at the specific moment in time when the stone starts to move (i.e. initiation of motion of stone).

The ranges with movements of stones are depicted in yellow in Figure 18. The ranges of  $\theta'_{\text{movements,range}}$  start at the minimal values of  $\theta'_{\text{McCall}}$  for which the first movements of stones are observed in the BIV analyzed video 05\_BIV\_0001. These minimal values are indicated with  $\theta_{\text{cr}}$  (shown in red in Figure 18). The first downslope movements of stones occur for a value of 0.018. The first upslope movements of stones are observed for a value of -0.054. The upper limits of the ranges are the positive and negative peaks of  $\theta'_{\text{McCall}}$ .

The mobility parameter  $\theta'_{\text{McCall}}$  determined with the new values for the coefficients  $c_f$  and  $c_{ir}$  are plotted over time for the 1:10 and 1:15 slopes in Figure 47 and Figure 52 in Appendix D respectively.

For each slope, the value of  $\theta_{\text{cr}}$  can be seen as a first estimate of the critical value for which movements of stones start to occur. The values of  $\theta_{\text{cr}}$  are given in Table 24.

Table 24 - Values of stability parameter  $\theta_{\text{cr}}$ , per slope

Slope	Downslope correction factor	$\theta_{\text{cr}}$ (-)
1:5	0.747	0.018
1:10	0.877	0.021
1:15	0.919	0.022
No correction factor (i.e. horizontal bottom)	1.000	0.024

**Note I:** the type of movements of stones, which has been used to derive the critical value of the 1:5 slope, is mainly rocking of stones (as was observed in the videos of the profile change experiments and the videos of the preparation of the BIV experiments of Kramer (2016) for the 1:5 slope).

**Note II:** for the 1:10 and 1:15 slopes, the ranges of  $\theta'_{\text{movements,range}}$  start at the minimal values of  $\theta'_{\text{McCall}}$  for which the first movements of stones are observed in the BIV analyzed video 05\_BIV\_0001. Thus, the value of  $\theta'_{\text{cr}}$  for initiation of motion of stones for the 1:10 and 1:15 slopes is derived from the value of  $\theta'_{\text{cr}}$  for the 1:5 slope (shown in red in Table 24), using the slope correction factors of Section 3.2.6.

When examining the value of the stability parameter  $\theta_{\text{cr}}$ , the following points have been found.

- It appears that the stability parameter  $\theta_{\text{cr}}$  could be a value of 0.024 (in case no slope correction factor is applied (i.e. for a horizontal bottom)). To define a threshold for initiation of motion of stones on mild slopes under wave attack, this value could be used as a first indication.
- The value of 0.024 of  $\theta_{\text{cr}}$  is lower than the value of 0.030 of  $\theta_{\text{cr,rocking}}$  (CIRIA et al., 2007).

### 5.7.3 Stability parameter $\theta_{cr}$ in bed-load transport formulas of Nielsen (2006) and Van Rijn (2007)

The stability parameter  $\theta_{cr}$  is included in the bed-load transport formulas of Nielsen (2006) and Van Rijn (2007) (elaborated in Section 2.5.4 and in Section 2.5.6 respectively). This  $\theta_{cr}$  has a value of 0.055 and corresponds to the upper limit of  $\theta_{cr,displacement}$  (examined in this research).

No transport ( $q = 0$ ) should be determined with the bed-load transport formulas if the values of the mobility parameters  $\theta'_{Nielsen,Test}$  and  $\theta'_{McCall}$  are below the values of  $\theta_{cr}$ . When looking at the results of the BIV analysis (see Figure 17 in Section 5.1 for the 1:5 slope and Figure 46 in Appendix D.2 for the 1:10 slope), the following points have been found.

- Movements of stones ( $q \neq 0$ ) are observed while the values of  $\theta'_{Nielsen,Test}$  and  $\theta'_{McCall}$  decrease below the value of  $\theta_{cr}$ .
- The value of 0.055 of the stability parameter  $\theta_{cr}$  seems to be incorrect and needs to be adjusted to define the threshold for initiation of motion for stones on mild slopes under wave attack more accurately. The values of  $\theta_{cr}$ , presented in Table 24, can be used as a first indication.
- A new value of the stability parameter could improve the amount of sediment transport modelled in XBeach-G with the bed-load transport formulas of Nielsen (2006) and Van Rijn (2007). In this way, the damage characteristics, derived from the modelled erosion profiles, can be determined more accurately.

From the above three points, it can be concluded that the sediment transport of stones on mild slopes under to wave attack cannot be determined accurately by the bed-load transport formulas of Nielsen (2006) and Van Rijn (2007), because the implemented stability parameter is not able to determine whether movements of stones occur or not.

## 5.8 Link mobility parameter $\theta'_{McCall}$ with numerical model XBeach-G

An attempt is made to link both parts of this research by connecting the mobility parameter regarding initiation of motion (part 2) with the numerical model XBeach-G (part 1). The mobility parameter  $\theta'_{McCall}$  and the erosion profiles modelled in XBeach-G with the wave characteristics based on  $S_{Wit}$  input are examined. The mobility parameter  $\theta'_{McCall}$  is treated in Section 3.2.6. The input parameters of the erosion profiles are given in Section 3.1.1. The mobility parameter  $\theta'_{McCall}$  has been investigated in Section 5.4, Section 5.6 and Section 5.7 for a few regular waves (i.e.  $N = 3 - 6$ ) and is now examined for irregular waves with  $N = 3000$ .

**Note:** the wave characteristics of the regular waves in the BIV experiments of Kramer (2016), given in Table 7, are based on the highest one percent irregular waves ( $H_{1\%}$ ) of the  $S_{Wit}$  input of the profile change experiments of Kramer (2016).

### 5.8.1 Mobility parameter $\theta'_{McCall}$ over time along length of slope

For the 1:5 slope and  $S_{Wit}$  input, the velocity and the acceleration over time along the length of the 1:5 slope are presented in Figure 53 and in Figure 54 in Appendix E.1. The velocity and the acceleration are substituted in the formula of the bed shear stress. The mobility parameter  $\theta'_{McCall}$  can be determined with the bed shear stress. The mobility parameter over time ( $t_{model}$  is 3,159 s for  $N = 3000$ ) along the length of the 1:5 slope ( $x = 0.00$  m to  $x = 4.70$  m) is shown in Figure 19.

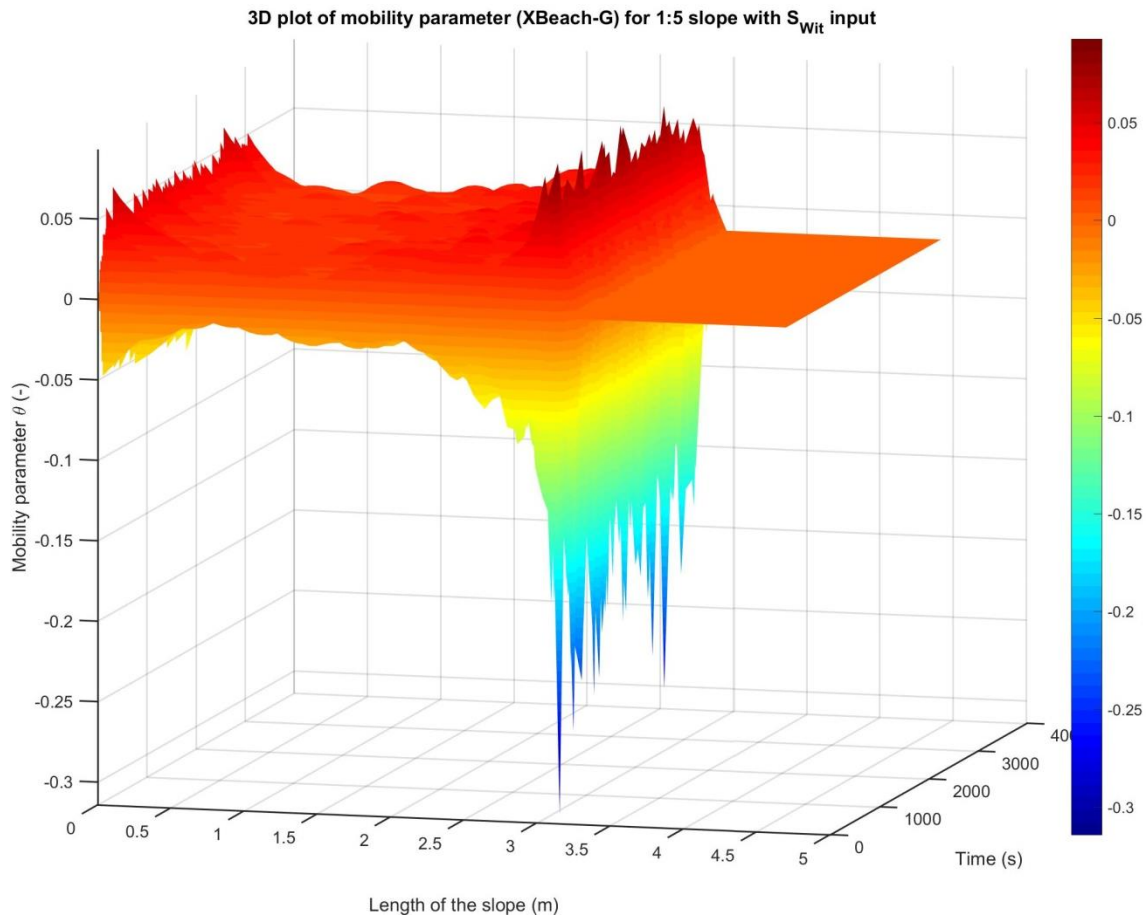


Figure 19 - Mobility parameter  $\theta'_{McCall}$  over time along length of 1:5 slope with  $S_{wit}$  input

In which: the mobility parameters have a negative value during run-up and the values of the mobility parameters are positive during run-down.

The velocity, the acceleration and the mobility parameter  $\theta'_{McCall}$  over time along the length of the 1:10 and 1:15 slopes are presented in Appendix E.2 and E.3 respectively.

The extreme minimum and maximum values of the velocity, the acceleration and the mobility parameter  $\theta'_{McCall}$  are given in Table 25.

Table 25 - Values of  $U$ ,  $dU/dt$  and  $\theta'_{McCall}$  from XBeach-G simulations with  $S_{wit}$  input, per slope

Slope		1:5	1:10	1:15
$U$ (m/s)	min	-0.323	-0.739	-0.998
	max	0.462	0.893	1.086
$dU/dt$ (m/s <sup>2</sup> )	min	-8.637	-23.946	-43.398
	max	3.365	5.751	7.614

Slope		1:5	1:10	1:15
$\theta'_{McCall}$ (-)	min	-0.307	-0.782	-1.080
	max	0.096	0.160	0.209

In which: the values are negative during run-up and the values are positive during run-down.

Based on the erosion profiles of the three slopes modelled in XBeach-G with the wave characteristics based on  $S_{Wit}$  input, the extreme minimum and maximum values in Table 25 occur in the damage zone, which can be described as the area where most damage occurs, located just below still water level (SWL) (see Appendix C). This is true for all three slopes.

The damage zone corresponds to the Field of View of the videos of the BIV experiments. Besides, the wave characteristics of the regular waves in the BIV experiments of Kramer (2016), given in Table 7, are based on the highest one percent (irregular) waves ( $H_{1\%}$ ) of the  $S_{Wit}$  input of the profile change experiments of Kramer (2016). For these  $H_{1\%}$  waves, initiation of motion of stones occurred. Because of this, the extreme minimum and maximum values in Table 19 (from the BIV analyzed videos) can be compared with the minimum and maximum values in Table 25 (from the XBeach-G simulations). The results with different slope angles cannot be compared with each other, because the type of wave breaking is not the same (as the Iribarren number is not constant, see Table 4).

When comparing the extreme minimum and maximum values of the horizontal velocity, the acceleration and the mobility parameter  $\theta'_{McCall}$  in Table 19 with the values in Table 25, the parameters do not match and the values differ significantly in magnitude. According to Postma (2016), the velocity and the acceleration in the hydrodynamics are modelled well in the numerical model XBeach-G. However, the extreme values of the velocity and the acceleration obtained with XBeach-G are significantly higher than the extreme values derived from the BIV analyzed videos. The difference in values is most extreme for the 1:15 slope. Moreover, very high and unrealistic values of the mobility parameter  $\theta'_{McCall}$  are determined in XBeach-G. These results were also found by Postma (2016). The higher values can be explained by the implemented hydrodynamics in XBeach-G, which is a one-layered model. Thus, the velocity and the acceleration are obtained for a depth-averaged flow in XBeach-G. The values of the local velocity and acceleration near the bed are lower (see the values derived locally using BIV).

The stones are not able to move in the FOV during the BIV experiments of Kramer (2016), because they are glued to a strip (see Section 3.2.1). Therefore, the influence of morphological updating of the bed in XBeach-G is investigated. The results of the XBeach-G simulations performed without morphological updating of the bed are shown in Table 41 in Appendix E.4.

- Without morphological updating of the bed, significantly lower values of the velocity, the acceleration and the mobility parameter  $\theta'_{McCall}$  are found for each slope.

Furthermore, the influence of the type of waves (i.e. regular vs. irregular waves) on the velocity, the acceleration and the mobility parameter  $\theta'_{McCall}$  is checked. The results of the XBeach-G simulations performed with regular waves are presented in Table 42 in Appendix E.5.

- With regular waves (and without morphological updating), the extreme minimum and maximum values of the velocity, the acceleration and the mobility parameter  $\theta'_{McCall}$  decrease even more.
- The values are still not in the range of the values derived from the BIV analyzed videos (given in Table 19).

The relation between the mobility parameter  $\theta'_{McCall}$  and the damage, which been described with the relative erosion depth  $d_e/D_{n50}$ , along the length of the slope is investigated in Appendix E.6.

## 6 Conclusions and recommendations

The conclusions and recommendations of this research are described in this chapter. The conclusions are summarized in Section 6.1. The recommendations for further research are given in Section 6.2.

### 6.1 Conclusions

The main conclusion is given by answering the main research question. The conclusion is further elaborated by means of the research objectives.

#### 6.1.1 Main research question

The main research question of this (and previous) research is repeated and elaborated below.

##### **How to describe the static stability of stones on mild slopes under wave attack?**

The static stability of stones on mild slopes under wave attack has been investigated in this research. Although not a specific design formula has been derived, suggestions for a design method based on the initiation of motion of stones are given.

- The effective, adapted Shields parameter  $\theta'_{McCall}$  can be used to describe movements of stones on mild slopes under wave attack.
- For initiation of motion of stones, the stability parameter  $\theta_{cr}$  has a value in the range of 0.024 (in case no slope correction factor is applied (i.e. for a horizontal bottom)). Minor optimization of this value is still required.

Furthermore, a lot of new insights have been gained regarding the hydrodynamics and the bed-load transport formulas of Nielsen (2006) and Van Rijn (2007) in the numerical model XBeach-G. These insights have been found by comparing the results of the XBeach-G simulations with the results of the physical scale model tests of Kramer (2016), which have been reanalyzed in this research.

- XBeach-G cannot determine the local velocity and acceleration near the bed, because the model solves the flow due to currents and waves for a single layer (i.e. the flow is depth-averaged).
- The bed-load transport formulas of Nielsen (2006) and Van Rijn (2007) are not able to model the sediment transport in XBeach-G accurately.
- XBeach-G cannot describe the static stability of stones on mild slopes under wave attack accurately.
- When applying XBeach-G as a tool to describe the static stability of stones on mild slopes under wave attack, the model gives (with the bed-load transport formula of Van Rijn (2007)) more conservative results than the extrapolated formula of Van der Meer (1988).

#### 6.1.2 Research objectives

The objectives of this research are repeated and elaborated below.

**Objective 1: To reproduce and analyse the results of the physical scale model tests regarding profile change of Kramer (2016) by means of the numerical model XBeach-G.**

The first objective has been investigated in Chapter 4 of this research. The erosion profiles modelled with the bed-load transport formulas of Nielsen (2006) and Van Rijn (2007) in XBeach-G are not in agreement with the erosion profiles of the profile change experiments of Kramer (2016), because the values of the damage characteristics and the profile development differ significantly. Therefore, the applied bed-load transport formulas are not able to model the sediment transport correctly in XBeach-G. XBeach-G should not be used to describe static stability of stones on mild slopes under

wave attack. Furthermore, the results obtained with the bed-load transport formula of Nielsen (2006) are very sensitive to the sediment friction factor and the phase lag angle. This has already been found by McCall (2015).

**Objective 2:** To validate/falsify the conclusions drawn by Postma (2016) about modelling sediment transport of stones on mild slopes under wave attack using the bed-load transport formulas of Nielsen (2006) and Van Rijn (2007).

The second objective has been met. In Chapter 4, the conclusions drawn by Postma (2016) about the bed-load transport formulas of Nielsen (2006) and Van Rijn (2007) have been validated/falsified. This has been done by comparing the results of the XBeach-G simulations with the (reanalyzed) results of the profile change experiments of Kramer (2016). Additionally, the conclusion of Postma (2016) about the hydrodynamics in XBeach-G has been refuted, because the hydrodynamics are not implemented correctly. The model cannot determine the local hydrodynamics near the bed, because the flow is solved for a single layer (i.e. the flow is depth-averaged). Therefore, the values of the velocity and the acceleration obtained with XBeach-G are significantly higher than the values derived from the BIV analysis of the videos of the BIV experiments of Kramer (2016). This also causes the significant differences in damage characteristics of the modelled and measured erosion profiles.

**Objective 3:** To describe initiation of motion of a stone by looking at the hydrodynamic forces that act on a stone on a mild sloping bed under wave attack.

The third objective has been set, because the first two objectives about XBeach-G did not give the expected outcome (i.e. the results of the physical scale model tests of Kramer (2016)). Therefore, the local hydrodynamic forces, which have been derived from the velocity and the acceleration near the bed, are examined with BIV. The results are presented in Chapter 5. The mobility parameter  $\theta'_{\text{McCall}}$ , which is an effective, adapted Shields parameter, is able to describe movements of stones on mild slopes under wave attack.

**Objective 4:** To develop a design method that describes the static stability of stones on mild slopes under wave attack based on the initiation of motion of stones.

The fourth objective elaborates on the results of the third objective. In Chapter 5, a critical value for which stones start to move has been found, when describing movements of stones with the mobility parameter  $\theta'_{\text{McCall}}$ . It appears that the stability parameter  $\theta_{\text{cr}}$  could be a value of 0.024 (in case no slope correction factor is applied (i.e. for a horizontal bottom)). To develop a design method that describes the static stability of stones on mild slopes under wave attack based on the initiation of motion of stones, the value of 0.024 of the stability parameter  $\theta_{\text{cr}}$  could be used. Furthermore, an attempt has been made to link both parts of this research by connecting the mobility parameter regarding initiation of motion (part 2) with the numerical model XBeach-G (part 1). It has been found that the hydrodynamics, implemented by McCall (2015), in XBeach-G are not in agreement with the hydrodynamics derived from the BIV analyzed videos.

## 6.2 Recommendations

The recommendations for further research are elaborated below.

- The values of the horizontal velocity and the acceleration obtained with XBeach-G (with irregular waves) are significantly higher than the values derived from the BIV analyzed videos (with regular waves). It is recommended to do more research on this subject. By improving the way to determine the velocity and the acceleration, the mobility parameter becomes more accurate.

This will lead to a better description of the initiation of movement of stones. The following recommendations are suggested.

- XBeach-G solves the flow due to currents and waves for a single layer (i.e. the flow is depth-averaged). No distinction has been made between the velocity and the acceleration at the water surface (where the wave breaking occurs) and the hydrodynamics near the bed. When examining the initiation of motion of stones near the bed, the local (i.e. near bed) velocity and acceleration are needed to determine the hydrodynamic forces that cause initiation of motion of stones accurately. A model that solves the hydrodynamics for multiple layers should be applied in further research. In this way, the local hydrodynamics near the bed can be used to determine the hydrodynamic forces (acting on the stones). Such a model could be the numerical model SWASH (Zijlema et al., 2011b). The model SWASH does not include morphological updating of the bed. However, this is not a requirement when investigating the static stability of stones, because for static stability no or only minor movements of stones are allowed.
  - Additionally, the velocity and the acceleration corresponding to the breaking of the irregular wave with the highest significant wave height (obtained with XBeach-G) could be investigated to validate/falsify the implemented hydrodynamics. By zooming in on this single wave, a spike (i.e. high peak) is expected to occur due to high values of the acceleration.
  - In this research, a smoothened line has been used to fit a curve through the scattered data of the horizontal velocity, which has been obtained from the BIV analysis. This flattens out the extreme values of the scattered data. To investigate the effects of this, a curve should be plotted through the extreme values only of the scattered data of the horizontal velocity.
- More experiments need to be executed to derive a design method for static stability of stones on mild slopes under wave attack. The focus of these experiments should be on the calibration of the stability parameter  $\theta_{cr}$  to optimize the value of 0.024. By using a statistical value for the stability parameter (like  $\theta_{cr,1\%}$ ), the stability parameter will describe the static stability of stones by means of a certain number of stones that are allowed to move (or by means of a certain acceptable damage) for a certain number of waves (i.e.  $N = 1000$  or  $N = 3000$ ). Preferably, the value of the stability parameter can be determined from the wave characteristics. This is the next step that has to be done to develop a design method that describes the static stability of stones on mild slopes under wave attack based on the initiation of motion of stones.
  - For different slope angles, profile change experiments and XBeach-G simulations need to be performed with a constant value of the Iribarren number. In this way, the quantitative and qualitative damage characteristics obtained from the measured/modelled erosion profiles of the profile change experiments and XBeach-G simulations for different slope angles can be compared with each other correctly, because the type of wave breaking is the same per slope.
  - In this research, the impermeable layer has been implemented in XBeach-G as an aquifer layer. This needs to be validated.
  - The bed-load transport formulas of Nielsen (2006) and Van Rijn (2007) with the stability parameter  $\theta_{cr}$  are not able to model the sediment transport in XBeach-G correctly. Besides improving the hydrodynamics and optimizing the value of 0.055 of the stability parameter  $\theta_{cr}$ , the method of how sediment transport has been described by both bed-load transport formulas needs to be researched. The implemented stability parameter is not able to determine the occurrence of movements of stones, because movements of stones ( $q \neq 0$ ) are observed when the values of the mobility parameters decrease below the value of  $\theta_{cr}$ . Even when the mobility parameter  $\theta'_{McCall}$  has a value of zero or changes in sign, movements of stones occur.



## References

- Bosboom, J., & Stive, M. J. (2013). *Coastal Dynamics 1, version 0.4 ed.*. Delft: Delft University of Technology, VSSD.
- Breusers, H., & Schukking, W. (1971). Begin van beweging van bodemmateriaal.
- CIRIA, CUR, & CETMEF. (2007). The Rock Manual, The use of rock in hydraulic engineering (2nd edition). *Centre for Civil Engineering Research and Codes: C683, CIRIA, London.*
- Dean, R. G., & Dalrymple, R. A. (1991). *Water wave mechanics for engineers and scientists* (Vol. 2): world scientific publishing Co Inc.
- Dessens, M. (2004). *The influence of flow acceleration on stone stability*. Delft: Delft University of Technology.
- Fredsøe, J., & Deigaard, R. (1992). Advanced series on ocean engineering. *World Scientific*, 3, 392.
- Hofland, B. (2005). *Rock and roll: Turbulence-induced damage to granular bed protections*. Delft: Delft University of Technology.
- Hofland, B., Battjes, J. A., & Booij, R. (2005). Measurement of fluctuating pressures on coarse bed material. *Journal of hydraulic engineering*, 131(9), 770-781.
- Hofland, B., Van Gent, M. R. A., Raaijmakers, T., & Liefhebber, F. (2011). Damage evaluation using the damage depth. *Coastal Structures 2011. Yokohama, Japan.*
- Hudson. (1953). Wave forces on Breakwaters. *Transactions ASCE 118, ASCE*, pp 653-674.
- Hudson, R. Y. (1959). Laboratory investigation of rubble-mound breakwaters.
- Huijsmans, M. A. (2006). *The influence of flow acceleration on the stability of stones*. Delft: Delft University of Technology.
- Kramer, R. (2016). *The stability of rock on mild slopes under wave attack*. Delft: Delft University of Technology.
- McCall, R. T. (2015). *Process-based modelling of storm impacts on gravel coasts*. Plymouth University, United Kingdom.
- Melby, J. A., & Kobayashi, N. (1998). Progression and variability of damage on rubble mound breakwaters. *Journal of waterway, port, coastal, and ocean engineering*, 124(6), 286-294.
- Morison, J., Johnson, J., & Schaaf, S. (1950). The force exerted by surface waves on piles. *Journal of Petroleum Technology*, 2(05), 149-154.
- Nielsen, P. (2002). Shear stress and sediment transport calculations for swash zone modelling. *Coastal Engineering*, 45(1), 53-60.
- Nielsen, P. (2006). Sheet flow sediment transport under waves with acceleration skewness and boundary layer streaming. *Coastal Engineering*, 53(9), 749-758.
- Postma, M. G. (2016). *XBeach-G as a Design Tool for Rock on mild slopes under wave loading*. Delft: Delft University of Technology.
- Puleo, J., Holland, K., Plant, N., Slinn, D., & Hanes, D. (2003). Fluid acceleration effects on suspended sediment transport in the swash zone. *Journal of Geophysical Research: Oceans*, 108(C11).
- Ryu, Y., Chang, K.-A., & Lim, H.-J. (2005). Use of bubble image velocimetry for measurement of plunging wave impinging on structure and associated greenwater. *Measurement Science and Technology*, 16(10), 1945.
- Saers, W. (2005). Erosion of rubble mound near-bed structures under irregular waves.
- Schierack, G. J. (1993). *Introduction to bed, bank and shore protection*: CRC Press.
- Schierack, G. J., & Fontijn, H. L. (1996). Pipeline protection in the surf zone. *Coastal Engineering*, 4228-4241.
- Schierack, G. J., & Verhagen, H. J. (2012). *Introduction to Bed, Bank and Shore Protection (2nd edition)*. Delft: VSSD.
- Shields, A. (1936). *Anwendung der Aehnlichkeitsmechanik und der Turbulenzforschung auf die Geschiebebewegung. [English title: Application of similarity principles and turbulence research to bed-load movement] translated by W.P. Ott and J.C. van Uchelen*. Retrieved from California Institute of Technology , Pasadena, CA

- Sisttermans, P. G. J. (1993). *Stability of Rock on Beaches*. Delft: TU Delft, Faculty of Civil Engineering and Geosciences, Hydraulic Engineering.
- Sleath, J. F. (1978). Measurements of bed load in oscillatory flow. *Journal of the Waterway, Port, Coastal and Ocean Division*, 104(3), 291-307.
- Soulsby, R., & Whitehouse, R. (1997). *Threshold of sediment motion in coastal environments*. Paper presented at the Pacific Coasts and Ports' 97: Proceedings of the 13th Australasian Coastal and Ocean Engineering Conference and the 6th Australasian Port and Harbour Conference; Volume 1.
- Steenstra, R., Hofland, B., Smale, A., Paarlberg, A., Huthoff, F., & Uijttewaai, W. (2016). Stone Stability under Stationary Nonuniform Flows. *Journal of hydraulic engineering*, 142(12), 04016061.
- Thielicke, W. (2014). The flapping flight of birds. *Diss. University of Groningen*.
- Thielicke, W., & Stamhuis, E. (2014). PIVlab—towards user-friendly, affordable and accurate digital particle image velocimetry in MATLAB. *Journal of Open Research Software*, 2(1).
- Tromp, M. (2004). *Influences of fluid accelerations on the threshold of motion*. Delft: Delft University of Technology.
- Van den Heuvel, H. (2013). The effect of multiple storms on the stability of near-bed structures.
- Van der Meer, J. W. (1988). *Rock slopes and gravel beaches under wave attack* (Vol. 396): Delft hydraulics.
- Van der Velden, E. T. J. M. (1989). *Coastal Engineering* (Vol. 2). Delft: Delft University of Technology, Department of Civil Engineering.
- Van Rijn, L. C. (1984). Sediment transport, part I: bed load transport. *Journal of hydraulic engineering*, 110(10), 1431-1456.
- Van Rijn, L. C. (1993). *Principles of sediment transport in rivers, estuaries and coastal seas* (Vol. 1006): Aqua publications Amsterdam.
- Van Rijn, L. C. (2007). Unified view of sediment transport by currents and waves. I: Initiation of motion, bed roughness, and bed-load transport. *Journal of hydraulic engineering*, 133(6), 649-667.
- Wit, E. M. (2015). *Stability of Gravel on Mild Slopes in Breaking Waves*. Delft: Delft University of Technology.
- Ye, L. (1996). *Stability of Rock on Beaches*. Delft: TU Delft, Faculty of Civil Engineering and Geosciences, Hydraulic Engineering.
- Zijlema, M., Stelling, G., & Smit, P. (2011a). *Simulating nearshore wave transformation with non-hydrostatic wave-flow modelling*. Paper presented at the Conference Proceedings, 12th Int. Workshop on Wave Hindcasting and Forecasting, Hawai'i, USA.
- Zijlema, M., Stelling, G., & Smit, P. (2011b). SWASH: An operational public domain code for simulating wave fields and rapidly varied flows in coastal waters. *Coastal Engineering*, 58(10), 992-1012.

## List of Symbols

Symbol	Unit	Description	Symbol	Unit	Description
A	m <sup>2</sup>	Exposed surface area	f' <sub>cw</sub>	-	Grain friction coefficient
A <sub>e</sub>	m <sup>2</sup>	Eroded area	f' <sub>c</sub>	-	Current-related friction coefficient
A <sub>w</sub>	m	Peak orbital diameter near the bed	f' <sub>w</sub>	-	Wave-related friction coefficient
a, dU/dt	m/s <sup>2</sup>	Acceleration	g	m/s <sup>2</sup>	Gravitational acceleration (=9.81 m/s <sup>2</sup> )
α	°	Slope angle	γ	-	Calibration coefficient (Van Rijn, 2007)
b <sub>Cl</sub>	-	Constant (= 0.9)	h	m	Water depth
β	°	Slope angle	H	m	Wave height
C	m <sup>1/2</sup> /s	Chézy coefficient	H <sub>m0</sub> , H <sub>s</sub>	m	Significant wave height
C <sub>B</sub>	-	Bulk coefficient	H <sub>1%</sub>	m	Highest 1% waves
C <sub>D</sub>	-	Drag coefficient	$\bar{H}$	m	Depth-averaged hydraulic head
C <sub>F</sub>	-	Friction coefficient	k	1/m	Wave number
C <sub>L</sub>	-	Lift coefficient	k <sub>x</sub>	m/s	Darcy-flow permeability coefficient
C <sub>M</sub> , C <sub>i</sub>	-	Acceleration coefficient	K	m/s	Hydraulic conductivity
C <sub>S</sub>	-	Shear coefficient	K <sub>D</sub>	-	Empirically determined constant
C <sub>0</sub>	-	Maximum bed concentration (=0.65)	k <sub>s</sub>	m	Characteristic roughness height
C <sub>a</sub>	-	Added mass coefficient	k <sub>m</sub>	-	Added mass for shape of stone
C <sub>b</sub>	-	Bed-load concentration	L	m	Wave length
C <sub>f</sub>	-	Bed friction factor	M	kg	Mass of stone
C <sub>m</sub>	-	Inertia coefficient	M <sub>e</sub>	-	Mobility parameter
C <sub>n</sub>	-	Coefficient for number of particles	N	-	Number of waves
C <sub>v</sub>	-	Volume shape factor	n <sub>p</sub>	-	Porosity
D <sub>50</sub>	m	Mean diameter of stone	ν	m <sup>2</sup> /s	Kinematic viscosity of water
D <sub>n50</sub>	m	Mean nominal diameter of stone	ν <sub>h</sub>	m <sup>2</sup> /s	Horizontal viscosity
D <sub>90</sub>	m	Diameter of stone with 90% passing	ν <sub>t</sub>	m <sup>2</sup> /s	Eddy viscosity
D*	-	Particle parameter	ξ <sub>m</sub>	-	Iribarren number related to T <sub>m</sub>
d <sub>e</sub>	m	Erosion depth	ξ	m	Bed level
Δ	-	Relative density	ρ	kg/m <sup>3</sup>	Density
δ	m	Boundary layer thickness	ρ <sub>s</sub>	kg/m <sup>3</sup>	Density of stone
δ <sub>wf</sub>	m	Thickness of the wetting front	ρ <sub>w</sub>	kg/m <sup>3</sup>	Density of water
E <sub>3</sub>	m	Damage depth (Hofland et al., 2011)	P	-	Notional permeability
ζ <sub>gw</sub>	m	Groundwater level	p	N/m <sup>2</sup>	Pressure
θ	-	Adapted Shields parameter	q <sub>b</sub>	kg/s/m	Sediment transport rate
θ'	-	Effective, adapted Shields parameter	$\bar{q}$	-	Normalized depth-averaged dynamic p
θ <sub>cr</sub>	-	Critical, adapted Shields parameter	q <sub>b</sub>	-	Dynamic pressure at the bed
F <sub>acc</sub>	N	Force caused by accelerations	Re*	-	Particle Reynolds number
F <sub>B</sub>	N	Bulk force	S	-	Damage level (Van der Meer, 1988)
F <sub>D</sub>	N	Drag force	S <sub>e</sub>	-	Source term for exfiltration
F <sub>F</sub>	N	Friction force	S <sub>i</sub>	-	Source term for infiltration
F <sub>G</sub>	N	Gravity force	S <sub>s</sub>	-	Source term for submarine exchange
F <sub>L</sub>	N	Lift force	s	-	Wave steepness
F <sub>S</sub>	N	Shear force	T	-	Transport stage parameter
f <sub>s</sub>	-	Sediment friction factor	T <sub>m</sub>	s	Mean wave period

Symbol	Unit	Description
$T_{m-1,0}$	s	Spectral mean period
$T_p$	s	Peak wave period
$t_r$	s	Time of latest velocity reversal
$\tau_b$	$N/m^2$	Bed shear stress
$\tau_{b,cr}$	$N/m^2$	Critical bed shear stress
$\tau'_{b,cw}$	$N/m^2$	Instantaneous bed shear stress
$\tau_c$	$N/m^2$	Critical shear stress
$U, u$	m/s	Velocity
$U_w$	m/s	Peak orbital velocity
$U_{\delta,cw}$	m/s	Instantaneous velocity at edge of boundary layer
$u_b$	m/s	Velocity near bottom
$\hat{u}_b$	m/s	Maximum orbital velocity
$u_c$	m/s	Critical velocity
$u_{c*}$	m/s	Critical bed shear velocity
$\hat{u}_\delta$	m/s	Peak bottom velocity
$u_e$	m/s	Effective velocity
$u_\theta$	m/s	Sediment mobilizing velocity
$u_\infty$	m/s	Free stream velocity
$u_*$	m/s	Bed shear velocity
$\Phi$	-	Ventilation parameter
$\varphi_\tau$	°	Phase lag angle
$\phi$	°	Internal angle of repose
$V$	$m^3$	Volume
$w_b$	m/s	Vertical velocity at the bed
$\Psi_{cr}$	-	Critical Shields (1936) parameter
$\omega_p$	rad/s	Angular peak velocity
$\Delta x$	m	Grid size in XBeach-G

## Glossary

Acronym	Description
BIV	Bubble Image Velocimetry
DOF	Depth of Field
FOV	Field of View
fps	frames per second
GUI	General User Interface
PIV	Particle Image Velocimetry
ROI	Region of Interest
SWASH	Simulating WAVes till SHore
SWL	Still Water Level
WAFO	Wave Analysis for Fatigue and Oceanography

## List of Figures

Figure 1 - Energy dissipation of plunging breaker and spilling breaker (Schierreck & Verhagen, 2012) .....	4
Figure 2 - Hydrodynamic forces acting on a stone (Huijsmans, 2006) .....	5
Figure 3 - Schematization of forces acting on a stone in accelerating flow (Tromp, 2004).....	6
Figure 4 - Original Shields diagram (Shields, 1936) .....	8
Figure 5 - Seven transport stages (Breusers & Schukking, 1971) .....	8
Figure 6 - Modified Shields-diagram for waves by Sleath (1978) (Schierreck & Verhagen, 2012) .....	9
Figure 7 - Comparison of formula of Van der Meer (1988) for plunging breakers with XBeach-G results of Wit (2015) (left) and comparison with experimental results of Schierreck & Fontijn (1996) (right) .....	11
Figure 8 - Damage of a rock protection with erosion parameters $A_e$ , $d_c$ , $d_e$ and $l_e$ (Melby & Kobayashi, 1998) ..	15
Figure 9 - XBeach-G results with submerged bar profile (left) and crest profile (right) (Wit, 2015) .....	16
Figure 10 - Test set up for BIV experiments of Kramer (2016) (length in cm) (Kramer, 2016) .....	20
Figure 11 - Schematization of DOF and FOV (Kramer, 2016).....	21
Figure 12 - Velocity vector field with ROI during run-down (left) and during run-up (right) for 1:5 slope .....	24
Figure 13 - Velocity (top) and acceleration (bottom) in ROI over time for 1:5 slope .....	25
Figure 14 - Erosion profiles for 1:10 slope and $S_{Wit}$ input .....	30
Figure 15 - Dimensionless stability parameter versus Iribarren number, adjusted graph of Kramer (2016) .....	37
Figure 16 - Velocity (top) and acceleration (bottom) in ROI over time for 1:5 slope .....	39
Figure 17 - Mobility parameters over time for 1:5 slope.....	40
Figure 18 - Mobility parameter $\theta'_{McCall}$ over time with new $c_f$ and $c_p$ for 1:5 slope.....	48
Figure 19 - Mobility parameter $\theta'_{McCall}$ over time along length of 1:5 slope with $S_{Wit}$ input.....	51
Figure 20 - Schematization of infiltration (left) and exfiltration (right) (McCall, 2015).....	68
Figure 21 - Horizontal pressure differences on a stone due to accelerations (Dessens, 2004).....	69
Figure 22 - Breaker types, according to Battjes (1974) (Schierreck, 1993) .....	72
Figure 23 - Notional permeability $P$ for various structures (Van der Meer, 1988) .....	73
Figure 24 - Damage level $S$ based on the erosion area $A$ (Van der Meer, 1988) .....	73
Figure 25 - Contributions of terms in sediment transport equation (A.39) (Bosboom & Stive, 2013) .....	75
Figure 26 - Free stream velocity (blue) and boundary layer thickness (black dotted) over time (Nielsen, 2002) ..	75
Figure 27 - Test set up for profile change experiments of Kramer (2016) (length in cm) (Kramer, 2016) .....	80
Figure 28 - Preparation of slope (left & middle) and Leica C10 scanner with trackers (right) (Kramer, 2016) ....	80
Figure 29 - Boundary restricted erosion profile for 1:15 slope and $S_{Wit}$ input.....	80
Figure 30 - FOV with black stones and DOF (left), DOF (middle) and setup of LED lights (right) (Kramer, 2016) ..	81
Figure 31 - Explanation of visual analysis of movements of stones with frames of video 05_BIV_0001 .....	81
Figure 32 - Effect of pre-processing techniques (Thielicke & Stamhuis, 2014) .....	82
Figure 33 - Screenshot of calibration image imported in PIVlab for the BIV analysis of 1:5 slope .....	83
Figure 34 - Ensemble average of wave periods $T_1$ , $T_2$ and $T_3$ of horizontal velocity for 1:10 slope.....	84
Figure 35 - Erosion profiles for 1:5 slope and $S_{norm}$ input .....	86
Figure 36 - Erosion profiles for 1:5 slope and $S_{Wit}$ input .....	87
Figure 37 - Erosion profiles for 1:10 slope and $S_{Wit}$ input .....	88
Figure 38 - Erosion profiles for 1:10 slope and $S_{S\&F}$ input.....	89
Figure 39 - Erosion profiles for 1:15 slope and $S_{Wit}$ input .....	90
Figure 40 - Erosion profiles for 1:15 slope and $S_{S\&F}$ input.....	91
Figure 41 - Bed shear velocity with formula of Nielsen (2006) over time for 1:5 slope .....	92
Figure 42 - Bed shear stress with formula of McCall (2015) over time for 1:5 slope .....	93
Figure 43 - Velocity (top) and acceleration (bottom) in ROI over time for 1:10 slope .....	94
Figure 44 - Bed shear velocity with formula of Nielsen (2006) over time for 1:10 slope .....	95
Figure 45 - Bed shear stress with formula of McCall (2015) over time for 1:10 slope .....	96
Figure 46 - Mobility parameters over time for 1:10 slope.....	97
Figure 47 - Mobility parameter $\theta'_{McCall}$ over time with new $c_f$ and $c_p$ for 1:10 slope.....	98
Figure 48 - Velocity (top) and acceleration (bottom) in ROI over time for 1:15 slope .....	100
Figure 49 - Bed shear velocity with formula of Nielsen (2006) over time for 1:15 slope .....	101
Figure 50 - Bed shear stress with formula of McCall (2015) over time for 1:15 slope .....	102
Figure 51 - Mobility parameters over time for 1:15 slope.....	103
Figure 52 - Mobility parameter $\theta'_{McCall}$ over time with new $c_f$ and $c_p$ for 1:15 slope.....	104
Figure 53 - Velocity over time along length of 1:5 slope with $S_{Wit}$ input .....	105
Figure 54 - Acceleration over time along length of 1:5 slope with $S_{Wit}$ input.....	105

Figure 55 - Velocity over time along length of 1:10 slope with $S_{Wit}$ input .....	107
Figure 56 - Acceleration over time along length of 1:10 slope with $S_{Wit}$ input.....	107
Figure 57 - Mobility parameter $\theta'_{McCall}$ over time along length of 1:10 slope with $S_{Wit}$ input.....	108
Figure 58 - Velocity over time along length of 1:15 slope with $S_{Wit}$ input .....	109
Figure 59 - Acceleration over time along length of 1:15 slope with $S_{Wit}$ input.....	109
Figure 60 - Mobility parameter $\theta'_{McCall}$ over time along length of 1:15 slope with $S_{Wit}$ input.....	110
Figure 61 - Extreme minimum and maximum values over time of mobility parameter $\theta'_{McCall}$ (top) and relative erosion depth $d_e/D_{n50}$ (bottom) along the length of the 1:5 slope.....	112
Figure 62 - Extreme minimum and maximum values over time of mobility parameter $\theta'_{McCall}$ (top) and relative erosion depth $d_e/D_{n50}$ (bottom) along the length of the 1:10 slope.....	113
Figure 63 - Extreme minimum and maximum values over time of mobility parameter $\theta'_{McCall}$ (top) and relative erosion depth $d_e/D_{n50}$ (bottom) along the length of the 1:15 slope.....	114

## List of Tables

Table 1 - Description of the seven transport stages (Breusers & Schukking, 1971) .....	8
Table 2 - Damage classification of $E_3$ for rock protection with layer thickness of $2D_{n50}$ (Hofland et al., 2011)....	15
Table 3 - Constant input parameters profile change experiments of Kramer (2016) and XBeach-G simulations	17
Table 4 - Variable input parameters of two wave characteristics, per slope .....	18
Table 5 - Sediment friction factor and phase lag angle (test values) derived from BIV experiments, per slope..	20
Table 6 - Constant input parameters used in BIV experiments of Kramer (2016).....	22
Table 7 - Wave characteristics of BIV experiments of Kramer (2016), per slope .....	22
Table 8 - Analyzed videos of BIV experiments of Kramer (2016), per slope.....	23
Table 9 - Overview of mobility parameters .....	26
Table 10 - Variable input parameters used to determine bed shear velocity and shear stress, per slope .....	27
Table 11 - Constant input parameters used to determine mobility parameter $\theta'_{McCall}$ with bed shear stress.....	27
Table 12 - Slope correction factors, per slope (according to Fredsøe and Deigaard (1992)) .....	28
Table 13 - Effective stability parameters, per slope .....	28
Table 14 - Overview of all simulations, including damage obtained from the erosion profiles .....	31
Table 15 - Theoretical damage levels and damage levels derived by Kramer (2016), per slope.....	36
Table 16 - Dimensionless stability parameter $H_s/\Delta D_{n50}$ determined with bed-load transport formula of Van Rijn (2007) using the numerical model XBeach-G, per slope (and corresponding wave characteristics) .....	36
Table 17 - Movements of stone for 1:5 slope (video 05_BIV_0001) .....	38
Table 18 - Critical, effective Shields parameter for 1:5 slope.....	41
Table 19 - Values of velocity, acceleration and mobility parameters from BIV analysis of videos, per slope .....	42
Table 20 - Values of $U$ and $dU/dt$ from BIV analysis derived by Kramer (2016), per slope .....	44
Table 21 - Values of coefficients $c_f$ and $c_i$ per slope (this research) .....	45
Table 22 - Values of coefficients $C_B$ and $C_M$ from previous research.....	46
Table 23 - Values of mobility parameter $\theta'_{McCall}$ with new $c_f$ and $c_i$ from BIV analysis of videos, per slope .....	46
Table 24 - Values of stability parameter $\theta_{cr}$ , per slope .....	49
Table 25 - Values of $U$ , $dU/dt$ and $\theta'_{McCall}$ from XBeach-G simulations with $S_{Wit}$ input, per slope .....	51
Table 26 - Overview of variables and their possible range of application (Van der Meer, 1988) .....	71
Table 27 - Check extreme values of horizontal velocity with linear wave theory for 1:5 slope .....	83
Table 28 - Phases determined from horizontal velocity over time for 1:10 slope (Figure 43) .....	85
Table 29 - Overview of simulations and damage obtained from erosion profiles for 1:5 slope and $S_{norm}$ input..	86
Table 30 - Overview of simulations and damage obtained from erosion profiles for 1:5 slope and $S_{Wit}$ input....	87
Table 31 - Overview of simulations and damage obtained from erosion profiles for 1:10 slope and $S_{Wit}$ input..	88
Table 32 - Overview of simulations and damage obtained from erosion profiles for 1:10 slope and $S_{S\&F}$ input .	89
Table 33 - Overview of simulations and damage obtained from erosion profiles for 1:15 slope and $S_{Wit}$ input..	90
Table 34 - Overview of simulations and damage obtained from erosion profiles for 1:15 slope and $S_{S\&F}$ input .	91
Table 35 - Ratio between velocity/drag term and acceleration/inertia term for 1:5 slope .....	93
Table 36 - Movements of stone for 1:10 slope (video 10_BIV_0003) .....	94
Table 37 - Ratio between velocity/drag term and acceleration/inertia term for 1:10 slope .....	96
Table 38 - Critical, effective Shields parameter for 1:10 slope .....	97
Table 39 - Ratio between velocity/drag term and acceleration/inertia term for 1:15 slope .....	102
Table 40 - Critical, effective Shields parameter for 1:15 slope .....	103
Table 41 - Values of $U$ , $dU/dt$ and $\theta'_{McCall}$ from XBeach-G simulations with $S_{Wit}$ input without morphological updating, per slope.....	111
Table 42 - Values of $U$ , $dU/dt$ and $\theta'_{McCall}$ from XBeach-G simulations with $S_{Wit}$ input with regular waves and without morphological updating, per slope .....	111

## Appendices - Table of Contents

<b>Appendix A</b>	<b>Additional literature .....</b>	<b>66</b>
A.1	Surface water for currents and waves .....	66
A.2	Groundwater .....	67
A.3	Surface water-groundwater exchange .....	67
A.4	Dimensionless relation between load and strength .....	68
A.5	Derivation of forces caused by accelerations.....	69
A.6	Coefficients $C_B$ , $C_D$ , $C_L$ and $C_M$ .....	70
A.7	Derivation of mobility parameter $\theta_{Force}$ .....	70
A.8	Limitations formula of Iribarren (1938) and Hudson (1953) .....	71
A.9	Overview parameters in Van der Meer (1988) tests .....	71
A.10	Parameters in formula of Van der Meer (1988) .....	71
A.11	Formulas in wave model ENDEC .....	74
A.12	Bed level change.....	74
A.13	Cross-shore sediment transport.....	74
A.14	Parameters in drag term and inertia term of bed shear stress.....	76
A.15	Parameters in formula of Nielsen (2006) .....	76
A.16	Parameters in formula of Van Rijn (1984) for currents.....	77
A.17	Parameters in formula of Van Rijn (2007) for currents and waves.....	77
A.18	Simplified formula of Van Rijn (2007) .....	78
<b>Appendix B</b>	<b>Verification previous physical scale model tests .....</b>	<b>80</b>
B.1	Test set up of profile change experiments of Kramer (2016) .....	80
B.2	Boundary restricted erosion profiles for 1:15 slope with $S_{Wit}$ input .....	80
B.3	Preparation of BIV experiments by Kramer (2016) .....	81
B.4	Visual analysis of movements of stones.....	81
B.5	Image pre-processing techniques in PIVlab .....	82
B.6	Calibration of images in PIVlab.....	83
B.7	Extreme values of horizontal velocity with linear wave theory .....	83
B.8	Ensemble averaging of horizontal velocity.....	84
<b>Appendix C</b>	<b>Results of XBeach-G simulations .....</b>	<b>86</b>
C.1	Erosion profiles for 1:5 slope with $S_{norm}$ input .....	86
C.2	Erosion profiles for 1:5 slope with $S_{Wit}$ input .....	87
C.3	Erosion profiles for 1:10 slope with $S_{Wit}$ input .....	88
C.4	Erosion profiles for 1:10 slope with $S_{S\&F}$ input .....	89
C.5	Erosion profiles for 1:15 slope with $S_{Wit}$ input .....	90
C.6	Erosion profiles for 1:15 slope with $S_{S\&F}$ input.....	91
<b>Appendix D</b>	<b>Results of BIV analysis .....</b>	<b>92</b>
D.1	Bed shear velocity and bed shear stress over time for 1:5 slope.....	92
D.2	Results of BIV analysis of video with 1:10 slope.....	94
D.3	Results of BIV analysis of video with 1:15 slope.....	100
<b>Appendix E</b>	<b>Results of mobility parameter from XBeach-G.....</b>	<b>105</b>
E.1	Velocity and acceleration in XBeach-G simulation for 1:5 slope.....	105
E.2	Mobility parameter $\theta'_{McCall}$ in XBeach-G simulation for 1:10 slope.....	107

E.3	Mobility parameter $\theta'_{\text{McCall}}$ in XBeach-G simulation for 1:15 slope.....	109
E.4	Influence of morphological updating of the bed.....	111
E.5	Influence of irregular waves.....	111
E.6	Mobility parameter and relative erosion depth along length of slope .....	112

## Appendix A Additional literature

### A.1 Surface water for currents and waves

The depth-averaged flow due to currents and waves can be described using the non-linear shallow water equations (NLSWE). The conservation of mass is given in equation (A.1). The first term describes the change in water level over time, the second term is the gradient influx and  $S$  is the source term to describe the exchange between surface water and groundwater. The conservation of momentum is presented in equation (A.2), in which a non-hydrostatic pressure term is included to model short waves.

$$\frac{\partial \zeta}{\partial t} + \frac{\partial hu}{\partial x} + S = 0 \quad (\text{A.1})$$

$$\underbrace{\frac{\partial u}{\partial t} + u \frac{\partial u}{\partial x}}_{\text{acceleration advection}} - \frac{\partial}{\partial x} \left( v_h \frac{\partial u}{\partial x} \right) = \underbrace{-\frac{1}{\rho} \frac{\partial(\rho \bar{q} + \rho g \zeta)}{\partial x}}_{\text{pressure gradient}} - \underbrace{\frac{\tau_b}{\rho h}}_{\text{bed friction}} \quad (\text{A.2})$$

In which:  $\zeta$  is the free surface elevation (m),  $u$  is the depth-averaged (cross-shore) velocity (m/s),  $h$  is the total water depth (m),  $S$  is the surface water-groundwater exchange flux,  $v_h$  is the horizontal viscosity ( $v_h = 2(0.1\Delta x)^2 \sqrt{2(\delta u / \delta x)^2}$  with  $\Delta x$  as the computational grid size, according to Smagorinsky (1963) (McCall, 2015)),  $\bar{q}$  is the depth-averaged dynamic pressure normalized by the density, and  $\tau_b$  is the bed shear stress (see equation (A.3) with the bed friction  $c_f$ , Chézy for turbulent flow and the characteristic roughness  $k_s$ ).

$$\tau_b = c_f \rho u |u| \quad \text{with} \quad c_f = \frac{g}{C^2} = \frac{g}{(18 \log(12h/k_s))^2} \quad \text{and} \quad k = 3D_{90} \quad (\text{A.3})$$

The normalized depth-averaged dynamic pressure  $\bar{q}$  is difficult to determine. Therefore, the average value of the dynamic pressure at the bed and the dynamic pressure at the surface (assumed to be zero) is often used. The dynamic pressure at the bed can be determined with equation (A.4), according to the Keller-Box applied by Stelling & Zijlema (2003) (McCall, 2015).

$$q_b = -\frac{h}{2} \left( \frac{\partial q}{\partial z} \Big|_s + \frac{\partial q}{\partial z} \Big|_b \right) \quad (\text{A.4})$$

Neglecting the advection and diffusion terms, the vertical momentum balance can be described by equation (A.5). In which:  $w_b$  is the vertical velocity at the bed.

$$\frac{\partial q}{\partial z} = -\frac{\partial w}{\partial t} \quad \text{and} \quad w_b = u \frac{\partial \xi}{\partial x} = u \frac{\partial(\zeta - h)}{\partial x} \quad (\text{A.5})$$

When substituting equation (A.4) into this balance, a new vertical momentum balance is obtained, see equation (A.6). The dynamic pressure at the bed can now be solved with equation (A.6), using the local continuity equation (A.7).

$$\frac{\partial w_s}{\partial t} = 2 \frac{q_b}{h} - \frac{\partial w_b}{\partial t} \quad (\text{A.6})$$

$$\frac{\partial u}{\partial x} + \frac{w_s - w_b}{h} = 0 \quad (\text{A.7})$$

## A.2 Groundwater

The groundwater is based on the conservation of mass, equations of motion and a parameterization for the non-hydrostatic groundwater pressure. For the conservation of mass, the continuity equation is used and an incompressible flow is assumed.

Laminar flow through a homogeneous structure can be described by the law of Darcy (1856), see equation (A.8). In which  $K$  is the hydraulic conductivity and  $\bar{H}$  is the depth-averaged hydraulic head.

$$u_{gw} = -K \frac{\partial \bar{H}}{\partial x} \quad (\text{A.8})$$

The hydraulic conductivity is determined with the laminar hydraulic conductivity and the Reynolds number (McCall, 2015). In which:  $n_p$  is the porosity (-) and  $\nu$  is the hydraulic viscosity.

- When  $Re > Re_{crit}$   $K(Re) = K_{lam} \sqrt{\frac{Re_{crit}}{Re}}$  with  $Re = \frac{|U|D_{50}}{n_p \nu}$  and  $Re_{crit} \approx 60$
- When  $Re \leq Re_{crit}$   $K(Re) = K_{lam}$

To determine the groundwater head, the following three assumptions are done:

- No exchange of water between the aquifer and the impermeable layer below the aquifer, so  $w_b = 0$  and  $\left. \frac{\delta H}{\delta \sigma} \right|_{\sigma=0} = 0$ .
- The groundwater head is equal to the head at the surface, so  $H(h_{gw}) = H_{bc}$ .
- The vertical velocity increases or decreases linearly from the aquifer bottom to the upper surface of the groundwater, so  $w(\sigma) = \alpha \sigma$  and  $\frac{\delta^2 H}{\delta \sigma^2} = \alpha$ .

These assumptions are fulfilled with the approximation of the vertical groundwater given in equation (A.9). The depth-averaged groundwater head presented in equation (A.10) can be found by integrating the approximation of equation (A.9) over the vertical. In which:  $\beta$  is a parabolic curvature coefficient,  $\sigma$  is the vertical coordinate above the bottom of the aquifer and  $H_{bc}$  is the head imposed at surface of the groundwater.

$$H(\sigma) = \beta(\sigma^2 - h_{gw}^2) + H_{bc} \quad (\text{A.9})$$

$$\bar{H} = \frac{1}{h_{gw}} \int_0^{h_{gw}} H(\sigma) d\sigma = H_{bc} - \frac{2}{3} \beta h_{gw}^2 \quad (\text{A.10})$$

## A.3 Surface water-groundwater exchange

The surface water-groundwater exchange can be determined with the equations for submarine exchange, infiltration and exfiltration. The parameter  $S$  is used to describe the exchange flux. Submarine exchange only occurs when the surface water is connected with the groundwater. Equation (A.8) is derived with the approximation of the hydraulic head in equation (A.9) (McCall, 2015).

$$S_s = -w(h_{gw}) = K \left. \frac{\delta H}{\delta \sigma} \right|_{\sigma=h_{gw}} = 2\beta h_{gw} K \quad (\text{A.11})$$

When the surface water and groundwater are not connected, infiltration and exfiltration occurs. Both phenomena are schematized in Figure 20. Infiltration occurs when the surface water table is above the groundwater table (e.g. during a swash event) and exfiltration happens due to a high groundwater table.

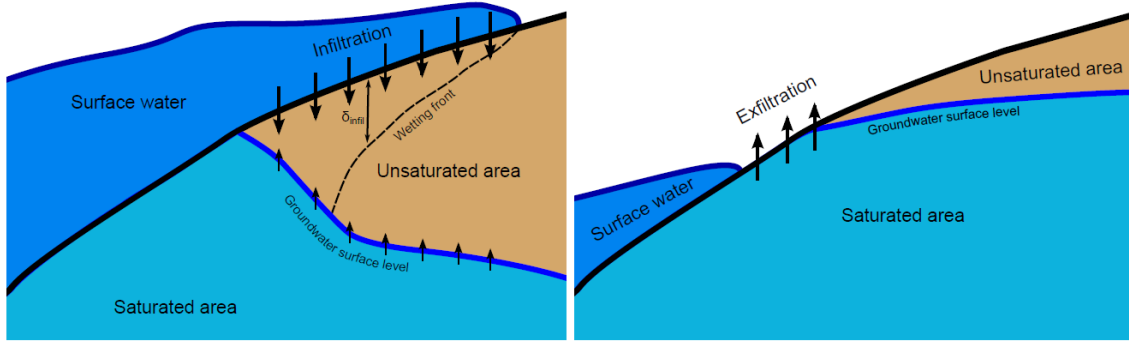


Figure 20 - Schematization of infiltration (left) and exfiltration (right) (McCall, 2015)

Infiltration can be calculated with equation (A.12), similar to the method of Packwood (1983). In which:  $\delta_{wf}$  is the thickness of the wetting front and  $p|^{z=\xi}$  is the total surface water pressure at the bed.

$$S_i = K \left( \frac{1}{\rho g} \frac{p|^{z=\xi}}{\delta_{wf}} + 1 \right) \quad \text{with} \quad \delta_{wf} = \int \frac{S_i}{n_p} dt \quad (\text{A.12})$$

Exfiltration can be determined with equation (A.13). In which:  $\xi$  is the bed level and  $\zeta_{gw}$  is the groundwater level.

$$S_e = n_p \frac{\partial(\xi - \zeta_{gw})}{\partial t} \quad (\text{A.13})$$

For every vertical grid cell, the overall groundwater effect is the sum of the submarine exchange, infiltration and exfiltration. This effect is implemented in the ventilation, which is part of the dimensionless friction factor  $c_f$  (see equation (A.3)).

Both the surface water level and the groundwater level changes due to the surface water-groundwater exchange. The surface water level (left) and the groundwater level (right) can be determined with equation (A.14) in case of submarine exchange. In case of infiltration/exfiltration, equation (A.15) needs to be used.

$$\frac{\partial \zeta}{\partial t} = -S_s \quad \text{and} \quad n_p \frac{\partial \zeta_{gw}}{\partial t} = w_{gw} + S_s = 0 \quad \text{with} \quad w_{gw,s} = \frac{\delta h_{gw} u_{gw}}{\delta x} \quad (\text{A.14})$$

$$\frac{\partial \zeta}{\partial t} = -S_i - S_e \quad \text{and} \quad n_p \frac{\partial \zeta_{gw}}{\partial t} = w_{gw} + S_i + S_e \quad (\text{A.15})$$

#### A.4 Dimensionless relation between load and strength

Equilibrium of the horizontal forces and vertical forces is given by equation (A.16), and equilibrium of momentum is given by equation (A.17).

$$\sum H = 0 \rightarrow F_D + F_S = C_F F_G, \quad \sum V = 0 \rightarrow F_L = F_G \quad (\text{A.16})$$

$$\sum M|_A = F_D a_1 + F_S a_2 + F_L b_2 = F_G b_1 + F_F a_3 \quad (\text{A.17})$$

The weight of the stone is proportional to the diameter by the third power. From the equilibrium of horizontal forces, vertical forces and momentum the proportionality in equation (A.18) remains. A dimensionless relation between load and strength can be deducted, using the critical velocity  $u_c$ , see equation (A.19).

$$\rho_w u_c^2 D_{50}^2 \propto (\rho_s - \rho_w) g D_{50}^3 \quad (\text{A.18})$$

$$u_c^2 \propto \left( \frac{\rho_s - \rho_w}{\rho_w} \right) g D_{50} = \Delta g D_{50} \rightarrow u_c^2 = K \Delta g D_{50} \quad (\text{A.19})$$

In which:  $\Delta$  is the relative density (-), given by  $\Delta = (\rho_s - \rho_w)/\rho_w$  and  $K$  is an empirical constant.

## A.5 Derivation of forces caused by accelerations

In a non-stationary flow, accelerations of a fluid motion around a stone create horizontal pressure differences. Tromp (2004) already investigated the influence of accelerations on the initiation of motion. The derivation of the forces due to the horizontal pressure differences is worked out with a schematization of a stone placed in an accelerating flow, see Figure 21.

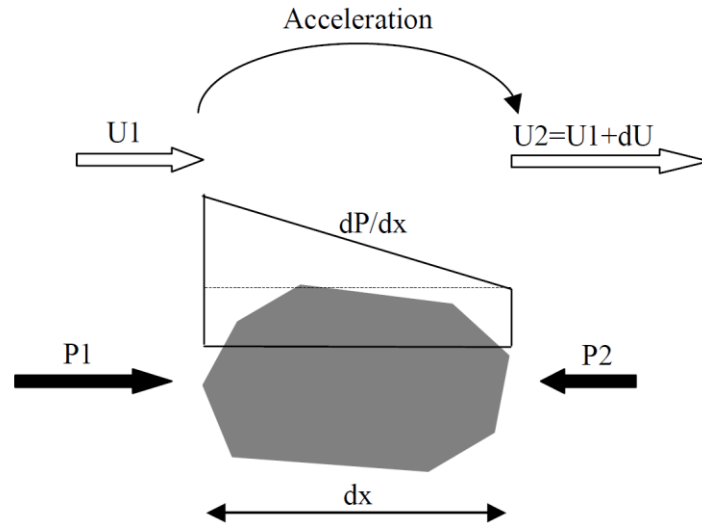


Figure 21 - Horizontal pressure differences on a stone due to accelerations (Dessens, 2004)

The pressure difference  $\Delta p$  is determined with the theory of Bernoulli, which is written into equation (A.20). This can be rewritten into equation (A.21).

$$p_1 + \frac{1}{2} \rho u_1^2 = p_2 + \frac{1}{2} \rho u_2^2 \quad (\text{A.20})$$

$$\Delta p = p_1 - p_2 = \frac{1}{2} \rho (u_2^2 - u_1^2) \quad (\text{A.21})$$

Assuming equally sized stones that are small compared to the variations in flow, equation (A.22) is valid.

$$\frac{dp}{dx} = \text{constant} \quad \text{and} \quad dp = \frac{dp}{dx} dx \quad (\text{A.22})$$

Due to the pressure differences, caused by accelerations of the flow, the force  $F_{acc}$  can be written as in equation (A.23). In which:  $V$  is the volume of the stone ( $\text{m}^3$ ) and  $\frac{dp}{dx}$  is a linear pressure gradient.

$$F_{acc} = \iiint \frac{dp}{dx} dx dy dz = V \frac{dp}{dx} \quad (\text{A.23})$$

Equation (A.24) is determined with the Euler equation, from which is known that  $\frac{dp}{dx}$  can be replaced by  $\rho \left( \frac{\partial u}{\partial t} \right)$ .

$$\nabla p = -\rho \frac{D\vec{u}}{Dt} \rightarrow \frac{dp}{dx} = -\rho \left( \frac{\partial u}{\partial t} + \bar{u} \frac{\partial u}{\partial x} \right) \quad (\text{A.24})$$

The force  $F_{acc}$  can now be expressed as equation (A.25). In case of small stones, the change of velocities along the length of a stone is small as well. Therefore,  $\frac{\partial u}{\partial x} \approx 0$  and equation (A.25) becomes equation (A.26). In which:  $a$  is the horizontal acceleration ( $\text{m/s}^2$ ). The force  $F_{acc}$  becomes larger for increasing stone sizes, because the volume of the stone in equation (A.26) is related to the diameter of the stone by  $V \propto D_{50}^3$ .

$$F_{acc} = V \frac{dp}{dx} = \rho \left( \frac{\partial u}{\partial t} + \bar{u} \frac{\partial u}{\partial x} \right) V \quad (\text{A.25})$$

$$F_{acc} = \rho \left( \frac{\partial u}{\partial t} \right) V = \rho a V \quad (\text{A.26})$$

## A.6 Coefficients $C_B$ , $C_D$ , $C_L$ and $C_M$

The bulk coefficient  $C_B$  includes the drag coefficient  $C_D$  and lift coefficient  $C_L$ , see equation (A.27). The left formula is according to Tromp (2004). In which:  $K$  depends on the angle  $\beta$  (see Figure 3). The right formula is according to Van den Heuvel (2013).

$$C_B \sim K(C_D + C_L) \quad \text{with} \quad K \leq 1 \quad \text{or} \quad C_B = \sqrt{C_L^2 + C_D^2} \quad (\text{A.27})$$

Various definitions are found in literature for the coefficients  $C_D$  and  $C_L$ . For example, the drag coefficient can be described by  $C_{D,0.15}$ ,  $C_{D,0}$ , and  $C_{D,*}$ , defined by the time-averaged velocity  $\bar{u}$  at 0.15d above the stone, or  $\bar{u}$  measured at the height of the centre of the stone, or the bed shear velocity  $u_*$ , respectively (Hofland et al., 2005). Hofland (2005) suggests that both  $C_D$  and  $C_L$  become fairly constant for high particle Reynolds numbers. However, the values of the coefficients have a certain range. For all protrusions, values between 0.23 and 0.30 are found for  $C_{D,0.15}$ .  $C_{L,0.15}$  has values between 0.15 and 0.22, in case the stone is placed between other (Hofland et al., 2005).

According to Dean and Dalrymple (1991), the acceleration coefficient  $C_M$  is given by equation (A.28). In which: 1 is the pressure gradient component and  $k_m$  is the added mass component, dependent on the shape of the stone. Tromp (2004) suggests a value between 2 and 3 for  $C_M$ , in case half the stone protrudes out of the bed.

$$C_M = 1 + k_m \quad (\text{A.28})$$

## A.7 Derivation of mobility parameter $\theta_{Force}$

The critical mobility parameter  $\theta_{Force}$  can be derived from the momentum balance of forces  $F_B$ ,  $F_{acc}$  and  $F_G$ , schematized in Figure 3 and given in equation (A.29) (Dessens, 2004; Tromp, 2004) to define a threshold of motion.

$$F_B \cos(\varphi - \beta) + F_{acc} \cos(\varphi) < F_G \sin(\varphi) \quad (\text{A.29})$$

When the left hand side is larger than the right hand side, the stone will start to move.  $F_G \sin(\varphi)$  can be seen as the critical force that has to be exceeded to initiate movement of the stone. The mobility parameter  $\theta_{Force}$  is derived in equation (A.30) and is found by substituting  $F_G$  (equation (2.2)),  $F_B$  and  $F_{acc}$  (equation (2.4)) into each other, using  $A = D_{n50}^2$  and  $V = D_{n50}^3$  and assuming that the slope effect (parameters  $\varphi$  and  $\beta$ ) is implicitly included in the coefficients  $C_B$  and  $C_M$  (Van den Heuvel, 2013). The result is shown in equation (A.31).

$$\theta_{Force} = \frac{F_B \cos(\varphi - \beta) + F_{acc} \cos(\varphi)}{F_G \sin(\varphi)} = \frac{\frac{1}{2} C_B u |u| \frac{\cos(\varphi - \beta)}{\sin(\varphi)} + C_M \frac{\partial u}{\partial t} D_{50} \frac{\cos(\varphi)}{\sin(\varphi)}}{\Delta g D_{50}} \quad (A.30)$$

$$\theta_{Force} = \frac{\frac{1}{2} C_B u |u| + C_M \frac{\partial u}{\partial t} D_{50}}{\Delta g D_{50}} \quad (A.31)$$

## A.8 Limitations formula of Iribarren (1938) and Hudson (1953)

The limitations of the formula of Iribarren (1938) and Hudson (1953) are listed below (Schierreck & Verhagen, 2012; Van der Meer, 1988).

- **Wave period:** the wave period is not included in the formulas, while the wave period influences the stability on two ways. The period is related to the wave length, hence to the wave steepness, which is important for the breaking pattern on the slope. Furthermore, the inertia forces on a particle depend on  $du/dt$ , hence on the wave period.
- **Permeability:** the permeability is absent in the formulas, while the permeability plays an important role when looking at the dissipation of waves breaking on a structure and the pressure build up in a structure.
- **Number of waves:** tests were carried out with regular waves over a certain time period (when the equilibrium damage-profile was reached). From tests with wave spectra can be concluded that the number of waves has some influence, because with more waves there is a greater chance of a large one occurring.
- **Damage level:** the damage level  $K_D$  and its definition are vague and unclear.

## A.9 Overview parameters in Van der Meer (1988) tests

Van der Meer (1988) performed scaled model tests for various parameters. The most governing parameters were tested with a certain range, see Table 26 below *from paragraph 3.4.1* (Van der Meer, 1988).

Table 26 - Overview of variables and their possible range of application (Van der Meer, 1988)

variable	expression	range
The wave height parameter	$H_s / \Delta D_{n50}$	1 - 4
The wave period parameters, wave steepness, and surf similarity parameter	$s_m$ $\xi_m$	0.01 - 0.06 0.7 - 7
The damage as a function of the number of waves	$S / \sqrt{N}$	< 0.9
The slope angle	$\cot \alpha$	1.5 - 6
The grading of the armour stones	$D_{85} / D_{15}$	1 - 2.5
The permeability of the structure	$P$	imperme.- hom.
The spectral shape parameter	$\kappa$	0.3 - 0.9
The crest height	$R_c / H_s$	-1 - 2

## A.10 Parameters in formula of Van der Meer (1988)

The design formulas of Van der Meer (1988) for plunging breakers and surging breakers are given in equation (A.32) and (A.33).

$$\frac{H_s}{\Delta D_{n50}} = 6.2 \cdot P^{0.18} \cdot \left( \frac{S}{\sqrt{N}} \right)^{0.2} \cdot \xi_m^{-0.5} \quad (A.32)$$

$$\frac{H_s}{\Delta D_{n50}} = 1.0 \cdot P^{-0.13} \cdot \left( \frac{S}{\sqrt{N}} \right)^{0.2} \cdot \xi_m^P \cdot \sqrt{\cot \alpha} \quad (\text{A.33})$$

In which:  $H_s/\Delta D_{n50}$  is a dimensionless stability parameter that describes both the load (significant wave height) on and strength (own weight) of the stone,  $H_s$  is the significant wave height (m),  $D_{n50}$  is the median nominal stone diameter (m),  $P$  is the notional permeability (-),  $N$  is the number of waves (-),  $S$  is damage level (-) and  $\xi_m$  is the Iribarren number related to the mean wave period (-). The elaboration on these implemented parameters is given below.

The transition between plunging and surging breakers is given by equation (A.34). For slopes more gentle than 1:4, the formula for plunging breakers is recommended to use.

$$\xi_{transition} = [6.2P^{0.31}\sqrt{\tan \alpha}]^{\left(\frac{1}{P+0.5}\right)} \quad (\text{A.34})$$

- When  $\xi < \xi_{transition}$  Apply equation (2.10) for plunging breakers.
- When  $\xi > \xi_{transition}$  Apply equation (A.33) for surging breakers.

The most important limitations of the formula of Iribarren (1938) and Hudson (1953) are overcome with the design formula of Van der Meer (1988). The implemented parameters are listed below.

- **Wave period:** the wave period is incorporated in Iribarren Number  $\xi$ , also called the surf similarity parameter. The parameter is given in equation (A.35) and the different types of breaking are shown in Figure 22, according to Battjes (1974). Van der Meer (1988) used both the surf similarity parameter and the wave steepness to describe the influence of the wave period on static stability (by damage) and dynamic stability (by profile).

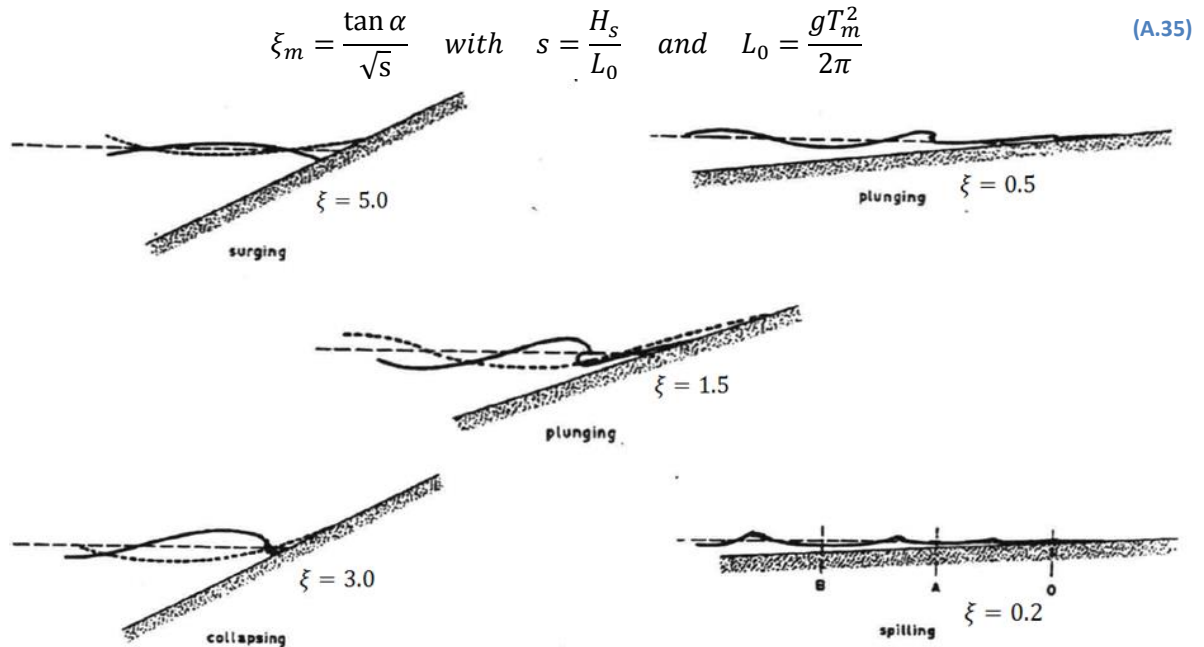


Figure 22 - Breaker types, according to Battjes (1974) (Schierack, 1993)

- **Permeability:** Van der Meer (1988) introduced the notional permeability  $P$ . This parameter ranges from 0.6 for a homogeneous core to 0.1 for an impermeable structure, see Figure 23. In paragraph 3.3.5 (Van der Meer, 1988) is found that the influence of permeability is only tested for  $\cot \alpha = 2$  and variable wave steepness. It is not certain that the influence of the permeability

is the same for more gentle slopes, because the wave absorption is more spread out over the slope increasing the stability even more.

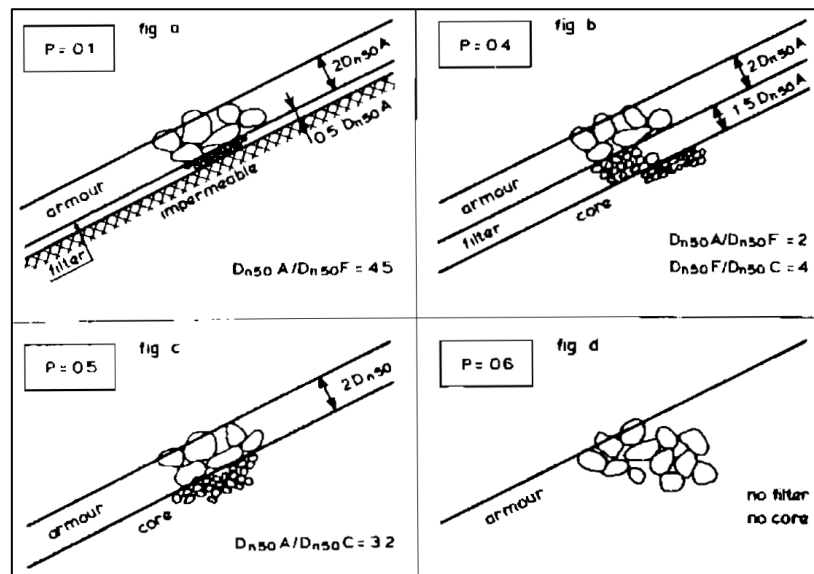


Figure 23 - Notional permeability P for various structures (Van der Meer, 1988)

- **Number of waves:** the parameter N represents the number of waves. After 7500 waves it is assumed that the damage erosion-profile has reached equilibrium. For storms with a short duration, lower values for N are used (cheaper). 3000 waves could represent a five hour storm.
- **Damage level:** the damage is based on the erosion profile after N waves, see Figure 24. It is described as  $S = \frac{A}{D_{n50}^2}$ . This is the erosion area divided by the square of the stone diameter. The erosion area A can be determined by measuring by soundings. The threshold for damage can be described with a value of S of 2 to 3. Failure of the structure (dependent on slope) occurs for a value of S of 10. The damage level only describes the eroded area and not the depth of the erosion. The design criteria to indicate whether the filter layer is visible or not is two times the diameter ( $2D_{n50}$ ) of the armour layer.

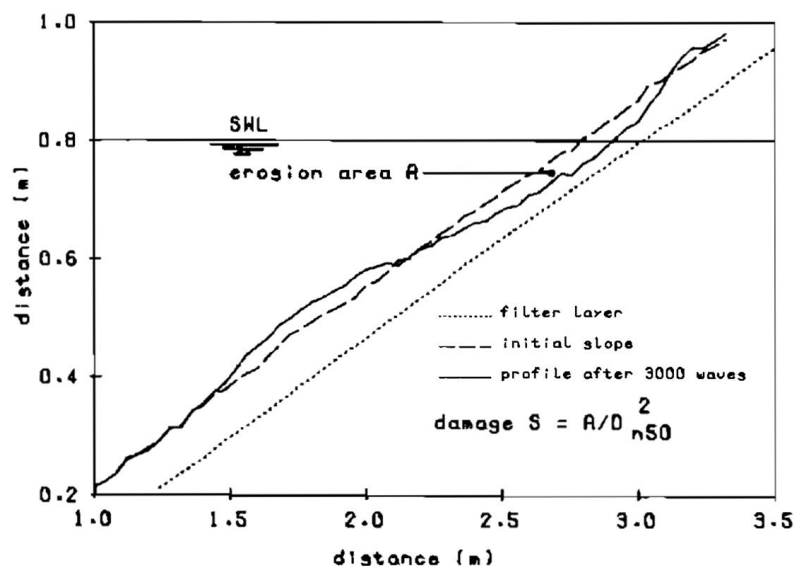


Figure 24 - Damage level S based on the erosion area A (Van der Meer, 1988)

### A.11 Formulas in wave model ENDEC

The experimental results of Sistermans (1993) and Ye (1996) are compared by Schiereck & Fontijn (1996) with computations according to Rance & Warren (1968) and computations according to Jonsson (1966) / Sleath (1978). These computations are obtained with the wave model ENDEC.

A modified relation of Rance & Warren (1968) is given in equation (A.36), in which the turbulent velocity  $q$  is added to the orbital velocity  $\hat{u}_b$  and a slope correction factor is included (Schiereck & Fontijn, 1996).

$$D_{n50} = \frac{2.15(\hat{u}_b + Fq)^{2.5}}{\sqrt{T}(\Delta g)^{1.5}} \frac{\sin \phi}{\sin(\phi - \alpha)} \quad (\text{A.36})$$

In which:  $q$  is the turbulent velocity (m/s),  $F$  is a calibration factor (-), and  $\phi$  is the angle of repose of stones (°).

The approach of Jonsson (1966) & Sleath (1978) is based on the equilibrium of forces on a single stone in a flow field, see also Section 2.2.1. By substituting the shear stress due to orbital velocities into the proportionality, the necessary diameter for stones on slopes is given by equation (A.37).

$$D_{n50} = \frac{0.84 \frac{1}{2} (f_w \hat{u}_b^2 + Fq^2)}{0.056 \Delta g} \frac{\sin \phi}{\sin(\phi - \alpha)} \quad (\text{A.37})$$

### A.12 Bed level change

The bed level change is computed from the spatial gradient in the bed-load transport, see equation (A.38). In which:  $\xi$  is the elevation of the bed (m), and  $n_p$  is the porosity of the sediment (-).

$$\frac{\partial \xi}{\partial t} + \frac{1}{(1 - n_p)} \frac{\partial q_b}{\partial x} = 0 \quad (\text{A.38})$$

A special type of bed level change is avalanching. This can be described as geotechnical slope collapse of the bed, and occurs when the angle of the bed exceeds the internal angle of repose.

- When  $|\tan \beta| > \phi$                       Avalanching.
- When  $|\tan \beta| \leq \phi$                       No avalanching.

### A.13 Cross-shore sediment transport

The cross-shore sediment transport can be described by equation (A.39) (Bosboom & Stive, 2013) and consists of the three terms worked out below. Their contributions can be found in Figure 25.

$$\langle \bar{U} | U|^2 \rangle = \underbrace{3 \langle \bar{U} | U_{hi}|^2 \rangle}_{\text{mean current / undertow}} + \underbrace{\langle U_{hi} | U_{hi}|^2 \rangle}_{\text{skewness}} + \underbrace{3 \langle U_{lo} | U_{hi}|^2 \rangle}_{\text{long waves}} \quad (\text{A.39})$$

- **Mean current/undertow:** Sediment is transported offshore due to the return current at the bottom. This undertow compensates the onshore transported mass of water due to waves.
- **Skewness:** Onshore sediment transport occurs due to skewness (horizontal asymmetric waves with smaller offshore velocities at wave trough than onshore velocities at wave crest).
- **Bound long waves:** Not relevant for this research. The direction of sediment transport changes when wave breaking occurs and the bound long waves become free long waves.

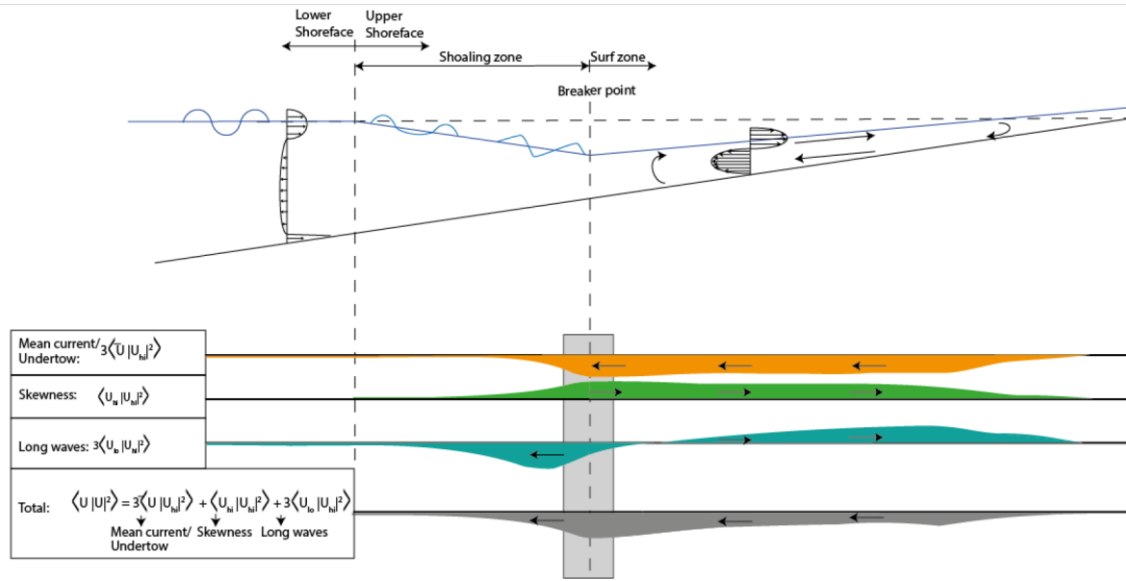


Figure 25 - Contributions of terms in sediment transport equation (A.39) (Bosboom & Stive, 2013)

In case of vertical wave asymmetry, no sediment transport seems to occur ( $\overline{u_\infty^3} = 0$ ) as the free stream velocity  $u_\infty$  is not skewed (onshore velocity is equal to offshore velocity in Figure 26). However, a net sediment transport does occur and is generated by significant acceleration skewness (Nielsen, 2002).

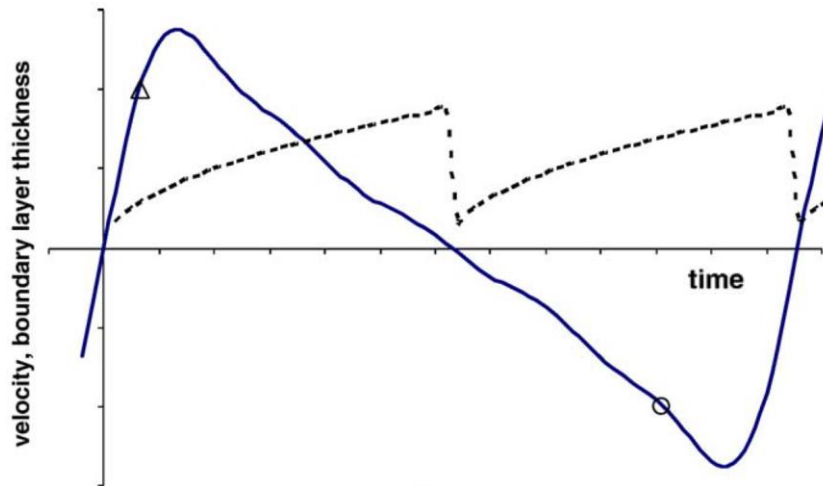


Figure 26 - Free stream velocity (blue) and boundary layer thickness (black dotted) over time (Nielsen, 2002)

The acceleration skewness is explained by means of a comparison between the points  $\Delta$  and  $O$  in Figure 26. The acceleration  $\dot{u}_\infty$  (described as steepness of blue line) and hence also the force  $F_{acc}$  due to pressure gradients (described in equation (2.3) in Section 2.2.2) is larger at point  $\Delta$  than at point  $O$ . Furthermore, the bed shear stress (given in equation (A.40)) is larger at point  $\Delta$ , because the boundary layer thickness  $\delta(t)$  is smaller at  $\Delta$ , while the free stream velocity is equal (Nielsen, 2002).

$$\tau_b(t) \approx \rho v_t \frac{u_\infty(t)}{\delta(t)} \quad \text{with} \quad \delta(t) = \sqrt{v_t(t - t_r)} \quad (\text{A.40})$$

In which:  $v_t$  is the eddy viscosity,  $u_\infty$  is the free stream velocity,  $\delta$  is the boundary layer thickness and  $t_r$  is the time of the latest velocity reversal.

### A.14 Parameters in drag term and inertia term of bed shear stress

The bed shear stress  $\tau_b$  is presented in equation (A.41), in which the drag term is the bed shear stress due to currents and the inertia term is the bed shear stress due to waves.

$$\tau_b = \underbrace{c_f \rho u |u|}_{\text{drag}} + \underbrace{\rho c_m c_v c_n D_{50} \frac{\partial u}{\partial t}}_{\text{inertia}} \quad (\text{A.41})$$

The drag term of the bed shear stress describes the forces exerted on the bed due to friction of currents. The drag term includes the dimensionless friction factor  $c_f$ , given in equation (A.42). This friction factor is determined according to Conley & Inman (1994) by including ventilated boundary layer effects in areas of infiltration and exfiltration (McCall, 2015).

$$c_f = c_{f,0} \left( \frac{\Phi}{e^{\Phi} - 1} \right) \quad \text{with} \quad \Phi = -\frac{1}{2} \frac{b_{cl}}{c_{f,0}} \frac{S}{|u|} \quad \text{and} \quad c_{f,0} = \frac{9.81}{\left( 18 \log \left( \frac{12h}{k_s} \right) \right)^2} \quad (\text{A.42})$$

In which:  $c_{f,0}$  is the dimensionless bed friction factor without ventilated boundary layer effects (-),  $\Phi$  is a dimensionless ventilation parameter,  $b_{cl}$  is a constant (= 0.9),  $k_s$  is the characteristic roughness height (assumed to be  $3D_{90}$ , as for flat beds according to Van Rijn (1982)). In XBeach-G, the boundary ventilation effects  $\left( \frac{\Phi}{e^{\Phi} - 1} \right)$  are limited (minimum of 0.1 and maximum of 3.0) (McCall, 2015).

The inertia term represents the bed shear stress due to asymmetric waves, as described in Section 2.5.2. The inertia term in equation (A.43) is computed in the same manner as the force exerted by the fluid motion on a stone due to pressure gradients created by accelerations in non-stationary flow, as the force  $F_{acc}$  due to pressure gradients (described in equation (2.3) in Section 2.2.2).

$$\tau_{b,inertia} = \rho c_m c_v c_n D_{50} \frac{\partial u}{\partial t} \quad (\text{A.43})$$

In which:  $c_m$  is an inertia coefficient ( $c_m = 1 + c_a$ ) with the added mass coefficient  $c_a$  (= 0.5 for spheres with zero autonomous acceleration),  $c_v$  is the volume shape factor ( $c_v = \pi/6$  for spheres), and  $c_n$  is a coefficient for the number of particles on the surface influenced by accelerations per unit of area. These coefficients can be replaced by one calibration coefficient for inertia  $c_i = c_m c_v c_n \approx O(1)$ .

### A.15 Parameters in formula of Nielsen (2006)

The sediment mobilizing velocity  $u_\theta(t)$  (which can be explained as the bed shear velocity) is given by equation (A.44) (Nielsen, 2002).

$$u_\theta(t) = \sqrt{\frac{f_s}{2}} \left( \underbrace{\cos \varphi_\tau \frac{u_\infty}{\text{velocity}}}_{\text{velocity}} + \underbrace{\frac{T_{m-1.0}}{2\pi} \sin \varphi_\tau \frac{\partial u_\infty}{\partial t}}_{\text{acceleration}} \right) \quad (\text{A.44})$$

In which:  $u_\theta(t)$  is a sediment mobilizing velocity,  $\varphi_\tau$  is the phase lag angle between the wave induced current and the period of the bed shear velocity ( $\varphi_\tau = 35-40^\circ$ ),  $f_s$  is the sediment friction factor (-) (for which a standard value of 0.025 is taken in XBeach-G) and  $T_{m-1.0}$  is the spectral mean period (s).

The influence of the phase lag angle and the sediment friction factor on the accuracy of the formula of Nielsen (2006) is significant. An elaboration of these two parameters is given below.

The phase lag angle is defined as the phase difference between the bed shear velocity and the free stream velocity. Postma (2016) used a value of 25° for the phase lag angle.

- When  $\varphi_\tau = 0^\circ$  Sediment transport is dominated by drag (i.e. velocity) term (Nielsen, 2006).
- When  $\varphi_\tau = 90^\circ$  Pressure gradient dominated sediment transport (Nielsen, 2006).
- When  $\varphi_\tau \approx 40^\circ$  Optimal phase lag angle according to transport rates in swash zone and to vertical sediment transport corresponding to sheet flow (Nielsen, 2002).

The sediment friction factor can be determined by equation (A.45).

$$f_s = \exp\left(5.5\left(\frac{2.5D_{50}}{A}\right)^{0.2} - 6.3\right) \quad \text{with} \quad A = \frac{\sqrt{2}}{\omega_p} \sqrt{\text{var}(u_\infty(t))} \quad (\text{A.45})$$

In which:  $\omega_p$  is the angular peak velocity ( $\omega_p = 2\pi/T_p$ , determined with  $T = T_p$  for regular waves).

In XBeach-G, the sediment friction factor is assumed to be a constant with a default value of 0.025.

### A.16 Parameters in formula of Van Rijn (1984) for currents

The bed-load transport formula of Van Rijn (1984) for currents only conditions is presented in equation (A.46) (for particles in the range of 200 to 2,000  $\mu\text{m}$ ).

$$q_b = 0.053 \sqrt{\Delta g D_{50}^3} \frac{T^{2.1}}{D_*^{0.3}} \quad (\text{A.46})$$

Van Rijn derived this formula by means of the saltation height  $\delta_b/D$ , the particle velocity  $u_b$  and the bed-load concentration  $c_b$  (Van Rijn, 1984). The formulas are given in equation (A.47). In these formulas, Van Rijn used a dimensionless particle parameter  $D_*$  and a transport stage parameter T to describe the bed-load transport rate, see equation (A.48).

$$\frac{\delta_b}{D} = 0.3D_*^{0.7}T^{0.5} \quad \text{and} \quad u_b = \sqrt{\Delta g D} 1.5T^{0.6} \quad \text{and} \quad \frac{c_b}{c_0} = 0.18 \frac{T}{D_*} \quad (\text{A.47})$$

$$D_* = D_{50} \left(\frac{\Delta g}{\nu^2}\right)^{1/3} \quad \text{and} \quad T = \frac{(u'_*)^2 - (u_{*,cr})^2}{(u_{*,cr})^2} \quad \text{with} \quad u'_* = \frac{\sqrt{g}}{C'} \bar{u} \quad (\text{A.48})$$

In which:  $c_0$  is the maximum bed concentration (= 0.65),  $u'_*$  is the bed shear velocity,  $\bar{u}$  is the mean flow velocity,  $u_{*,cr}$  is the critical bed shear velocity according to Shields (1936),  $\nu$  is the kinematic viscosity of water ( $\text{m}^2/\text{s}$ ) ( $\approx 10^{-6} \text{ m}^2/\text{s}$ ), and  $C'$  is the Chézy coefficient related to grains (Van Rijn, 1984).

### A.17 Parameters in formula of Van Rijn (2007) for currents and waves

The bed-load transport formula of Van Rijn (2007) for currents and waves is given in equation (A.49).

$$q_b = \gamma \rho_s f_{silt} D_{50} D_*^{-0.3} \sqrt{\frac{\tau'_{b,cw}}{\rho}} \left[ \frac{(\tau'_{b,cw} - \tau_{b,cr})}{\tau_{b,cr}} \right]^\eta \quad (\text{A.49})$$

In which:  $q_b$  is the volumetric bed-load transport rate (excluding pore space) ( $\text{kg}/\text{s}/\text{m}$ ),  $\gamma$  is a calibration coefficient ( $\gamma = 0.5$  according to Van Rijn (2007)),  $D_*$  is the non-dimensional particle diameter, and for gravel beaches, both  $f_{silt}$  and  $\eta$  have a value of 1.  $\tau_{b,cr}$  is the critical bed-shear

stress according to Shields (1936) and  $\tau'_{b,cw}$  is the instantaneous grain-related bed-shear stress due to currents and waves, which is given in equation (A.50).

$$\tau'_{b,cw} = 0.5\rho_w f'_{cw} (U_{\delta,cw})^2 \quad \text{with} \quad f'_{cw} = \alpha\beta f'_c + (1 - \alpha)f'_w \quad (\text{A.50})$$

In which:  $f'_{cw}$  is the grain friction coefficient due to currents and waves,  $U_{\delta,cw}$  is the instantaneous velocity due to currents and waves at edge of wave boundary layer,  $\alpha$  is the coefficient related to relative strength of wave and current motion (see equation (A.51)), and  $\beta$  is the coefficient related to the vertical structure of the velocity profile (according to Van Rijn (1993)).  $f'_c$  is the current-related grain friction coefficient (based on the Darcy-Weisbach), and  $f'_w$  is the wave-related grain friction coefficient (based on Swart (1974) (Saers, 2005)). As can be seen in equation (A.52), both these friction coefficients are based on  $k_{s,grain} = 1D_{90}$  (Van Rijn, 2007).

$$\alpha = \frac{u_c}{u_c + U_w} \quad (\text{A.51})$$

$$f'_c = \frac{8g}{\left[18 \log\left(\frac{12h}{k_{s,grain}}\right)\right]^2} \quad \text{and} \quad f'_w = \exp\left(-6 + 5.2\left(\frac{A_w}{k_{s,grain}}\right)^{-0.19}\right) \quad (\text{A.52})$$

In which:  $u_c$  is the depth-averaged current velocity (m/s),  $U_w$  is the peak orbital velocity near the bed (m/s),  $A_w$  is the peak orbital diameter near the bed (m).  $A_w$  is given in equation (A.53) with the linear wave theory for a situation without varying water depth to estimate  $U_w$ .

$$A_w = \frac{U_w T}{2\pi} \quad \text{with} \quad U_w = \frac{\pi H_{m0}}{T} \frac{1}{\sinh(kh)} \quad (\text{A.53})$$

In which: T is the characteristic wave period (s) ( $T_{m-0,1}$  is used), k is the wave number (1/m), and h is the water depth at the ROI (m).

### A.18 Simplified formula of Van Rijn (2007)

The simplified formula of Van Rijn (2007) to compute bed-load transport for steady flow (with or without waves) is derived using the detailed, numerical intra-wave TR2004 model (Van Rijn, 2007). The formula is given in equation (A.54).

$$q_b = 0.015\rho_s u h \left(\frac{D_{50}}{h}\right)^{1.2} M_e^{1.5} \quad \text{with} \quad M_e = \frac{u_e - u_{cr}}{\sqrt{\Delta g D_{50}}} \quad (\text{A.54})$$

In which:  $M_e$  is a mobility parameter,  $u_e$  is the effective velocity (see equation (A.55)) with  $\gamma = 0.4$  for irregular waves (and 0.8 for regular waves), u is the depth-averaged flow velocity and  $U_w$  is the peak orbital velocity based on linear wave theory with the significant wave height  $H_s$  and the peak wave period  $T_p$ .

$$u_e = u + \gamma U_w \quad \text{and} \quad U_w = \frac{\pi H_s}{T_p \sinh(kh)} \quad (\text{A.55})$$

The critical velocity, given in equation (A.56), is divided into the critical velocity for currents  $u_{cr,c}$  based on Shields (1936) and the critical velocity for waves  $u_{cr,w}$  based on Komar & Miller (1975) (Van Rijn, 2007).

$$u_{cr} = \beta u_{cr,c} + (1 - \beta)u_{cr,w} \quad \text{and} \quad \beta = \frac{u}{u + U_w} \quad (\text{A.56})$$

For  $0.05 < D_{50} < 0.50$  mm, the critical velocity for currents and waves is given by equation (A.57).

$$u_{cr,c} = 0.19(D_{50})^{0.1} \log\left(\frac{12h}{3D_{90}}\right) \quad \text{and} \quad u_{cr,w} = 0.24(\Delta g)^{0.66} D_{50}^{0.33} (T_p)^{0.33} \quad (\text{A.57})$$

For  $0.50 < D_{50} < 2.00$  mm, the critical velocity for currents and waves is given by equation (A.58).

$$u_{cr,c} = 8.5(D_{50})^{0.6} \log\left(\frac{12h}{3D_{90}}\right) \quad \text{and} \quad u_{cr,w} = 0.95(\Delta g)^{0.57} D_{50}^{0.43} (T_p)^{0.14} \quad (\text{A.58})$$

## Appendix B Verification previous physical scale model tests

### B.1 Test set up of profile change experiments of Kramer (2016)

The test set up for the profile change experiments of Kramer (2016) is schematized in Figure 27. The Leica C10 laser scanner is shown as a circle in the upper left corner. The bold lines are wave gauges and the dashed line is the EMS.

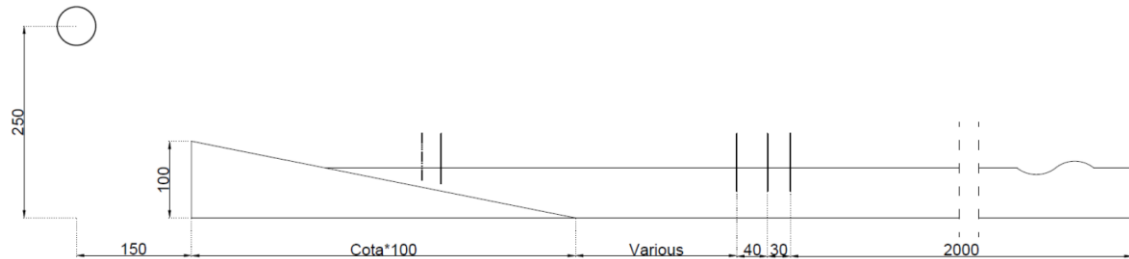


Figure 27 - Test set up for profile change experiments of Kramer (2016) (length in cm) (Kramer, 2016)

The preparation of the slope in the wave flume with the stone layer (thickness of  $2D_{n50}$ ) is shown in Figure 28 (left & middle). In Figure 28 (right), the Leica C10 laser scanner (red box) and three trackers (red circles) are shown.

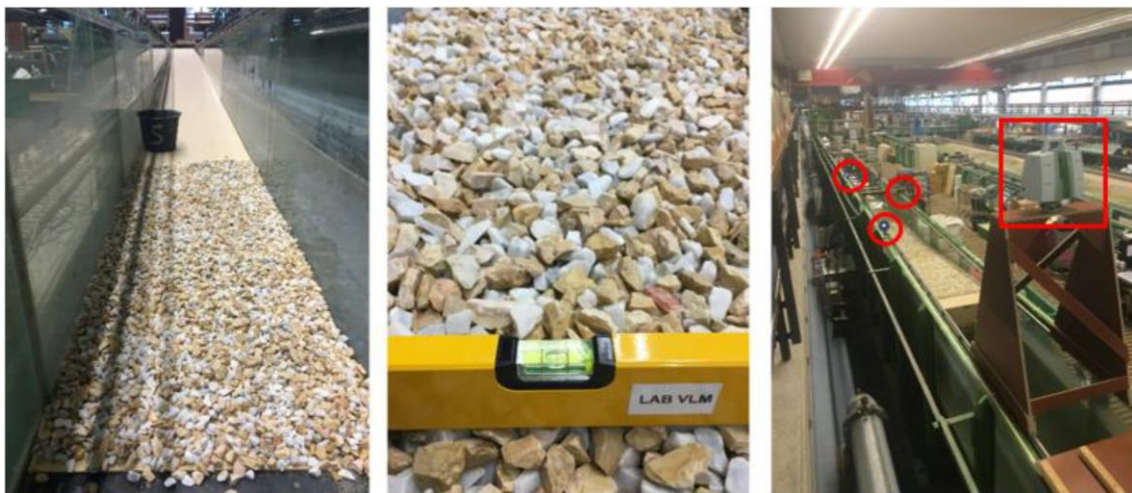


Figure 28 - Preparation of slope (left & middle) and Leica C10 scanner with trackers (right) (Kramer, 2016)

### B.2 Boundary restricted erosion profiles for 1:15 slope with $S_{Wit}$ input

The boundary restricted erosion profile for 1:15 slope with  $S_{Wit}$  input, modelled with the bed-load transport formula of Nielsen (2006) with standard values, is presented in Figure 29. The right boundary restricts the sediment transport. Therefore, the original length of the 1:15 slope of the profile change experiments of Kramer (2016) is extended in upslope direction to overcome this problem.

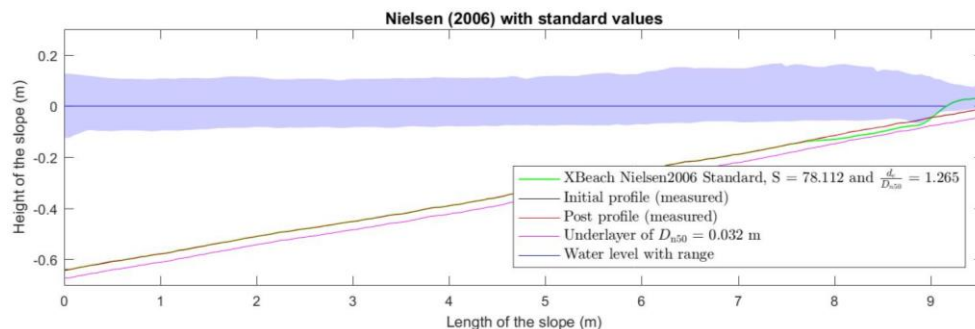


Figure 29 - Boundary restricted erosion profile for 1:15 slope and  $S_{Wit}$  input

### B.3 Preparation of BIV experiments by Kramer (2016)

The Field of View (FOV) with black stones and Depth of Field (DOF) (left), the DOF (middle) and the setup of the two 50W LED lights (right) are shown in Figure 30.



Figure 30 - FOV with black stones and DOF (left), DOF (middle) and setup of LED lights (right) (Kramer, 2016)

### B.4 Visual analysis of movements of stones

The analysis of the movements of stones of the videos of the BIV experiments of Kramer (2016) by means of visual observation is explained with Figure 31. The frames of video 05\_BIV\_0001 show the movements of the stone from the moment before the incoming wave, the wave breaking on the 1:5 slope, flow reversal, and the return flow. The movements of stone in the red box, which represents the ROI, are examined. The time of each frame in the video can be determined with the fps of 132.

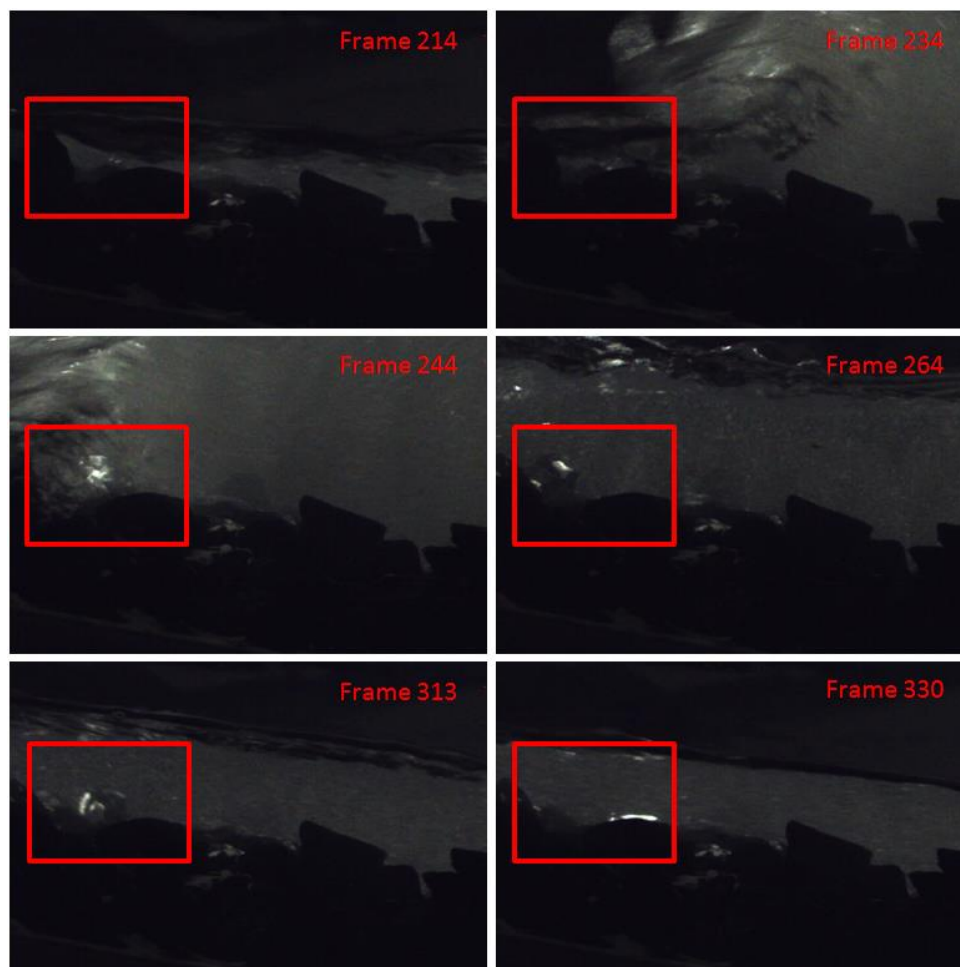


Figure 31 - Explanation of visual analysis of movements of stones with frames of video 05\_BIV\_0001

In which: frame 214 shows the moment before the incoming wave with a stable stone. Frame 234 represents the start of the breaking of the wave on the slope at the location of the stone. The stone starts to move (displacement) in upslope direction. Frame 244 shows the passing of the wave and the displacement of the stone in upslope direction. Furthermore, the horizontal velocity has the maximum (negative) value at frame 244. Frame 264 represents the moment of flow reversal (from the breaking wave to the return flow) and the stone moves a little in downslope direction (rocking). Frame 302 (not shown) shows the start of displacement of the stone in downslope direction. Frame 313 gives the return flow of the water and displacement of the stone in downslope direction. Frame 330 shows the return flow and a stable stone, settled in the bed.

The direction of the movement of the water and the stone can be upslope or downslope directed. The movement of wave in upslope direction is called run-up and the movement of water in downslope direction is called run-down.

The visual analysis in Figure 31 is only done for a single incoming wave with subsequent return flow to explain the methodology. The visual analysis is performed for all frames of the videos. In this way, the movements of stones in the ROI can be found for each incoming wave and the subsequent return flow. The results of the visual analysis can be found per slope/video in Appendix D. With the results of the visual analysis, the horizontal velocity and acceleration can be determined at the specific moment in time when the stone starts to move (initiation of motion).

The type and the direction of the movements of the stone are indicated in the figures of the horizontal velocity, the acceleration and the mobility parameters in Section 5.1 and Appendix D.

## B.5 Image pre-processing techniques in PIVlab

The effects of pre-processing techniques to improve the measurement quality by the enhancement of the images are shown in Figure 32. The pre-processing techniques are elaborated briefly below, using the research of Thielicke and Stamhuis (2014).

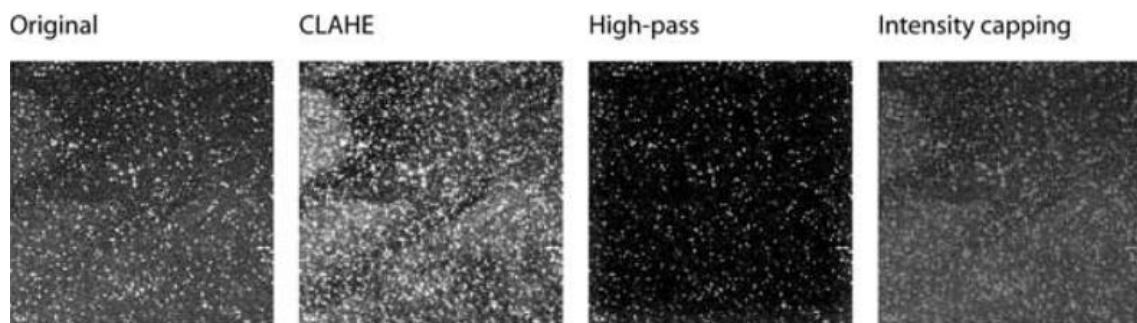


Figure 32 - Effect of pre-processing techniques (Thielicke & Stamhuis, 2014)

- **CLAHE** (contrast limited adaptive histogram equalization) filter increases the readability of the image data. Improves image by 4.7 + 3.2 %.
- **High-pass** filter conserves the high frequency information by removing low frequency background information caused by inhomogeneous lighting.
- **Intensity capping** filter prevents that brighter particles/spots contribute (statistically) more to the correlation signal. Improves image by 5.2 + 2.5 %.

## B.6 Calibration of images in PIVlab

A calibration image is, imported in PIVlab, to calibrate the images for the BIV analysis of the 1:5 slope is shown in Figure 33.

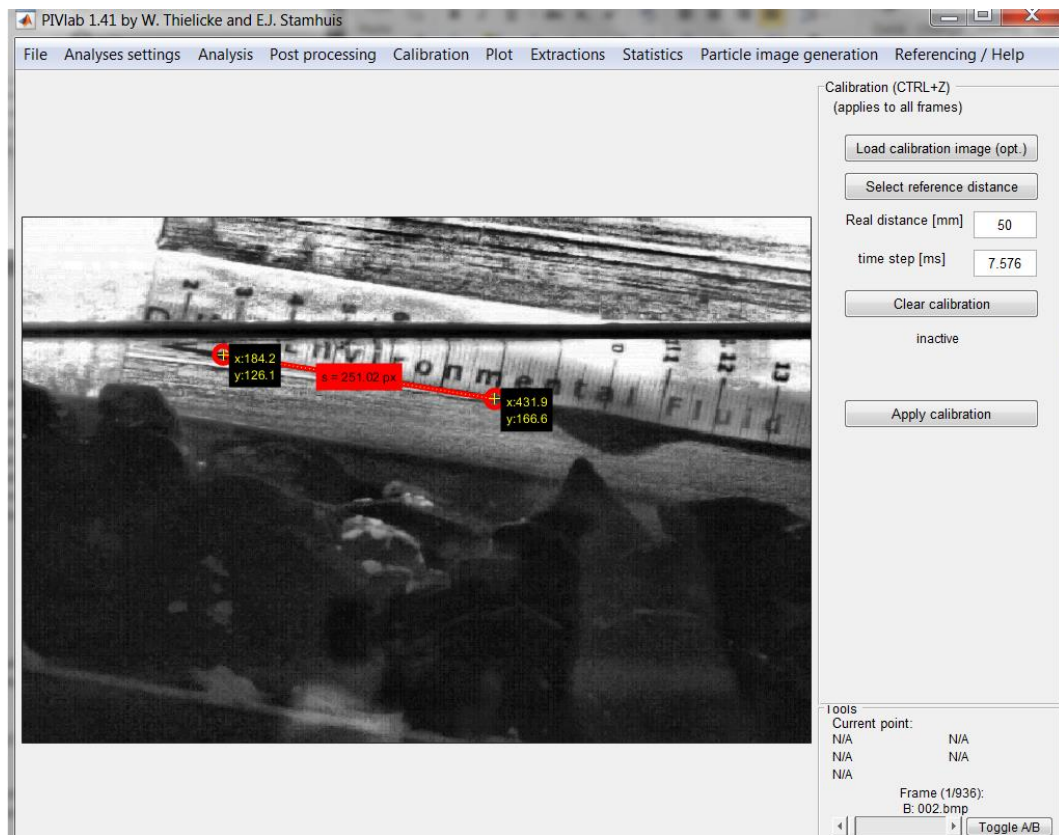


Figure 33 - Screenshot of calibration image imported in PIVlab for the BIV analysis of 1:5 slope

## B.7 Extreme values of horizontal velocity with linear wave theory

The extreme values of the horizontal velocity are compared with linear wave theory in Table 27. The extreme values of the data points of the horizontal velocity are used for this comparison, and not the extreme values of the fitted curve of the horizontal velocity. As can be seen in Table 27, the extreme values agree well with each other. The maximum value of the velocity of the BIV experiment could be lower than the maximum value of the velocity according to linear wave theory due to friction (as the water moves downslope in case of positive values). The extreme values according to linear wave theory are determined with equation (B.1).

Table 27 - Check extreme values of horizontal velocity with linear wave theory for 1:5 slope

<b>U</b> BIV experiment (m/s)	min	-0.895
	max	0.555
<b>U</b> Linear wave theory (m/s)	min	-0.737
	max	0.737

$$U = \frac{1}{2} H \sqrt{\frac{g}{h}} \sin(\omega t) \quad (\text{B.1})$$

In which: U is the horizontal velocity (m/s), h is the water depth at the ROI (m), and for extreme values  $\sin(\omega t)$  becomes -1 or 1.

## B.8 Ensemble averaging of horizontal velocity

Because the BIV experiments are executed with regular waves, the methodology of curve fitting of the horizontal velocity can be investigated with ensemble averaging. With ensemble averaging, the velocity data points of the BIV analysis with the same phase are plotted in one phase, and a curve is fitted through all these scattered data points with the fit-function in MATLAB using 'smoothingspline' with a value of 0.997 for the option 'SmoothingParam'. In this way, local uncertainties in the scattered data can be averaged out and the curve can be fitted more accurately.

The negative peaks of the horizontal velocity, derived from the video of the BIV experiment of Kramer (2016) for 1:10 slope, are checked with the negative peak of the horizontal velocity obtained with ensemble averaging.

As can be seen in Figure 34, the horizontal velocity of the three wave periods (3T) are plotted in one wave period (T) for the 1:10 slope.

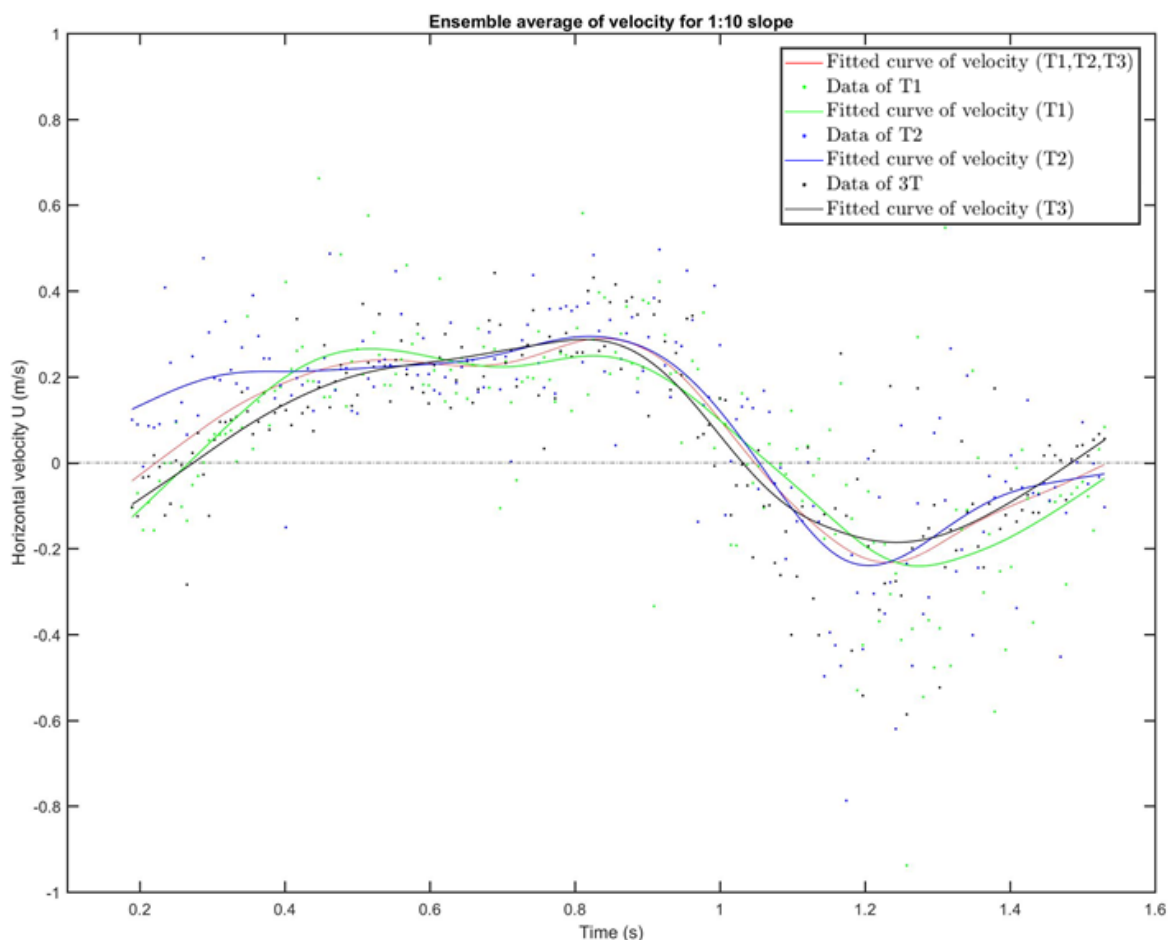


Figure 34 - Ensemble average of wave periods T1, T2 and T3 of horizontal velocity for 1:10 slope

In which: the velocities have a negative value during run-up (in case of incoming waves) and the values of the velocities are positive during run-down (in case of return flow).

Ensemble averaging does not result in higher values of the negative and positive peaks of the horizontal velocity, because the scattered data is present in all three phases. Therefore, ensemble averaging will not be used further.

**NOTE:** the wave period  $T$  has a value of 1.5503 s. The wave period should be in agreement with the duration of each phase. A phase can be defined as the time between the two moments where the velocity becomes positive. When looking at the horizontal velocity over time (see Figure 43 in Appendix D.2), the wave period does not correspond exactly to the phase. The duration of each phase is shown in Table 28. However, the negative and positive peaks of the horizontal velocity of the three phases apart can still be compared with the peaks of the horizontal velocity obtained with ensemble averaging.

**Table 28 - Phases determined from horizontal velocity over time for 1:10 slope (Figure 43)**

Phase	Time (s)			Frame (-)		
	from	to	$\Delta T$	from	to	$\Delta f$
T1	0.189	1.530	1.341	25	202	177
T2	1.538	2.879	1.341	203	380	177
T3	2.886	4.227	1.341	381	558	177

## Appendix C Results of XBeach-G simulations

### C.1 Erosion profiles for 1:5 slope with $S_{norm}$ input

The erosion profiles for 1:5 slope with  $S_{norm}$  input, modelled with the bed-load transport formulas of Nielsen (2006) and Van Rijn (2007), are presented in Figure 35.

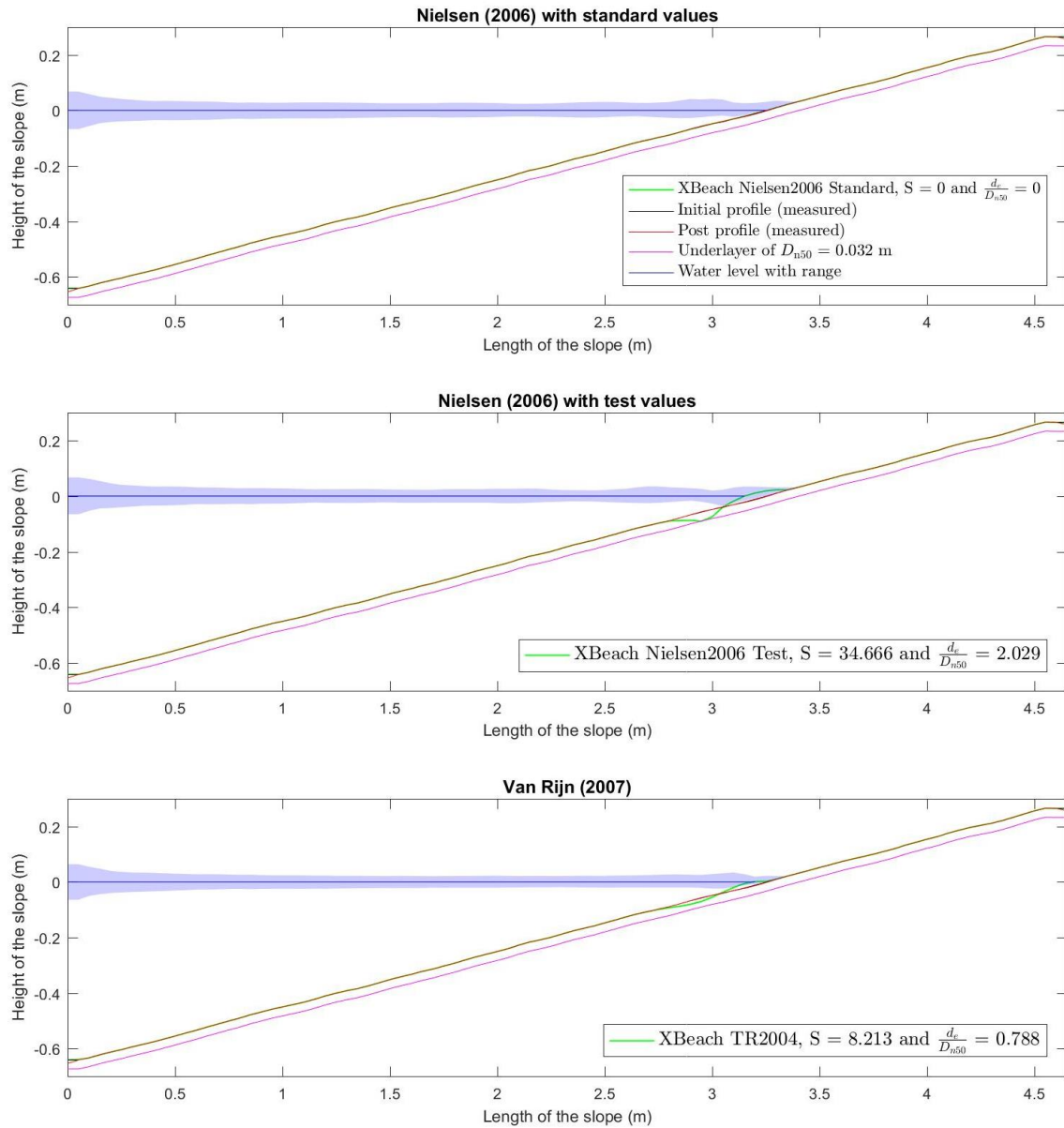


Figure 35 - Erosion profiles for 1:5 slope and  $S_{norm}$  input

An overview is given in Table 29 of the simulations and the damage derived from the erosion profiles modelled with 1:5 slope and  $S_{norm}$  input.

Table 29 - Overview of simulations and damage obtained from erosion profiles for 1:5 slope and  $S_{norm}$  input

	1:5 slope & $S_{norm}$ input	$A_e$ (m <sup>2</sup> )	$S$ (-)	$d_e/D_{n50}$ (-)	$E_3$ (%)	Profile development
1	Experiment of Kramer (2016)	-1.44E-04	0.55	-	35.8	-
2	XBeach-G Nielsen (2006) Standard	0.00	0.00	0.000	0.0	No erosion profile
3	XBeach-G Nielsen (2006) Test	-9.10E-03	34.67	2.029	203.1	Reversed transport, crest profile
4	XBeach-G Van Rijn (2007)	-2.20E-03	8.21	0.788	79.0	Reversed transport, crest profile

## C.2 Erosion profiles for 1:5 slope with $S_{Wit}$ input

The erosion profiles for 1:5 slope with  $S_{Wit}$  input, modelled with the bed-load transport formulas of Nielsen (2006) and Van Rijn (2007), are presented in Figure 36.

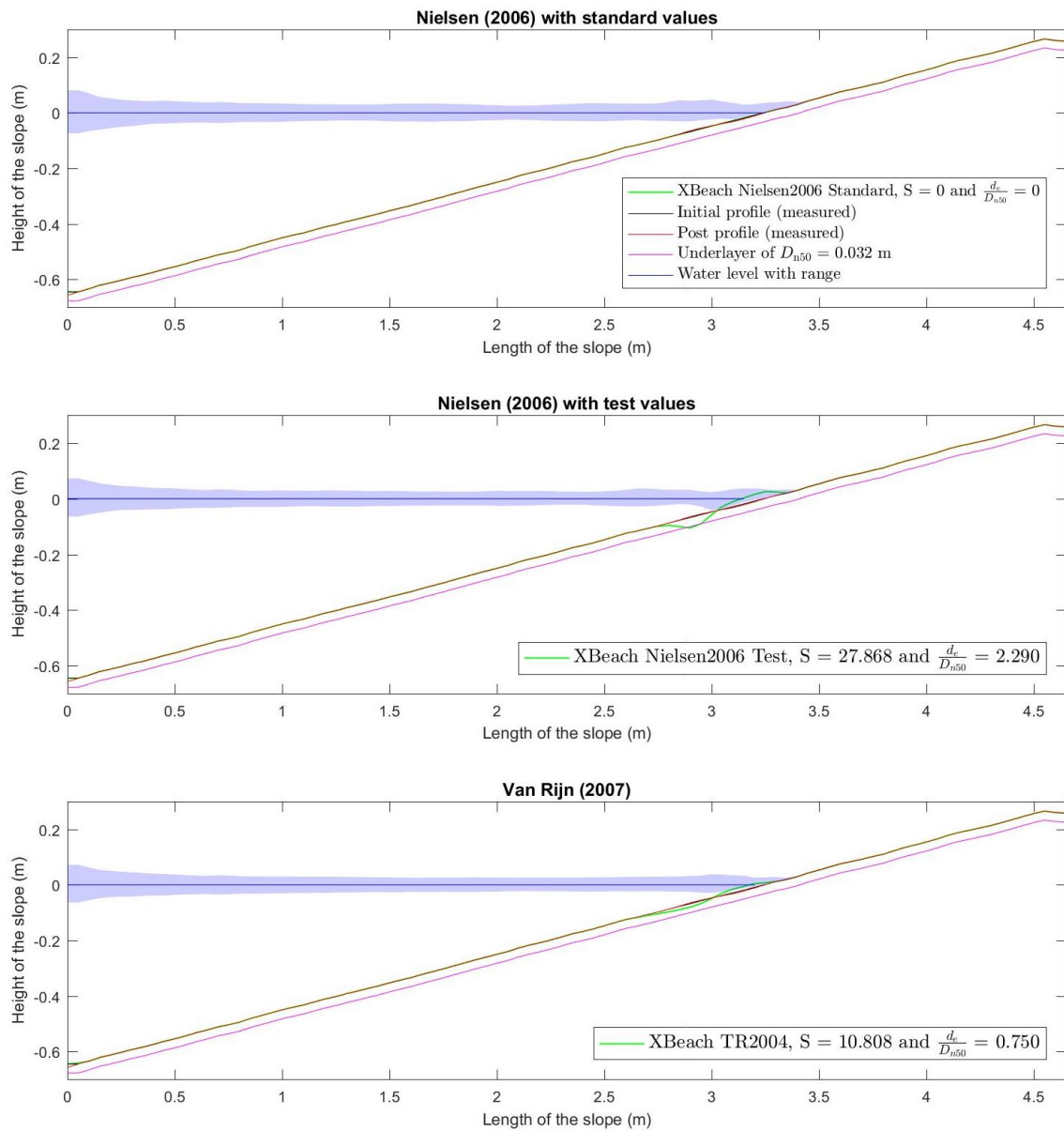


Figure 36 - Erosion profiles for 1:5 slope and  $S_{Wit}$  input

An overview is given in Table 30 of the simulations and the damage derived from the erosion profiles modelled with 1:5 slope and  $S_{Wit}$  input.

Table 30 - Overview of simulations and damage obtained from erosion profiles for 1:5 slope and  $S_{Wit}$  input

	1:5 slope & $S_{Wit}$ input	$A_e$ (m <sup>2</sup> )	$S$ (-)	$d_e/D_{n50}$ (-)	$E_3$ (%)	Profile development
1	Experiment of Kramer (2016)	-2.77E-04	1.02	-	6.3	-
2	XBeach-G Nielsen (2006) Standard	0.00	0.00	0.000	0.0	No erosion profile
3	XBeach-G Nielsen (2006) Test	-7.30E-03	27.87	2.290	229.0	Reversed transport, crest profile
4	XBeach-G Van Rijn (2007)	-2.80E-03	10.81	0.750	74.7	Reversed transport, crest profile

### C.3 Erosion profiles for 1:10 slope with $S_{wit}$ input

The erosion profiles for 1:10 slope with  $S_{wit}$  input, modelled with the bed-load transport formulas of Nielsen (2006) and Van Rijn (2007), are presented in Figure 37.

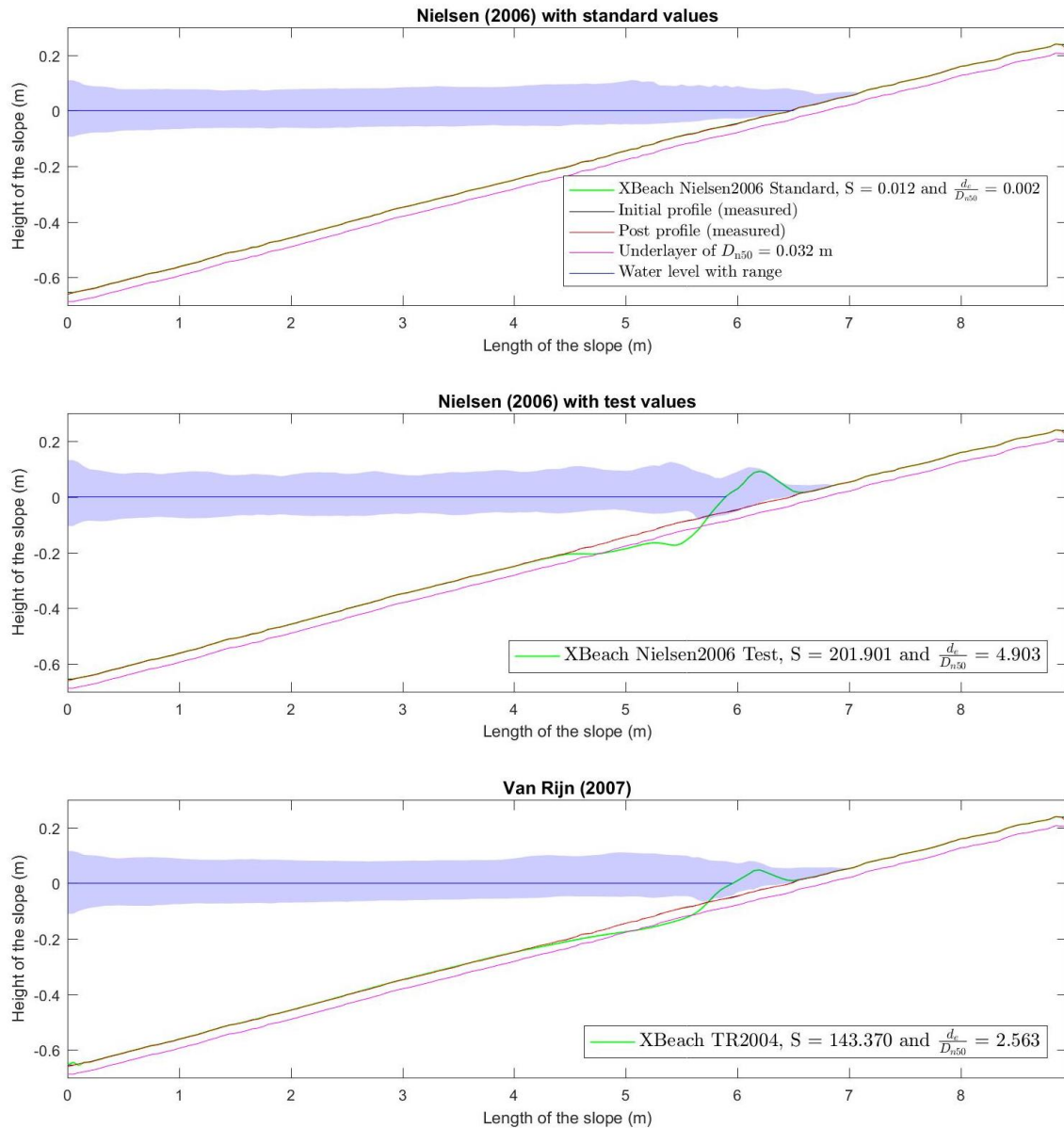


Figure 37 - Erosion profiles for 1:10 slope and  $S_{wit}$  input

An overview is given in Table 31 of the simulations and the damage derived from the erosion profiles modelled with 1:10 slope and  $S_{wit}$  input.

Table 31 - Overview of simulations and damage obtained from erosion profiles for 1:10 slope and  $S_{wit}$  input

	1:10 slope & $S_{wit}$ input	$A_e$ (m <sup>2</sup> )	S (-)	$d_e/D_{n50}$ (-)	$E_3$ (%)	Profile development
1	Experiment of Kramer (2016)	-5.29E-04	2.01	-	44.4	-
2	XBeach-G Nielsen (2006) Standard	-3.02E-06	0.01	0.002	0.2	No erosion profile
3	XBeach-G Nielsen (2006) Test	-5.30E-02	201.90	4.903	490.1	Very large crest profile
4	XBeach-G Van Rijn (2007)	-3.76E-02	143.37	2.563	255.6	Very large crest profile

## C.4 Erosion profiles for 1:10 slope with $S_{S\&F}$ input

The erosion profiles for 1:10 slope with  $S_{S\&F}$  input, modelled with the bed-load transport formulas of Nielsen (2006) and Van Rijn (2007), are presented in Figure 38.

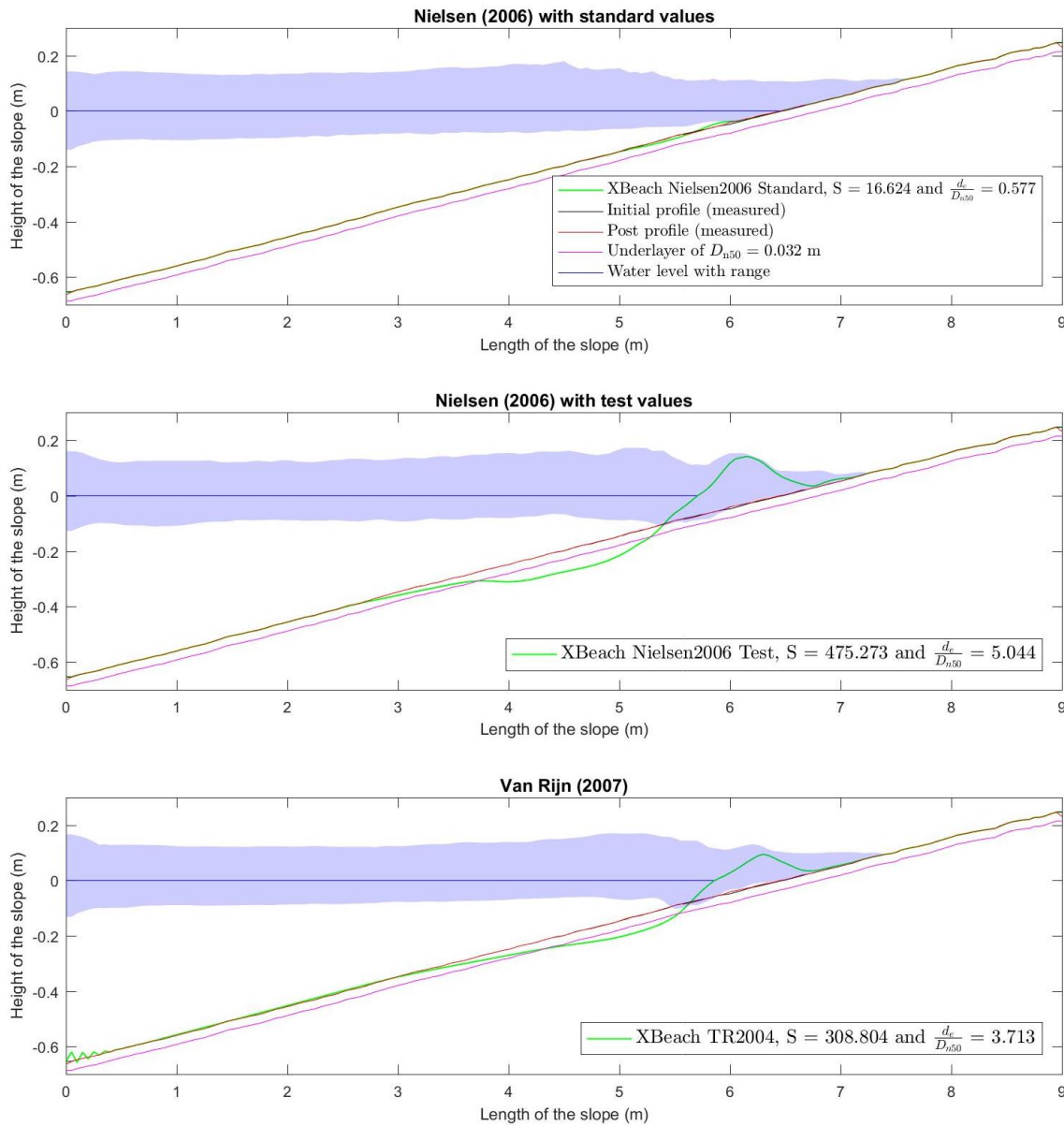


Figure 38 - Erosion profiles for 1:10 slope and  $S_{S\&F}$  input

An overview is given in Table 32 of the simulations and the damage derived from the erosion profiles modelled with 1:10 slope and  $S_{S\&F}$  input.

Table 32 - Overview of simulations and damage obtained from erosion profiles for 1:10 slope and  $S_{S\&F}$  input

	1:10 slope & $S_{S\&F}$ input	$A_e$ (m <sup>2</sup> )	$S$ (-)	$d_e/D_{n50}$ (-)	$E_3$ (%)	Profile development
1	Experiment (adapted*) of Kramer (2016)	-3.07E-04	1.07	-	50.0	-
2	XBeach-G Nielsen (2006) Standard	-4.40E-03	16.62	0.577	57.4	Wide erosion profile
3	XBeach-G Nielsen (2006) Test	-1.25E-01	475.27	5.044	504.3	Very large crest profile
4	XBeach-G Van Rijn (2007)	-8.10E-02	308.80	3.713	371.6	Very large crest profile

\*Kramer (2016) adapted the results of this experiment to exclude significant boundary effects.

## C.5 Erosion profiles for 1:15 slope with $S_{Wit}$ input

The erosion profiles for 1:15 slope with  $S_{Wit}$  input, modelled with the bed-load transport formulas of Nielsen (2006) and Van Rijn (2007), are presented in Figure 39.

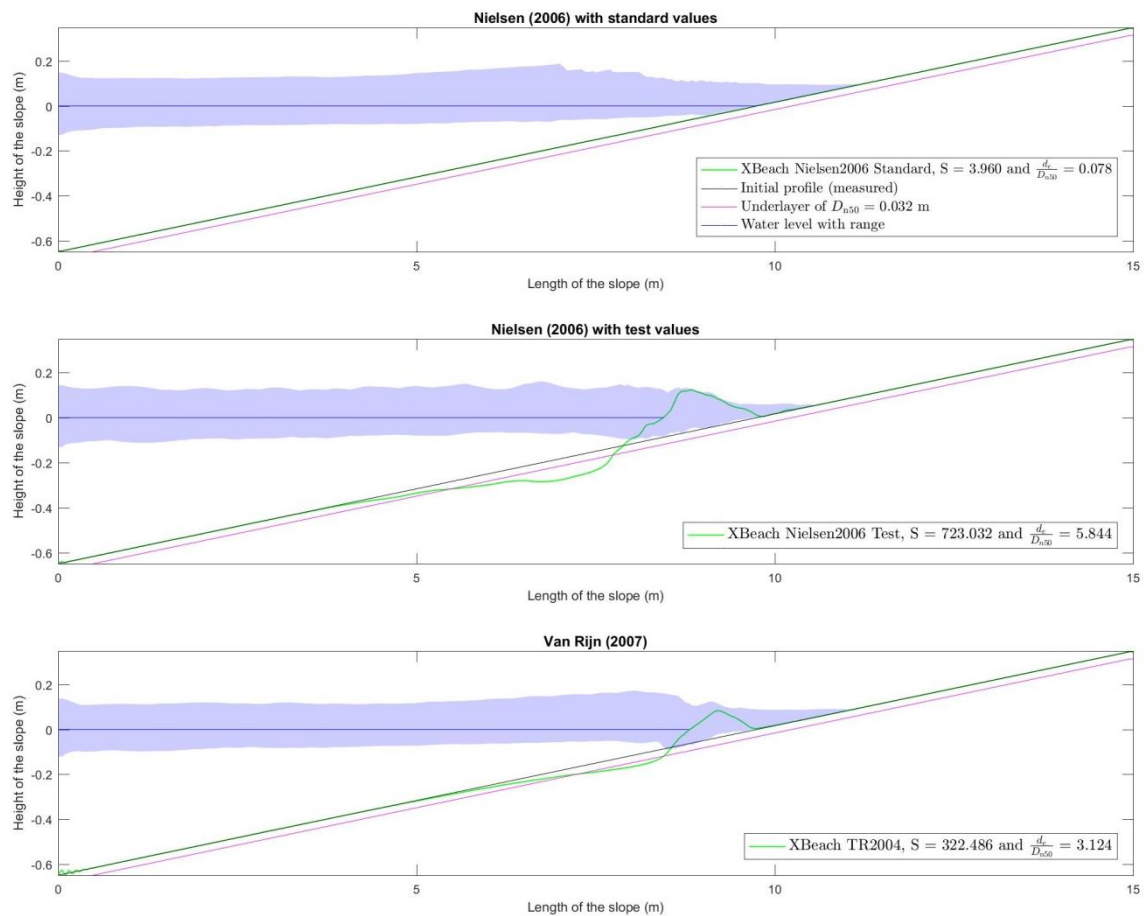


Figure 39 - Erosion profiles for 1:15 slope and  $S_{Wit}$  input

An overview is given in Table 33 of the simulations and the damage derived from the erosion profiles modelled with 1:15 slope and  $S_{Wit}$  input.

Table 33 - Overview of simulations and damage obtained from erosion profiles for 1:15 slope and  $S_{Wit}$  input

	1:15 slope & $S_{Wit}$ input	$A_e$ (m <sup>2</sup> )	$S$ (-)	$d_e/D_{n50}$ (-)	$E_3$ (%)	Profile development
1	Experiment of Kramer (2016)	-2.76E-04	1.05	-	33.3	-
2	XBeach-G Nielsen (2006) Standard	-1.00E-03	3.96	0.078	8.0	Wide erosion profile
3	XBeach-G Nielsen (2006) Test	-1.90E-01	723.03	5.844	584.6	Very large crest profile
4	XBeach-G Van Rijn (2007)	-8.46E-02	322.49	3.124	312.3	Very large crest profile

## C.6 Erosion profiles for 1:15 slope with $S_{S\&F}$ input

The erosion profiles for 1:15 slope with  $S_{S\&F}$  input, modelled with the bed-load transport formulas of Nielsen (2006) and Van Rijn (2007), are presented in Figure 40.

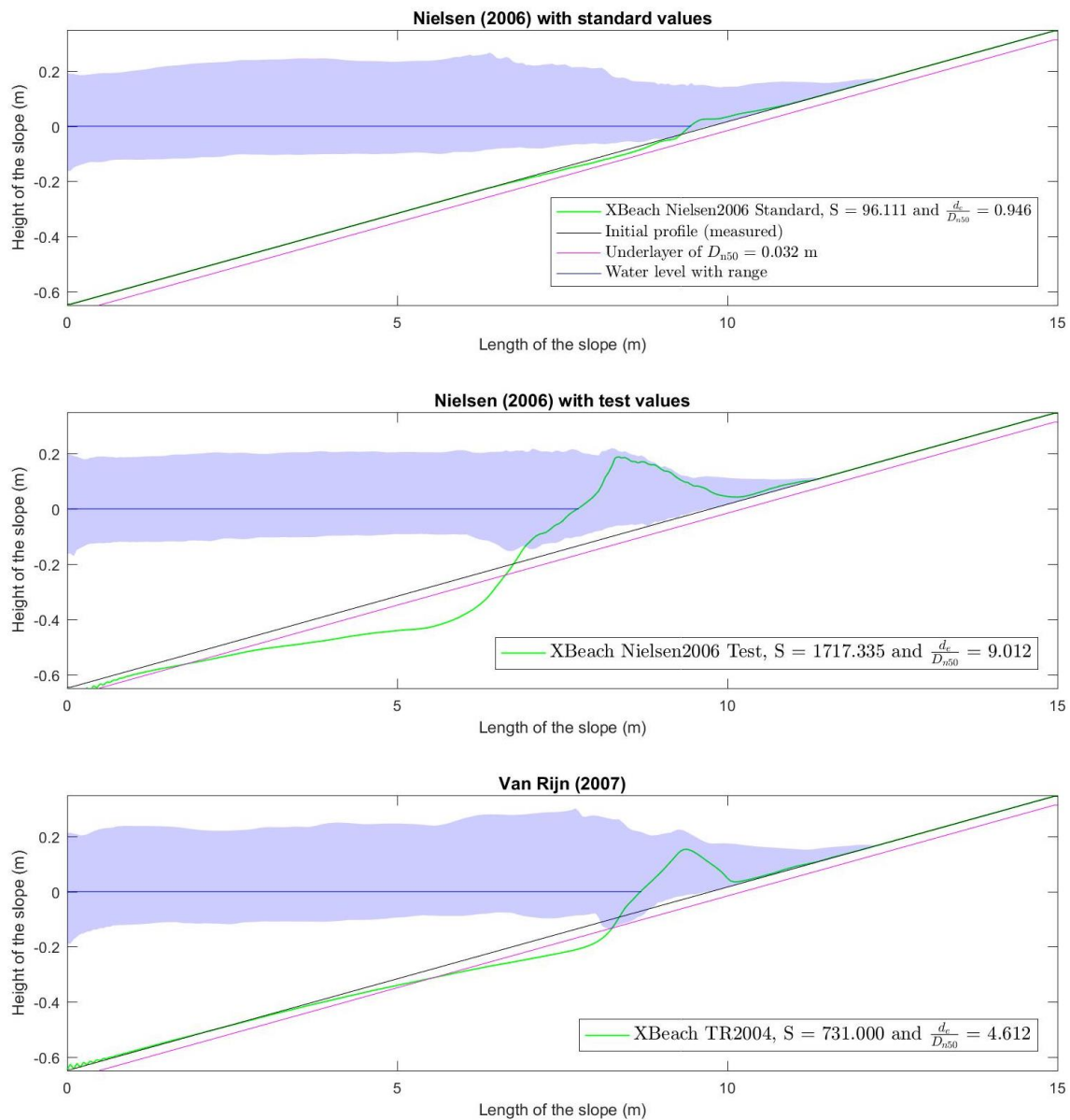


Figure 40 - Erosion profiles for 1:15 slope and  $S_{S\&F}$  input

An overview is given in Table 34 of the simulations and the damage derived from the erosion profiles modelled with 1:15 slope and  $S_{S\&F}$  input.

Table 34 - Overview of simulations and damage obtained from erosion profiles for 1:15 slope and  $S_{S\&F}$  input

	1:15 slope & $S_{S\&F}$ input	$A_e$ (m <sup>2</sup> )	S (-)	$d_e/D_{n50}$ (-)	$E_3$ (%)	Profile development
1	Experiment of Kramer (2016)	-1.85E-04	0.70	-	46.3	-
2	XBeach-G Nielsen (2006) Standard	-2.52E-02	96.11	0.946	94.4	Very wide crest profile
3	XBeach-G Nielsen (2006) Test	-4.51E-01	1717.34	9.012	901.2	Very large crest profile
4	XBeach-G Van Rijn (2007)	-1.92E-01	731.00	4.612	461.1	Very large crest profile

## Appendix D Results of BIV analysis

### D.1 Bed shear velocity and bed shear stress over time for 1:5 slope

For the 1:5 slope, the bed shear velocity over time is presented in Figure 41 and the bed shear stress over time is shown in Figure 42.

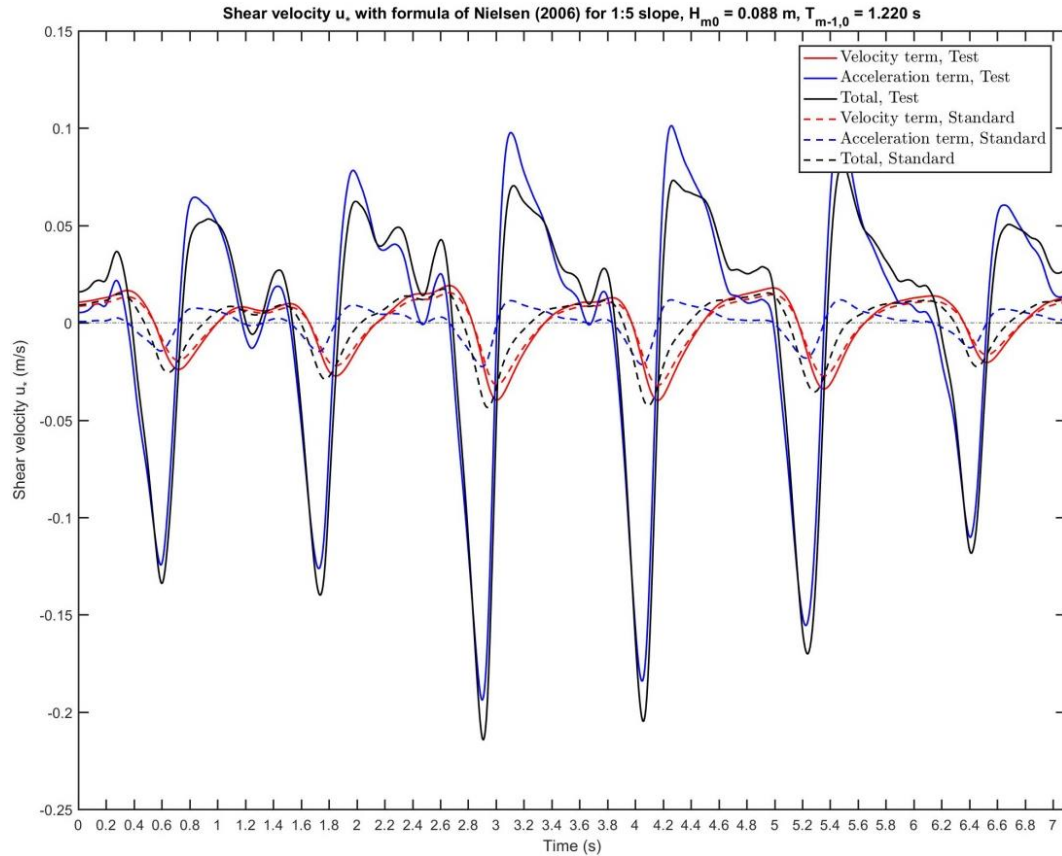


Figure 41 - Bed shear velocity with formula of Nielsen (2006) over time for 1:5 slope

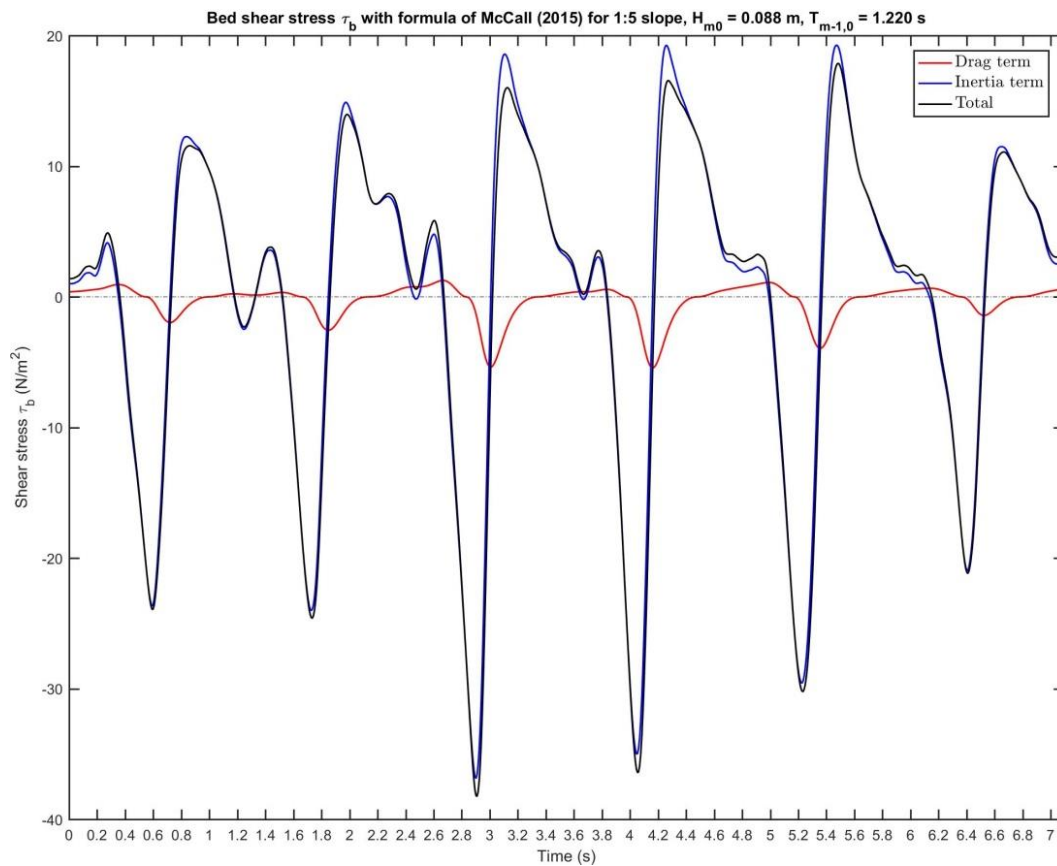


Figure 42 - Bed shear stress with formula of McCall (2015) over time for 1:5 slope

The ratio between the velocity/drag term and the acceleration/inertia term of the bed shear velocity and the bed shear stress is given in Table 35.

Table 35 - Ratio between velocity/drag term and acceleration/inertia term for 1:5 slope

Shear velocity	min	max	Shear stress	min	max
Velocity term (m/s)	-0.040	0.019	Drag term (N/m <sup>2</sup> )	-5.443	1.255
Acceleration term (m/s)	-0.194	0.101	Inertia term (N/m <sup>2</sup> )	-36.868	19.261
Ratio (-)	4.9	5.3	Ratio (-)	6.8	15.3

## D.2 Results of BIV analysis of video with 1:10 slope

### Visual analysis of video 10\_BIV\_0003

The results of the visual analysis of the movements of the stone of video 10\_BIV\_0003 are shown in Table 36. The methodology of the visual analysis of the movements of the stone is treated Section 3.2.3 and elaborated in Appendix B.4. Only limited movements of stones are observed in video 10\_BIV\_0003, because the FOV contains stones that are glued to a strip (explained in Section 3.2.1). However, from videos of the preparation of the BIV experiments of Kramer (2016) with regular waves could be observed that frequent movements of stones occur at many locations over the width of the flume. This corresponds to transport stage 4 of Breusers and Schukking (1971). The type of movement is mainly rocking, but some stones move to another location (i.e. displacements).

Table 36 - Movements of stone for 1:10 slope (video 10\_BIV\_0003)

Type of movement	Direction	Time (s)		Frame (-)	
		from	to	from	to
Rocking	Upslope	1.098	1.152	145	152
Rocking	Downslope	3.848	3.924	508	518
Rocking	Upslope	3.924	4.008	518	529

### Horizontal velocity and acceleration

After the visual analysis of the movements of stone, the horizontal velocity  $U$  and the acceleration  $dU/dt$  are derived from the BIV analysis of video 10\_BIV\_0003. The horizontal velocity  $U$  and the acceleration  $dU/dt$  over time are presented in Figure 43.

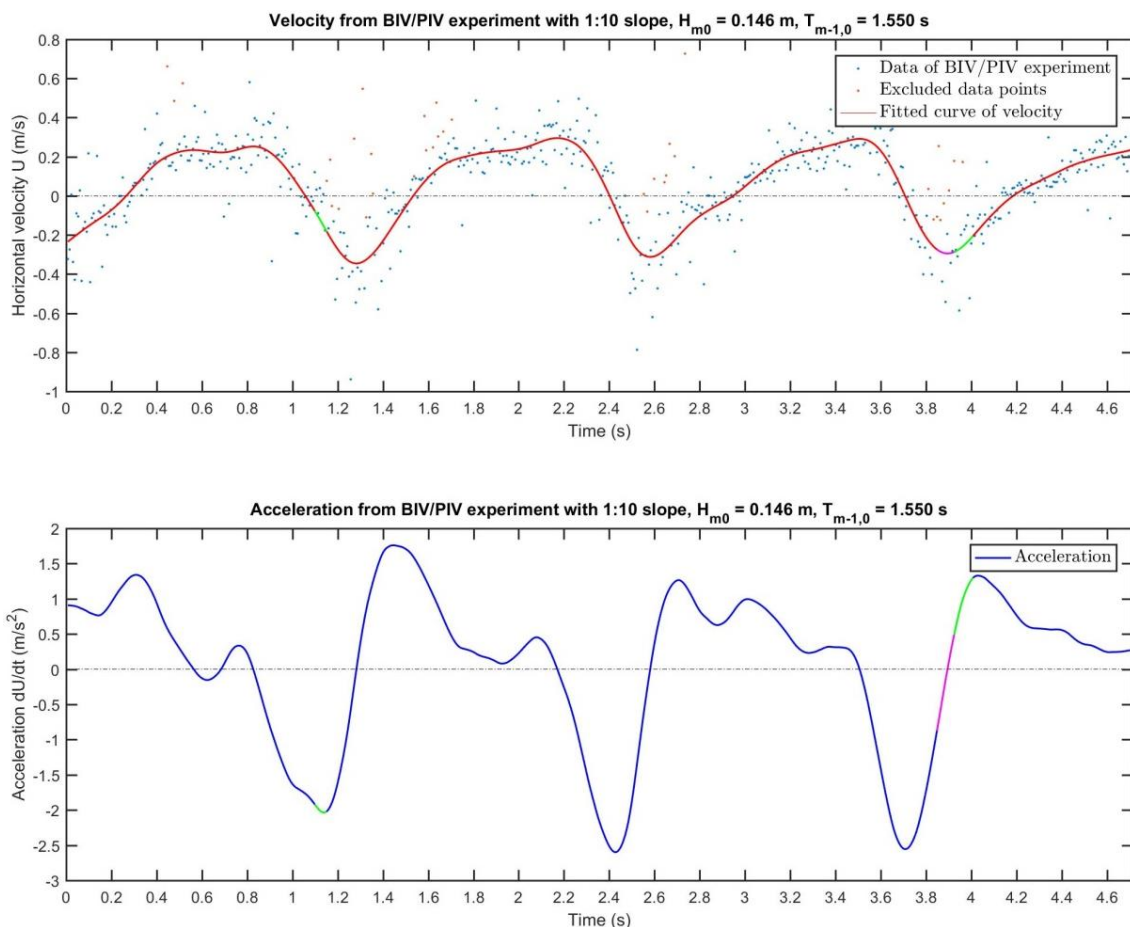


Figure 43 - Velocity (top) and acceleration (bottom) in ROI over time for 1:10 slope

In which: the velocities have a negative value during run-up (in case of incoming waves) and the values of the velocities are positive during run-down (in case of return flow).

Furthermore, the type and the direction of the movements of the stone (from the visual analysis, see Table 36) are indicated in the plots of the horizontal velocity and the acceleration. The green line shows rocking of a stone in upslope direction. The pink line indicates rocking of a stone in downslope direction. In this way (with the results of the visual analysis), the horizontal velocity and acceleration can be determined at the specific moment in time when the stone starts to move (i.e. initiation of motion of stone).

As can be seen in Figure 43, the negative peaks (during run-up) are larger in magnitude than the positive peaks (during run-down) for both the velocity and the acceleration. At  $t = 1.098$  s, rocking of a stone in upslope direction is observed. The negative value of the velocity increases in magnitude at this moment and the acceleration reaches the negative peak. At  $t = 3.848$  s, rocking of a stone in downslope direction occurs. The velocity is at the negative peak and the acceleration changes from negative values to positive values. After this, the stone moves in upslope direction (at  $t = 3.924$  s) with a decreasing negative value for the velocity and a positive increase of the acceleration.

### Bed shear stress and bed shear velocity

The horizontal velocity  $U$  and acceleration  $dU/dt$  are substituted into the velocity/drag term and the acceleration/inertia term of the formula of the bed shear stress of McCall (2015), as used in XBeach-G with the modified bed-load transport formula of Van Rijn (2007), and the formula of the bed shear velocity, as used in the bed-load transport formula of Nielsen (2006). The bed shear stress and bed shear velocity are treated in Section 2.5.3 and Section 2.5.4. For the 1:10 slope, the bed shear velocity over time and the bed shear stress over time are presented in Figure 44 and Figure 45 respectively.

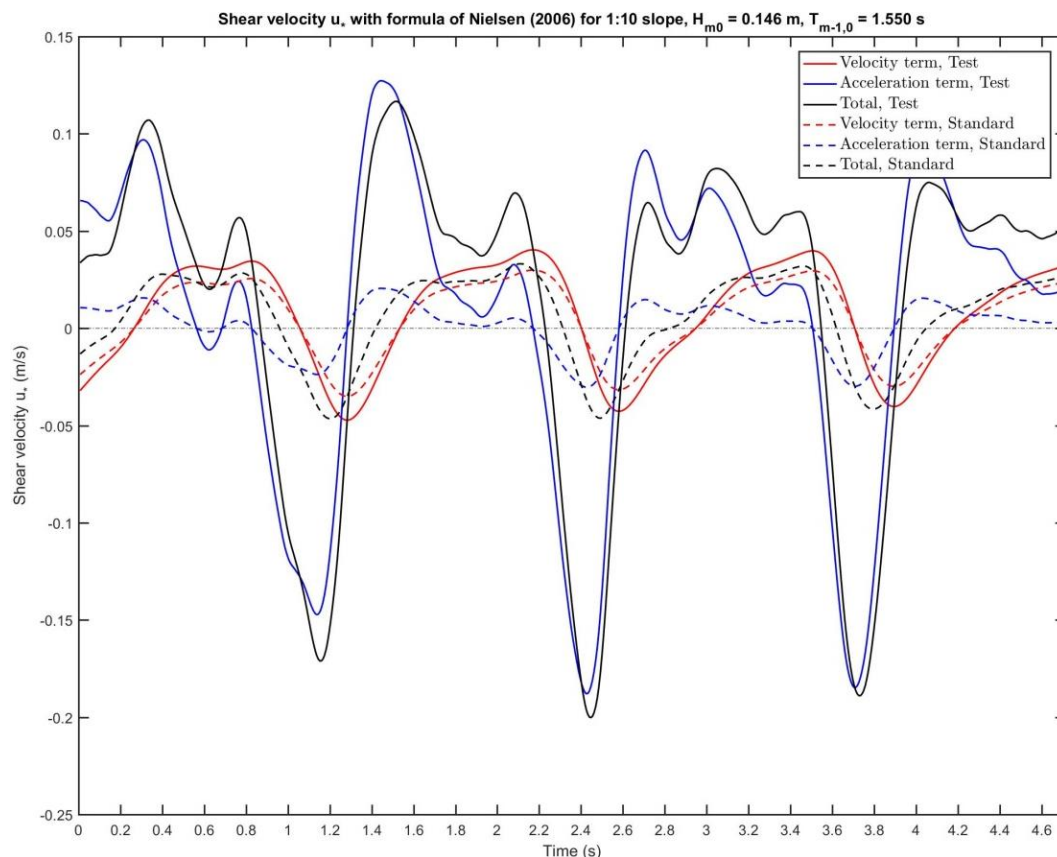


Figure 44 - Bed shear velocity with formula of Nielsen (2006) over time for 1:10 slope

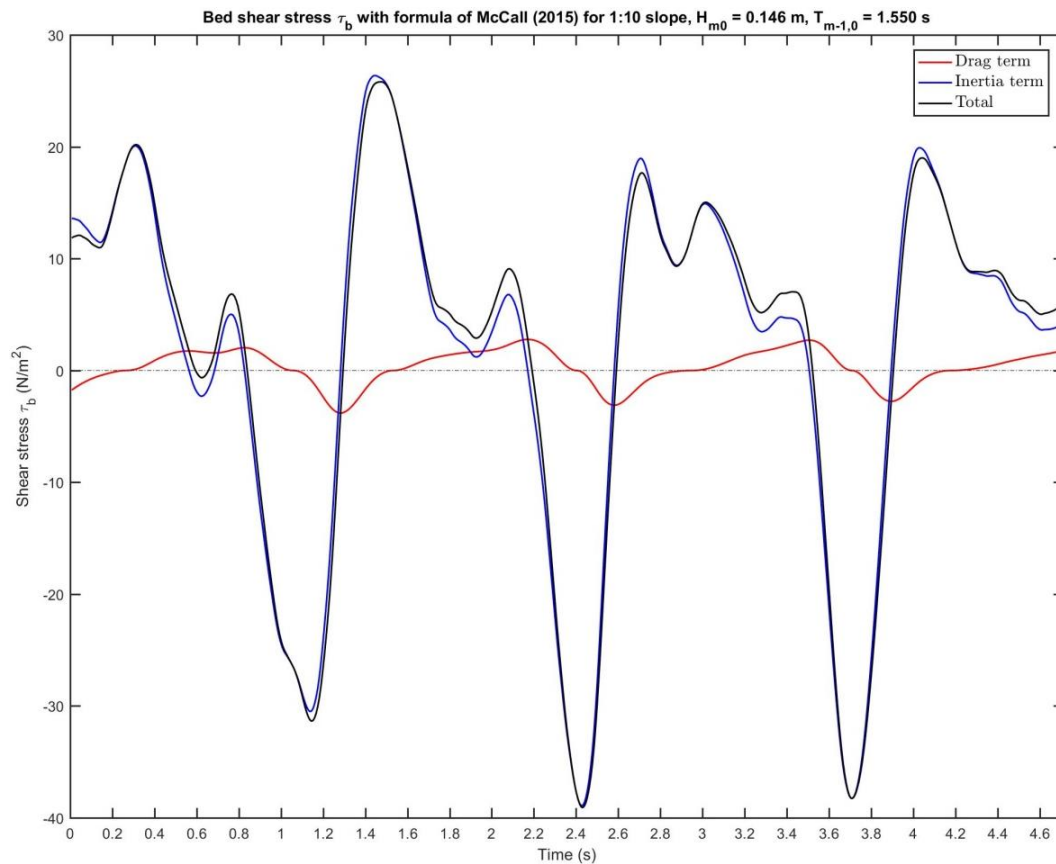


Figure 45 - Bed shear stress with formula of McCall (2015) over time for 1:10 slope

The ratio between the velocity/drag term and the acceleration/inertia term of the bed shear velocity and the bed shear stress is given in Table 37. The acceleration/inertia term is dominant over the velocity/drag term for both the bed shear stress and the bed shear velocity (as is also found for the 1:5 slope). However, the dominance is less pronounced for the 1:10 slope, because the ratio between the terms is lower (see difference in ratio in Table 35 and Table 37).

Table 37 - Ratio between velocity/drag term and acceleration/inertia term for 1:10 slope

Shear velocity	min	max	Shear stress	min	max
Velocity term (m/s)	-0.047	0.040	Drag term (N/m <sup>2</sup> )	-3.805	2.777
Acceleration term (m/s)	-0.188	0.127	Inertia term (N/m <sup>2</sup> )	-38.916	26.369
Ratio (-)	4.0	3.2	Ratio (-)	10.2	9.5

### Mobility parameters

The bed shear stress and the bed shear velocity over time are substituted in the formulas of the mobility parameters  $\theta'_{\text{Nielsen,Test}}$ ,  $\theta'_{\text{Nielsen,Standard}}$  and  $\theta'_{\text{McCall}}$ . An elaboration on how these three mobility parameters (i.e. effective, adapted Shields parameters) are determined is given in Section 3.2.6. The mobility parameters over time are presented in Figure 46.

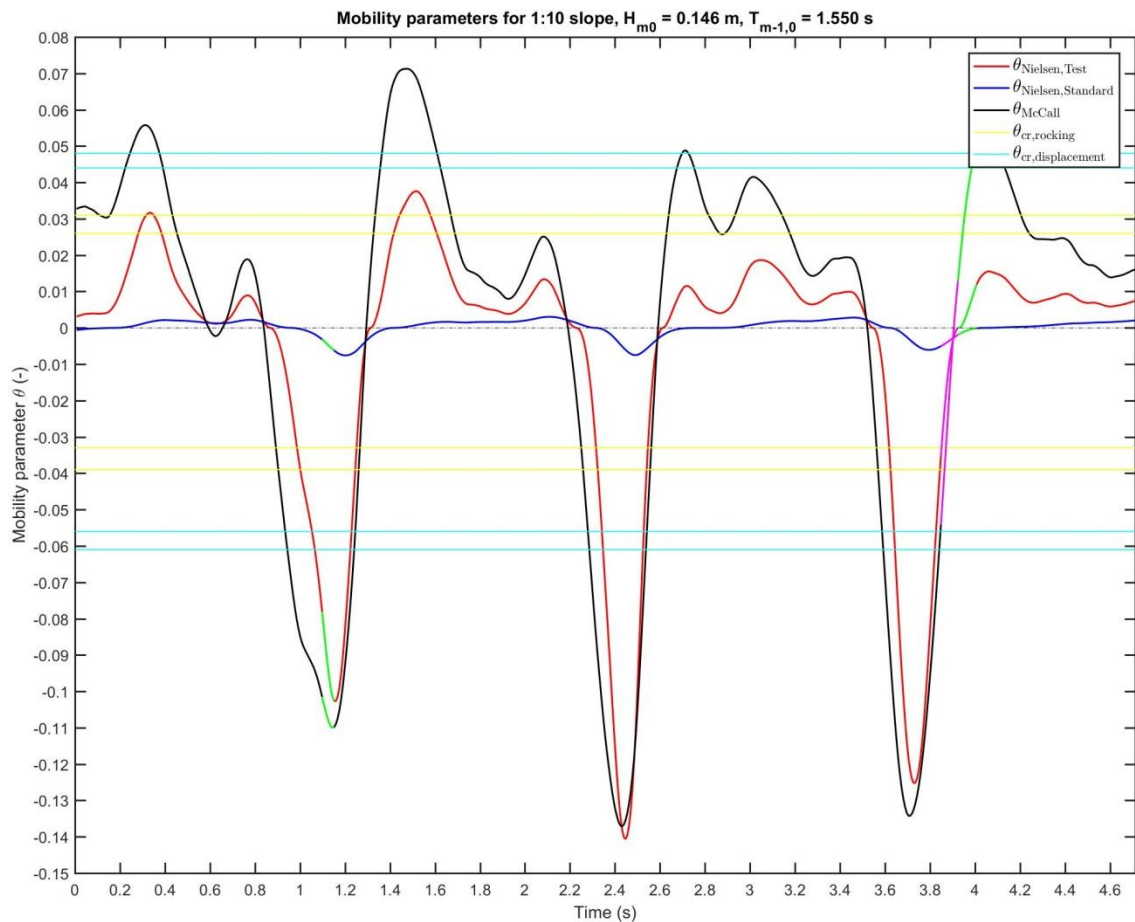


Figure 46 - Mobility parameters over time for 1:10 slope

In which: the mobility parameters have a negative value during run-up and the values of the mobility parameters are positive during run-down.

Furthermore, the type and the direction of the movements of the stone (from the visual analysis, see Table 36) are indicated in Figure 46. The green line shows rocking of a stone in upslope direction. The pink line indicates rocking of a stone in downslope direction. In this way (with the results of the visual analysis), the stability parameters can be determined at the specific moment in time when the stone starts to move (i.e. initiation of motion of stone).

The critical, effective Shields parameters for rocking  $\theta'_{cr,rocking}$  and displacement  $\theta'_{cr,displacement}$  are shown in Figure 46 as horizontal lines. The critical, effective Shields parameters for the 1:10 slope are given in Table 38 (and elaborated in Section 3.2.7).

Table 38 - Critical, effective Shields parameter for 1:10 slope

Slope	Description of movements of stones		Direction	$\theta'_{cr}$	
1:10	Rocking	First stones start to move	Upslope	-0.033	-0.039
			Downslope	0.026	0.031
	Displacement	Beginning of transport of stones	Upslope	-0.056	-0.061
			Downslope	0.044	0.048

In which: the values of  $\theta'_{cr}$  are positive during run-down and  $\theta'_{cr}$  has a negative value during run-up.

As can be seen in Figure 46, the positive peaks of the mobility parameter  $\theta'_{McCall}$  (shown with black line) are in the range of the stability parameter for displacement  $\theta'_{cr,displacement}$  for downslope movement (indicated with horizontal, light blue lines). The positive peaks of  $\theta'_{Nielsen,Test}$  (shown with red line) are lower and come closer to  $\theta'_{cr,rocking}$  for downslope movement (indicated with horizontal, yellow lines). Both the negative peaks of the mobility parameters  $\theta'_{Nielsen,Test}$  and  $\theta'_{McCall}$  exceed  $\theta'_{cr,displacement}$  for upslope movement significantly, and movements of stones in upslope direction occur (type: rocking and displacements). The values of  $\theta'_{Nielsen,Standard}$  do not correspond to the values of  $\theta'_{Nielsen,Test}$  and  $\theta'_{McCall}$ .

At  $t = 1.098$  s, rocking of a stone in upslope direction (indicated in green) is observed when the mobility parameters  $\theta'_{Nielsen,Test}$  and  $\theta'_{McCall}$  reaches the negative peak. However, movements of stones were expected to occur when  $\theta'_{cr,displacement}$  and  $\theta'_{cr,rocking}$  for upslope movement are exceeded for the first time (which is not observed in Figure 46). At  $t = 3.848$  s, rocking of a stone in downslope direction occurs (shown in pink), while  $\theta'_{Nielsen,Test}$  and  $\theta'_{McCall}$  decrease to values below the stability parameters (and thus, no movement was expected). At  $t = 3.924$  s, the stone moves in upslope direction (indicated in green), while  $\theta'_{Nielsen,Test}$  and  $\theta'_{McCall}$  do not exceed  $\theta'_{cr,rocking}$  for downslope movement.

#### New values for stability parameter $\theta_{cr}$ determined with $\theta'_{McCall}$ with new $c_f$ and $c_i$

The mobility parameter  $\theta'_{McCall}$ , determined with the new values for the coefficients  $c_f$  and  $c_i$ , is plotted over time for the 1:10 slope in Figure 47.

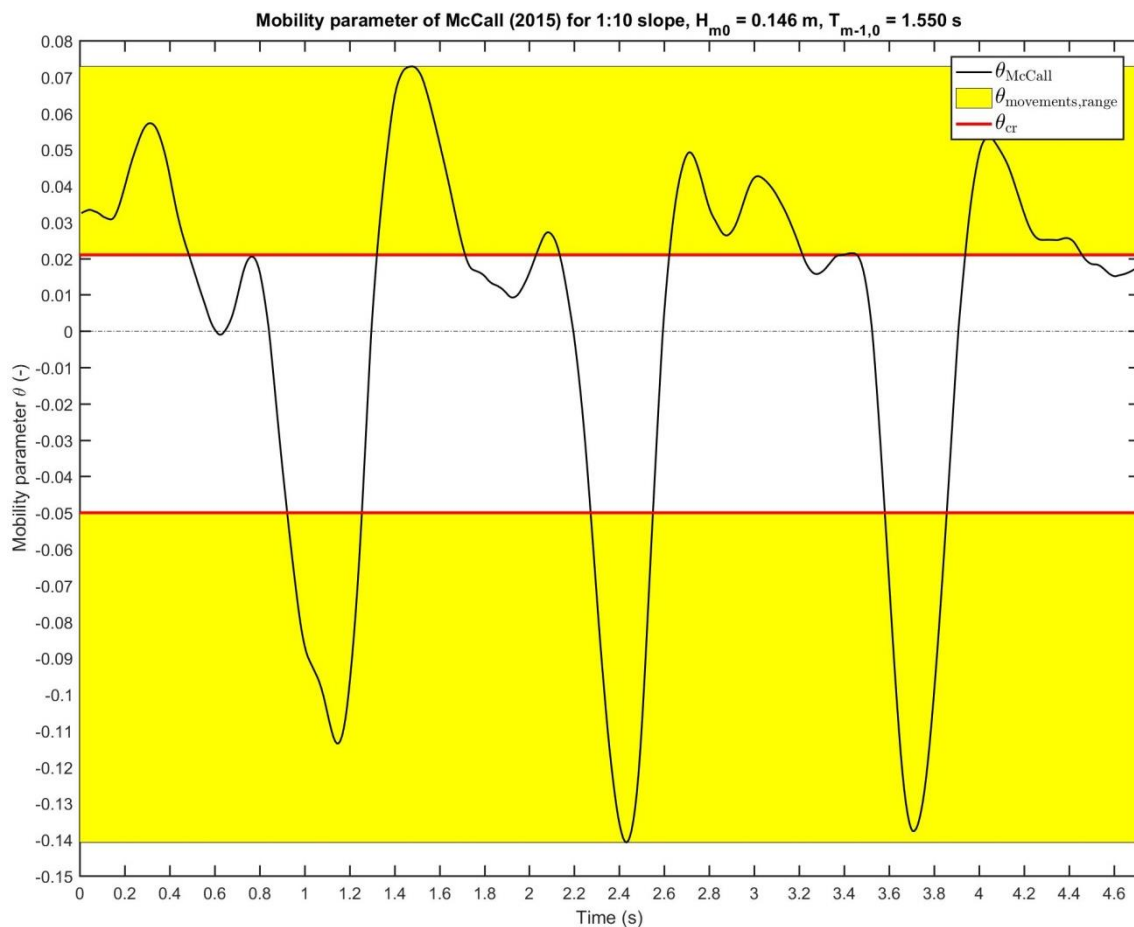


Figure 47 - Mobility parameter  $\theta'_{McCall}$  over time with new  $c_f$  and  $c_i$ , for 1:10 slope

In which: the mobility parameters have a negative value during run-up and the values of the mobility parameters are positive during run-down.

The ranges with movements of stones are depicted in yellow in Figure 47. The minimal values are indicated with  $\theta'_{cr}$  (shown in red in Figure 47). The first downslope movements of stones (with positive values) occur for a value of 0.021. The first upslope movements of stones (with negative values) are observed for a value of -0.050. The upper limits of the ranges are the positive and negative peaks of  $\theta'_{McCall}$ .

**Note:** for the 1:10 slope, the ranges of  $\theta'_{movements,range}$  start at the minimal values of  $\theta'_{McCall}$  for which the first movements of stones are observed in the BIV analyzed video 05\_BIV\_0001. Thus, the critical value of  $\theta'_{cr}$  for initiation of motion of stones for the 1:10 slope is derived from the critical value of  $\theta'_{cr}$  for the 1:5 slope (shown in red in Table 24), using the slope correction factors of Section 3.2.6.

### D.3 Results of BIV analysis of video with 1:15 slope

#### Visual analysis of video 15\_BIV\_0005

No movements of stones are found from the visual analysis of the movements of the stone of video 15\_BIV\_0005, because the FOV contains stones that are glued to a strip (explained in Section 3.2.1). However, from videos of the preparation of the BIV experiments of Kramer (2016) with regular waves could be observed that frequent movements of stones occur at many locations over the width of the flume. This corresponds to transport stage 4 of Breusers and Schukking (1971). The type of movement is mainly rocking, but some stones move to another location (i.e. displacements).

The methodology of the visual analysis of the movements of the stone is treated Section 3.2.3 and elaborated in Appendix B.4.

#### Horizontal velocity and acceleration

After the visual analysis of the movements of stone, the horizontal velocity  $U$  and the acceleration  $dU/dt$  are derived from the BIV analysis of video 15\_BIV\_0005. The horizontal velocity  $U$  and the acceleration  $dU/dt$  over time are presented in Figure 48.

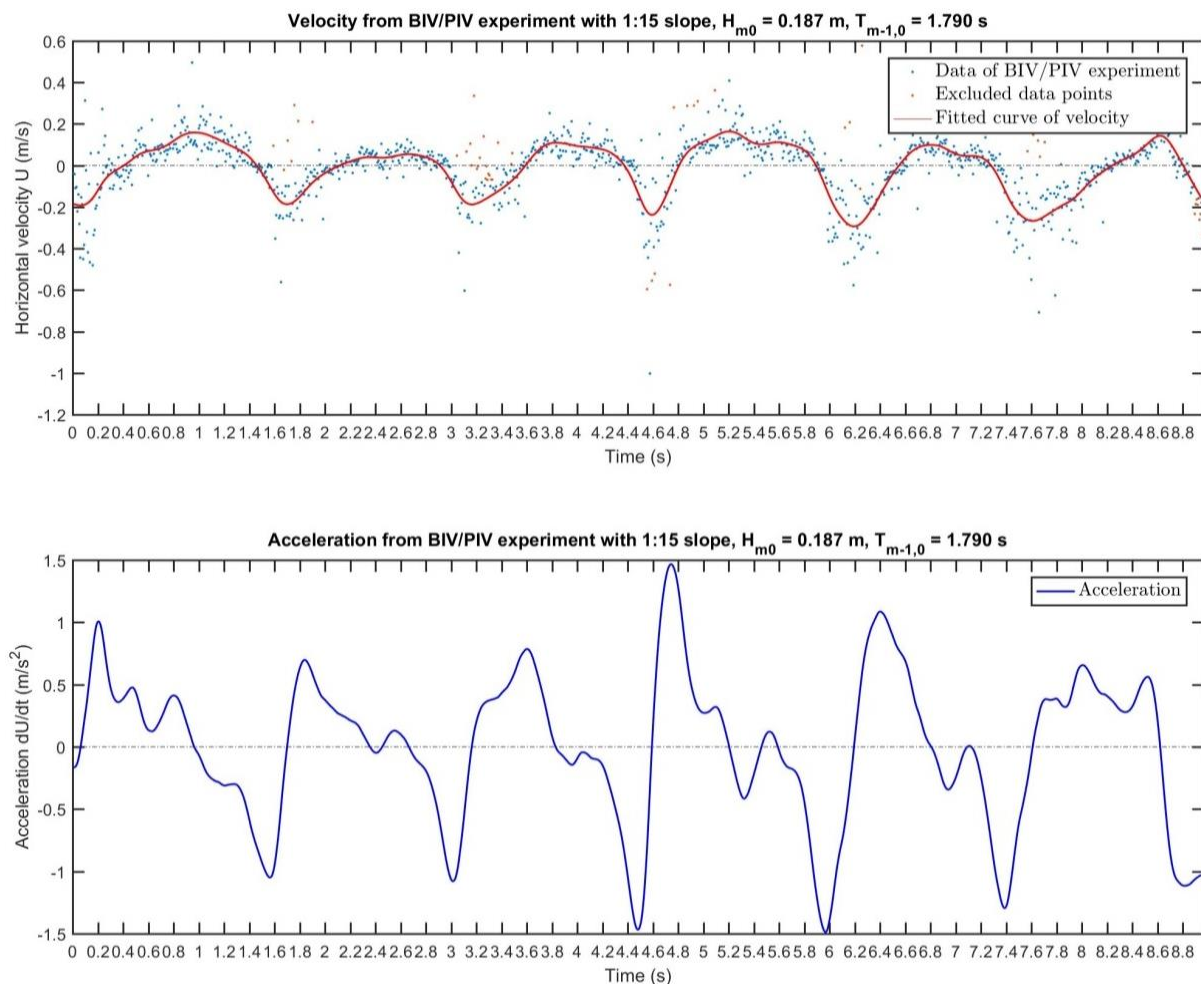


Figure 48 - Velocity (top) and acceleration (bottom) in ROI over time for 1:15 slope

In which: the velocities have a negative value during run-up (in case of incoming waves) and the values of the velocities are positive during run-down (in case of return flow).

As can be seen in Figure 48, the negative peaks (during run-up) are larger in magnitude than the positive peaks (during run-down) for both the velocity and the acceleration. However, the difference in magnitude between the positive and negative peaks is less than in case of the 1:5 and 1:10 slopes.

### Bed shear stress and bed shear velocity

The horizontal velocity  $U$  and acceleration  $dU/dt$  are substituted into the velocity/drag term and the acceleration/inertia term of the formula of the bed shear stress of McCall (2015), as used in XBeach-G with the modified bed-load transport formula of Van Rijn (2007), and the formula of the bed shear velocity, as used in the bed-load transport formula of Nielsen (2006). The bed shear stress and bed shear velocity are treated in Section 2.5.3 and Section 2.5.4. For the 1:15 slope, the bed shear velocity over time and the bed shear stress over time are presented in Figure 49 and Figure 50 respectively.

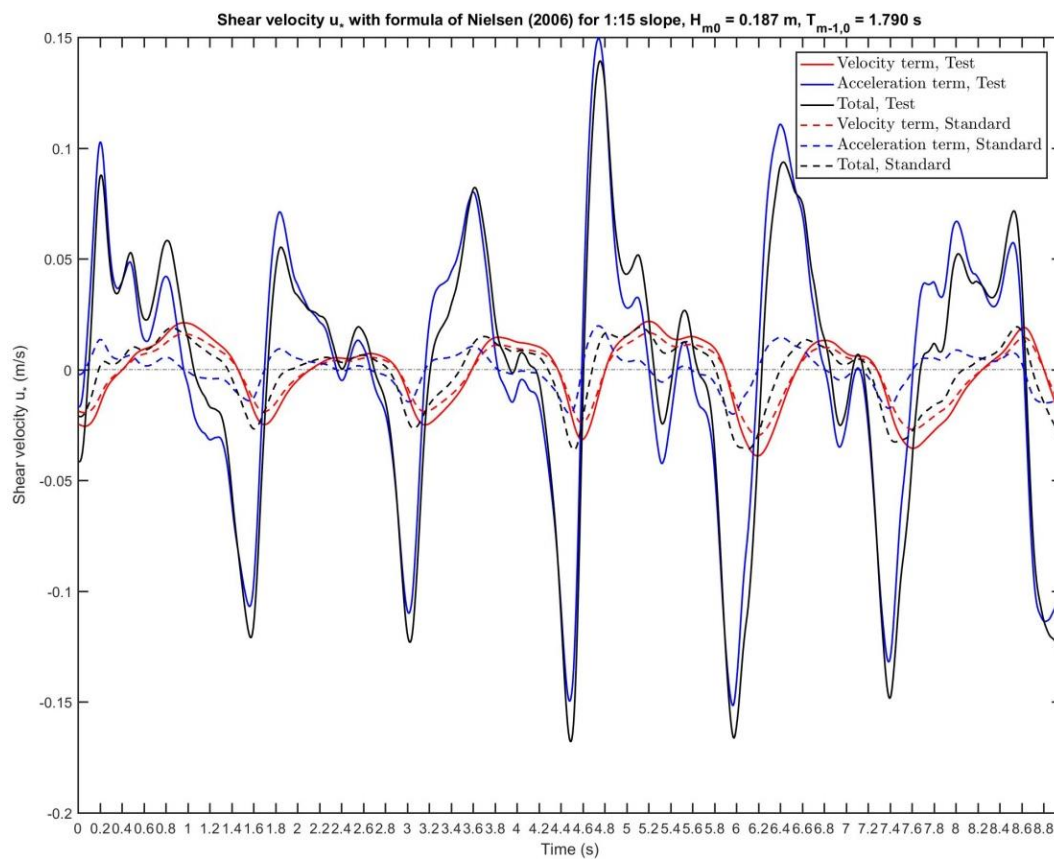


Figure 49 - Bed shear velocity with formula of Nielsen (2006) over time for 1:15 slope

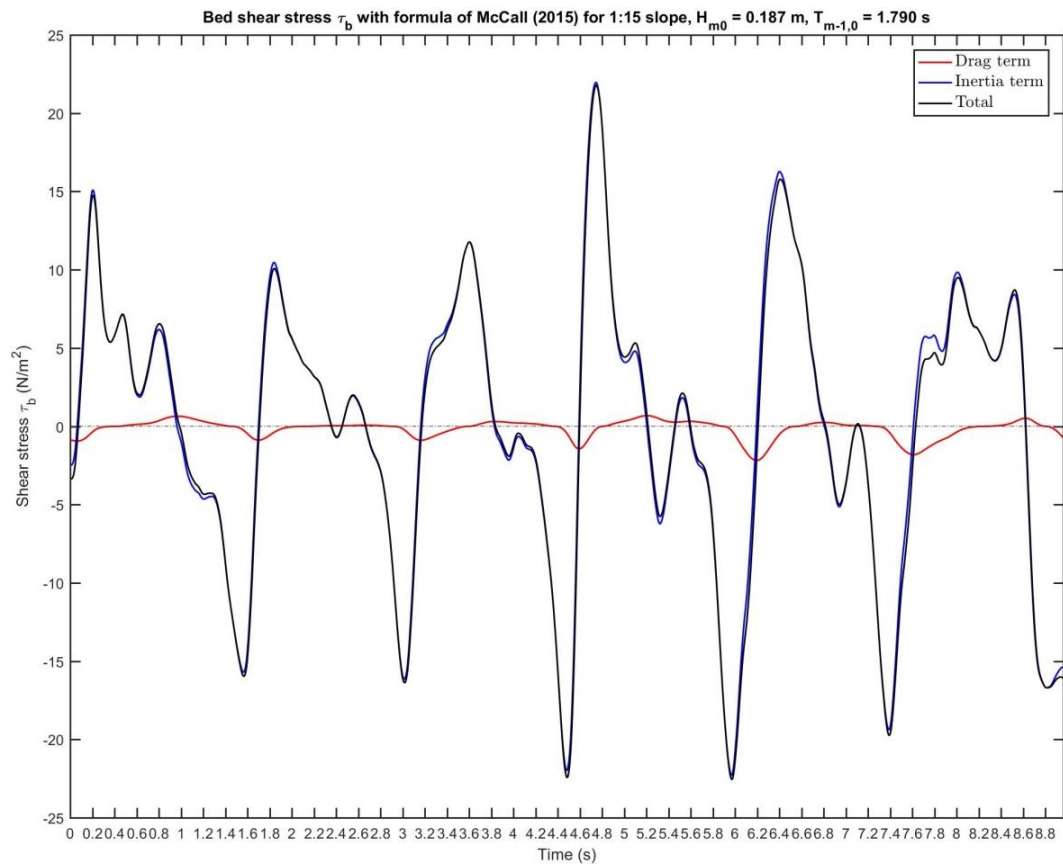


Figure 50 - Bed shear stress with formula of McCall (2015) over time for 1:15 slope

The ratio between the velocity/drag term and the acceleration/inertia term of the bed shear velocity and the bed shear stress is given in Table 39. The acceleration/inertia term is dominant over the velocity/drag term for both the bed shear stress and the bed shear velocity (as is also found for the 1:5 and 1:10 slope). However, the dominance is more pronounced for the 1:15 slope, because the ratio between the terms is higher (see difference in ratio in Table 35, Table 37 and Table 39).

Table 39 - Ratio between velocity/drag term and acceleration/inertia term for 1:15 slope

Shear velocity	min	max	Shear stress	min	max
Velocity term (m/s)	-0.039	0.022	Drag term (N/m <sup>2</sup> )	-2.181	0.684
Acceleration term (m/s)	-0.152	0.150	Inertia term (N/m <sup>2</sup> )	-22.281	21.976
Ratio (-)	3.9	6.9	Ratio (-)	10.2	32.1

### Mobility parameters

The bed shear stress and the bed shear velocity over time are substituted in the formulas of the mobility parameters  $\theta'_{\text{Nielsen,Test}}$ ,  $\theta'_{\text{Nielsen,Standard}}$  and  $\theta'_{\text{McCall}}$ . An elaboration on how these three mobility parameters (i.e. effective, adapted Shields parameters) are determined is given in Section 3.2.6. The mobility parameters over time are presented in Figure 51.

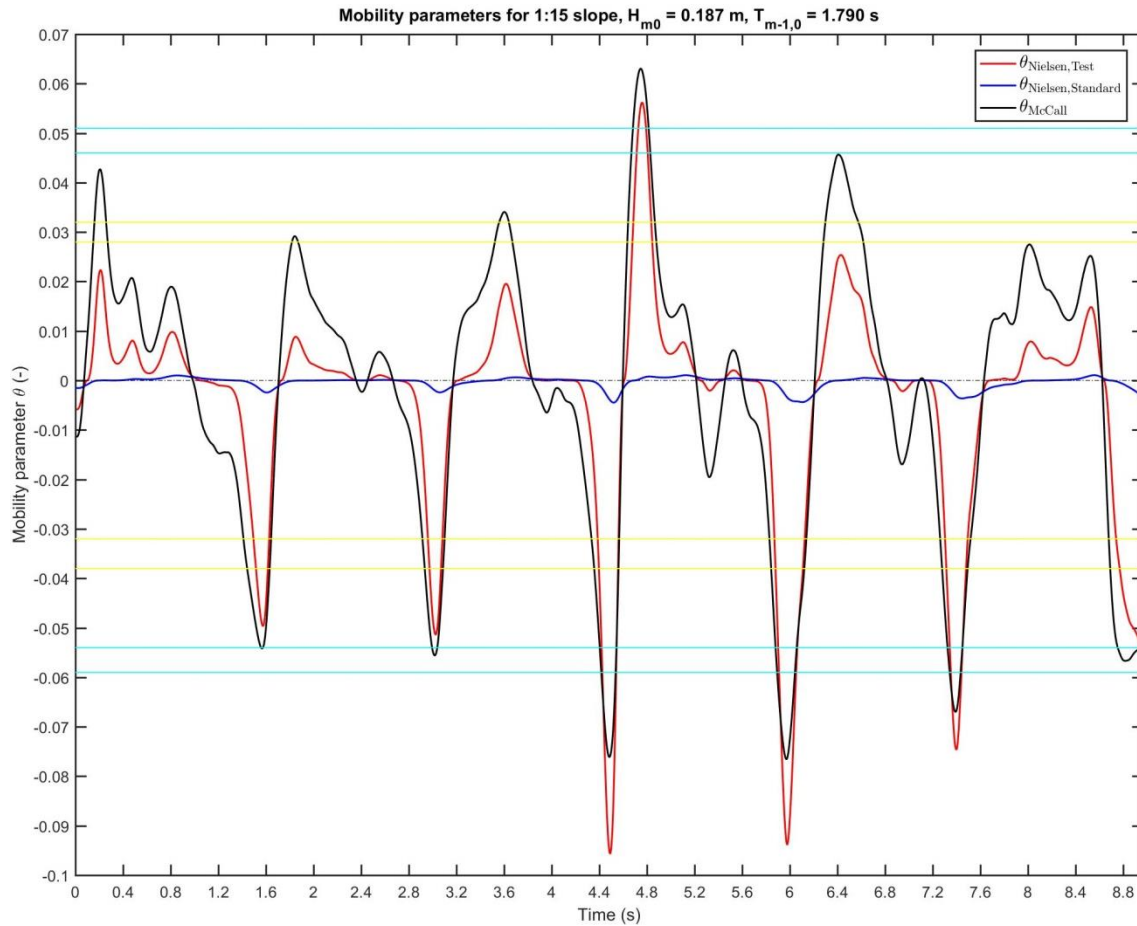


Figure 51 - Mobility parameters over time for 1:15 slope

In which: the mobility parameters have a negative value during run-up and the values of the mobility parameters are positive during run-down.

The critical, effective Shields parameters for rocking  $\theta'_{cr,rocking}$  and displacement  $\theta'_{cr,displacement}$  are shown in Figure 51 as horizontal lines. The critical, effective Shields parameters for the 1:15 slope are given in Table 40 (and elaborated in Section 3.2.7).

Table 40 - Critical, effective Shields parameter for 1:15 slope

Slope	Description of movements of stones		Direction	$\theta'_{cr}$	
1:15	Rocking	First stones start to move	Upslope	-0.032	-0.038
			Downslope	0.028	0.032
	Displacement	Beginning of transport of stones	Upslope	-0.054	-0.059
			Downslope	0.046	0.051

In which: the values of  $\theta'_{cr}$  are positive during run-down and  $\theta'_{cr}$  has a negative value during run-up.

As can be seen in Figure 51, the positive peaks of the mobility parameter  $\theta'_{McCall}$  (shown with black line) are in the range of the stability parameter  $\theta'_{cr,rocking}$  for downslope movement (indicated with horizontal, yellow lines). The positive peaks of  $\theta'_{Nielsen,Test}$  (shown with red line) remain below  $\theta'_{cr,rocking}$ . One positive peak of both  $\theta'_{Nielsen,Test}$  and  $\theta'_{McCall}$  exceeds  $\theta'_{cr,displacement}$  for downslope movement (indicated with horizontal, light blue lines). Both the negative peaks of the mobility parameters  $\theta'_{Nielsen,Test}$  and  $\theta'_{McCall}$  exceed  $\theta'_{cr,displacement}$  for upslope movement, and rocking of stones in upslope direction occur (and sometimes also displacements are observed). The exceedance is less

significant than for the 1:5 and 1:10 slopes. The values of  $\theta'_{\text{Nielsen,Standard}}$  are very small and are not in agreement with the values of  $\theta'_{\text{Nielsen,Test}}$  and  $\theta'_{\text{McCall}}$ .

#### New values for stability parameter $\theta_{\text{cr}}$ determined with $\theta'_{\text{McCall}}$ with new $c_f$ and $c_i$

The mobility parameter  $\theta'_{\text{McCall}}$ , determined with the new values for the coefficients  $c_f$  and  $c_i$ , is plotted over time for 1:15 slope in Figure 52.

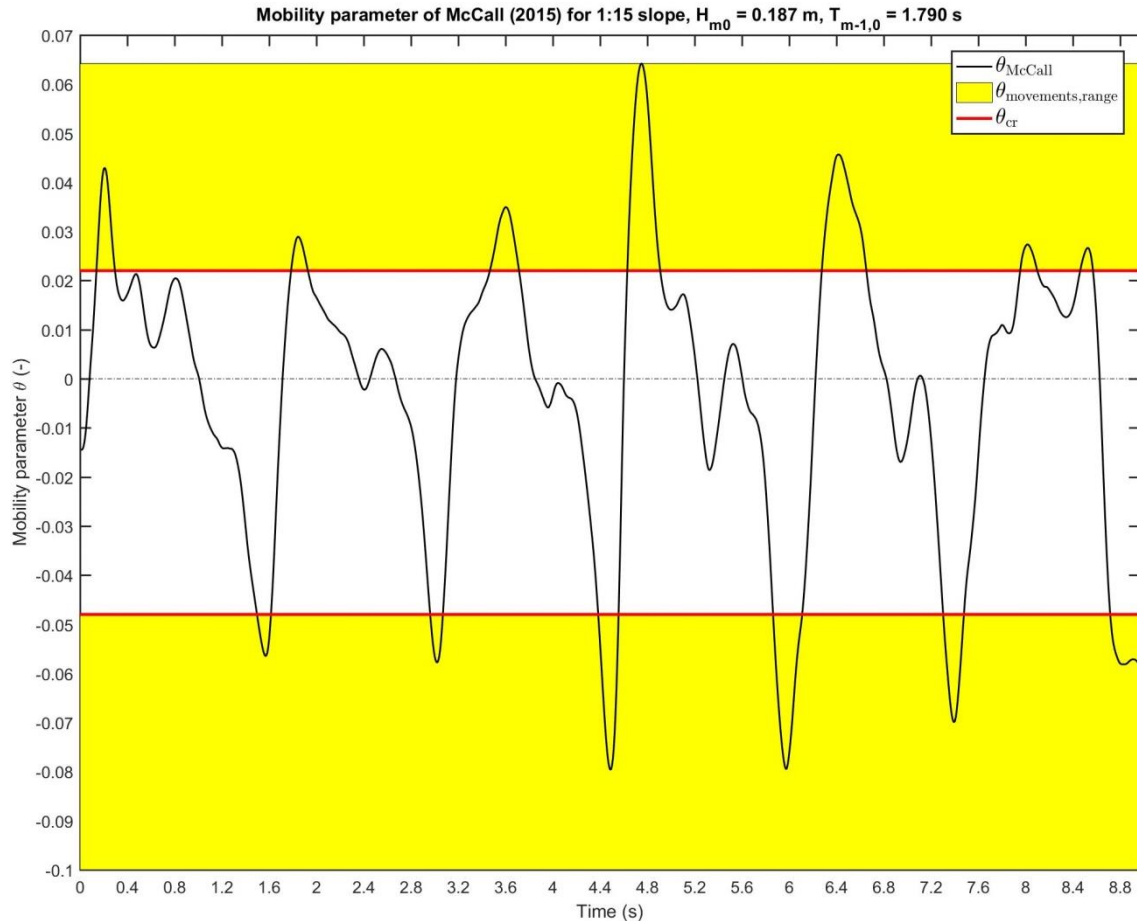


Figure 52 - Mobility parameter  $\theta'_{\text{McCall}}$  over time with new  $c_f$  and  $c_i$ , for 1:15 slope

In which: the mobility parameters have a negative value during run-up and the values of the mobility parameters are positive during run-down.

The ranges with movements of stones are depicted in yellow in Figure 52. The minimal values are indicated with  $\theta'_{\text{cr}}$  (shown in red in Figure 52). The first downslope movements of stones (with positive values) occur for a value of 0.021. The first upslope movements of stones (with negative values) are observed for a value of -0.048. The upper limits of the ranges are the positive and negative peaks of  $\theta'_{\text{McCall}}$ .

**Note:** for the 1:15 slope, the ranges of  $\theta'_{\text{movements,range}}$  start at the minimal values of  $\theta'_{\text{McCall}}$  for which the first movements of stones are observed in the BIV analyzed video 05\_BIV\_0001. Thus, the critical value of  $\theta'_{\text{cr}}$  for initiation of motion of stones for the 1:15 slope is derived from the critical value of  $\theta'_{\text{cr}}$  for the 1:5 slope (shown in red in Table 24), using the slope correction factors of Section 3.2.6.

## Appendix E Results of mobility parameter from XBeach-G

### E.1 Velocity and acceleration in XBeach-G simulation for 1:5 slope

For the 1:5 slope, the velocity and the acceleration over time along the length of the slope is presented in Figure 53 and in Figure 54.

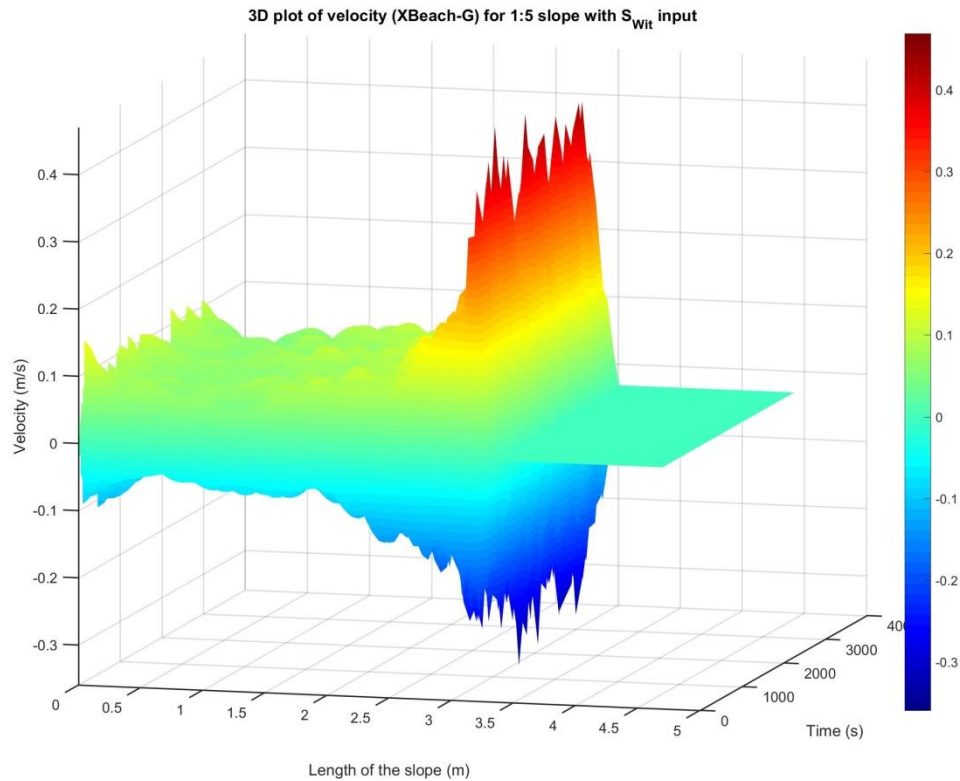


Figure 53 - Velocity over time along length of 1:5 slope with  $S_{wit}$  input

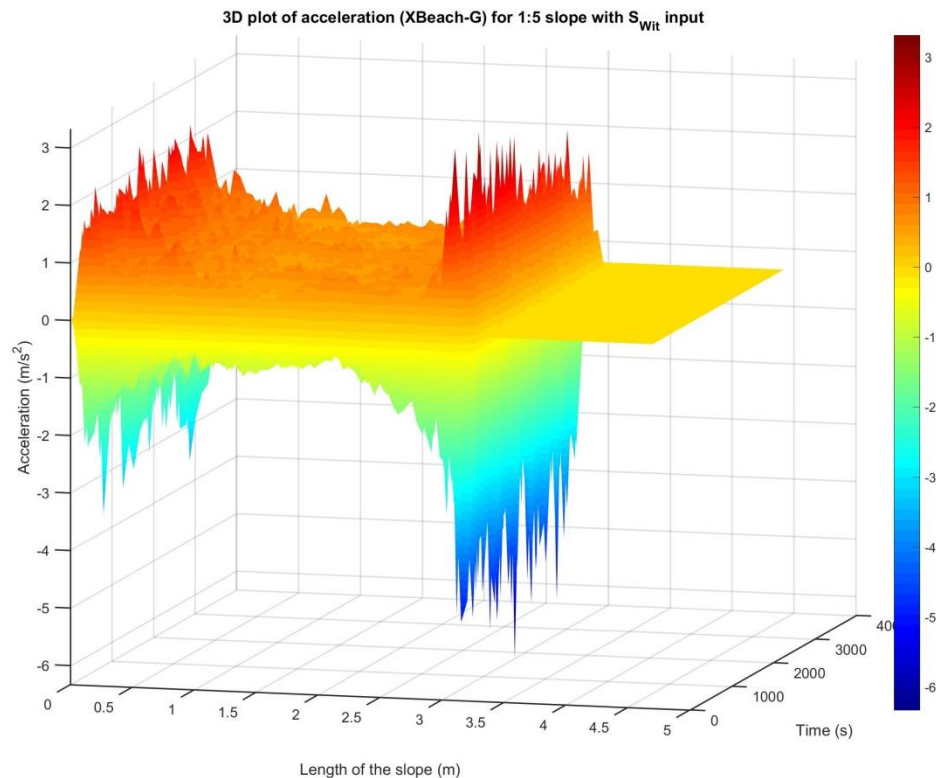


Figure 54 - Acceleration over time along length of 1:5 slope with  $S_{wit}$  input

The velocity and the acceleration are substituted in the formula of the bed shear stress. The mobility parameter  $\theta'_{\text{McCall}}$  can be determined with the bed shear stress. The mobility parameter over time along the length of the slope is shown in Figure 19 in Section 5.8.

## E.2 Mobility parameter $\theta'_{McCall}$ in XBeach-G simulation for 1:10 slope

For the 1:10 slope, the velocity and the acceleration over time along the length of the 1:10 slope are presented in Figure 55 and in Figure 56.

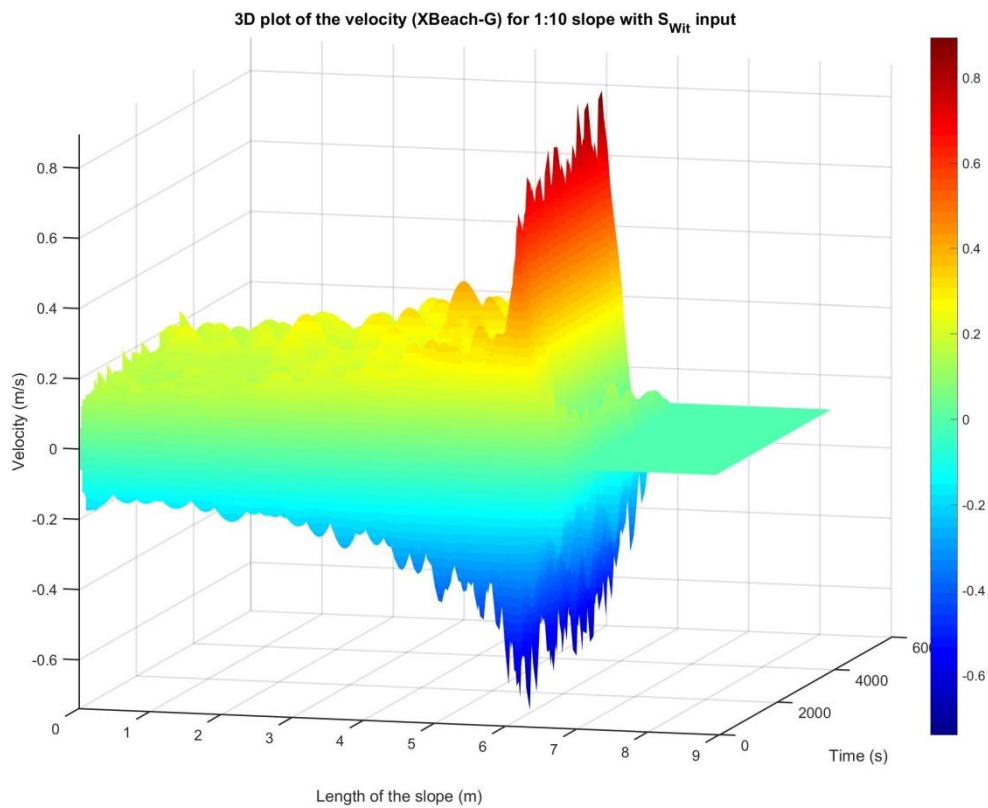


Figure 55 - Velocity over time along length of 1:10 slope with  $S_{Wit}$  input

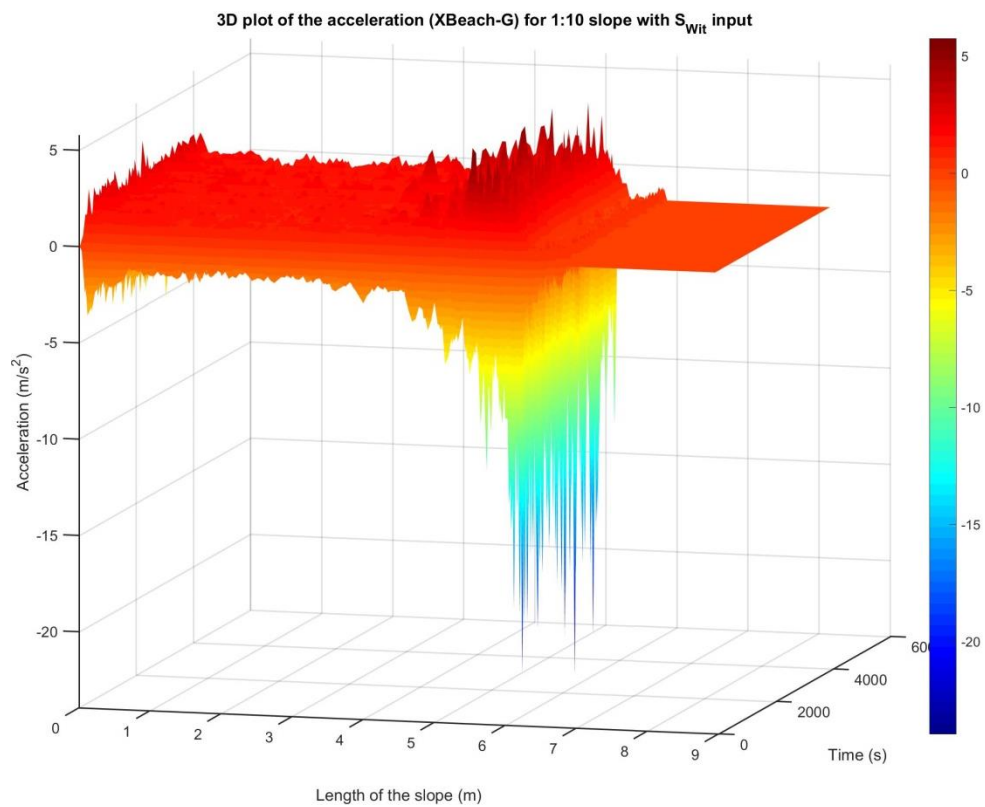


Figure 56 - Acceleration over time along length of 1:10 slope with  $S_{Wit}$  input

The velocity and the acceleration are substituted in the formula of the bed shear stress. The mobility parameter  $\theta'_{McCall}$  can be determined with the bed shear stress. The mobility parameter over time ( $t_{model}$  is 4,023 s for  $N = 3000$ ) along the length of the 1:10 ( $x = 0.00$  m to  $x = 8.95$  m) slope is shown in Figure 57.

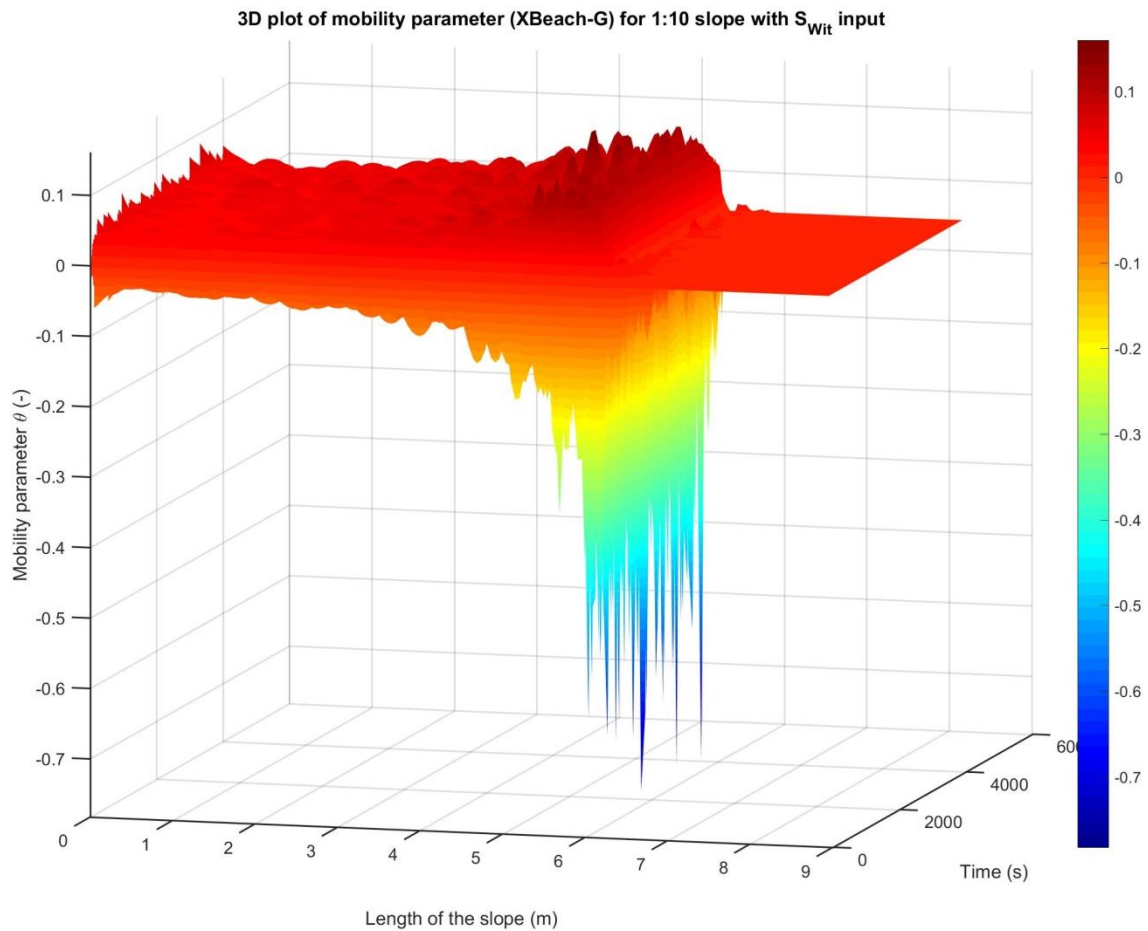


Figure 57 - Mobility parameter  $\theta'_{McCall}$  over time along length of 1:10 slope with  $S_{Wit}$  input

In which: the values are negative during run-up and the values are positive during run-down.

### E.3 Mobility parameter $\theta'_{McCall}$ in XBeach-G simulation for 1:15 slope

For the 1:15 slope, the velocity and the acceleration over time along the length of the 1:15 slope are presented in Figure 58 and in Figure 59.

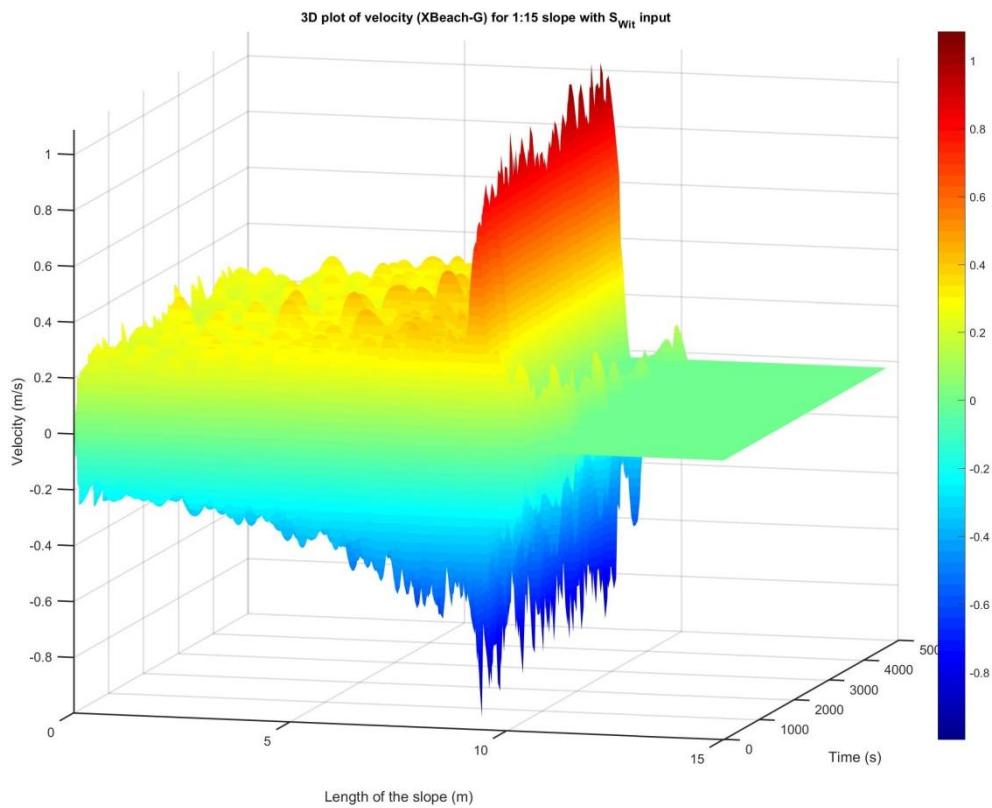


Figure 58 - Velocity over time along length of 1:15 slope with  $S_{wit}$  input

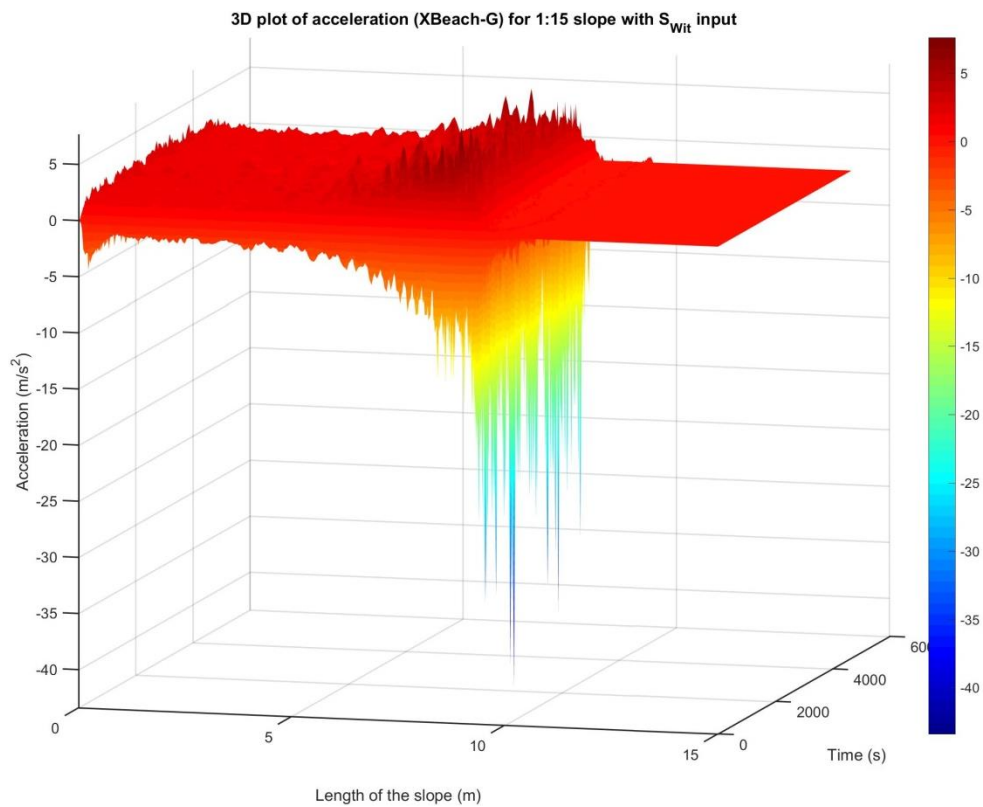


Figure 59 - Acceleration over time along length of 1:15 slope with  $S_{wit}$  input

The velocity and the acceleration are substituted in the formula of the bed shear stress. The mobility parameter  $\theta'_{McCall}$  can be determined with the bed shear stress. The mobility parameter over time ( $t_{model}$  is 4,677 s for  $N = 3000$ ) along the length of the 1:15 slope ( $x = 0.00$  m to  $x = 15.00$  m) is shown in Figure 60.

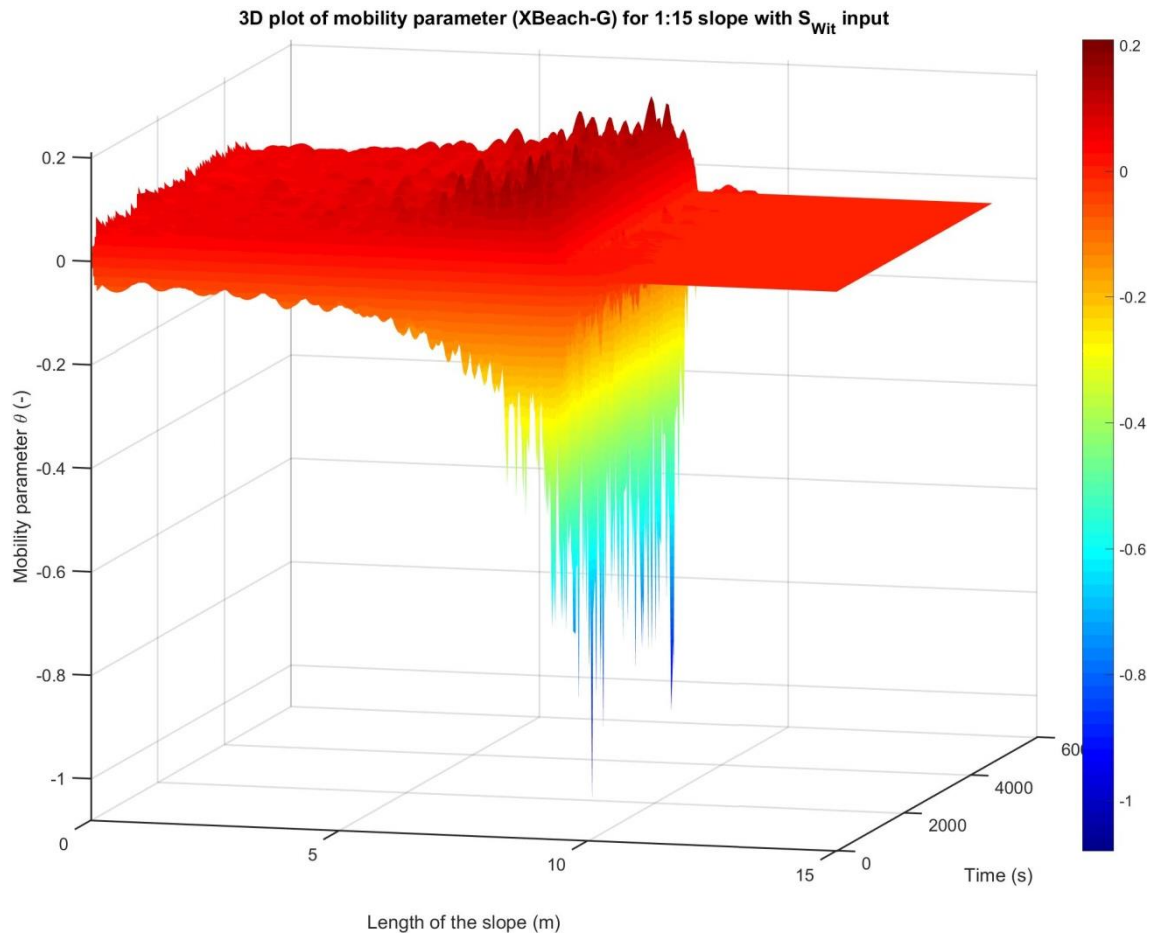


Figure 60 - Mobility parameter  $\theta'_{McCall}$  over time along length of 1:15 slope with  $S_{Wit}$  input

In which: the values are negative during run-up and the values are positive during run-down.

## E.4 Influence of morphological updating of the bed

The results of the XBeach-G simulations performed without morphological updating of the bed are shown in Table 41.

**Table 41 - Values of  $U$ ,  $dU/dt$  and  $\theta'_{McCall}$  from XBeach-G simulations with  $S_{Wit}$  input without morphological updating, per slope**

Slope		1:5	1:10	1:15
<b>U</b> (m/s)	min	-0.295	-0.532	-0.748
	max	0.369	0.472	0.586
<b>dU/dt</b> (m/s <sup>2</sup> )	min	-6.767	-15.953	-23.886
	max	3.178	5.946	7.962

Slope		1:5	1:10	1:15
<b><math>\theta'_{McCall}</math></b> (-)	min	-0.253	-0.572	-0.648
	max	0.089	0.146	0.189

The extreme minimum and maximum values of the horizontal velocity, the acceleration and the mobility parameter  $\theta'_{McCall}$  obtained with the XBeach-G simulations without morphological (given in Table 41) are lower than the values of the XBeach-G simulations with morphological updating (given in Table 25). For all three slopes, the extreme minimum values (during run-up) decrease more than the maximum values (during run-down). Higher negative values of the velocity and the acceleration are found in the modelled erosion holes in case of morphological updating, because the slope can change in the modelled erosion holes (i.e. slope can become steeper or milder). The values of the XBeach-G simulations without morphological updating (given in Table 41) are still not in the range of the values derived from the BIV analyzed videos (given in Table 19).

## E.5 Influence of irregular waves

The results of the XBeach-G simulations performed with regular waves and without morphological updating of the bed are shown in Table 42.

**Table 42 - Values of  $U$ ,  $dU/dt$  and  $\theta'_{McCall}$  from XBeach-G simulations with  $S_{Wit}$  input with regular waves and without morphological updating, per slope**

Slope		1:5	1:10	1:15
<b>U</b> (m/s)	min	-0.179	-0.425	-0.552
	max	0.244	0.321	0.337
<b>dU/dt</b> (m/s <sup>2</sup> )	min	-3.936	-11.802	-18.205
	max	1.790	5.593	6.955

Slope		1:5	1:10	1:15
<b><math>\theta'_{McCall}</math></b> (-)	min	-0.160	-0.407	-0.502
	max	0.057	0.131	0.156

The extreme negative and positive values of the velocity, the acceleration and the mobility parameter  $\theta'_{McCall}$  obtained with the XBeach-G simulations with regular waves and without morphological (given in Table 42) are lower than the values of the XBeach-G simulations with irregular waves and with morphological updating (see Table 25) and lower than the values obtained with irregular waves and without morphological updating (see Table 41). However, the values in Table 42 are still not in the range of the values derived from the BIV analyzed videos (see Table 19).

## E.6 Mobility parameter and relative erosion depth along length of slope

Although very high and unrealistic values of the mobility parameter  $\theta'_{\text{McCall}}$  are determined in XBeach-G, the relation between the mobility parameter  $\theta'_{\text{McCall}}$  and the damage, which has been described with the relative erosion depth  $d_e/D_{n50}$ , along the length of the slope can be examined qualitatively (assuming that the extreme minimum and maximum values of the mobility parameter  $\theta'_{\text{McCall}}$  occur at the same location of the slope, but the magnitude of these values can be different).

The extreme minimum and maximum values over time of the mobility parameter  $\theta'_{\text{McCall}}$  along the length of the 1:5 have been determined by taking the extreme minimum and maximum value of  $\theta'_{\text{McCall}}$  in time ( $t_{\text{model}}$  is 3,159 s, with  $\Delta t = 1.00$  s) at each grid point  $x$  ( $x = 0.00$  m to  $x = 4.70$  m, with  $\Delta x = 0.05$  m). The extreme minimum and maximum values over time of the mobility parameter  $\theta'_{\text{McCall}}$  along the length of the 1:5 slope are plotted in Figure 61. The relative erosion depths  $d_e/D_{n50}$ , derived from the profile change experiments of Kramer (2016) and the erosion profile modelled with XBeach-G, have been plotted along the length of the 1:5 slope as well. In this way, the mobility parameter can be linked with the obtained damage.

The extreme minimum and maximum values over time of the mobility parameter  $\theta'_{\text{McCall}}$  along the length of the 1:10 and 1:15 slopes are plotted in Figure 62 and Figure 63 respectively.

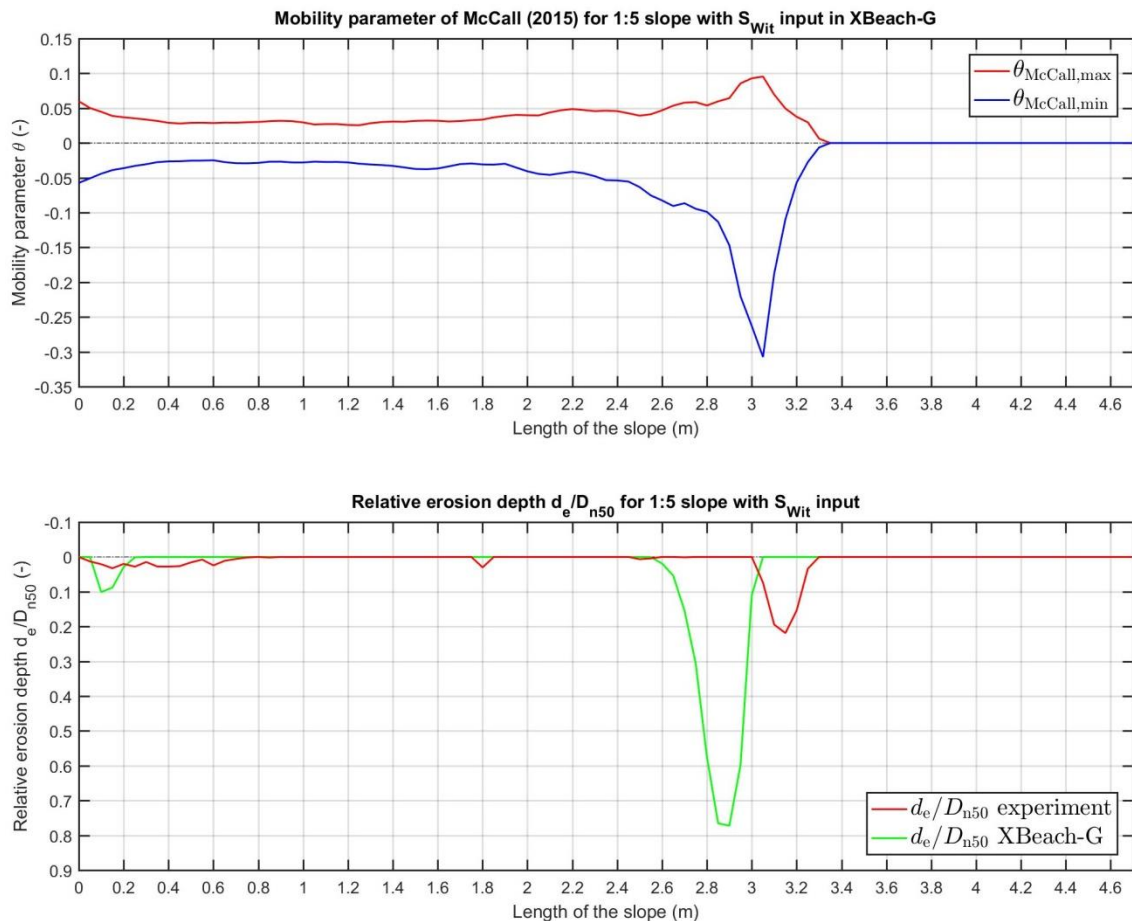


Figure 61 - Extreme minimum and maximum values over time of mobility parameter  $\theta'_{\text{McCall}}$  (top) and relative erosion depth  $d_e/D_{n50}$  (bottom) along the length of the 1:5 slope

In which: the values of the mobility parameter are positive during run-down and the values of the mobility parameter are negative during run-up. The relative erosion depth has a positive value when the profile is eroded (i.e. damage to the profile). The relative erosion depth has a value of zero when no changes to the profile occurred or when the profile increases (e.g. due to sedimentation).

As can be seen in Figure 61, the extreme maximum damage does not occur at the location where the mobility parameter  $\theta'_{\text{McCall}}$  has its extreme minimum and maximum value. The relative erosion depth is maximum more upslope than the extreme minimum and maximum of the mobility parameter for the profile change experiment of Kramer (2016) and more downslope in case of the XBeach-G simulation. The same trend has been found for the XBeach-G simulations with 1:10 and 1:15 slopes.

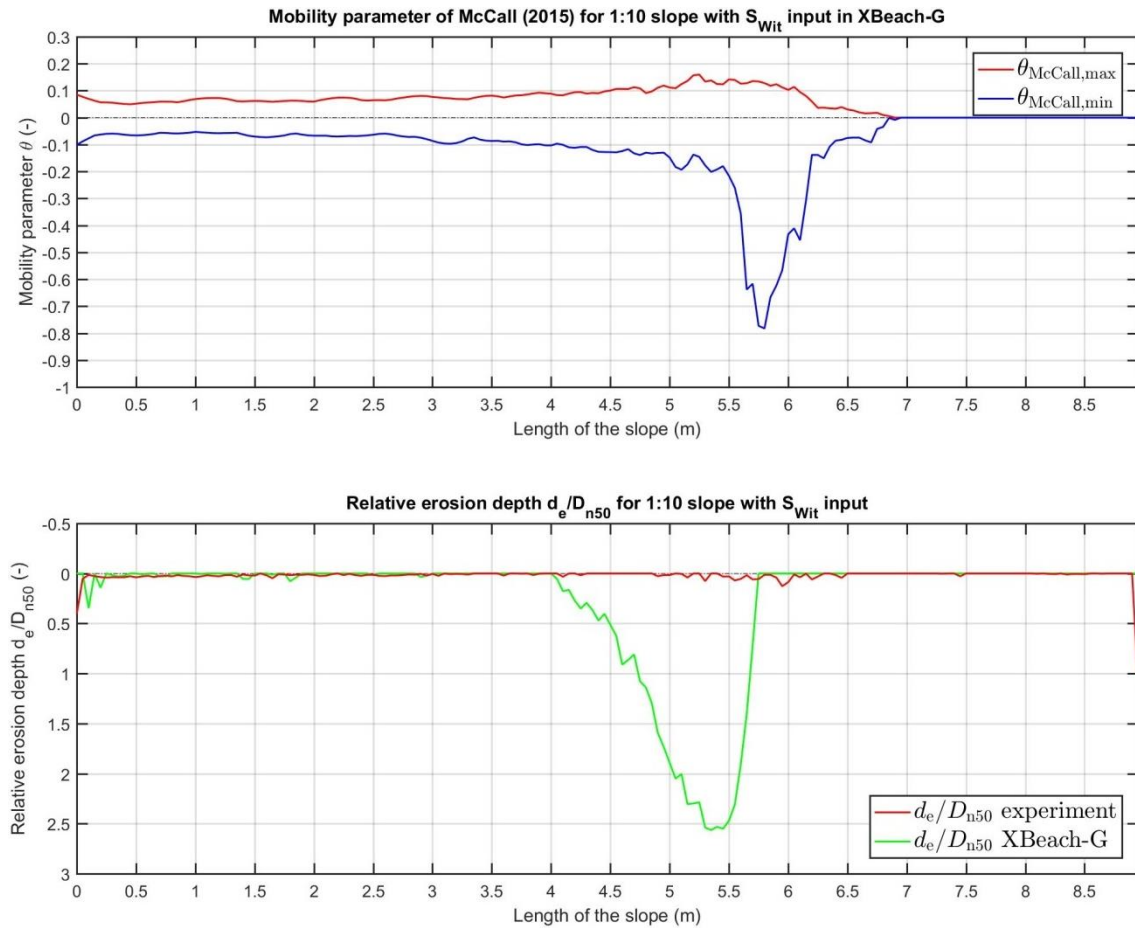


Figure 62 - Extreme minimum and maximum values over time of mobility parameter  $\theta'_{\text{McCall}}$  (top) and relative erosion depth  $d_e/D_{n50}$  (bottom) along the length of the 1:10 slope

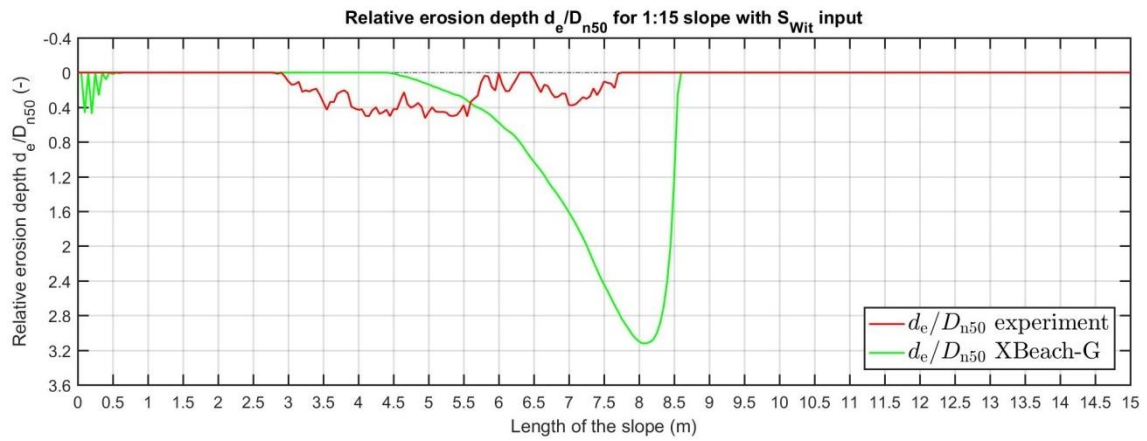
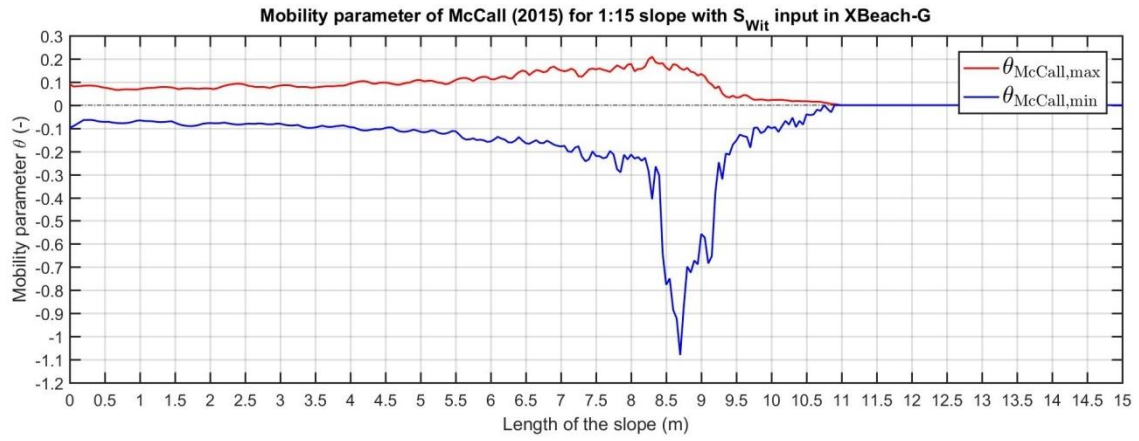


Figure 63 - Extreme minimum and maximum values over time of mobility parameter  $\theta'_{McCall}$  (top) and relative erosion depth  $d_e/D_{n50}$  (bottom) along the length of the 1:15 slope